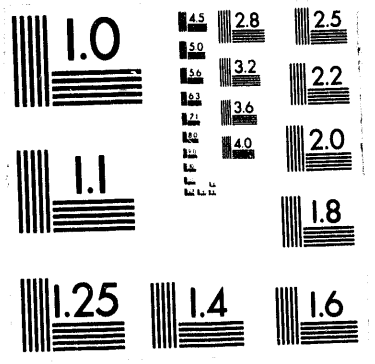
1.0
1.1
1.25
1.4
1.6
1.8
2.0
2.2
2.5
2.8
3.2
3.6
4.0
4.5
5.0
5.6
6.3
7.1
8.0
9.0

1 of 3

UCRL-LR-114875
Distribution Category UC-700

On the Hypothesis that Quantum Mechanics Manifests Classical Mechanics: Numerical Approach to the Correspondence in Search of Quantum Chaos

Sang-Bong Lee

Manuscript date: September 1993

LAWRENCE LIVERMORE NATIONAL LABORATORY
University of California • Livermore, California • 94551

On The Hypothesis That Quantum Mechanics Manifests Classical Mechanics:

Numerical Approach To The Correspondence In Search Of Quantum Chaos.

By

SANG-BONG LEE

B. A. (San Francisco State University) 1987
M. S. (University of California, Davis) 1989

DISSERTATION

Submitted in partial satisfaction of the requirements for the degree of

DOCTOR OF PHILOSOPHY

in

APPLIED SCIENCE

in the

GRADUATE DIVISION

of the

UNIVERSITY OF CALIFORNIA

DAVIS

Approved:

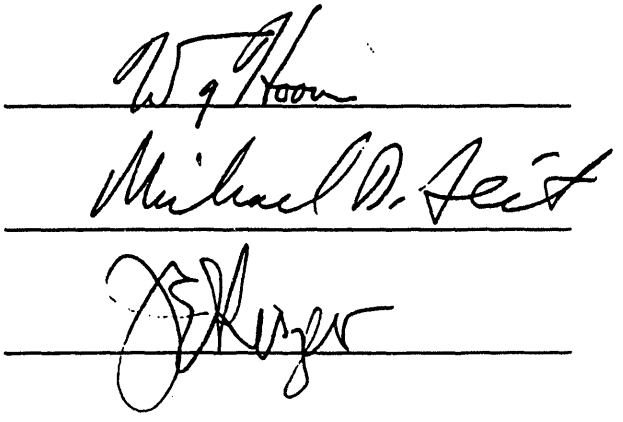

Committee in Charge

1993

ABSTRACT

Quantum manifestation of classical chaos has been one of the extensively studied subjects for more than a decade. Yet clear understanding of its nature still remains to be an open question partly due to the lack of a canonical definition of *quantum chaos*. The classical definition seems to be unsuitable in quantum mechanics partly because of the Heisenberg quantum uncertainty. In this regard, *quantum chaos* is somewhat misleading and needs to be clarified at the very fundamental level of physics. Since it is well known that quantum mechanics is more fundamental than classical mechanics, the quantum description of classically chaotic nature should be attainable in the limit of large quantum numbers. The focus of my research, therefore, lies on the correspondence principle for classically chaotic systems. The chaotic damped driven pendulum is mainly studied numerically using the split operator method that solves the time-dependent Schrödinger equation. Other chaotic systems such as the kicked rotator, the superconducting Josephson junction, the forced Duffing's oscillator and the nonequilibrium three-body oscillator are also discussed in a quantum context. For classically dissipative chaotic systems in which (multi)fractal strange attractors often emerge, several quantum dissipative mechanisms are also considered. For instance, Hoover's and Kubo-Fox-Keizer's approaches are studied with some computational analyses. But the notion of complex energy with non-Hermiticity is extensively applied. Moreover, the Wigner and Husimi distribution functions are examined with an equivalent classical distribution in phase-space, and dynamical properties of the wave packet in configuration and momentum spaces are also explored. The results indicate that quantum dynamics embraces classical dynamics although the classical-quantum correspondence fails to be observed in the classically chaotic regime. Even in the semi-classical limits, classically chaotic phenomena would eventually be suppressed by the quantum uncertainty. The quantum measurement problem appears to hold a part of key solution. It is also suggested that time-varying uncertainty fluctuations can be used as a quantitative measure of quantum chaos even in systems that have no classical analogs.

PREFACE

Ich sage euch:
man muss noch Chaos in sich haben,
um einen tanzenden Stern gebären zu können.
Ich sage euch:
ihr habt noch Chaos in euch.

Yea verily, I say unto you:
A man must have Chaos yet within him,
To birth a dancing star.
I say unto you:
You have yet Chaos in you.

Friedrich Nietzsche's "Thus spake Zarathustra"

The universal concept underlying chaos in a quantum system has yet to come. It is believed that quantum mechanics is one of the most fundamental and important concepts in science today. Quantum theory governs many laws of nature and innumerable phenomena in the world around us. However, the so-called quantum chaos, unlike ubiquitous classical chaos, not only fails to be observed, but lacks a canonical definition. My thesis therefore treats mostly the damped driven pendulum as an example to search and to examine quantum chaotic nature specifically in the context of the correspondence principle. Our aim is focused on theoretical and numerical investigation.

The basic picture of the thesis is mentioned in Chapters one and two. These chapters deal with primary operational ideas. The numerical method extensively used in this study is the split operator method that takes advantage of easily used fast Fourier transforms. This method effectively solves the time-dependent Schrödinger equation by treating the dependence of the solution on kinetic and potential energies separately. Then the expectation values of classically dynamical variables are computed and are compared with classical values. Moreover the numerous distributions representing different probabilities in phase-space are also considered since

the quantum wave function physically represents a probability. One with knowledge of non-relativistic quantum mechanics and advanced mathematics should have little difficulty to follow the contents with the exception of some numerical techniques. An able person who has no or little facility in this field can learn these techniques in a moderate amount of time.

In Chapter three, numerical results from the pendulum with some quantum distribution functional analyses of a simple harmonic oscillator are presented. The Wigner and Husimi distributions as the quantum counterparts of a classical probability distribution will be used to determine the correspondence within the break time. The break time is identified in my study as the time where the magnitude of the uncertainty is comparable to the action taken by motions in phase-space. It will be interesting to see the claim that the Husimi representation is better than the Wigner one solely for the purpose of checking the correspondence. On the other hand, it will also be of importance to observe whether or not the Husimi formulation is better to describe quantum dynamics since it ignores some of dynamical information through the Gaussian smoothing mechanism adapted. These discussions are in Chapter three more specifically and also in Chapter four. A condensed version of some of these materials in Chapter four has been published in Phys. Rev. E. **47**(6), 4552-5 (1993).

At this juncture I must mention that a postulate is proposed in Chapter four since there exists a seriously different nature between classical and quantum mechanics. Quantum mechanics deals with a closed system, whereas classical mechanics deals with an open system, especially when the viscous damping is present. In the study, a possible consideration of this classical dissipation into quantum mechanics, specifically into Schrödinger equation, is suggested by using a term resembling the classical Rayleigh energy. In this regard, the non-Hermitian nature is only mentioned, but not thoroughly considered. Also, Kubo-Fox-Keizer approach to this problem is reviewed, and Nosé-Hoover mechanics is briefly introduced as a more general quantum mechanical description of the classical dissipation mechanism.

In Chapter five, the comparisons with the kicked rotator and Josephson junction are provided. Analyses of the well-known kicked rotator and the Josephson junction problem as possible applications of the numerical method are carried out in this chapter. A two-dimensional case is also considered in

this chapter to see Heller's 'scars' left out by the quantum wave packet. A possible non-equilibrium approach to many-body quantum system is also considered using Gauss' principle of least constraint to modify linear Schrödinger equation nonlinear.

The nature of the quantum uncertainty will be considered in Chapter six to see if the correspondence can be better represented. In this regard, the possible explanation to this matter will be established using a quantum mechanical measurement problem like Schrödinger's cat paradox. Moreover, the possibility that there might exist an unknown non-linear coupling term in Schrödinger equation will be also considered for the case where quantum chaos can naturally arise. This chapter concludes with possible future research directions.

Again, this writing was intended initially to inform as many people as possible in the field as well as in other fields of science. In writing this dissertation, I have experienced pleasures of fostering a rough initial version. On the other hand, I have also felt great difficulties, partly because of the perpetual need to make a change, sometimes considerably, and partly because of the inhibition of the many topics to be included. It is clear that the current trend in search of quantum chaos includes a very wide range of topics and a fair amount of new materials relating both to recent research and to earlier results that have now become of greater significance. However, I found that the reviews of all these materials were not possible, though some were mentioned. Yet, the process of the writing was a challenging and fruitful experience to me. I finally confess that any errata are strictly the results of my own ineptitude and blind enthusiasm. Any misreadings of existing theories or findings are the results of similar impulses, not malicious intent.

Some of the contents in this text have been either published or presented in various means by the author. See *University of California, Lawrence Livermore Laboratory Reports: UCRL-JC-112292 (Dec. 1992); UCRL-JC-111922 (Sept. 1992); UCRL-JC-111443 (Aug. 1992); UCRL-JC-111444-ABS (Nov. 1992); UCRL-JC-111446-ABS (Nov. 1992)*. See also *Phys. Rev. E. 47(6), 4552-5 (1993); Bull. Am. Phys. Soc. 37(7), 1686 (1992); Bull. Am. Phys. Soc. 37(3), 1108 (1992); Abstract for Physics Computing, 27 (June, 1991); Proceedings of the International Conference for Advancement of Science and Technology (Korea Univ., Korea, Aug, 1993). For other materials by the author related to this thesis topic, see UCRL-JC-112922 (Feb. 1993); Bull. Am. Phys. Soc. 38(1), 529, (1993).*

ACKNOWLEDGMENT

I am greatly indebted to Dr. Michael Feit who has given not only important meaning to my project but also endless support. During this research, I have been fortunate to observe and share his seemingly unbounded wisdom and intellect. In addition, for his scholarly brilliancy I admire Professor William Hoover from whom I have benefited immensely in preparing the thesis. I am very grateful for many friendly, inspiring conversations with both of them, which found their way into the text. I also acknowledge deeply Professor Joel Keizer who has offered valuable criticism and suggestions. I was also able to write this thesis as the results of longstanding hospitality and kindness from many others, making it almost impossible to express sufficient recognition to all of them. But I would remiss not to thank Drs. Minh Duong-van, Ricky Ratowski, David Hwang, Fred Wooten, Yin Yeh, John DeGroot, Ann Orel-Woodin, Blake Temple, Ron Soohoo, Tom Wainwright, and Rudy Bauer.

Furthermore, I express my sincere dedication to my wife, Sohyun. I am very grateful for her abiding patience and encouragement as we journeyed through various emotional peaks and valleys together. Without her support, this work would never be possible. She and my delightful daughter, Juhyé, have been the constant sources of my strong withstanding and boundless joy throughout the years of this research, especially during difficult times.

Last but far from least, I profoundly thank my teachers, Young-Ho Lee and Gary Ling who led me into this fascinating world of physical sciences, and all of my confreres, especially Doug Sparks for his detailed comments and corrections. It is regrettable that my thanks to all others who have aided me in some ways have to be omitted at this juncture. But these people will always remain unforgettable in my heart.

Computations in this thesis were mainly carried out using CRAY through Open/Secure Computing Facilities in FORTRAN at the Lawrence Livermore National Laboratory. This thesis work was partly supported and performed under auspices of the U. S. Department of Energy by the Lawrence Livermore National Laboratory under contract No. W-7405-ENG-48.

Livermore, CA. 1993. *Sang-Bong Lee*

To Sohyun and Juhyé

TABLE OF CONTENTS

LIST OF SYMBOLS

The major symbols utilized throughout the paper are listed here to grasp the contents better and to avoid confusion with other conventions.

θ	Angle of oscillation	ψ, φ	Wave functions
$\dot{\theta}$	Angular velocity	A, χ	Gauges
q	Canonical position (angle)	$\hat{O}$	Operator
$\dot{q}$	Canonical velocity	$\hat{U}$	Evolution operator
p	Canonical momentum	σ	Width of wave packet
m	Mass of an oscillator	$P(\omega_k)$	Power spectral density
μ	Dimensionless (effective) mass	$V(t)$	Uncertainty product $(\Delta q \Delta p)$
f	External field strength	$U(t)$	Uncertainty product $(\Delta q \Delta \dot{q})$
γ	Dimensionless field strength	T	Kinetic energy
b	Damping coefficient	V	Potential energy
β	Dimensionless damping coefficient	λ	Lagrange multiplier
l	Length of an oscillator	I	Characteristic action
ω	External field frequency	P_c	Classical distribution
ω_o	Natural frequency of oscillation	P_w	Wigner distribution
H_o	Unperturbed Hamiltonian	P_h	Husimi distribution
H_{pert}	Perturbing Hamiltonian	C	Correlation function
H_{cl}	Classical Hamiltonian	R	Rayleigh energy
H_{qm}	Quantum Hamiltonian	H	Other Hamiltonians

Note that quantum mechanical operators and dimensionless variables are designated by the superscript ^ and –, respectively.

CHAPTER 1

INTRODUCTION

In the beginning there was Apsu the Primeval,
and Tīāmat, who is chaos.

Myths of the world

In this chapter, an introduction to the main focus of this thesis is described. The dimensional issues of the model are also described with possible physical configurations.

1-1. Introductory notes

In 1963, E. N. Lorenz published [1] his seminal numerical results from a set of simple first-order differential equations for fluid convection with a nonlinearity in the equations. The discovery he made in this completely deterministic system of three equations was unstable irregular fluctuation that never repeats itself in any predictable pattern. Lorenz had found unpredictability which generates complexity: richly organized patterns, now called chaos.

The word 'chaos' is defined as *a state of utter confusion or disorder, a total lack of organization or order* in the Random House Dictionary [2]. Its original meaning in Greek '*Khaos*' is *formless matter*. Scientists adopted this word to describe states of unpredictability and complexity containing a high sensitivity to initial conditions.

At around the same time, the theory known as the KAM theorem [3] emerged from Russia. It states that invariant surfaces formed by a trajectory of integrable regions in phase-space continue to exist for most initial conditions for systems perturbed away from the regions. These surfaces are isolated and are called the KAM surfaces. As the perturbation strength increases, however, a transition can occur in which the isolating KAM surfaces disappear and the stochastic layers merge. With this theoretical support, nonlinear researchers started looking on chaos problems such as Lorenz's hydrodynamical model more and more.

As the 1960s went on, individual scientists made discoveries that paralleled Lorenz's. Among them, M. Feigenbaum discovered the striking universality lying under the several chaotic motions described by, for example, the logistic map or Hénon map. More theoretical and experimental

realizations of the field have followed by seemingly much richer and broader applications. Some have even called *chaos* as a revolutionary science heading towards the twenty-first century. To make this more drastic, *relativity* and *quantum mechanics* were put on to the equivalent level by a few of them. No matter what one can say about the significance of this new field, there is no doubt that it has provided and will provide a better understanding of nature.

However, as this classical means of chaos [4] develops further, many of scientists, G. Casati and J. Ford, for instance, started speculating about the possibility that quantum mechanics manifests classical chaos. In principle, this quantum manifestation must be true since quantum mechanics is known to be more fundamental. Therefore, a search for quantum chaos becomes a new exciting challenge for quantum physicists. But permitting the definition of classical chaos for that of quantum chaos, nobody is able to find its existence. Since then, many investigators have contributed their own definitions, and defended them with some supporters. Despite the fact that there exists no canonical definition of quantum chaos, much of this research, as once J. Ford puts it [5], is still recognized as an encouraging exploration and innovation. However, the problems still have remained: the lack of a serious research in the context of the correspondence principle, the roles of quantum eigen-values, eigen-functions in quantum chaos in terms of classical definitions. The right questions then we have to ask are the following: How can we justify the ambiguity of classical means of chaos in the underlying quantum mechanics? Does the randomness of eigen-values play a classical chaotic role in quantum mechanics? It is these simple questions that brought up this research project initially. The first question can be answered by rather direct investigations using the quantum methods corresponding to classical method for defining chaos and by studying their results. On the other hand, it

is difficult to establish the relationship between quantum eigen-values and classical energy of a system. The only specific indication of certain chaotic nature is in this case randomness. Since this randomness is necessary, but not sufficient for chaos [6], this thesis will focus mainly on the first problem or rather the first question.

Bearing this in mind, we will choose a model that is describable in both classical and quantum mechanics. It is of better interest that a system contains at least two control parameters for developing chaos. A good choice seems to be a driven system that is simple and familiar enough to many people and also has very small quantum energy level differences so that it may be regarded as an almost classical system. It is quite possible there are many systems that satisfy these conditions, but a proper choice seems to be the driven pendulum. This model also contains the analog of a linearly driven harmonic oscillator as a limiting case where the oscillation is small.

In the next section, the description of a dimensional issue is presented with some possible physical configurations using the hydrogen atom. In Chapter two, general features of the model and its numerical scheme are discussed. Basic mathematical approaches to the problem are all contained in this chapter. Quantum mechanical distributions are introduced in Chapter three. Without dissipation, the correspondence is checked using numerical results in this chapter. In Chapter four, a possible dissipation mechanism is introduced and used. The results of calculations are also presented and compared. As an application problem in Chapter five, we consider several different models described in Chapter two. For example, a single parameter system such as the kicked rotator and the Josephson junction will be discussed in Chapter five. In addition, Nosé-Hoover approach to chaos is introduced in this chapter. Finally, our conclusions are summarized in

Chapter six. Potential future directions are also indicated in the same chapter. To see an overview of the study, the readers should consult Preface.

1-2. System of units with physical interpretation

As we will see in the next chapter, we are basically concerned with classical equations of motion and Schrödinger equation for an externally driven pendulum. The potential term contains an earth gravitational constant g, and mass m, length l. The external field strength is f. Then classically, the motion is described by (see Section 2-1 for complete details)

$$\dot{\theta} = \frac{p}{m\, l^2}, \tag{1-1a}$$

$$\dot{p} = -\, m\, g\, l \sin\theta + m\, l^2 f \cos(\omega t) = m\, l^2 \ddot{\theta}. \tag{1-1b}$$

This reduces to

$$\ddot{\theta} = -\frac{g}{l}\sin\theta + f\cos(\omega t). \tag{1-1c}$$

If the damping torque, $F_D = -b\,\dot{\theta}$, is present, this equation becomes

$$\ddot{\theta} = -\frac{g}{l}\sin\theta + f\cos(\omega t) - \frac{b}{m\, l^2}\dot{\theta}. \tag{1-1d}$$

Since b has the unit of [mass] [length]^2/[time] in this case, F_D is the moment of damping force (damping torque). Now, we divide both sides of equation (1-1a) by $\sqrt{\frac{g}{l}}$, then we find

$$\dot{\theta}\sqrt{\frac{l}{g}} = \frac{p}{m'} \rightarrow \bar{\dot{\theta}} = \frac{p}{m'},$$

where the bar sign on the top of the variable means dimensionless. Here, $m' = m\,l\sqrt{g\,l}$, so the term p/m' becomes dimensionless. If we divide (1-1d) or (1-1c) this time by (g/l), then we get

$$\ddot{\theta}\,\frac{l}{g} = -\sin\theta + f\,\frac{l}{g}\cos(\omega t) - \frac{b}{m\,l^2}\sqrt{\frac{l}{g}}\left(\sqrt{\frac{l}{g}}\,\dot{\theta}\right).$$

This equation then finally reduces to the following closed form with notations $\bar{\dot{\theta}} = \sqrt{\frac{l}{g}}\,\dot{\theta}$, $\bar{\ddot{\theta}} = \ddot{\theta}\,\frac{l}{g}$.

$$\bar{\ddot{\theta}} = -\sin\bar{\theta} + \gamma\cos(\omega t) - \beta\bar{\dot{\theta}}, \qquad (1\text{-}2)$$

where $\gamma = f\frac{l}{g}$, and $\beta = \frac{b}{m\,l^2}\sqrt{\frac{l}{g}}$; these are also dimensionless as well as the product ωt since b contains m implicitly. This (1-2) is a classical dimensionless equation of motion for a driven damped pendulum. Note that the mass term drops out.

Quantum mechanically, if we ignore the dissipation due to damping, the corresponding Schrödinger equation will be

$$\hat{E}\,\varphi = \hat{H}\,\varphi = \left[\,\hat{H}_o + \hat{H}_{pert}\,\right]\varphi,$$

$$= \left[-\frac{\hbar^2}{2m\,l^2}\frac{\partial^2}{\partial\theta^2} + mgl\,(1-\cos\theta)\right]\varphi - ml^2 f\,\theta\cos(\omega t)\varphi, \qquad (1\text{-}3)$$

$$\approx \left[-\frac{\hbar^2}{2m\,l^2}\frac{\partial^2}{\partial\theta^2}+\frac{1}{2}\,mgl\,\theta^2\right]\varphi \;-\; ml^2 f\,\theta\cos(\omega t)\varphi,$$

$$= \left[-\frac{\hbar^2}{2m}\frac{\partial^2}{\partial(l\theta)^2}+\frac{1}{2}\,m\frac{g}{l}(l\theta)^2\right]\varphi \;-\; mlf\,(l\theta)\cos(\omega t)\varphi, \qquad (1\text{-}4)$$

$$= \left[-\frac{\hbar^2}{2m}\frac{\partial^2}{\partial x^2}+\frac{1}{2}\,m\omega_o^2 x^2\right]\varphi \;-\; mlf\,x\cos(\omega t)\varphi,$$

where $x = l\theta$, and $\omega_o^2 = g/l$ with the assumption of a small angle oscillation. Note that l has a unit of length, and so does $l\theta$; θ is the angle measured in radian.

Hence, if we ignore the perturbation term, $-\,mlf\,x\cos(\omega t)$, a unit of energy becomes $\hbar\omega_o$ $(=\hbar\sqrt{\frac{g}{l}}\,)$ just like the case of a simple harmonic oscillator. Hence it may be assumed that the quantized energy levels for small angle oscillations, E_n, would be $\sim n\,\hbar\sqrt{\frac{g}{l}}$. If we carry this out further, we get the dimensionless equation. We divide both sides of equation (1-3) or (1-4) by $\hbar\omega_o$, and find

$$\overline{E}\,\overline{\varphi} = \left[-\frac{\hbar}{2m\sqrt{g}l^{3/2}}\frac{\partial^2}{\partial\theta^2}+\frac{1}{2}\frac{m}{\hbar}\sqrt{g}l^{3/2}\,\theta^2-\frac{m}{\hbar}\sqrt{g}l^{3/2}\left(\frac{f}{g}\right)(l\,\theta)\cos(\omega t)\right]\overline{\varphi}, \qquad (1\text{-}5)$$

where dimensionless $\overline{E} = i\,(\frac{\partial}{\partial t})$. The wave function consequently needs to be changed in the following form for completeness,

$$\varphi(\theta,t) = \sum_n^{\infty} A_n\,u_n(\theta)\,exp\,(-iE_n t/\hbar) \rightarrow \overline{\varphi}(\theta,t) = \sum_n^{\infty} A_n\,u_n(\theta)\,exp\,(-i\overline{E}_n t)$$

where A_n is an arbitrary complex number. Thus, by setting $M = m\,(\sqrt{\frac{g}{l}}\,)$, we finally get

$$i\frac{\partial\bar{\varphi}}{\partial t} = \left[-\frac{1}{2}\left(\frac{\hbar}{Ml^2}\right)\frac{\partial^2}{\partial\theta^2} + \frac{1}{2}\left(\frac{Ml^2}{\hbar}\right)\theta^2 - \frac{Ml^2}{\hbar}\frac{fl}{g}\theta\cos(\omega t)\right]\bar{\varphi},$$

$$= \left[-\frac{1}{2\mu}\frac{\partial^2}{\partial\theta^2} + \frac{1}{2}\mu\,\theta^2 - \mu\frac{fl}{g}\theta\cos(\omega t)\right]\bar{\varphi}, \qquad (1\text{-}6)$$

where the dimensionless $\mu = [Ml^2/\hbar] = \left[\frac{m}{\hbar}\right] l\sqrt{g\,l}$. Hereafter we will change the notation of $\bar{\varphi} \rightarrow \varphi$, but φ means $\bar{\varphi}$. It is plausible from here to interpret that the equation (1-3) becomes

$$i\frac{\partial\varphi}{\partial t} = \left[-\frac{1}{2\mu}\frac{\partial^2}{\partial\theta^2} + \mu(1-\cos\theta) - \mu\gamma\theta\cos(\omega t)\right]\varphi, \qquad (1\text{-}7)$$

where $\gamma = fl/g$; it is also dimensionless as we have seen in the classical case, since the dimension of $[f]$ = [Time]$^{-2}$.

We will also come across another form of (1-3), namely a gauge transformed version, in the next chapter. After a gauge transformation, the Hamiltonian becomes

$$\widehat{H} = \frac{1}{2ml^2}\{\hat{p} + \frac{ml^2 f}{\omega}\sin(\omega t)\}^2 + mgl\,(1-\cos\widehat{\theta}). \qquad (1\text{-}8)$$

This equation can then be reduced to a dimensionless equation by applying the same techniques. Then, Eq. (1-8) yields the following dimensionless form:

$$\begin{aligned}\widehat{H}_{qm} &= \frac{1}{2\mu}\{\overline{p} - \overline{A}\}^2 + \overline{V}, \\ &= \frac{1}{2\mu}\left[\overline{p} + \mu\frac{fl}{g}\frac{\sin(\overline{\omega}\,\overline{t})}{\overline{\omega}}\right]^2 + \mu(1-\cos\theta), \\ &= \frac{1}{2\mu}\left[\overline{p} + \mu\gamma\frac{\sin(\overline{\omega}\,\overline{t})}{\overline{\omega}}\right]^2 + \mu(1-\cos\theta), \end{aligned} \tag{1-9}$$

where the variables $\overline{p} = -i\dfrac{\partial}{\partial\theta}$, and parameters $\overline{\omega} = \omega\sqrt{\dfrac{l}{g}}$, $\overline{t} = t\sqrt{\dfrac{g}{l}}$ are also dimensionless. Note that the product $\overline{\omega}\,\overline{t} = \omega t$. Then the dimensionless gauges $\overline{A} \rightarrow \widehat{\mathbf{A}}$, and $\overline{\chi} \rightarrow \widehat{\chi}$ are

$$\begin{aligned}\widehat{\mathbf{A}} &= -\mu\gamma\frac{\sin(\overline{\omega}\,\overline{t})}{\overline{\omega}}, \\ \widehat{\chi} &= \mu\gamma\theta\frac{\sin(\overline{\omega}\,\overline{t})}{\overline{\omega}}, \end{aligned} \tag{1-10}$$

such that gauges after the transformation,

$$\begin{aligned}\widehat{\mathbf{A}}' &= \widehat{\mathbf{A}} + \frac{\partial\widehat{\chi}}{\partial\theta} = 0, \\ \widehat{\mathbf{V}}' &= \widehat{\mathbf{V}} - \frac{\partial\widehat{\chi}}{\partial\overline{t}} = \mu(1-\cos\theta) - \mu\gamma\theta\cos(\overline{\omega}\,\overline{t}), \\ &= \mu(1-\cos\theta) - \mu\gamma\theta\cos(\omega t), \end{aligned} \tag{1-11}$$

yield the same dimensionless equation (1-7). The final form of Schrödinger equation then becomes

$$i\frac{\partial\psi}{\partial t} = \frac{1}{2\mu}\left[-i\frac{\partial}{\partial\theta} + \mu\gamma\frac{\sin(\overline{\omega}\,\overline{t})}{\overline{\omega}}\right]^2\psi + \mu(1-\cos\theta)\psi. \tag{1-12}$$

These equations (1-7) and (1-12) are equivalent dimensionless forms of Schrödinger equation with parameters μ, γ and $\overline{\omega}$ (denote ω hereafter). Note the relation $\varphi = exp(i\hat{\chi})\psi$.

In later chapters, the importance of the parameters μ, γ, ω will become clear. Whenever we choose the combinatory parameter $\mu = \lambda$, λ = any real number, we are actually setting $ml\sqrt{gl}/\hbar = \lambda$ such that the quantity $(m\ l\sqrt{l})$ is being fixed since the values of g and $\hbar$ are constants. Here we call μ the effective mass since it is the parameter we will change numerically. So unless it is specified, μ always means the effective mass. However, it is easier to think of $\mu = m$ numerically by assuming $g = l = \hbar = 1$ such that $\gamma = f$ and $\omega_0 = 1$. This is so because final values of the combinations in μ, γ are important instead of the individual parameters contained in those such as m, l as far as computers are concerned. In fact, this is numerically valid when we solve Schrödinger equation in dimensionless form.

So whenever we set μ to a certain number numerically, we are actually setting the quantity $(ml\sqrt{l})$. Let us briefly find out what the actual physical situation might be when we set $\mu = 1$. Now first imagine a bob made of the hydrogen atom. Then a unit effective mass may represent the hydrogen atom swinging at the end of a rod of length 7.4×10^{-6} meters [7]. That is to say, a particle 100 times the mass of the H-atom swinging at the end of the same rod would take a value of $\mu = 100$. On the other hand, this value ($\mu = 100$) may also be the H-atom moving at the end of 1.6×10^{-6} meter rod. It is obvious from these that more classical behavior is certainly expected for values $\mu > 1$. This corresponds to usual physics of gravity such that the heavier a particle (or longer the rod) is, the more valid classical mechanics is.

For an external perturbation strength, a similar analogy can be applied.

For instance, when μ = 1 for the H-atom, $\gamma = fl/g$ =1 means $f = g/l$. So f = 1.3×10^{6} $(\text{sec})^{-2}$, which is in terms of energy $ml^2 f \sim 1.2 \times 10^{-31}$ Joules = 7.5 $\times 10^{-13}$ eV. Even when μ = 100, γ = 1 represents the case where ~ 2.6×10^{-30} Joules = 1.6 $\times 10^{-11}$ eV. This is not a small energy, but it is an effective one in the quantum mechanical treatment of gravity, which we will explain shortly. As we increase the effective mass, the corresponding value of f will increase linearly.

In the case of the external field frequency, ω ~ 1150 Hz, which means the period ~ 5.5 $\times 10^{-4}$ seconds when dimensionless $\overline{\omega}$ = 1 for μ = 1 (H-atom). For μ = 100, ω ~ 247 Hz, which also means the period ~ 2.5 $\times 10^{-2}$ seconds when dimensionless $\overline{\omega}$ = 1. In both cases, The product $\hbar\omega \approx \Delta E$ as it should be since $\overline{\omega}$ = 1 corresponds to resonance.

Now let us interpret time scale. For $\overline{\omega}$ = 1 and μ = 1 (H-atom), $\overline{t}$ = 1 sets the real physical time to be 8.7×10^{-4} seconds. In other words, when we choose the integration time step $\Delta \overline{t}$ = 0.01 in this case, a real physical time step becomes 8.7×10^{-6} seconds so that the number of time steps to reach the period (5.5 $\times$ 10^{-4} seconds) would be about 628 (~ 100 $\times$ 2π). But in a case of $\overline{\omega}$ = 1 and μ = 100 (H-atom), $\overline{t}$ = 1 sets the real physical time to be 4.0×10^{-3} seconds. By the same token, we would need the same number of time steps to reach a period (2.5×10^{-2} seconds in this case) with $\Delta \overline{t}$ = 0.01 ($\Delta t = 4.0 \times 10^{-5}$ seconds). As a result, the size of a time step should be reduced to 2.2×10^{-3} for μ = 100 in order to have the same physical time as for μ = 1. Therefore, we need a smaller $\Delta \overline{t}$ for a larger μ. It is clear that there are virtually many other possible interpretations of this kind using different atoms. We will see more physical examples of the pendulum consisting of the hydrogen atom in the next chapter and Appendix therein.

Nonetheless, the role of gravity in quantum mechanics appears as a rather different situation: whenever $\hbar$ appears, m is also expected to appear. In our case, μ contains both implicitly. It is important from this point of view that we must make an appropriate semi-classical approximation ($\mu \to \infty$, but not just $\hbar \to 0$). We will come to this point again in the next chapter when we study how to take a semi-classical limit.

It is interesting to see that the quantity $[\hbar\sqrt{g/l}]$ is really a small number. It is about ~ 1.2×10^{-31} Joules ~ 7.6×10^{-13} eV when $l = 7.4\times10^{-6}$ meters (This length was explained previously); ω_o = 1150 Hz. This is expected because of a very small quantum effect on gravitation unless we deal with a scale length of ~ 10^{-35} m, the so-called the 'Planck length' L_P, where $L_P \approx (G\hbar/c^3)^{1/2}$, where G is Newton's universal constant, and c the speed of light. It is at this scale of fundamental length in nature that we might expect to see some quantum mechanical effects of gravity. The sizes of an atom and nucleus which are in the order of 10^{-10} m and 10^{-15} m, respectively should be noted for comparison. To study this length scale, we need 10^{18} ~ 10^{19} GeV, the so-called the 'Planck mass' in unit of energy M_P, where $M_P \approx (\hbar c/G)^{1/2}$. This value can be obtained from the uncertainty principle using L_P alone. Nevertheless, it seems highly unlikely that this enormous amount of energy will ever be achieved by us since the largest particle accelerator works in present time at around 10^3 GeV.

In the case of a linearly driven harmonic oscillator, the dimensionless Schrödinger equation is easily reduced to the following form by just inspecting (1-12),

$$i\frac{\partial\psi}{\partial t} = \frac{1}{2\mu}\left[-i\frac{\partial}{\partial\xi} + \mu\gamma\frac{\sin(\bar{\omega}\bar{t})}{\bar{\omega}}\right]^2\psi + \frac{\mu}{2}\xi^2\psi, \qquad (1\text{-}13)$$

where the dimensionless variable $\xi = x/a$, a is a scaling length, and dimensionless parameters $\mu = \hbar/ma^2\omega_o$, $\gamma = f/a\omega_o^2$, $\overline{\omega} = \omega/\omega_o$ and $\overline{t} = t\omega_o$. In this case f has a unit of acceleration. With the use of atomic units, however, the variations in μ is not applicable. To take semi-classical limits, (1-13) makes more sense than simply using atomic units in Schrödinger equation. Then the similar physical interpretations can be conjectured.

In Chapter five, however, we shall consider a Josephson junction in which the unit system is different since it involves electromagnetic units. But the same basic principles and techniques apply, so we will not discuss these units explicitly here. One can easily derive the appropriate scale factors from the equation (2-12) in this case.

References

[1] E. N. Lorenz, *Deterministic Nonperiodic Flow*, J. Atmos. Sci. **20**, 130 (1963).

[2] *The Random House Dictionary of the English Language*, 2nd Edition, Unabridged, Random House (N. Y., 1987).

[3] A. N. Kolmogorov, Dokl. Akad. Nauk. SSSR, **98**, 527 (1954); V. I. Arnold, Sov. Math. Dokl. **3**, 136 (1963); **4**, 1153 (1963); J. Moser, Nachr. Akad. Wiss. Göttingen. Math. Phys. **K1**, 1 (1962).

[4] To see many kinds of definitions, for example, B. Eckhardt, Phys. Rep. **163**, 205 (1988).

[5] J. Ford, in *Directions in Chaos*, Vol. II, edited by H. Bai-Lin (World Scientific, Singapore, 1988); see also by the same author, *The New Physics*, edited by P. Davis (Cambridge Univ. Press, Cambridge, 1989).

[6] To see recent discussions on quantum chaos, refer to the whole volume of J. Stat. Phys, **68**, July issue (1992).

[7] This can be easily checked by substituting the mass of the H-atom which is 1.6611×10^{-27}kg into μ.

CHAPTER 2

BASIC MATHEMATICAL AND NUMERICAL OPERATIONS

All stable processes
we shall predict,
all unstable processes
we shall control.

J. von Neumann ~1950
(F. Dyson's "Infinite in all directions")

The driven pendulum model is introduced in this chapter. The integration methods for numerical simulations are discussed. Method of controlling semi-classical limits is extensively investigated with two supplemental appendices.

2-1. Numerical models

In this section we discuss briefly the numerical models that will be investigated throughout this study. Let us consider a quantum mechanical system whose corresponding classical motion exhibits chaos. Time-dependent, one-degree of freedom, non energy-conserving Hamiltonian systems are perhaps simple to analyze numerically. The simplest but physically real and general system is the forced quantum pendulum as shown in the figure below.

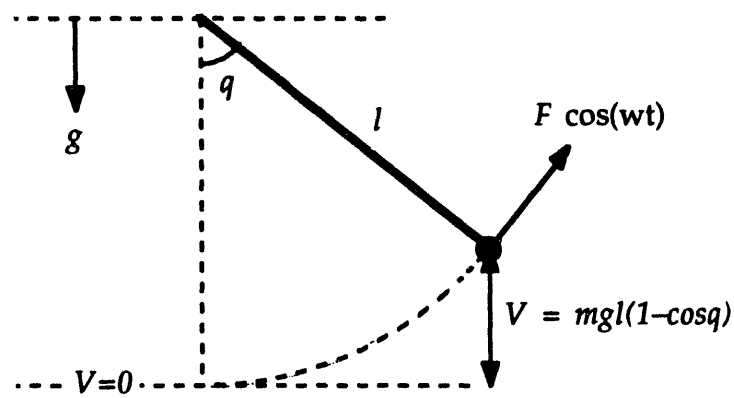

The canonical variable q is written here and hereafter instead of θ used in the previous chapter.

We are interested in a pendulum subjected to a continuous time-dependent external perturbation, $F\cos(\omega t)$. The classical Hamiltonian of the pendulum is not integrable; the pendulum's motion shows very rich classical chaotic structures [1]. This classical pendulum is represented by the full Hamiltonian without simplification in Section 1-2,

$$H_{cl} = H_0 + H_{pert} = T + V + H_{pert}$$

$$= \frac{p^2}{2ml^2} + mgl\,(1-\cos q) - ml^2 f\, q\cos(\omega t). \qquad (2\text{-}1)$$

This equation describes a pendulum in a gravitational acceleration g driven by an external field of amplitude f with a frequency ω. Here p is the angular momentum, q is the angular position, m is the mass of the pendulum. The length of the pendulum is l. The Hamilton's canonical equations of motion,

$$\dot{q} = \frac{dH}{dp} = \frac{p}{ml^2}, \qquad (2\text{-}2a)$$

$$\dot{p} = -\frac{dH}{dq} = -mgl\,\sin q + ml^2 f\cos(\omega t), \qquad (2\text{-}2b)$$

are then integrated to find a trajectory in phase-space for a given initial condition by a fourth-order Runge-Kutta method that will be discussed in the next section. If we combine these two equations, we get the usual classical equation of motion for a pendulum.

$$\ddot{q} + \frac{g}{l}\sin q = \ddot{q} + \omega_0^2 \sin q = f\cos(\omega t). \qquad (2\text{-}2c)$$

As we expected, the mass term drops out: so a feather and an iron ball would swing in the same way classically in the absence of friction (air resistance). In the case of quantum mechanics they would move differently because of the mass dependence in quantum mechanical dynamics of gravity [2]. Yet the classical damping is not considered here.

For a quantum model, we shall be concerned with the classical counterpart of our pendulum model. The corresponding quantum version becomes a time-dependent Hamiltonian operator $\widehat{H}_{qm} = \widehat{H}_{qm}(\hat{p}, \hat{q}, t)$:

$$\hat{H}_{qm} = \frac{1}{2ml^2}\{\hat{p} + \frac{ml^2 f}{\omega}\sin(\omega t)\}^2 + mgl(1-\cos\hat{q}),$$
$$= \frac{1}{2ml^2}\{\hat{p} - \hat{A}\}^2 + \hat{V}, \qquad (2\text{-}3)$$

where we recover an equivalent Hamiltonian to the classical one after a gauge transformation with the following gauges.

$$\hat{A} \rightarrow \hat{A}' = \hat{A} + \frac{\partial\hat{\chi}}{\partial q}, = 0, \qquad (2\text{-}4a)$$

$$\hat{V} \rightarrow \hat{V}' = \hat{V} - \frac{\partial\hat{\chi}}{\partial t} = mgl(1-\cos\hat{q}) - ml^2 f\,\hat{q}\cos(\omega t), \qquad (2\text{-}4b)$$

where $\hat{A} = -ml^2 f\sin(\omega t)/\omega$ and $\hat{\chi} = ml^2 f\,\hat{q}\sin(\omega t)/\omega$. Here the single component term, $\hat{A}$, acting like a vector potential commutes with $\hat{p}$ and its divergence vanishes; gauges in time-domain only. The reason to use the gauge transformed Hamiltonian (2-3) instead of (2-1) in this case will become clear in Section 2-3. As a check, we easily see that this transformation yields

$$\hat{H}_{qm}' = \frac{1}{2ml^2}\{\hat{p} - \hat{A}'\}^2 + \hat{V}',$$
$$= \frac{\hat{p}^2}{2ml^2} + mgl(1-\cos\hat{q}) - ml^2 f\,\hat{q}\cos(\omega t) = \hat{H}_{cl}. \qquad (2\text{-}5)$$

So the classical Hamiltonian (2-1) is gauge invariant.

It is interesting to note that this transformation is also canonical since phase-space volume is invariant, having a unit Jacobian. To see that, let $P = p - A = p + \frac{ml^2 f}{\omega}\sin(\omega t)$ and $Q = q$, then by definition,

$$\frac{\partial(Q,P)}{\partial(q,p)} = \frac{\partial Q}{\partial q}\frac{\partial P}{\partial p} - \frac{\partial P}{\partial q}\frac{\partial Q}{\partial p} = 1.$$

The nature of this gauge invariance is totally equivalent to the case where a particle with a unit charge is moving under the influence of electromagnetic vector potential A and scalar potential V. We will come back and study extensively the Hamiltonian (2-3) which is our main focus in the next section and in Chapter three.

We may also consider a quantum kicked rotator from this model. If one assumes a discrete potential whose form takes a periodic delta function, the Hamiltonian in (2-1) becomes that of the quantum kicked rotator [3]. In this case there is no need for extra external field term (set $f = 0$). Then the corresponding classical version produces the well-known standard mapping equations [3].

$$H = \frac{p^2}{2ml^2} + mgl\,(1 - \cos q) \sum_{n=-\infty}^{\infty} \delta(t - nT), \tag{2-6}$$

where T is the kick period and the term, mgl, is the potential strength. We set $(mgl) = \eta$, and $I = ml^2$, then

$$H = \frac{p^2}{2I} + \eta\,(1 - \cos q) \sum_{n=-\infty}^{\infty} \delta(t - nT). \tag{2-7}$$

Classically, using equations (2-2), one can derive the mapping equations by expressing the time derivatives on the left-hand sides of equations (2-2) as first-order differences, that is,

$$\dot{q} = \frac{q(t + \Delta t) - q(t)}{\Delta t} \quad \text{and} \quad \dot{p} = \frac{p(t + \Delta t) - p(t)}{\Delta t}. \tag{2-8}$$

Discretizing q and p, we get a set of equations:

$$p_{n+1} = p_n - \left[\frac{\partial H}{\partial q}\right]_{q=q_n} \Delta t = p_n - \left[\frac{\partial V}{\partial q}\right]_{q=q_n} \Delta t,$$
$$q_{n+1} = q_n + p_n \Delta t, \qquad (2\text{-}9)$$

where dimensionless $p_{n+1} = p(t+\Delta t)$ and $q_{n+1} = q(t+\Delta t)$. This transformation is very close to an area-preserving transformation since the Jacobian of eq. (2-8),

$$\frac{\partial(q_{n+1}, p_{n+1})}{\partial(q_n, p_n)} = \begin{vmatrix} 1 & -\Delta t \dfrac{\partial^2 V}{\partial q_n^2} \\ \Delta t & 1 \end{vmatrix} = 1 + (\Delta t)^2 \frac{\partial^2 V}{\partial q_n^2} \approx 1, \qquad (2\text{-}10)$$

for small Δt. Then the mapping equation (2-9) becomes the standard mapping equations with the integration taken over one period T, from $t = nT$ to $t = (n+1)T$.

$$p_{n+1} = p_n - K \sin q_n ,$$
$$q_{n+1} = q_n + p_{n+1}. \qquad (2\text{-}11)$$

For $K = \eta T >> 1$ (see Ch. 5), delicately interwoven chaotic motions appear in phase-space which will be explained in the next section. It is also worth mentioning that the equation (2-11) is different in the sign of K than the usual standard mapping equations, also exhibiting chaos for $K >> 1$.

The Hamiltonian in (2-1) is also equivalent to the Hamiltonian for a superconducting Josephson junction if a damping term is ignored in the classical equation for superconducting phase φ. Consider a current-driven

shunted-Josephson-junction oscillator with microwave field and applied external dc current [4]. Then the superconducting phase φ is determined by the junction capacitance C, the resistance R, and the potential difference V across the junction.

$$C\frac{dV}{dt} + \frac{V}{R} + I_c \sin\varphi = I_{rf}\cos(\omega_d t) + I_{dc}, \tag{2-12}$$

$$\frac{d\varphi}{dt} = \frac{2e}{\hbar} V, \tag{2-13}$$

where I_c is the critical current and I_{rf} is the microwave field amplitude at the driving frequency ω_d. Combining (2-12) and (2-13), and expressing the result in terms of dimensionless variables, we get

$$\frac{d^2\varphi}{dt^2} + \beta\frac{d\varphi}{dt} + \Omega_o^2 \sin\varphi = \Gamma_1 \cos(RC\beta\omega_d t) + \Gamma_0. \tag{2-14}$$

In this equation, $\beta = \Omega_o/RC\omega_o$, $\omega_o = (2eI_c/\hbar C)^{1/2}$, $\Gamma_0 = (2\ e\Omega_o^2/\hbar C\ \omega_o^2)I_{dc}$ and $\Gamma_1 = (2e\Omega_o^2/\hbar C\ \omega_o^2)I_{rf}$. This equation is exactly the same as a forced-damped pendulum; for $\beta \approx 0$, the Hamiltonian (2-13) is approximately the same. In a later chapter, we shall investigate the case where $\beta \neq 0$. Classically, it is interesting that current and voltage characteristics of this junction show the strange phenomenon known as the 'devil's staircase' [5].

It is also obvious that the Hamiltonian (2-1) can be extended to a case where we represent an ionic molecule as a Morse oscillator driven by strong laser field simply by replacing the potential term, $mgl\ (1 - \cos\hat{q})$, with the Morse potential, $D\ [\ 1 - \exp(-ax)\ ]^2$, where D is the dissociation energy. For example, a possible Hamiltonian is

$$H = \frac{p^2}{2m} + D\,[\,1 - \exp(-ax)\,]^2 - d(x)f(t)\cos(\omega t), \qquad (2\text{-}15)$$

where $x = r - r_0$, r_0 is the equilibrium separation of nuclei, $d(x)$ is the molecular dipole moment function, $f(t)$ is the time-dependent pulse envelope. We will consider a couple of these models mentioned here in more details in Ch. 5.

2-2. Classical method of integration

A classical system with n-degrees of freedom can be described by a Hamiltonian H whose canonically conjugate variables are q_k and p_k, $k = 1, 2, \cdots, n$. Its motion obeys the principle of least action [6] which is reduced to a set of first-order differential equations in the form:

$$\frac{dq_k}{dt} = \frac{\partial H}{\partial p_k},$$
$$\frac{dp_k}{dt} = -\frac{\partial H}{\partial q_k}, \qquad (2\text{-}16)$$

where $H = H(q_1, q_2, \cdots, q_n, p_1, p_2, \cdots, p_n; t)$, where H, in this case, is called non-autonomous (time-dependent).

If these canonical Hamilton's equations of motion contain nonlinear terms that either couple their variables together or have higher order than quadratic in powers, chaotic motions often appear for some coupling strength. These chaotic motions are represented in a mathematical space, so-called phase-space, representing the conjugate variables as orthogonal coordinates. For example, a time-dependent system such as a particle moving in one

dimension forms a trajectory in a three-dimensional phase-space specified by its position q, momentum p, and time t. In most cases, the time coordinate is deleted to reduce a dimension of phase-space. Hence, phase-space becomes a two-dimensional plane in this case. In general, a set of solutions, $\{ q_k, p_k \}, k = 1, \cdots, n$, defines a trajectory in the $2n$-dimensional phase-space.

However, integrating a nonlinear differential equation analytically is usually not easy except for some special cases. It is practically impossible to solve it analytically for many cases. Therefore, in those situations, we must use a numerical integration method to determine system's behaviors in phase-space. The method that is used in this study to integrate classical equations of motion is a fourth-order Runge-Kutta algorithm [7].

The equations (2-a) and (2-b) (actually (1-2)) are integrated for q and dq/dt to find phase-space trajectories in the following way: let $\dot{x} = f(t, x)$, where x can be either q or p, then

$$x(t+h) = x(t) + \frac{1}{6}(F_1 + 2F_2 + 2F_3 + F_4), \tag{2-17}$$

where

$$\begin{cases} F_1 = h f(t, x) \\ F_2 = h f(t + \frac{1}{2}h, x + \frac{1}{2}F_1) \\ F_3 = h f(t + \frac{1}{2}h, x + \frac{1}{2}F_2) \\ F_4 = h f(t + h, x + F_3) \end{cases} \tag{2-18}$$

Here, h is the integration step size. This contains the error terms in the Taylor series up to and including the one involving h^4. A reduction of the order in a differential equation can be easily achieved before the application of this

method. In our case of the pendulum, we simply set $\dot{x} \equiv \ddot{q}$, for example. The numerical stability will be discussed in the following sections in more details.

2-3. Quantum mechanical method of integration

In the quantum case, the motion of the pendulum is governed by the time-dependent Schrödinger equation in dimensionless form: see Section 1-2. From (2-3), we have with the effective mass μ

$$i \frac{d\psi}{dt} = \hat{H}_{qm}\, \psi = [\frac{1}{2\mu} \{\hat{p} - \hat{\mathbf{A}}\}^2 + \hat{\mathbf{V}}]\psi, \tag{2-19}$$

where $\hat{\mathbf{A}} = -\mu\gamma \sin(\omega t)/\omega$, and $\hat{\mathbf{V}} = \mu\,(1 - \cos q)$. We have used and will use the notation ω, t instead of $\overline{\omega}, \overline{t}$ unless specified. Now the gauge invariant transformation, describing the corresponding classical system, yields

$$\begin{aligned} i \frac{d\psi'}{dt} &= \hat{H}'_{qm}\, \psi' = [\frac{1}{2\mu} \{\hat{p} - \hat{\mathbf{A}}'\}^2 + \hat{\mathbf{V}}']\psi', \\ &= -\frac{1}{2\mu}\frac{\partial^2}{\partial q^2}\psi' + \mu\,(1 - \cos q)\psi' - \mu\,\gamma q \cos(\omega t)\psi'. \end{aligned} \tag{2-20}$$

These equations are more difficult to analyze numerically than both the classical differential equations of motion (2-2) and the Hamiltonian (2-19). Here the usual dimensionless canonical momentum operator $p = -\,i\,\partial/\partial q$ is used with prescriptions $p = \hat{p}$, $q = \hat{q}$ with $\hat{\mathbf{A}}' = 0$, $\hat{\mathbf{V}}' = \mu\,(1 - \cos q) - \mu\,\gamma\,q \cos(\omega t)$, and $\hat{\chi} = \mu\gamma q \sin(\omega t)/\omega$. It is worth remembering that here $\mu = [Ml^2/\hbar]$, is the effective mass that we are controlling throughout the study.

Now we use (2-19) to solve ψ first, then we find the required solution ψ'. The Schrödinger equation (2-19) is formally solved to give

$$\psi(q, t) = \exp(- i \int_0^t \hat{H}_{qm}(t')\, dt')\, \psi(q, 0). \qquad (2\text{-}21)$$

Then the split operator algorithm [8,9] splits $\hat{H}_{qm}$ into $\hat{T}(p)$, $\hat{V}(q)$, and results in a discrete form with a time-ordering operator $\hat{\Theta}$ as

$$\psi(q,t+\Delta t) = \hat{\Theta} \exp [- i \int_t^{t+\Delta t} \hat{H}(t')\, dt']\, \psi(q,t),$$

$$= \hat{U}(p, q, t; t')\, \psi(q,t) + \vartheta\{(\Delta t)^3\}, \qquad (2\text{-}22)$$

where $\hat{U} = \exp\{ - i \int_t^{t+\Delta t} (\hat{T}/2)\, dt' \exp\{ - i \int_t^{t+\Delta t} (\hat{V})\, dt' \exp\{ - i \int_t^{t+\Delta t} (\hat{T}/2)\, dt'$

$$= \exp\{ - i \int_t^{t+\Delta t} [\frac{1}{4\mu}(p + \frac{\mu\gamma}{\omega}\sin\omega t')^2]\, dt'\} \exp\{ - i \int_t^{t+\Delta t} \mu(1-\cos q)\, dt'\}$$

$$\times \exp\{ - i \int_t^{t+\Delta t} [\frac{1}{4\mu}(p + \frac{\mu\gamma}{\omega}\sin\omega t')^2]\, dt'\}, \qquad (2\text{-}23)$$

$$= \exp\{ - i \int_t^{t+\Delta t} [\frac{\Pi^2}{4\mu}]\, dt'\} \exp\{ - i \int_t^{t+\Delta t} \hat{V}(q)\, dt'\} \exp\{ - i \int_t^{t+\Delta t} [\frac{\Pi^2}{4\mu}]\, dt'\},$$

$$= \hat{T}(p, t)\ \hat{Y}(q)\hat{T}(p, t) = \hat{T}_{eff}\ \hat{Y}_{eff}\ \hat{T}_{eff}.$$

The effect of applying the kinetic operator $\hat{T}$ is evaluated in terms of discrete Fourier transforms and the FFT algorithm [9], and the mechanical

(kinematical) momentum, $p+\mu\gamma\sin(\omega t)/\omega$ [10], where p is canonical momentum. After all the integrals are evaluated analytically for more accurate numerical results, the terms containing q and p in exponents are applied to the wave function in coordinate and momentum space respectively by forward and inverse FFT's. The normalization of the wave function is checked in Appendix 2.I.

The reason to use $\hat{H}_{qm}$ instead of $\hat{H}_{qm}'(=\hat{H}_{cl})$ is the following: if the usual Hamiltonian (2-1), $\hat{H}_{cl}$, is used instead in FFT's, Gibb's phenomena [11] at the boundaries of a grid will have a significant effect on a result unless we take very large coordinates (to be exact, infinitely large). Therefore, it was wise to use the gauge transformation to preserve periodic nature of the potential whose Fourier transformation only requires one full period of the periodic potential. This in turn allows one to shorten computer time considerably. Their final form after analytic integrations are

$$\hat{T} = \exp[-i\frac{p^2}{4\mu}\Delta t]$$
$$\times \exp\left[-i\frac{1}{2}\frac{p\gamma}{\omega}\left\{\sin(\omega t)\frac{\sin(\omega\Delta t)}{\omega} - \cos(\omega t)\left(\frac{\cos(\omega\Delta t)-1}{\omega}\right)\right\}\right]$$
$$\times \exp\left[-i\frac{1}{2}\frac{\mu\gamma^2}{2\omega^2}\left\{\frac{\Delta t}{2} - \sin(2\omega t)\frac{\cos(2\omega\Delta t)-1}{4\omega} - \cos(2\omega t)\frac{\sin(2\omega\Delta t)}{4\omega}\right\}\right], \quad (2\text{-}24)$$

$$\hat{Y} = \exp[-i\mu(1-\cos q)\Delta t]. \quad (2\text{-}25)$$

We immediately notice that the operator $\hat{T}$ has a part that does not depend on either p or q. Therefore, in actual computations, we use operators $\hat{T}_{eff}$ and $\hat{Y}_{eff}$ to save computation time since $\hat{T}$ operations must be done twice.

$$\hat{T}_{eff}(p) = \exp[-i\frac{p^2}{4\mu}\Delta t]$$
$$\times \exp\left[-i\frac{1}{2}\frac{p\gamma}{\omega}\left\{\sin(\omega t)\frac{\sin(\omega\Delta t)}{\omega} - \cos(\omega t)\left(\frac{\cos(\omega\Delta t)-1}{\omega}\right)\right\}\right], \quad (2\text{-}26)$$

$$\hat{Y}_{eff}(q) = \exp[-i\mu(1-\cos q)\Delta t]$$
$$\times \exp\left[-i\frac{\mu\gamma^2}{2\omega^2}\left\{\frac{\Delta t}{2} - \sin(2\omega t)\frac{\cos(2\omega\Delta t)-1}{4\omega} - \cos(2\omega t)\frac{\sin(2\omega\Delta t)}{4\omega}\right\}\right]. \quad (2\text{-}27)$$

It is also simple to see that the operator $\hat{U} = \exp(-i\int\hat{H}_{qm}\,dt')$ is unitary:

$$\hat{U}^{\dagger} = [\exp(-i\int\hat{H}_{qm}\,dt')]^{\dagger}$$

$$= \exp(i\int\hat{H}_{qm}{}^{\dagger}dt') = \exp(i\int\hat{H}_{qm}\,dt') = \hat{U}^{-1}, \quad (2\text{-}28)$$

since $\hat{H}_{qm}$ is Hermitian. The notation $\hat{U}^{\dagger}$ means the transpose of $\hat{U}^{*}$.

However, because of the gauge transformation, the required solution $\psi'(q, t)$, describing the same classical physics [12] and corresponding to $\hat{H}_{qm'}$, should be the following:

$$\psi'(q, t) = \exp[i\hat{\chi}(q, t)]\psi(q, t), \quad (2\text{-}29a)$$

$$= \exp[i\hat{\chi}(q, t)]\exp(-i\int\hat{H}_{qm}\,dt')\psi(q, 0),$$

$$= \exp[i\mu\gamma q\sin(\omega t)/\omega]\exp(-i\int\hat{H}_{qm}\,dt')\psi(q, 0). \quad (2\text{-}29b)$$

Then the expectation values of an observable $\hat{O}$ can be calculated.

$$< \hat{O} > = < \psi'(q,t) \mid \hat{O} \mid \psi'(q,t) >$$

$$= < \psi_o' \mid (\hat{U}^+)^n \hat{O} (\hat{U})^n \mid \psi_o' >, \qquad (2\text{-}30)$$

where $\psi'_o = \psi'(q,0) = \exp[i \hat{\chi} (q, 0)] \psi(q, 0) = \psi(q, 0)$, $t = n\Delta t$ and n is the number of integration steps. We are interested in canonical variables $< q(t) >$, $< p(t) >$ for expectation-value phase-space. For $< q(t) >$, we have

$$< q(t) > = < \psi'(q,t) \mid q \mid \psi'(q,t) >, \qquad (2\text{-}31a)$$

$$= < \psi(q,t) \mid \exp[-i \hat{\chi} (q,t)] q \exp[i \hat{\chi} (q,t)] \mid \psi(q,t) >,$$

$$= < \psi(q,t) \mid q \mid \psi(q,t) >, \qquad (2\text{-}31b)$$

since $[\hat{q}, \exp\{ -i \hat{\chi} (q,t)\}] = 0$; they commute. For $< p(t) >$, we have

$$< p(t) > = < \psi'(q,t) \mid p \mid \psi'(q,t) >, \qquad (2\text{-}32a)$$

$$= < \psi(q,t) \mid \exp[-i \hat{\chi} (q,t)] (- i \frac{\partial}{\partial q}) \exp[i \hat{\chi} (q,t)] \mid \psi(q,t) >,$$

$$= < \psi(q,t) \mid \exp[-i \hat{\chi} (q,t)] \exp[i \hat{\chi} (q,t)] \ (- i \frac{\partial}{\partial q}) \mid \psi(q,t) >$$
$$+ < \psi(q,t) \mid \exp[-i \hat{\chi} (q,t)] \exp[i \hat{\chi} (q,t)] \frac{\partial \hat{\chi}}{\partial q} \mid \psi(q,t) >,$$

$$= < \psi(q,t) \mid p \mid \psi(q,t) > + < \psi(q,t) \mid \frac{\partial \hat{\chi}}{\partial q} \mid \psi(q,t) >,$$

$$= < \psi(q, t) | p | \psi(q, t) > + \mu\gamma \sin(\omega t)/\omega. \qquad (2\text{-}32b)$$

From these expressions we readily notice that only the canonical momentum is manifestly gauge dependent in the sense that its expectation value depends on the particular gauge chosen while the kinematical momentum and the probability flux are gauge invariant.

Therefore, the required expectation values can be computed for a given initial wave function $\psi(q, 0)$. The following minimum uncertainty Gaussian wave packet is used as an initial wave function.

$$\psi(q,0) = \left(\frac{1}{\sqrt{\pi\sigma^2}}\right)^{1/2} \exp[-\frac{(q-q_o)^2}{2\sigma^2} + ip_o q\ ], \qquad (2\text{-}33)$$

where $< q\ (0)> = q_o$, $< p(0)> = p_o$ and σ is the Gaussian width. The final form of a solution is just (2-29a). It is of interest to note that the solutions corresponding to the classical simple harmonic motion can be analytically obtained using this initial function.

Computation of the power spectrum is also carried out using the FFT algorithm. A discrete time series $< q(t) >$ from (2-31) (or, $< p(t) >$ from (2-32)) is windowed by a Hanning window function [8]. Then the power spectral density $P(\omega_k)$ with frequency ω_k becomes

$$\begin{aligned} P(\omega_k) &= |q\ (\omega_k)\ |^2\ , \\ &= \left| \int_{-\infty}^{+\infty} \exp(i\omega_k t\ )\ <q(t)>\ W(t)\ dt \right|^2 , \end{aligned} \qquad (2\text{-}34)$$

where a Hanning window function $W(t)$ is

$$W(t) = \begin{cases} 1 - \cos\left(\frac{2\pi t}{\tau}\right), & 0 \le t \le \tau \\ 0, & t > \tau \end{cases} \quad . \qquad (2\text{-}35)$$

The total propagation time (evolution time) is τ. This window is designed to adjust the discontinuity of a series at τ. One may design another form of the window to exhibit rather distinct peaks. Here the same results are expected if the correlation $< C(t) >$ is Fourier analyzed, where

$$< C(t) > = \; < q(0) \mid q(t) > . \qquad (2\text{-}36)$$

Finally, we are also interested in computing the uncertainty product $V(t) = \{ <(p - < p >)^2> <(q - < q >)^2> \}^{1/2}$ to determine how expectation-values in phase-space are shadowed by uncertainty. Similar to (2-31), (2-32), we would get the following expressions:

$$(\Delta q)^2 = <(q - < q >)^2 > = < q^2 > - < q >^2 ,$$

$$= < \psi'(q,t) \mid q^2 \mid \psi'(q,t) > - < \psi'(q,t) \mid q \mid \psi'(q,t) >^2 ,$$

$$= < \psi(q,t) \mid q^2 \mid \psi(q,t) > - < \psi(q,t) \mid q \mid \psi(q,t) >^2 . \qquad (2\text{-}37)$$

Because of the same reason we have Eq. (2-31), and using Eq. (2-32),

$$(\Delta p)^2 = <(p - < p >)^2 > = < p^2 > - < p >^2 ,$$

$$= < \psi'(q,t) \mid p^2 \mid \psi'(q,t) > - < \psi'(q,t) \mid p \mid \psi'(q,t) >^2 ,$$

$$= < \psi(q,t) | \exp[-i\hat{\chi}(q,t)] (-\frac{\partial^2}{\partial q^2}) \exp[i\hat{\chi}(q,t)] | \psi(q,t) >$$

$$- [< \psi(q,t) | \exp[-i\hat{\chi}(q,t)] (-i\frac{\partial}{\partial q}) \exp[i\hat{\chi}(q,t)] | \psi(q,t) >]^2,$$

$$= - < \psi(q,t) | \exp[-i\hat{\chi}(q,t)] \{ \exp[i\hat{\chi}(q,t)] (i\frac{\partial\hat{\chi}}{\partial q}) (\frac{\partial}{\partial q}) | \psi(q,t) >$$

$$+ \exp[i\hat{\chi}(q,t)] (\frac{\partial^2}{\partial q^2}) | \psi(q,t) > + \exp[i\hat{\chi}(q,t)] (i\frac{\partial\hat{\chi}}{\partial q})^2 | \psi(q,t) >$$

$$+ \exp[i\hat{\chi}(q,t)] (i\frac{\partial^2\hat{\chi}}{\partial q^2}) | \psi(q,t) > + \exp[i\hat{\chi}(q,t)] (i\frac{\partial\hat{\chi}}{\partial q}) (\frac{\partial}{\partial q}) | \psi(q,t) > \}$$

$$- [< \psi(q,t) | p | \psi(q,t) > + \mu\gamma \sin(\omega t)/\omega]^2,$$

$$= 2(\mu\gamma \sin(\omega t)/\omega) < \psi(q,t) | p | \psi(q,t) > + < \psi(q,t) | p^2 | \psi(q,t) >$$

$$+ [\mu\gamma \sin(\omega t)/\omega]^2 - [< \psi(q,t) | p | \psi(q,t) >]^2$$

$$- 2(\mu\gamma \sin(\omega t)/\omega) < \psi(q,t) | p | \psi(q,t) > - [\mu\gamma \sin(\omega t)/\omega]^2,$$

$$= < \psi(q,t) | p^2 | \psi(q,t) > - [< \psi(q,t) | p | \psi(q,t) >]^2 \qquad (2\text{-}38)$$

Thus, we finally get

$$V(t) = \{ <(p - < p >)^2> <(q - < q >)^2> \}^{1/2},$$

$$= \{ < \psi(q,t) | q^2 | \psi(q,t) > - < \psi(q,t) | q | \psi(q,t) >^2 \}^{1/2},$$

$$\times \{ < \psi(q,t) | p^2 | \psi(q,t) > - [< \psi(q,t) | p | \psi(q,t) >]^2 \}^{1/2}. \qquad (2\text{-}39a)$$

Note that the uncertainties (2-37) and (2-38) are gauge invariant as required. In general, because the wave function is not known at any arbitrary time, $V(t)$ cannot be determined analytically. For a simple harmonic oscillator with the

initial wave function of the form (2-33), however, we would get a steady solution with a minimum value of 0.5 if $\gamma = 0$. But numerically, we calculate $U(t)$ where

$$U(t) = \{ <(\dot{q} - <\dot{q}>)^2> <(q - <q>)^2> \}^{1/2}. \qquad (2\text{-}39b)$$

This uncertainty volume is more useful since we will plot trajectories in phase-space which has the angular velocity axis rather than the momentum axis. We can directly compare this uncertainty with the trajectory. One can always go back to calculate the original uncertainty product $V(t)$ using the relation $V(t) = \mu U(t)$ and $\dot{q} = [p - A(t)] / \mu$.

It is also of our interest to determine eigen-values and eigen-states. Eigen-values are easily calculated by forming a correlation between the initial wave function $\sim \sum_n^{\infty} A_n u_n(q)$ and the final wave function $\sim \sum_n^{\infty} A_n u_n(q) \exp(-iE_n t)$. The correlation is

$$C_\psi(t) = < \psi(q, 0) \mid \psi(q, t) >,$$

$$= \sum_n^{\infty} |A_n|^2 \exp(-iE_n t). \qquad (2\text{-}40)$$

This correlation function is then Fourier transformed to formulate a delta function. Its final form takes

$$\tilde{C}_\psi(\lambda) = \int C_\psi(t) \exp(i\lambda t)\, dt = \sum_n^{\infty} |A_n|^2 \delta(\lambda - E_n). \qquad (2\text{-}41)$$

As a result, we get spectral peaks located at E_n with an amplitude of $|A_n|^2$.

To project out a single eigen-state with an eigen-value λ_k, we take the following integral.

$$\int \psi(q,t)\exp(i\lambda_k t)\,dt = \sum_n^{\infty} A_n u_n(q) \int \exp(i[\lambda_k - E_n]t) \qquad (2\text{-}42)$$

Consequently, we get the desired eigen-state because of the delta function property. In actual computation, however, we use the method of fitting a line shape function similar to the Hanning window function. The method is described well in the references [13].

Before we use the basic numerical tools we have developed here, let us first focus on the problem of taking semi-classical limit. It is very important to note that the canonical momentum, $p - A$, in this quantum scheme should be divided by μ to get dq/dt, which is offered by the classical integration scheme. Otherwise, quantum and classical trajectories will have a scale difference in p -axis (or dq/dt -axis) in phase-space.

2-4. Method of controlling semi-classical limit

It can be shown that in the limit $\hbar \to 0$, quantum mechanics resembles classical mechanics. To see it in one way, first write the wave function in standard polar form

$$\psi(q,t) = R(q,t)\exp[\,i\,S(q,t)/\hbar], \qquad (2\text{-}43)$$

where R and S are real. Substitute this into Schrödinger equation. Then one finds

$$-\frac{\hbar^2}{2m}\frac{1}{R}\frac{\partial^2 R}{\partial q^2}+\frac{1}{2m}\left(\frac{\partial S}{\partial q}\right)^2+V=-\frac{\partial S}{\partial t}, \tag{2-44a}$$

$$-\frac{1}{2m}\left[R\frac{\partial^2 S}{\partial q^2}+2\frac{\partial R}{\partial q}\frac{\partial S}{\partial q}\right]=\frac{\partial R}{\partial t}. \tag{2-44b}$$

In the limit $\hbar \to 0$, These equations become

$$\frac{1}{2m}\left(\frac{\partial S}{\partial q}\right)^2+V=-\frac{\partial S}{\partial t}, \tag{2-45a}$$

$$\frac{\partial \rho}{\partial t}+\frac{\partial}{\partial q}\cdot[\rho v]=0. \tag{2-45b}$$

The (2-45.a) is a classical Hamilton-Jacobi equation whose solution is S . Then the form of a continuity equation (2-45.b) where the velocity $v=\frac{1}{m}\frac{\partial S}{\partial q}$, and $\rho = R^2$ describes conservation of probability. Therefore the limit $\hbar \to 0$ can be taken alone as a semi-classical approximation in many cases of which there is no gravity involved. It really means, however, that the ratio of $\hbar$ to some classical characteristic action of the system with the same dimension approaches zero [14]. This limit is also discussed in both quantum and classical perturbation theories [15]. The term,

$$-\frac{\hbar^2}{2m}\frac{1}{R}\frac{\partial^2 R}{\partial q^2}, \tag{2-46}$$

is D. Bohm's quantum mechanical potential [16].

In our case, however, we must consider the effective mass, $ml\sqrt{gl}/\hbar$ as a semi-classical approximation. This is so because of the reason we discussed

in Section 1-2. It is obvious that the gravitational field strength g and Planck's constant $\hbar$ are fixed numbers, so what we really have to consider is the quantity $(ml\sqrt{l})$ where m is not the effective mass, but the mass of the pendulum. To see this more clearly, we first consider the classical equation of motion in general in the absence of air resistance:

$$m\dot{q}^{\cdot} = -\, m\, \nabla_q \Phi_{grav}\,, \tag{2-47}$$

so that we get $\ddot{q} - \nabla_q \Phi_{grav} = 0$ because the mass term cancels as we mentioned briefly in Section 2-1. We, of course, assume that the gravitational and the inertial mass are equal (principle of equivalence). We can see this point also using the Hamilton's classical approach, based on

$$\delta \int_{t_1}^{t_2} dt \left(\frac{m}{2} \dot{q}^2 - m\, \nabla_q \Phi_{grav} \right) = 0\,, \tag{2-48}$$

where m clearly drops out again.

In the quantum mechanical formulation, however, the equation analogous to (2-44) is

$$\left[-\frac{\hbar^2}{2m} \nabla_q^2 + m\, \Phi_{grav} \right] \psi = i\hbar \frac{\partial \psi}{\partial t}\,. \tag{2-49}$$

The mass term does not drop out: it appears in the form of a ratio $(\hbar/m)$. Analogous to the classical Hamilton's approach, we try the Feymann path-integral formulation of this case.

$$< \psi(q, t+\Delta t) \mid \psi(q, t) >$$

$$= \sqrt{\frac{m}{2\pi i \Delta t \hbar}} \exp\left[i \int_t^{t+\Delta t} dt' \frac{m}{\hbar} (\dot{q}^2 - \nabla_q \Phi_{grav}) \right], \Delta t \to 0. \qquad (2\text{-}50)$$

In this case, the combination $(\hbar/m)$ also appears. This is a clear distinction from the classical approach [17]. In our case, this combination appears in the effective mass implicitly.

To support our idea of semi-classical approximation more, we may carry out the argument physically in the following way. Consider a double-slit experiment which shows a pure quantum effect with the separation of two slits d, de Broglie wave length λ. Then the equation for successive interference pattern becomes $n\lambda = d \sin\theta_n$ where $\lambda = 2\pi \hbar/mv$ and θ_n is the angle between the n th and $(n\text{-}1)$ th maxima. Therefore $2\pi \hbar/m = (vd/n)\sin\theta_n$, where m is the mass of the particles (we shall not consider a photon case here) passing through the slits with the velocity v.

Now, in classical limit the successive interference pattern of quantum phenomenon disappears such that $\theta_n \approx \theta_{n-1} \approx \cdots\cdots \approx \theta_1 \approx 0$. In other words the ratio $\hbar/m$ is required to be small in semi-classical limit [18]. In practical computation, there is no difference as to whether letting $\hbar$ decrease or m increase. What it matters is the combination, $\hbar/m$, implicitly contained in μ. In physical sense it is more appropriate to adjust m than $\hbar$.

The same argument can also be applied by EBK quantization rule [19]. The rule gives rise to the approximate integer number n of bound states.

$$\int_{\text{closed}} p\, dq = (n + \tfrac{1}{2})\hbar, \; p = \sqrt{2m\,[E_{max} - V(q)]}, \qquad (2\text{-}51)$$

where E_{max} is the maximum available bound state energy (see Appendix 2.II).

Therefore as the mass is increased, the number of bound states will be increased accordingly. This corresponds to higher energy states contributing to a total system, which makes the system more classical. So in either case, μ is an appropriate factor to be adjusted in corresponding limits. Thus, EBK quantization also requires $\hbar/m$ to be a small constant in the semi-classical limit for larger n. In fact, quantum mechanical commutator in gravity $[\,\hat{\mathbf{A}},\,\hat{\mathbf{B}}\,]$ becomes classical Poisson bracket $\{A,\,B\}$ in the limit $\hbar/m \rightarrow 0$ if $A=q$ and $B=dq/dt$.

In practical computations, it is easier to think of $\mu = m$ numerically by assuming $g = l = \hbar = 1$ such that $\gamma = f$ and $\omega_o = 1$ without considering the physics of units [20] since the computer (machine) will not recognize the difference. This method is always numerically valid whenever we solve dimensionless equations. To get a feeling for a possible physical situation, one can always go back to the kind of calculations we have done in Section 1-2. As a consequence, the parameter to control semi-classical approximation is just reduced to effective mass only.

2-5. Computational stability consideration

In this case, the numerical error comes from the commutator since the splitting of a Hamiltonian is based on the commutation of operators. To see more clearly, we expand the following two unitary operators in Taylor series;

$$\hat{U}_a(t\,;t') = \exp\left[-i\int_{t-\Delta t}^{t}\hat{H}(t')\,dt'\right] = \exp\left[-i\,\mathbf{H}\,\Delta t\,\right],$$

$$\hat{U}_b(t;t') = \exp\left[-\frac{i}{2}\int_{t-\Delta t}^{t}\hat{T}(t')\,dt'\right]\times\exp\left[-i\int_{t-\Delta t}^{t}\hat{V}(t')\,dt'\right]$$
$$\times\exp\left[-\frac{i}{2}\int_{t-\Delta t}^{t}\hat{T}(t')\,dt'\right],$$

$$= \exp\left[-i\frac{\mathbf{T}}{2}\Delta t\right]\exp\left[-i\,\mathbf{V}\,\Delta t\right]\exp\left[-i\frac{\mathbf{T}}{2}\Delta t\right]. \qquad (2\text{-}52)$$

Then we get

$$\hat{U}_a(t;t') = 1 - i\,(\Delta t)(\mathbf{T}+\mathbf{V}) - \frac{(\Delta t)^2}{2}(\mathbf{T}^2+\mathbf{V}^2+\mathbf{TV}+\mathbf{VT})$$
$$+ i\,\frac{(\Delta t)^3}{6}(\mathbf{T}^3+\mathbf{V}^3+\mathbf{T}^2\mathbf{V}+\mathbf{V}^2\mathbf{T}+\mathbf{T}\mathbf{V}^2+\mathbf{V}\mathbf{T}^2+\mathbf{TVT}+\mathbf{VTV})+\cdots,$$

$$\hat{U}_b(t;t') = 1 - i\,(\Delta t)(\mathbf{T}+\mathbf{V}) - \frac{(\Delta t)^2}{2}(\mathbf{T}^2+\mathbf{V}^2+\mathbf{TV}+\mathbf{VT})$$
$$+ i\,\frac{(\Delta t)^3}{6}(\mathbf{T}^3+\mathbf{V}^3+\frac{3}{4}\mathbf{T}^2\mathbf{V}+\frac{3}{4}\mathbf{V}^2\mathbf{T}+\frac{3}{2}\mathbf{TVT}+\cdots)+\cdots.$$

Therefore, the difference between the two is the error term ϑ, where

$$\vartheta = \frac{(\Delta t)^3}{6}\{[\mathbf{T}^2,\mathbf{V}],[\mathbf{V}^2,\mathbf{T}]\}. \qquad (2\text{-}53)$$

The computational stability due to this error is described in the reference [21] for several different numerical models. This reference shows that the split operator method is very stable, and reliable for small enough integration steps, which can be optimized.

Appendix 2.I Normalization

Normalization property can be checked using a Taylor series expansion of the wave function in terms of the Hamiltonian of a system.

$$< \psi(t+\Delta t) \mid \psi(t+\Delta t) >$$

$$= \left[< \psi(t) \mid + \frac{i\Delta t}{\hbar} < \psi(t) \mid \hat{H} + \frac{(\Delta t)^2}{2\hbar} \left\{ i < \psi(t) \mid \frac{d\hat{H}}{dt} - \frac{1}{\hbar} < \psi(t) \mid \hat{H}^2 \right\} + \cdots \right]$$

$$\times \left[\mid \psi(t) > - \frac{i\Delta t}{\hbar} \hat{H} \mid \psi(t) > - \frac{(\Delta t)^2}{2\hbar} \left\{ i \frac{d\hat{H}}{dt} \mid \psi(t) > + \frac{1}{\hbar} \hat{H}^2 \mid \psi(t) > \right\} + \cdots \right],$$

$$=$$

$$\begin{aligned}
&< \psi(t) \mid \psi(t) > - \frac{i\Delta t}{\hbar} < \psi(t) \mid \hat{H} \mid \psi(t) > - \frac{i\,(\Delta t)^2}{2\hbar} < \psi(t) \mid \frac{d\hat{H}}{dt} \mid \psi(t) > \\
&\quad - \frac{(\Delta t)^2}{2\hbar^2} < \psi(t) \mid \hat{H}^2 \mid \psi(t) > + \frac{i\Delta t}{\hbar} < \psi(t) \mid \hat{H} \mid \psi(t) > \\
&\quad + \frac{(\Delta t)^2}{\hbar^2} < \psi(t) \mid \hat{H}^2 \mid \psi(t) > + \frac{(\Delta t)^3}{2\hbar^2} < \psi(t) \mid \hat{H} \frac{d\hat{H}}{dt} \mid \psi(t) > \\
&\quad + \frac{i\,(\Delta t)^3}{2\hbar^3} < \psi(t) \mid \hat{H}^3 \mid \psi(t) > + \frac{i\,(\Delta t)^2}{2\hbar} < \psi(t) \mid \frac{d\hat{H}}{dt} \mid \psi(t) > \\
&\quad - \frac{(\Delta t)^2}{2\hbar^2} < \psi(t) \mid \hat{H}^2 \mid \psi(t) > + \frac{(\Delta t)^3}{2\hbar^2} < \psi(t) \mid \frac{d\hat{H}}{dt} \hat{H} \mid \psi(t) > \\
&\quad - \frac{i\,(\Delta t)^3}{2\hbar^3} < \psi(t) \mid \hat{H}^3 \mid \psi(t) > + \cdots,
\end{aligned}$$

$$= < \psi(t) \mid \psi(t) > + \frac{(\Delta t)^3}{2\hbar^2} < \psi(t) \mid \hat{H} \frac{d\hat{H}}{dt} + \frac{d\hat{H}}{dt} \hat{H} \mid \psi(t) > + \cdots,$$

$$= \langle \psi(t) \mid \psi(t) \rangle + \vartheta\left[\frac{(\Delta t)^3}{2\hbar^2}\left\{ \widehat{H}, \frac{d\widehat{H}}{dt} \right\}\right], \qquad \text{(A2I-1)}$$

where $\{\widehat{A}, \widehat{B}\} = \widehat{A}\widehat{B} + \widehat{B}\widehat{A}$. For simplicity, we show only the time variable explicitly. Now for a time-independent Hamiltonian, $\frac{d\widehat{H}}{dt} = \frac{\partial \widehat{H}}{\partial t} + \left[\widehat{H}, \widehat{H}\right] = 0$; so the wave functions are normalized at all times. But for the time-dependent Hamiltonian of our pendulum, we have

$$\frac{d\widehat{H}_{qm}}{dt} = \frac{\partial \widehat{H}_{qm}}{\partial t} = p\,\gamma\cos(\omega t) + f(t),$$

where $f(t)$ is a function of time only and commutes with $\widehat{H}_{qm}$. Therefore, the commutator bracket would be left with $\{\cos q, p\}$. So for a small Δt, normalization can be satisfied. In this analysis, we have ignored the error due to Eq. (2-53).

Appendix 2.II Quantization of a pendulum

To find the number of bound states in a pendulum-like potential, we use the Wilson-Bohr-Sommerfeld semiclassical quantization rule [22].

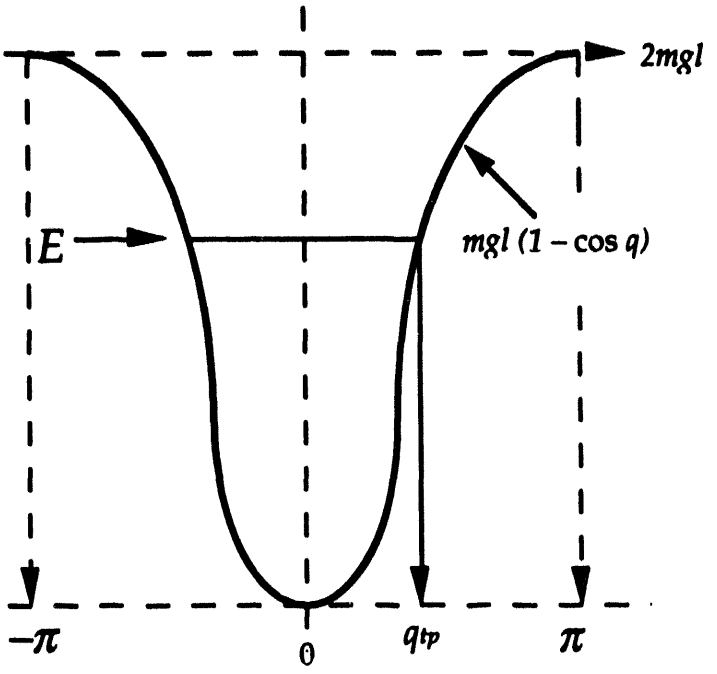

This diagram assumes a periodic potential well with $V = V_0 (1 - \cos q)$, and $E = V_0 (1 - \cos q_{tp})$. The point q_{tp} represents the turning point where a particle with energy E bounces at the potential wall in a classical sense. Then the rule requires that a closed integral, I, of momentum equals to $2\pi n\hbar$, n is integer.

$$\mathrm{I} = 4\int_0^{q_{tp}} \sqrt{2ml^2(E - V)}\, dq \,,$$

$$= 4\int_0^{q_{tp}} \sqrt{2ml^2E\,(1 - \frac{V}{E})}\, dq \,,$$

$$= 4\sqrt{2m\,l^2E}\int_0^{q_{tp}} \sqrt{[1-\frac{V_o(1-\cos q)}{V_o(1-\cos q_{tp})}]}\,dq\,,$$

$$= 4\sqrt{2m\,l^2E}\int_0^1 \sqrt{\frac{1-y}{2ay-y^2}}\,dy\,. \qquad \text{(A2II-1)}$$

Here we let $y = a\,(1-\cos q)$, where $a = (1-\cos q_{tp})^{-1}$, then $dy = a\,\sin q\,dq = \sqrt{2ay-y^2}\,dq$, where $0 < q < \pi$, since

$$\begin{aligned}(a\sin q)^2 &= a^2(1-\cos^2 q) + 2a^2\cos q - 2a^2\cos q \\ &= [a(1-\cos q)]^2 + 2a^2\cos q\,(1-\cos q) \\ &= a(1-\cos q)[\,a(1-\cos q) + 2a\cos q\,] \\ &= a(1-\cos q)[\,-a(1-\cos q) + 2a\,] \\ &= 2ay - y^2.\end{aligned}$$

Then,

$$\begin{aligned}\mathrm{I} &= 4\sqrt{2m\,l^2E}\int_0^1 \sqrt{\frac{1-y}{(2a-y)(y-0)}}\,dy\,, \\ &= 2\sqrt{2a}\;G(\nu,\kappa) - \frac{2(2a-1)}{\sqrt{2a}}F(\nu,\kappa),\end{aligned} \qquad \text{(A2II-2)}$$

where the functions F and G are elliptic integrals of the first and second kinds, respectively [23]. Since $\nu = \mathrm{Arcsin}(1) = \frac{\pi}{2}$, $0 \le q \le \pi$, and $\kappa = \sqrt{\frac{1}{2a}}$, they form complete elliptic integrals whose series representations are given by

$$G\left(\frac{\pi}{2},\kappa\right) = \frac{\pi}{2}\left\{1 - \frac{1}{2^2}\kappa^2 - \frac{1^2\cdot 3}{2^2\cdot 4^2}\kappa^4 - \cdots - \left[\frac{(2n-1)!!}{2^n\cdot n!}\right]^2\frac{\kappa^{2n}}{2n-1} - \cdots\right\},$$

$$F\left(\frac{\pi}{2}, \kappa\right) = \frac{\pi}{2}\left\{1 + \frac{1}{2^2}\kappa^2 + \frac{1^2 \cdot 3^2}{2^2 \cdot 4^2}\kappa^4 + \cdots + \left[\frac{(2n-1)!!}{2^n \cdot n!}\right]^2 \kappa^{2n} + \cdots\right\}.$$

Now, for angles less than $\pi/2$, $1 < 2a < \infty$ since $a = (1 - \cos q_{tp})^{-1}$;

so for κ, $0 < (1/2a)^{1/2} < 1$. Then the functions G and F can be approximated.

$$G\left(\frac{\pi}{2}, \kappa\right) \approx \frac{\pi}{2}\left\{1 - \frac{1}{2^2}\kappa^2\right\}, \text{ and } F\left(\frac{\pi}{2}, \kappa\right) \approx \frac{\pi}{2}\left\{1 + \frac{1}{2^2}\kappa^2\right\}.$$

Thus, we finally get

$$\begin{aligned} \mathrm{I} &= 4\sqrt{2m\,l^2E}\left[\sqrt{2a}\,\pi\left\{1 - \frac{1}{8a}\right\} - \frac{2a-1}{\sqrt{2a}}\,\pi\left\{1 + \frac{1}{8a}\right\}\right], \\ &= 4\sqrt{2m\,l^2E}\left[\frac{1+4a}{8a\sqrt{2a}}\,\pi\right]. \end{aligned} \qquad \text{(A2II-3)}$$

Now $4a >> 1$, for $0 < q_{tp} << \pi/2$, and $a = V_o/E$, so we get

$$\mathrm{I}^2 \approx \frac{4\,\pi^2 m\,l^2E^2}{V_o} = [2\pi\, n\,\hbar]^2.$$

Solve first for E. One finds the quantized energy levels for small angles with $V_o = mgl$,

$$E\,(n) = E_n \approx n\,\hbar\sqrt{\frac{g}{l}}. \qquad \text{(A2II-4)}$$

Now by substituting the classical-like energy $E = mgl\,(1 - \cos q_{tp})$, $n \approx \left(\frac{m}{\hbar}\right) l\sqrt{g\,l}\,(1 - \cos q_{tp})$. But since we have assumed $q_{tp} < \pi/2$, the actual total number of energy levels becomes

$$n > 2 \times \left(\frac{m}{\hbar}\right) l\sqrt{g\,l}\,q_{tp}^2 >> \mu\, q_{tp}^2. \qquad \text{(A2II-5)}$$

The inequality is due to the fact that the energy level spacing becomes narrower as the energy of a particle becomes closer to the top of a potential well.

It is interesting to see that the energy level spacing ΔE agrees with that of Section 1-2 from the unit analysis in Schrödinger equation. Moreover, the quantity $\left[\frac{m}{\hbar}\right] l\sqrt{g\,l}$, we called the effective mass, is directly related to the number of energy levels as we have also seen from both Sections 1-2 and 2-4.

For real physical situations, one can estimate numbers for the parameters. Substituting the values of fundamental constants, we find the effective mass $\mu \sim 3 \times 10^{34}\, ml^{3/2}$. So for 1 kg objects swinging at the end of 1 meter string for small angles, the number of energy levels approximately becomes $\sim 10^{34}$. For a proton at a distance of 1 Å, there hardly exists any quantized energy level. For a particle a hundred times heavier than a proton at the same distance, there are probably more than 100 quantized levels. Here are some examples of number of energy levels in the H-atom case;

i) for $\mu = 1, l = 7.4 \times 10^{-6}$ meters, then $\Delta E = 1.2 \times 10^{-31}$ J. But the potential energy $\sim mgl \approx 1.661 \times 10^{-27}$ kg $\times$ 9.8 (m/sec^2) $\times$ 7.4×10^{-6} meter $= 1.2 \times 10^{31}$ J. So the depth of the well 2μ provides ~ only a few quantized energy levels in crude approximation.

ii) for $\mu = 10, l = 3.5 \times 10^{-5}$ meters, then $\Delta E = 5.6 \times 10^{-32}$ J. But the potential energy $\sim mgl \approx 5.7 \times 10^{-31}$ J. So in this case there are about in the order of ten energy levels.

iii) for $\mu = 100$, $l = 1.6 \times 10^{-4}$ meters, then $\Delta E = 2.6 \times 10^{-32}$ J. But the potential energy ~ $mgl \approx 2.6 \times 10^{-30}$ J. So in this case there are more than a hundred energy levels.

It is obvious from here that the approximate number of energy levels linearly increases with the value of μ, and that this value corresponds to those one might get directly from (A2II-5). This is what exactly we should expect since the gravitational effect becomes negligibly smaller in a more microscopic system. It is also interesting to note again that the effective mass is the only parameter to control semi-classical limit.

References

[1] E. G. Gwinn, R. M. Westervelt, Phys. Rev. Lett. **54**, 1613 (1985); E. G. Gwinn, R. M. Westervelt, Phys. Rev. A. **33**, 4143 (1986); D. D'Humieres, M. R. Beasley, B. A. Hubermann, A. Libchaber, Phys. Rev. A. **26**, 3483 (1982); J. B. McLaughlin, J. Stat. Phys. **24**, 375 (1981).

[2] This requires a little bit of explanation. In principle, they swing differently, but it is impossible to distinguish or detect the difference practically because of a negligible quantum gravity effect as we have seen in Section 1-2 and Appendix 2.II. It is too weak to be observable in present time.

[3] G. Casati, J. Ford, I. Guarneri, F. Vivaldi, Phys. Rev. A. **34**, 1413 (1986); see also for classical mapping equations corresponding to ours, B. V. Chirikov, Phys. Rep. **52**, 263 (1979); see also *Quantum Chaos* edited by H. A. Cerdeira, R. Ramasmeny, M. C. Gutzwiller, G. Casati (World Scientific, Singapore, 1991).

[4] W. C. Stewart, Appl. Phys, Lett. 12, 277 (1968); E. E. McCumber, J. Appl. Phys. 39, 3113 (1968).

[5] V. N. Belykh, N. F. Pedersen, O. H. Soerensen, Phys. Rev. B. **16**, 4853 (1977); see also P. Bak, Physics Today, 39 (Dec. 1986).

[6] For a review, see H. Goldstein, *Classical Mechanics* (2nd Ed. Addison-Wesley, Reading, Ma, 1980); see also J. B. Marion, *Classical Dynamics of Particles and Systems* (2nd Ed., Academic Press, Orlando, Fl, 1970).

[7] S. S. Kuo, *Computer Applications of Numerical Method* (Addison-Wesley, N. Y. 1972); R. W. Hornbeck, *Numerical Method* (Prentice-Hall, N. J. 1975); D. Kincaid, W. Cheney, *Numerical Analysis* (Brooks 'Cole Pub. Co.,Pacific Grove, CA. 1991).

[8] M. D. Feit, J. A. Fleck. Jr., J. Chem. Phys. **80**, 2578 (1984).

[9] M. D. Feit, J. A. Fleck. Jr., A. Steiger, J. Comput. Phys. **47**, 412 (1982); J. N. Bardsley, A. Szöke, and J. M. Comella, J. Phys. B. **21**, 3899 (1988); C. Leforestier,R. H. Bisseling, C. Cerjan, M. D. Feit, R. Friesner, A. Guldberg, A. Hammerich, G. Jolicard, W. Karrlein, H.-D. Meyer, N. Lipkin, O. Roncero, R. Kosloff, J. Comp. Phys. **94**, 59 (1991).

[10] See *The Feynman Lectures on Physics*, Vol III (Addison-Wesley, Reading, Ma. 1964); see also J. J. Sakurai, *Modern Quantum Mechanics* (Benjamin Cummings, Menlo Park, CA, 1985).

[11] F. J. Harris, Proceedings of IEEE, **66**, 51 (1978).

[12] I. J. R. Aitchison, A. J. G. Hey, *Gauge Theories in Particle Physics* (2nd Ed., Adam Hilger, Bristol, England, 1989).

[13] M. D. Feit, J. A. Fleck, Jr., Appl. Opt. **19**, 1154 (1980); **20**, 848 (1981); **20**, 2843 (1981); see also J. H. Povlsen, P. Davidsen, G. Jacobsen, J. Opt. Soc. Am. **72**, 1506 (1982).

[14] In this case, the action term is $\int_{\text{closed}} \left(\frac{\partial S}{\partial q}\right) dq$. see also M. V. Berry, *Dynamical Chaos* (Princeton Univ. Press, Princeton, N. J. 1987), p 194.

[15] J. H. Jensen, Phys. Rev. A. **45**, 2686 (1992).

[16] D. Bohm, Phys. Rev. **85**, 166 (1952); **85**, 180 (1952); Nature, **315**, 294 (1985).

[17] I follow here J. J. Sakurai's argument. See his quantum text book, *Modern Quantum Mechanics* (Benjamin Cummings, Menlo Park, CA, 1985).

[18] For a comprehensive argument about taking a classical limit, see for example, D. H. Freedman, Science, 253, 626 (1991)

[19] D. W. Noid, M. L. Koszykowski, R. A. Marcus, Annu. Rev. Phys. Chem. **32**, 267 (1981); W. P. Reinhardt, *Chaotic Behaviors in Quantum Systems: Theory and Applications*, edited by G. Casati (Plenum, N. Y. 1985), p 235; see also M. Tabor, *Chaos and Integrability in Nonlinear Dynamics* (John Wiley & Sons, N. Y. 1989), p 236.

[20] See Section 1-2 for possible physical situations.

[21] C. Leforestier, R. H. Bisseling, C. Cerjan, M. D. Feit, R. Friesner, A. Guldberg, A. Hammerich, G. Jolicard, W. Karrlein, H.-D. Meyer, N. Lipkin, O. Roncero, R. Kosloff, J. Comp. Phys. **94**, 59 (1991); see also M. Thachuk, G. C. Schatz, J. Chem. Phys. **97**, 7297 (1992).

[22] EBK quantization contains the zero point energy, but in this analogy the zero point energy is not important.

[23] See page 232 (3.14)-8 in I. S. Gradshteyn, I. M. Ryzhik, *Table of Integrals, Series, and Products* (Academic Press, Orlando, FL. 1980): the equations 8.112(1), (2), 8.113 (1), and 8.114 (1) are also required for the series.

CHAPTER 3

NON-DISSIPATIVE SYSTEMS

A violent order is disorder; and
A great disorder is order. These two things are one.

W. Stevense's "Connoisseur of chaos" (1942)

Phase-space behaviors are extensively studied in this chapter using both a single system and a distribution of systems. A possible general description of a break time is introduced. The results indicate the correspondence does not hold in classically chaotic regime.

3-1. Classical and quantum Lyapunov exponents

3-1-1. Classical Lyapunov exponent

Classical Lyapunov exponents specify the exponential growth of the two initially nearby trajectories in phase-space. Any system containing at least one positive Lyapunov exponent is defined to be chaotic [1]. To find the exact quantity of the growth (negative growth in the case of dissipation), we first linearize the given nonlinear equations of motion giving rise to a stochastic motion. First, we may write a set of nonlinear differential equations in a form:

$$\dot{x}_i = f_i(x_1, x_2, \cdots, x_n), i = 1, 2, \cdots, n. \tag{3-1a}$$

Then we can write

$$\delta\dot{x}_i \approx \sum_k f_i(x_1^0, x_2^0, \cdots, x_n^0)\delta x_k + \vartheta[\sum_{k \neq j} \delta x_k \delta x_j], \tag{3-1b}$$

where x_i^0 represents the fixed points of the motion, for which the phase flow is stationary (i.e., those points for which $\dot{x}_i = 0$, that is, $f(x_i^0) = 0$. This linearized equation then can be expressed as a matrix $\underline{M}$.

$$\frac{d}{dt}(\delta\dot{x}_i) = \underline{M}\,\delta x_i. \tag{3-2}$$

The general solution is obtained by $\det|\,\underline{M} - \lambda I\,| = 0$, where I is a unit matrix. So we get

$$\delta \vec{x} = \sum_k a_k \vec{D}_k \exp(\lambda_k t), \tag{3-3}$$

where $\vec{D}_k$'s are the eigen-vectors associated with eigen-values λ_i, which determine the actual directions of the local phase flows. Here the eigen-value λ_i is the characteristic exponent called Lyapunov exponent. The diagram below shows a possible phase flow of the pendulum in three dimensional phase-space.

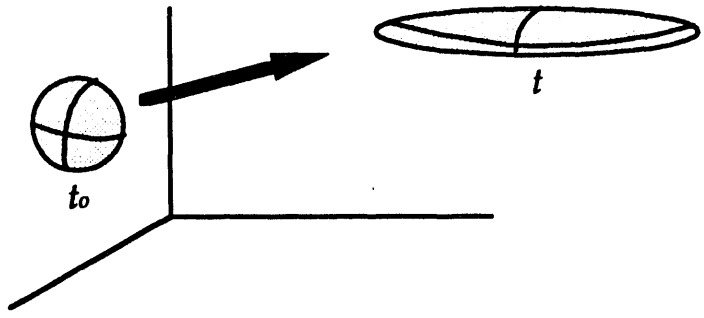

To find the linearized equations of motion in our pendulum case, we first write (1-2) or (2-2) as

$$\begin{cases} \dot{x}_1 = -\beta x_1 - \sin(x_2) + \gamma \cos(x_3) \\ \dot{x}_2 = x_1 \\ \dot{x}_3 = \omega \end{cases}, \tag{3-4}$$

where ω is the frequency of driving force. Then the linearized equations of motion for our pendulum model can be easily obtained by applying the method [2] described earlier.

$$\begin{cases} \dot{x}_1 = -\beta x_1 - x_2 \cos(x_2) - \gamma x_3 \sin(x_3) \\ \dot{x}_2 = x_1 \\ \dot{x}_3 = 0 \end{cases}, \tag{3-5}$$

where $\dot{x}_1 = \dot{q}$, $\dot{x}_2 = \dot{q}$, and $\dot{x}_3 = \omega$. The time evolutions of each variable are then orthonormalized by Gram-Schmidt method [3]. The diagram below depicts this process.

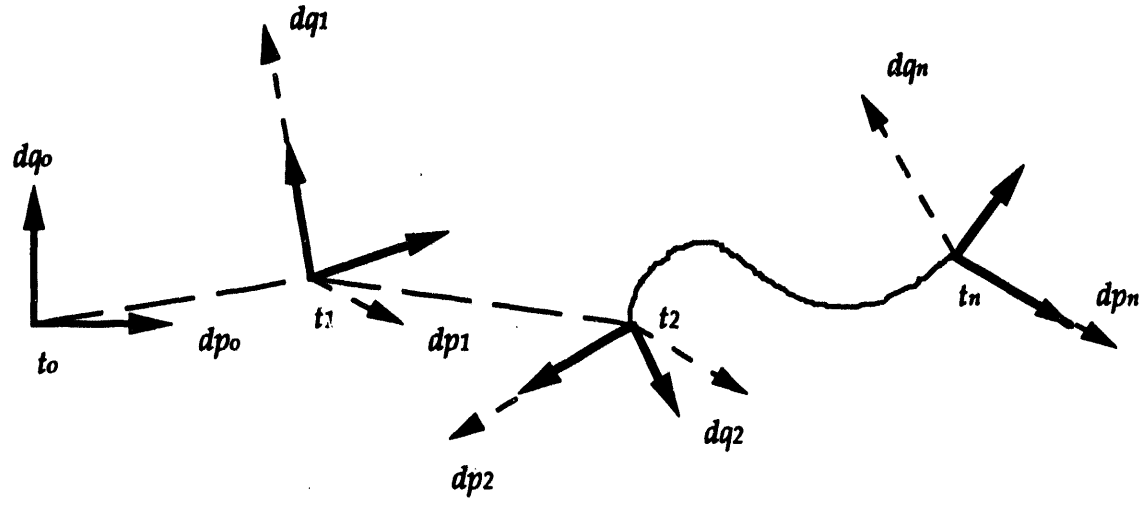

Thick solid lines represent the orthogonal unit vectors. Thin dashed lines are vectors after the unit vectors evolved. Therefore, we can compute the exponent, say, for q using the following formal expression:

$$\lambda_q \sim \lim_{n\to\infty}\left[\frac{1}{n}\left(\sum_{i=1}^{n} \ln|\Delta q_i|\right)\right], \qquad (3\text{-}6)$$

where $\Delta q = dq_i - dq_{i-1}^{norm}$, and dq_{i-1}^{norm} is a normalized unit vector depicted as a solid line in the above diagram.

Figure 3.1 shows the time variations of exponents for cases where γ = 0.2, 5.0 with ω = 2. It clearly exhibits a positive exponent for γ = 5.0, whose phase-space trajectory is not predictable. We will see the trajectories of these cases in Section 3-2.

3-1-2. Quantum Lyapunov exponent

Classical chaos is usually characterized by the existence of a positive Lyapunov exponent as we have discussed previously. In this sense, the quantum version of it becomes subtle and ambiguous because the concept of a small variation in initial conditions resulting a large change in outcomes cannot be applied to quantum mechanics. To show this, we consider a small perturbation ε on the position vector of wave function ψ_1. Then the displaced wave function ψ_2 can be written by Taylor expansion as follows.

$$\begin{aligned}\psi_2(\mathbf{q}, t+dt) &= \psi_1(\mathbf{q}+\varepsilon, t+dt) = \sum_{n=0}^{\infty} \frac{(\varepsilon\cdot\frac{\partial}{\partial \mathbf{q}})^n}{n!}\ \psi_1(\mathbf{q},t+dt) \\ &= \exp(\varepsilon\cdot\frac{\partial}{\partial \mathbf{q}})\ \psi_1(\mathbf{q},t+dt) = \exp(i\,\mathbf{p}\cdot\varepsilon)\ \psi_1(\mathbf{q},t+dt). \qquad (3\text{-}7)\end{aligned}$$

By definition of Lyapunov exponent, we are interested in the difference between the two trajectories at every step formed by their expected values in phase space. The expectation values of an operator $\hat{O}_i = \hat{O}_i(\mathbf{p}, \mathbf{q})$, i=1,2, can be calculated according to the following operations:

$$<\hat{O}>_1 = <\psi_1(\mathbf{q}, t+dt)|\ \hat{O}\ |\psi_1(\mathbf{q}, t+dt)>, \qquad (3\text{-}8a)$$

$$\begin{aligned}<\hat{O}>_2 &= <\psi_2(\mathbf{q}, t+dt)|\ \hat{O}\ |\psi_2(\mathbf{q}, t+dt)>, \\ &= <\psi_1(\mathbf{q}, t+dt)|\ \exp(-i\,\mathbf{p}\cdot\varepsilon)\,\hat{O}\ \exp(i\,\mathbf{p}\cdot\varepsilon)\ |\psi_1(\mathbf{q}, t+dt)>, \\ &= <\psi_1(\mathbf{q}, t+dt)|\ \hat{U}_p^{+}(\varepsilon)\,\hat{O}\ \hat{U}_p(\varepsilon)\ |\psi_1(\mathbf{q}, t+dt)>. \qquad (3\text{-}8b)\end{aligned}$$

Apparently, expectation values of any function of the momentum operator are unchanged when the states are displaced. On the other hand, if $\hat{O}$ is the function of the coordinate operator q, it can be shown easily using (3-7) that [4]

$$< q >_2 = < q_1 + \varepsilon >, \tag{3-9}$$

since $\hat{U}_p(\varepsilon)\ |\psi_1(q,t+dt)> = |\psi_2(q,t+dt)>$, where $\hat{U}_p(\varepsilon) = \exp(i\,p\cdot\varepsilon)$. Therefore, for this kind of perturbational method which is common in classical dynamics, the Lyapunov exponent becomes zero. We arrive at this result by applying the conceptual definition of Lyapunov exponent to quantum mechanics.

Symmetrically we would get the same result for a small perturbation on the momentum vector of the initial wave function if we treat this case in momentum space. In general, however, the situation becomes more complicated for the initial perturbation on both the momentum and the position vectors. It is not difficult to conjecture though that there exist no positive exponents even in this case. It is easy to determine that the classical method in the previous section cannot be exactly applied here. The process of linearization is not appropriate in quantum mechanics.

Nonetheless, we looked at the similar quantum mechanical process analogous to classical method in the previous section. To do that, we used a Gaussian wave function (2-33) initially with q_o with $< q(0) >$ and p_o with $< p(0) >$. We next calculated changes in the norm of each expectation value at every time step. The wave function was then brought back to the form of (2-33) by replacing $< q(t-\Delta t) >$ with $< q(t) >$ and $< p(t-\Delta t) >$ with $< p(t) >$. The results showed that a positive exponent is possible, but it is quite different

from the classical value. It also showed that trajectories in phase-space were not even close to the corresponding classical ones. This excludes this set of method. A study [5] reveals that at very high values of spin in a driven quantum spin system, one could find a positive exponent without any resemblance to the classical exponent. A spin value of $\sim 10^8$ in this study, however, is not realistic.

In the following section, even though there are no positive exponents, we will look at actual trajectories in phase-space, and see if we can understand quantum chaotic phenomena better using the techniques developed so far.

3-2. Phase-space behaviors

The phenomena of classical chaos have fascinated physicists since the development of computational techniques in nonlinear dynamics. Much attention has also been directed toward determining possible quantum analogs of chaos (QC). It is well established that, in principle, quantum mechanics provides a more fundamental description than classical mechanics [6]. Ehrenfest's theorem [7] as well as the correspondence principle, then supports our expectation of the existence of QC. Unexpectedly the fundamental theory of QC is still somewhat speculative. For example, extreme sensitivity of quantum dynamics to initial conditions is lacking because of the smoothing nature of wave mechanics and of the quantum suppression of classical chaos (CC) [8-10]. Even the existence of Lyapunov exponents is not well understood (as seen in Section 3-1). In general, classical chaos is characterized by the existence of a positive Lyapunov exponent λ, i.e., $d(t) \sim d(0) \exp(\lambda t)$, where d is the phase space distance between two initially nearby trajectories as we discussed in details in the previous section. This

classical concept of exponential growth of two initially nearby trajectories in 2N-dimensional phase space cannot be applied if the initial trajectories are within Planck cells (P-cells) of volume h^N for a system with N degrees of freedom [11]. In fact, phase space trajectories have no meanings in quantum mechanics because of this uncertainty unless we introduce the concept of quantum trajectories as the evolution of expectation values of classical observables surrounded by P-cells.

The stringent classical definitions of chaos however may not be appropriate for quantum dynamics since classical and quantum mechanics are different descriptions of nature. Some studies have used the classification of energy level spectra and their statistics [12-17] or stationary states [18-21] as the quantum definitions of chaos. These approaches to QC have no analogues in classical mechanics. Our approach is formulated in the context of classical-quantum correspondence. To do that, we focus explicitly on phase-space behavior.

In this chapter, we will investigate mainly the correspondence principle by comparing classical trajectories with quantum mechanical expectation-value trajectories without dissipation. The classical Hamiltonian of the pendulum is not integrable; the pendulum's motion shows very rich classical chaotic structures [22,23]. The similar quantum model of a kicked rotor has been extensively studied [24-27]. It is similar in the sense that the gravitational potential in our model is applied as a periodic delta function kick as mentioned earlier in Chapter two. Our model can be regarded as a generalized version of this since the external field is added.

The correspondence principle is also studied by varying the effective mass μ in the Schrödinger equation. The degree of correspondence is quantified in terms of the Fourier power spectra of expectation values of

classical observables. In other words, we examine the temporal behavior of the quantum expectation values and their power spectra to compare with the classical values. The power spectra generally exhibit the effect of uncertainty through their noise level. Therefore we expect close correspondence between classical and quantum spectra as long as the P-cells are small compared to the expectation values, or the uncertainty does not grow constantly in time. Especially in the classical regime of regular or mild chaos, this has been assumed to be valid. It has been shown analytically that the strong classical-quantum correspondence exists for a bound potential in one degree of freedom system [28].

In addition, the transition to chaotic behavior will be signaled by changes in the spectral peak distribution. For instance the power spectrum of a Morse oscillator driven by an intense laser pulse briefly mentioned in Section 2-5 undergoes a transition from clear spectral peaks to a chaotic spectrum as one goes to high intensity pulses [29]. A similar observation is expected in our model if there exists any transition.

We also examine time variations of the P-cell volume in both the classically regular and chaotic regimes. This uncertainty volume, if large, may prevent the assignment of a corresponding unique time trajectory in the expectation-value phase space. In this case, the expectation values represent averages over many trajectories within that volume, analogous to Feynman's *sum over paths* formulation. Therefore it has been assumed [see last reference in Ref. 26] that the expectation-value trajectory resembles very closely a unique one if the energy-time uncertainty volume is relatively small compared to the *action* of the system. On the other hand, a non-stationary variation or a large increase of the volume would eliminate the correspondence. We test this novel assumption using phase space trajectories.

The numerical examples of phase-space behaviors are depicted in figures at the end of this chapter along with the results from Sections 3-3, and 3-4.

However, one of the fascinating contents of classical mechanics is energy dissipation (damping) due to friction or heat loss to the surrounding environment. Although strange attractors characterize a classical dissipative system, little is known about the respective quantum system [24,33]. To the author's knowledge, no theory illustrating the comparability of classical damping into quantum calculation has been regarded universal. We will carry further this model with dissipation in the next chapter. Nonetheless, it seems to be more appropriate to first check the correspondence in non-dissipative cases using a classical probability distribution, given by the quantum mechanical probability, $\psi^*\psi$, of initial conditions.

3-3. Classical distribution function

We assume that an initial classical distribution is the same as the probability amplitude of an initial wave function. The initial distribution in configuration space is then taken to be $|\psi_o|^2$. Then the momentum space distribution is

$$|\phi_o|^2 = |\phi(p,0)|^2 = \left|\int dq\, \psi(q,0) \exp(-ipq)\right|^2 .$$

Therefore, the initial classical distribution P_c in phase-space for a minimum uncertainty wave packet becomes

$$P_c(p, q, 0) = \frac{1}{2\pi} |\psi(q,0)|^2 |\phi(p,0)|^2 ,$$

$$= \frac{1}{2\pi}\frac{1}{\pi\sigma}\exp\left[-\frac{(q-q_0)^2}{\sigma^2}\right]\exp\left[-\sigma^2(p-p_0)^2\right]. \qquad (3\text{-}10)$$

To make the distribution closely resembling the quantum wave function, we should pick as many points as possible in phase-space so that the density of those points follows the quantum probability amplitude. Then each point in the distribution represents either a single classical system or a single initial condition. In either case, the resulting distribution would be the same since each point is governed by the same classical equations of motion. If one uses $|\psi_o'|$ instead, the only difference would be that the center of the resulting distribution changes from (q, p) to $(q, p+\mu\gamma\sin(\omega t)/\omega)$. We will see clearly this effect in the following section.

Now, we use the Monte-Carlo random number generator to pick an initial distribution of points in phase-space such that a random point at (q_{rm}, p_{rm}) satisfies the inequality $P_C(q_{rm}, p_{rm}, 0) \leq P_C(p, q, 0)$. Then each of these initial points is governed by the given classical equations of motion, for example, Eq. (3-4) and collected after the required propagation time τ to give a final distribution of points.

To compare, we also examine properties of quantum distribution functions since the wave function itself cannot be compared with the classical distribution given by the method above. In the next section we introduce the Wigner and Husimi quantum distribution functions in phase-space, and study their advantages and disadvantages in the context of our model.

3-4. Quantum distribution functions

In the last few years, interest in the Wigner distribution function has been revived to study quantum dynamics in the classical-like phase-space. This function, first formulated by Wigner [34,35], represents the Weyl transform of a density matrix. The Wigner function provides the quantum analogue to a classical phase-space density, known as the Poincaré surface of section [36,37]. However, starting from the Schrödinger wave function, it is difficult to carry out the calculation of the Wigner distribution *function*, the so-called phase-space distribution function or PSD function because Schrödinger equation is in general not easily solvable especially for potentials which give rise to classically chaotic behaviors [38]. Instead, the Wigner *equation* [36,39,40] governing the time evolution of an initially localized Wigner PSD function has been studied in various problems. This equation is the PSD analogue in the Heisenberg picture [41] since it is considered as the quantum version of the classical Liouville equation when h is considered negligible [34,35,42].

For example, some studies have used the Wigner equation to simulate quantum effects in semiconductor devices [43] numerically. Other applications of the equation such as the photodissociation cross section calculation [44], stellar dynamics [45] and collision problems [46] have been considered. Takahashi and Saito [47] examined the Wigner equation to discuss quantum manifestations of chaos. Interestingly, they also added a computational analysis of the Husimi equation describing the time development of the Husimi PSD function [48] in the Heisenberg equations of motion.

In addition, using a coherent state wave function, the Wigner function is useful in wave optics to measure the uncertainty distribution [49]. Possible transitions into a squeezed state are of interest also. Nonetheless, in the course of recent developments in semi-classical mechanics to search for quantum chaos, the Wigner function has been directly investigated as the PSD analogue in the Schrödinger picture [50] using several different systems in the context of classical-quantum correspondence [51]. On the basis of these studies, it is plausible to characterize quantum chaos as the appearance of a stochastic Wigner phase-space density. On the other hand, it still does not seem sufficient to generalize and relate the stochastic Wigner density to a classical one. Therefore, one of our purposes is to investigate further and to derive a clearer picture of the classical-quantum correspondence.

We also study the Husimi representation of chaos in the Schrödinger picture. Takahashi and Saito have claimed that the Husimi representation was better for describing the correspondence principle than the Wigner representation. This study also supports Heisenberg's correspondence that relates quantum mechanical matrix elements to Fourier components of a classical motion. However, their results also seem to indicate that correspondence becomes obscured at long times. We have tested their claim by checking the correspondence at long times.

One obvious advantage of the Husimi function is that this function is non-negative, whereas the Wigner PSD function may be negative so that its meaning as a probability density becomes unclear. In spite of its compact form that can be readily identified as a probability function, the Husimi function has not attracted much attention until recently. We use the Husimi PSD function to study its connection to the corresponding classical (Liouville) and quantum (Wigner) PSD functions.

Moreover, our earlier results [52] indicate that the correspondence fails after the break time. We characterized the break time when the uncertainty product ($\Delta q \Delta p$) in phase-space becomes significant compared to the characteristic *action* of the system formed by the expectation-value trajectory. We therefore concluded that the correspondence cannot be checked by comparing merely a single classical trajectory with a quantum (expectation-value) trajectory in phase-space. This result will be shown again in the next section with discussions. Thus, we have suggested that a classical distribution is the more appropriate choice to check the correspondence. A classical distribution describes initial conditions of the system corresponding to the quantum probability amplitude as in Sec. 3-3.

In this section, we present numerical evidence of the correspondence between quantum mechanical and semi-classical phase space densities. These densities are formed by the Wigner and the Husimi functions corresponding to classical motions of the classical distribution. Extension of the earlier study by Takahashi and Saito to the forced pendulum is applied to verify their conclusions. We are especially interested in the classically chaotic regime of the pendulum [22,52].

In doing so, we first discuss the correspondence among the three schemes of a simple harmonic oscillator analytically. Then, we briefly describe numerical methods of the calculations, and show the numerical examples for both a simple harmonic oscillator and a forced pendulum. Finally, the results are compared and discussed in several different semi-classical approximations followed by the summary in Sec. 3-6.

First in the case of a simple harmonic motion, the minimum uncertainty Gaussian wave packet initially displaced by an amount a spatially can exhibit all the eigen-states [53]. The simple harmonic oscillations are well

predictable with the given oscillator strength $k \sim \mu\omega_0^2$, where μ is the dimensionless mass of the oscillator and ω_0 is the dimensionless natural frequency of the oscillation. The initial Gaussian shape of a probability density is always spatially preserved if there is no external perturbation. Therefore, the probability density is invariably the same Gaussian shape oscillating with amplitude a and frequency ω_0. The corresponding classical motion is described by the quantum expectation-values located at the point of peaks of the Gaussian in both configuration and momentum spaces [54].

Classically, however, we are to use the Liouville distribution that is initially displaced by the same amount as the quantum initial wave packet. This distribution then expresses the probability distribution, $\psi^*\psi$, of the initial conditions of an oscillator. Then this Gaussian distribution keeps the same distribution centered at some position in phase-space at a later time. This is apparent because the initial distribution with an additional oscillation term is the solution of the Liouville equation for the simple harmonic oscillator. Then it is not difficult to show the close correspondence among three different PSD functions analytically.

First, consider the Wigner PSD function. This function, P_w, represents a system in a mixed state represented by a density matrix $\hat{\rho}$ [35].

$$P_w(\mathbf{p}, \mathbf{q}, t) = \frac{1}{(2\pi\hbar)^n} \int_{-\infty}^{\infty} d\mathbf{y} \, \langle \mathbf{q} - \frac{\mathbf{y}}{2}, t \left| \hat{\rho} \right| \mathbf{q} + \frac{\mathbf{y}}{2}, t \rangle \exp\left(\frac{i\,\mathbf{p}\cdot\mathbf{y}}{\hbar}\right), \qquad (3\text{-}11)$$

where n specifies dimensions of a system. In our case of a pure state, ψ, in one dimension

$$P_w(p, q, t) = \frac{1}{2\pi\hbar}\int_{-\infty}^{\infty} dy\ \psi^*(q+\frac{y}{2}, t)\ \psi(q-\frac{y}{2}, t)\exp(\frac{ipy}{\hbar}), \qquad (3\text{-}12a)$$

$$= \frac{1}{2\pi\hbar}\int_{-\infty}^{\infty} dy\ C(q, y; t)\ \exp(\frac{ipy}{\hbar}). \qquad (3\text{-}12b)$$

Note that P_w is just the Fourier transform of $C(q, y; t)$.

The Husimi PSD function can be obtained by a Gaussian smoothing method [55] and is given by the following expression:

$$P_h(p, q, t) = \frac{1}{2\pi\hbar}\,|\langle f(p, q; x)\,|\,\psi(x, t)\rangle|^2$$

$$= \frac{1}{2\pi\hbar}\left|\int_{-\infty}^{\infty} f^*(p, q; x)\ \psi(x, t)\,dx\right|^2. \qquad (3\text{-}13)$$

where $f(p, q; x) \equiv f_x(p, q)$ is the coherent Gaussian-type test function with the minimum uncertainty. It is given by

$$f_x(p, q) = \left(\frac{1}{2\pi\sigma^2}\right)^{1/4}\exp(-\frac{(x-q)^2}{4\sigma^2}+\frac{ipx}{\hbar}). \qquad (3\text{-}14)$$

Here, the usual Gaussian width is represented by σ specifying the uncertainty of the classical variables p and q.

Therefore, once the wave function is known from Schrödinger equation, the formulation of the Wigner or the Husimi function is considerably less difficult than solving the Wigner or the Husimi equation.

This is because we use a well-known Fourier transformation method in the Wigner case. In the Husimi case, a simple projection scheme into the test function f makes so.

Finally, the classical Liouville distribution at a certain time t becomes

$$P_l(p, q, t) = \frac{1}{2\pi\hbar}|\psi(q, t)|^2 |\phi(p, t)|^2. \qquad (3\text{-}15)$$

where $\phi(p, t) = \int \psi(q, t) \exp(-ipq/\hbar)\, dq$. We used the probability density of the wave function $\psi(q, t)$. Obviously, this is not a general description, but a special one that works only for a simple harmonic oscillator. In general, a classical distribution does not have to always resemble the wave function at time t.

To show the correspondence analytically, substitute the following Gaussian function into the equations (3-12), (3-13) and (3-15):

$$\psi(q, t) = \left(\frac{1}{2\pi s^2}\right)^{1/4} \exp\left(-\frac{(q - q_0)^2}{4s^2} + \frac{ip_0 q}{\hbar}\right) \exp(-i\theta t/\hbar), \qquad (3\text{-}16)$$

whose width is s and peak is located at (q_0, p_0) in phase-space. The width s is generally not a ground state Gaussian width [53]. The time dependence is involved implicitly in q_0, p_0 and in the time-dependent phase θ [4], i.e., $q_0 = a\cos(\omega_0 t)$, $p_0 = -a\mu\omega_0\sin(\omega_0 t)$. The variable q in Eq. (3-16) should become x when $\psi(q)$ is substitute into Eq. (3-13). It is also worth noting that the gauge transformation of our kind effects the solution (3-16) such that p_0 changes to $p_0 + \mu\gamma\sin(\omega t)/\omega$; $\psi(q, t) \rightarrow \psi'(q, t)$. But the actual results from Eqs. (3-12), (3-13) and (3-15) are gauge invariant.

The analytic results from the equation (3-12) is

$$P_w(p, q, t) = \frac{1}{\pi\hbar} \exp\left(-\frac{(q - q_o)^2}{2s^2}\right) \exp\left(-\frac{2s^2(p - p_o)^2}{\hbar^2}\right). \qquad (3\text{-}17)$$

We get a circular contour in phase-space from this equation for $s^2 = 0.5$. From the equation (3-13), we get

$$P_h(p, q, t) = \frac{1}{\pi\hbar} \frac{\sigma s}{\sigma^2 + s^2} \exp\left(-\frac{(q - q_o)^2}{2(\sigma^2 + s^2)}\right) \exp\left(-\frac{2\sigma^2 s^2}{(\sigma^2 + s^2)} \frac{(p - p_o)^2}{\hbar^2}\right). \qquad (3\text{-}18)$$

In the case where $\sigma = s$, this equation becomes

$$P_h(p, q, t) = \frac{1}{2\pi\hbar} \exp\left(-\frac{(q - q_o)^2}{4s^2}\right) \exp\left(-\frac{s^2(p - p_o)^2}{\hbar^2}\right). \qquad (3\text{-}19)$$

The classical result from the equation (3-15) is

$$P_c(p, q, t) = \frac{1}{\pi\hbar} \exp\left(-\frac{(q - q_o)^2}{2s^2}\right) \exp\left(-\frac{2s^2(p - p_o)^2}{\hbar^2}\right). \qquad (3\text{-}20)$$

These equations, (3-17)~(3-20), satisfy the normalization condition $\int P_{(w,h,l)}(p, q)\, dpdq = 1$. Now, compare the equations (3-17), (3-18) (or (3-19)) and (3-20). The classical distribution in this case is exactly the same as the Wigner distribution. Also notice that the phase-space contours of three results become circles for $s^2 = 0.5$, but for other values of s (or σ), an elliptical shape of contours would be yielded. Although the Husimi PSD function does not exactly match with the other two, its overall shape is quite close to those distribution functions. If the solution, ψ' after the gauge transform is used, the

centers of three distributions (3-17), (3-18) and (3-20) will lie at ($q_o, p_o + \mu\gamma \sin(\omega t)/\omega$). We will use ψ' from now on.

Therefore we showed the correspondence for a simple harmonic oscillator using three different probability density functions in phase-space in this section. It is interesting to note that the width σ of the test Gaussian function can be adjusted to give different uncertainties of Δp and Δq. In other words, externally 'squeezed' states can be generated. The results of numerical calculations of Sections 3-3, 3-4 for the cases of the pendulum will be shown in the next section.

3-5. Numerical results

First, we will compare directly classical trajectories with quantum mechanical expectation-value trajectories in phase-space. The initial conditions for Figures 3.1 - 3.6 of Section 3-2 are $q_o = 0.05$, $p_o = -0.02$ and $\mu = 1$, 50, 200, for cases (b), (c) and (d) with $\sigma^2 = 0.6$, 0.02 and 0.005 respectively. For a case (a), a simple harmonic motion is plotted with $\mu = 10$, $\sigma^2 = 0.1$. More spatial grid points are required as the mass increases since $\sigma^2 \sim 1/\mu$; the width and depth of the potential well is directly dependent upon the value of μ. All runs were made with 32768 integration steps with $\omega = 2.0$. In the regular regime, $\gamma = 0.2$ is used whereas in the chaotic regime, $\gamma = 5.0$ is used. The number of abscissa points of power spectra is taken to be 512 steps out of the total integration steps for a spectral peak blow-up. All the initial data used in this chapter are summarized in Table 3.I. Most runs were carried out with $\Delta t = 0.005$. This value permits an accuracy in determining the phase space trajectories comparable with that obtainable with the very accurate classical calculations [22,23] using a fourth-order Runge-Kutta method.

The time variations of Lyapunov exponents calculated using Eq. (3-6) for the regular ($\gamma = 0.2$) and the chaotic ($\gamma = 5.0$) cases are shown in Figure 3.1. For the regular motion, the exponent is zero, whereas the exponent approaches ~ ±0.248 for the chaotic case.

Figure 3.2, which shows cases (a)-(d), exhibits motions in the classically regular regime whose Lyapunov exponents are zero as seen in Fig. 1. The rectangles inside (c) and (d) represent the uncertainty products

$$U(t) = \{ <(\dot{q} - <\dot{q}>)^2> <(q - <q>)^2> \}^{1/2},$$

whose area shadows each point on the trajectories (called "the shadow effect"). In this regime, it is assumed that the each point on the trajectory is at the center of the rectangle. We notice that the area decreases as we increase μ. However, the fluctuation dU/U is very small so that one may assume a steady $U(t)$ for $\mu = 50$ as shown in Fig. 6 (We will come back to Fig. 3). In fact, the minimum uncertainty is being kept with the negligible fluctuation in this case. For $\mu = 200$, the steady $U(t)$ is so small that the scale of Fig. 6 is not appropriate to plot the case. In the case where $\mu = 1$, however, the size of the area $U(t)$, which is 0.5, is larger than that of the phase-space shown in Fig. 1(b). In other words, $\Delta q \sim 0.7$ and $\Delta \dot{q} \sim 0.7$ in this case where $\dot{q} = (p - A)/\mu$. Although the volume $U(t)$ is considered steady in this case, the shadow effect is big enough to dissociate the correspondence. The bottom two in this figure exhibit the power spectra of the cases (a) and (d), respectively. We hardly notice the difference between (a) and (d) because of a negligible noise level due to the volume $U(t)$.

Figure 3.3 exhibits the power spectra of the cases (a) - (d), respectively. The power spectra are calculated by using Eq. (2-34). We hardly notice the

difference between (a) and (d) because of a negligible noise level due to the volume $U(t)$. We should note here that more trials of similar cases in classically regular regimes indicate the same results. The larger the values of μ are, the better the correspondence is. We do not observe that the correspondence fails in classically regular regimes. It is appropriate to ignore those figures here.

Figure 3.4, however, shows big differences for the cases (a) - (d). The external force is twenty-five times stronger than the previous one shown in Fig. 3.2. Obviously, the classical system is in chaotic motion, i.e., there exist a positive Lyapunov exponent (see Fig. 3.1). There is an external force range where intermittence appears. But we are interested in the fully developed chaotic regime. The figure displays that all the quantum trajectories appear to be quite chaotic with no resemblance to the classical one and to each other. Here the volume $U(t)$ spreads almost the entire phase space. Because the sizes and shapes of the volume $U(t)$ always change, the rectangles like shown in Fig. 3.2 cannot be drawn in this case. Fig. 3.6 clearly exhibits this effect even in the case where μ = 200. We noticed from another calculation in the chaotic regime using μ = 100 that the volumes with smaller values of μ are always larger than the one with greater values of μ. Moreover its initial expansion limits the correspondence to be satisfied within a very short time, and its fluctuation permits many other possible trajectories.

In addition, the fact that the expectation values of q trace out into a smaller region for the larger μ tells us that the wave packet expands more so that the average values (expectation values) of q become smaller. Figure 3.5 supports the idea because of the noise rise due to the large $U(t)$. Therefore the *real* trajectory can never be determined in this case after the short characteristic time, so-called the break time, [15,26] which gives the time of

close correspondence between the classical and quantum trajectories. In our case, the break time can be characterized as the time when the uncertainty volume becomes significant compare to the *action* of the system. The same findings are also deduced from many other trials in the classically chaotic regimes. We will not show them here.

Despite the appearance of abrupt changes in the quantum trajectories in Fig. 4, the initial values are brought back by the reverse-time calculations of the Schrödinger equation as an accuracy test [30,31]. The fact that no apparent changes are observed with the use of different number of time steps and grid points also supports the accuracy of the algorithm. The power spectrum calculations utilize the window function [32]. Now let us move our focus to the distribution functions.

Figs. 7-10 are plotted for cases where initial values are $\mu = 20.0$, $\Delta t = 0.00383349$, $\omega = 4/3$, $q_o = 0.5$, $p_o = 0$. The values of γ in these cases are 0.5, 0.8, and 1.25. The uncertainty products of these three different cases are shown in Figure 3.7. The uncertainty product grows in time with higher values of γ as it should be expected. Fig 3.8 depicts the exponents for same cases. Their values are easily noticeable directly from the figure.

Before we discuss about later figures, a word is in order concerning contour plots of the Wigner distribution function. The contour plots are taken from the norm of Eq. (3-12), $|P_w|$, to avoid possible negative values. This treatment is applied throughout the following chapters for the Wigner function.

The next two figures exhibit (a) the initial classical distribution, (b) the later classical distribution, (c) Husimi distribution function, and (d) Wigner distribution function. For Figure 3.9, we initially start with 1000 different initial conditions with $\gamma = 0.5$. This Gaussian initial distribution is shown in

(a). Then the later classical distribution after the time $t = 20T/3 \approx 7T$, $T = 2\pi/\omega$, is shown in (b). The spiral structures are easily noticeable. Both (c) and (d) show similar spiral structures. From these contours of the distributions, we may say that the Husimi case (d) manifests more than the Wigner case (c) in overall structure in phase-space. On the contrary, the case (d) is better in details of the distribution in phase-space since it does not have a smoothing mechanism of Husimi kind.

Figure 3.10 with $\gamma = 1.25$ also supports this idea. In this case, 2000 different initial conditions are used, and the evolution time is about $3T$. The picture in (b) clearly exhibits classically chaotic motion. The obvious difference between (c) and (d) exists, but the similarity between (b) and (d) can be easily spotted. Since the correspondence breaks down earlier at higher values γ, the less evolution time is used in this case even for a larger value $\mu = 40.0$. It is interesting that Wigner distribution shown in (c) spreads almost all the phase-space. We believe that the initial wave function quickly spreads out in this case so that equation (3-12) contains a complex structure. However, it is a surprising fact that Husimi distribution can still project out the result somewhat closer to the classical one (b). The width of the Husimi's test function (3-14) is 0.25 for both cases of Figures 3.9, 3.10. One can indeed control the projection of Husimi distribution into phase-space by adjusting the width.

Figure 3.11 shows the uncertainty product U for two different cases of other trials. The first one in Fig. 3.12 is at resonance with the values $\omega = 1.0$, $\gamma = 0.35$, and the second one $\omega = 1.5$, $\gamma = 0.5$. It is easy to acknowledge that the Husimi one (c) is much closer to (b) than the Wigner one (d) in the first case after $t = 5T$. In Figure 3.13, the similar phenomenon is observed for the second case. But the case (d) is not very different from (b) although the kind of

a spiral in (b) is difficult to detect. Typical three dimensional distributions of this case are shown in Figure 3.14.

Figure 3.15 exhibits another classical chaotic case where $\omega = 1.05$, $\gamma = 0.5$ whose Lyapunov exponent is ± 0.065. It is certain that the Husimi representation resembles the classical one more closely than the Wigner representation in the classical chaotic regime. Additional example in classical chaotic motions are shown in the final figure. In Fig. 3.16, the different values of wave packet widths from the previous figure were used. The results somewhat support our idea and the previous findings of Takahashi et al., that the Husimi is better to represent the correspondence, but it is actually difficult to judge. It is safe to say that generic behavior of the Husimi is more reliable in the context of the correspondence. On the other hand, the Wigner will be better in the classically regular regime since it will not lose detailed information of the distribution through the Gaussian smoothing as we see in the figure. Now we summarize our results.

3-6. Summary

It has been shown clearly that the correspondence principle holds more closely for trajectories and their power spectra near the semi-classical limit, especially in the regular regime. It is not surprising that the correspondence fails even in the regular regime for $\mu \approx 1$ since the effects of spreading and distortion of the wave packets cause relatively large deviations from the classical counterparts. Conversely, the level of correspondence increases as μ gets bigger with considerably smaller time steps at a cost of much more computer time. A recent study [56] mainly focused on classical regular regime using the Floquet states [57] reveals the close association of eigenstates with

classical invariant tori [58]. However it is impossible to check the quantum chaotic behavior in a classically chaotic regime because the uncertainty dominates the phase space taken by the characteristic *action* within a short time. This fact is well supported by the power spectrum in the chaotic regime. The noise rise due to the large variations in $U(t)$ is large enough to veil the *real* spectrum. It is worth mentioning that several distinct peaks are due to the initial transient effect that will disappear at a large time.

Also, the assumption that the correspondence does not hold after the break time in the chaotic regime was tested numerically to be valid. On the other hand, the correspondence holds with relatively long break time in the regular regime, of the highly semi-classical limit. A study by G. P. Berman *et al.* [27] also indicates the evolution of atoms in a resonant cavity essentially quantal after a certain time has elapsed (break time). They find that quasi-classical approximation breaks down after the break time. Therefore, it does not seem to be an accurate guide for us to use the expectation-value phase-space trajectory in classically chaotic regime for predicting whether a given wave packet will exhibit classical means of chaotic behavior in a certain constraint. In other words, the correspondence between the quantum mechanical and the classical system cannot be complete in the classically chaotic regime at this stage.

We also find from the results of the three distributions that the Husimi representation is better than the Wigner's within the break time. This is in agreement with Takahasi and Saito's results. Our results also suggest that there is no contradiction qualitatively within their correspondence time (our break time). It is very interesting to see that especially in the chaotic regime, the higher degree of correspondence in the Husimi case can be easily noticeable. On the other hand, we find that the Wigner representation is good

enough to represent the correspondence itself in the non-dissipative cases, and is in fact better in the interests of detailed structure of phase-space. The details of the Wigner resembles the classical one more than the Husimi. Classically more dense areas are simulated as more intense distinct peaks of the Wigner distribution unlike the Husimi where the smoothing takes place.

Additionally, we checked the time domain beyond the correspondence limit up to few orders of the break time, and found the support to the previous conclusion of correspondence breaking. It really appears at this juncture the manifestations of classical chaos in quantum mechanics in this model without dissipation cannot be established. However, our results do not indicate that quantum mechanics in general describes a different mechanics than classical mechanics. All the classical trajectories examined lie well within the regions covered by the quantum uncertainty.

We learned that others have found similar results. For example, in a quantum version of the map associated with the classically chaotic Arnol'd cat, a failure of the correspondence principle in an appropriate limit is claimed [59]. Also, J. Kimball, et. al. indicates that an agreement between the quantum equations of an electron in a periodic potential with an additional periodic pulsed kick and the corresponding classical motion disappears very quickly [60]. This effect is due to our claim of the uncertainty growth. Another study [61] uses this growth as an possible indicator of semi-classical chaos. Our results agrees with these.

As a final note, Husimi representation is not useful when we deal with quantum dynamics. The information about the dynamics is being lost due to Gaussian smoothing that is somewhat coarse-grained version of Wigner representation. This loss is a significant fact for quantum dynamics. We will see of more evidence in the next chapter.

Appendix 3.I A characterization of break time

The break time, τ_b can be generally identified as a finite time interval during which the uncertainty product $U(t)$ is comparable to the classical characteristic action, I_{cl}.

$$U(t) \approx U(0) \exp(\lambda \tau_b) \approx I_{cl}, \tag{A3I-1}$$

where λ is a positive constant (or zero) specifying the average growth rate, and the classical action for a dimensionless Lagrangian L is

$$I_{cl} = \int_{t_1}^{t_2} L[q(t), \dot{q}(t), t]\, dt. \tag{A3I-2}$$

It is assumed in (A3I-1) that in principle, the growth can be unbounded. In practice, $U(t)$ would eventually saturate phase-space that is bounded by limited size of numerical grids for a positive growth rate. This quantity (A3I-2) is in general not integrable, especially for our model, but it can be approximated using a numerical integration. It should also be noted that the growth rate λ is only applicable before the saturation of phase-space by $U(t)$ occurs. Then this indicates the break time to be

$$\tau_b = \frac{1}{\lambda} \ln\left[\frac{I_{cl}}{U(0)}\right], \tag{A3I-3}$$

$$= \frac{1}{\lambda} \ln[2\mu I_{cl}], \tag{A3I-4}$$

provided that $I_{cl} \geq 1/2\mu$ since $U(0)$ is $1/2\mu$ for a minimum uncertainty wave packet. Consequently the correspondence holds for that time interval only. The expression (A3I-3) is quite general since it contains general features although I_{cl} is not easy to obtain. Moreover the dependence on μ in our case should be of importance. Now if the value of λ has a certain universal behavior, the limit of correspondence can be determined. It would also be very interesting to see that the substitution of the positive Lyapunov exponents in place of λ in (A3I-3) yields approximately the same τ_b provided that I_{cl} is known. In other words, τ_b becomes shorter for classically more chaotic motions. Nonetheless it seems that the reasonable correspondence holds for longer time intervals than our limits of integration time $\sim n\Delta t$ in the classically regular regime. This kind of the logarithmic law has been proposed originally by G. M. Zaslavsky [62]. But much of it requires a further study.

References

[1] R. Shaw, Z. Naturforsch, **36A**, 80 (1981).

[2] A. Wolf, J. B. Swift, H. L. Swinney, J. A. Vastano, Physica **16D**, 285 (1985).

[3] See for example, J. Stoer, R. Bulirsch, *Introduction to Numerical Analysis* (Springer-Verlag, N. Y. 1980).

[4] L. I. Schiff, *Quantum Mechanics* (3rd edition), Section 26 (McGraw-Hill, N. Y. 1968).

[5] J. J. Mikeska, J. Frahm, *Chaos, Noise and Fractals* edited by E. R. Pike, L. A. Lugiato (Adam Hilger, Bristol, England, 1987).

[6] See, for example, L. D. Landau, E. M. Lifshitz, *Quantum Mechanics* (Nonrelativistic Theory, 3rd Edition, Pergamon Press, 1977); see also A. J. Lichtenberg, M. A. Lieberman, *Regular and stochastic Motion* (Springer-Verlag, New York, 1985), p 462.

[7] P. Ehrenfest, Z. Physik, **45**, 455 (1927); see also ref. 4, and A. Yariv, *Quantum Electronics*, 3rd Edition, Ch. 1 (John Wiley & Sons, N. Y. 1989); J. L. Powell, B. Crasemann, *Quantum Mechanics* (Addison-Wesley, Reading, MA, 1961).

[8] B. V. Chirikov, F. M. Izrailev, D. L. Shepelyansky, Soviet Sci. Rev. C. **2**, 209 (1981); F. M. Izrailev, Phys. Rep. **196**, 299 (1990).

[9] S. Fishman, D. R. Grempel, R. E. Prange, Phys. Rev. Lett. **49**, 509 (1982).

[10] D. R. Grempel, Phys. Rev. A. **29**, 1639-47 (1984).

[11] W. Firth J. N. Elgin, J. S. Satchell, *Quantum Measurement and Chaos*, edited by E.R. Pike, S. Sarkar (Nato ASI Series, Plenum Press,1986), p 251.

[12] I. C. Percival, J. Phys. B. **6**, L229 (1973).

[13] T. H. Seligman (Ed.) *et al.*, *Quantum Chaos and Statistical Nuclear Physics* (Springer-Verlag, 1986).

[14] M. C. Gutzwiller, *Chaos in Classical and Quantum Mechanics* (Springer-Verlag, 1990); see also *Quantum Chaos* edited by H. A. Cerdeira, R. Ramasmeny, M. C. Gutzwiller, G. Casati (World Scientific, Singapore, 1991).

[15] F. M. Izrailev, Phys. Rep. **196**, 299 (1990)

[16] G. Casati (Ed), *Chaotic Behavior in Quantum Systems* (NATO ASI Series, Plenum Press, New York, 1983).

[17] M. Feingold, S. Fishman, Physica D, **25**, 181 (1987).

[18] K. S. J. Nordholm, S. A. Rice, J. Chem. Phys. **61**, 203 (1974); **61**, 768 (1974); **62**, 157 (1975).

[19] M. V. Berry, Phil. Trans. Roy. Soc. **A287**, 237-71 (1977); J. Phys. A. **10**, 2083-91 (1977); with M. Robnik, J. Phys. A. **19**, 1365 (1986).

[20] S. W. Mcdonald, A. N. Kaufman, Phys. Rev. Lett. **42**, 1189 (1979); E. J. Heller, Phys. Rev. Lett. **16**, 1515 (1984).

[21] To see more recent development, refer to the whole volume of J. Stat. Phys, **68** July issue (1992).

[22] E. G. Gwinn, R. M. Westervelt, Phys. Rev. Lett. **54**, 1613 (1985); E. G. Gwinn, R. M. Westervelt, Phys. Rev. A. **33**, 4143 (1986); D. D'Humieres, M. R. Beasley, B. A. Hubermann, A. Libchaber, Phys. Rev. A. **26**, 3483 (1982); J. B. McLaughlin, J. Stat. Phys. **24**, 375 (1981).

[23] G. L. Baker, J. P. Gollub, *Chaotic dynamics*, (Cambridge Univ. Press. N. Y., 1990); A. R. Bishop, Nature, **344**, 290 (1990).

[24] T. Hogg, B. A. Huberman, Phys. Rev. A. **28**, 22 (1983).

[25] H. G. Schuster, *Deterministic Chaos*, see Sec. 7 (Physik-Verlag, Berlin, 1984).

[26] G. Casati, J. Ford, I. Guarneri, F. Vivaldi, Phys. Rev. A. **34**, 1413 (1986); for excellent discussions of the break time, see also G. M. Zaslavsky, Phys. Rep. **80**, 157 (1981); *Chaos in Dynamic Systems* (Harwood, N. Y. 1985) by the same author; for numerical results, see for example, R. F. Fox, Phys. Rev. A. **41**, 2969 (1990).

[27] G. P. Berman, A. R. Kolovskii, F. M. Izrailev, A. M. Iomin, Chaos, **1**(2), 220 (1991).

[28] E. J. Heller, Physica 7D, 356 (1983).

[29] S. Chelkowski, A. D. Bandrauk, Phys. Rev. A. **44**, 788 (1991).

[30] M. D. Feit, J. A. Fleck, Jr, J. Chem. Phys. **80**, 2578 (1984).

[31] M. D. Feit, J. A. Fleck, Jr., A. Steiger, J. Comput. Phys. **47**, 412 (1982); J. N. Bardsley, A. Szöke, and J. M. Comella, J. Phys. B. **21**, 3899 (1988); C. Leforestier,R. H. Bisseling, C. Cerjan, M. D. Feit, R. Friesner, A. Guldberg, A. Hammerich, G. Jolicard, W. Karrlein, H.-D. Meyer, N. Lipkin, O. Roncero, R. Kosloff, J. Comp. Phys. **94**, 59 (1991).

[32] F. J. Harris, Proceedings of IEEE, **66**, 51 (1978): M. D. Feit, J. A. Fleck. Jr., J. Chem. Phys. **78**(1), 301 (1983).

[33] B. A. Huberman, *Dynamical Systems and Chaos*, edited by L. Garrido

(Springer-Verlag, New York, 1982).

[34] E. P. Wigner, Phys. Rev. 40, 749 (1932). For a detailed exposition of the original theory, see J. E. Moyal, Proc. Cambridge Philos. Soc. 45, 99 (1949); L. Cohen, J. Math. Phys. 7, 781 (1966).

[35] For more recent versions, see M. Hillery, R. F. O'connell, M. O. Scully, E. P. Wigner, Phys. Rep. 106, 121 (1984); S. K. Ghosh, A. K. Dhara, Phys. Rev. A. 44, 65 (1991).

[36] Y. Weissman, J. Jortner, J. Chem. Phys. 77, 1486 (1982)

[37] For the definitions of the Poincaré sections, see for example, J. M. T. Thompson, H. B. Stewart, *Nonlinear Dynamics and Chaos* (John Wiley & Sons, N. Y. 1986). To see many examples of Poincaré plots in a classically damped driven pendulum, refer to G. L. Baker, J. P. Gullub, *Chaotic Dynamics: An Introduction* (Cambridge, N. Y. 1990); M. Tabor, *Chaos and Integrability in Nonlinear Dynamics* (John Wiley & Sons, N. Y. 1989).

[38] Here we convert the quantum Hamiltonian H to the classical one that gives rise to the nonlinear classical equations of motion. This Hamiltonian then generates classical chaos whose definition usually means the existence of a positive Lyapunov exponent λ, where $\lambda \sim \lim_{n\to\infty}\left[\frac{1}{n}\left(\sum_{i=1}^{n} ln\left|\frac{d(t_i)}{d(0)}\right|\right)\right]$, $d(t)$ is the distance between the two initially nearby trajectories in phase-space at time t. See Section 3-1.

[39] Y. S. Kim, E. P. Wigner, Am. J. Phys. 58(5), 439 (1990); H. J. Korsch, M. V. Berry, Physica 3D, 627 (1981); F. Nier, Ph.D. Thesis (Ecole Polytechnique, Palaiseau Cedex, France, 1991).

[40] V. I. Tatarskii, Sov. Phys. Usp. 26, 311 (1983).

[41] Here we treat the Wigner PSD function as a dynamical variable in the von Neumann equation [Gött. Nachr. 273 (1927)], $i\hbar\frac{dP_w}{dt} = [H, P_w]$, which plays the same role in quantum mechanics as the classical Liouville equation.

[42] E. Prugovecki, Ann. Phys. 110, 102 (1978);
B. L. Lan, R. F. Fox, Phys. Rev. A. 43, 646 (1991).

[43] N. C. Klüksdahl, A. M. Kriman, D. K. Ferry, C. Ringhofer, Phys. Rev. B. 39, 7720 (1989); W. R. Frensley, Phys. Rev. B. 36, 1570 (1987); U. Ravaioli, M. A. Osman, W. Pötz, N. C. Klüksdahl, D. K. Ferry, Physica, 134B, 36

(1985); K. Hirakawa, H. Sakaki, Phys. Rev. B. 33, 8291 (1986); P. Degond, F. Guyot-Delaurens, J. Comput. Phys. 90, (1990).

[44] R. C. Brown, E. J. Heller, J. Chem. Phys. 75(1),186 (1981).

[45] J. Batt, W. Faltenbacher, E. Horst, Arch. Rat. Mech. Anal. 93, 159 (1986)

[46] P. Carruthers, F. Zachariasen, Rev. Mod. Phys. 55, 245 (1983).
H. W. Lee, M. O. Scully, J. Chem. Phys. 73, 2238 (1980).

[47] K. Takahasi, N. Saito, Phys. Rev. Lett. 55, 645 (1985); K. Takahasi, J. Phys. Soc. Jpn. 55, 762 (1986).

[48] K. Husimi, Pro. Phys. Math. Soc. Jpn. 22, 264 (1940). See reference 42 by Prugovecki for a comprehensive review. See also R. F. O'Connel, L. Wang, H. A. Willians, Phys. Rev. A. 30, 2187 (1984); G. Radons, R. E. Prange, Phys. Rev. Lett. 61, 1691 (1988); for more recent discussions on both Wigner and Husimi functions, see D. Lalovic, D. M. Dacidovic, N. Bijedic, Phys. Rev. A. 46, 1206 (1992).

[49] For a review and excellent references therein, see M. C. Teich, B. E. A. Saleh, Physics Today, 43, 26 (June 1990).

[50] The calculation of the Wigner function is carried out in this case using the wave function that varies in accordance with the time-dependent Schrödinger equation. The results from the both pictures are same, but it is only a matter that the degree of difficulty to solve makes the difference. In his book *Quantum mechanics* (3rd edition, McGraw-Hill, N. Y. 1968), Schiff describes both pictures well. See for more detailed discussions, C. J. Joachain, *Quantum Collision Theory*, 3rd edition, in Ch.13 (part III) (North-Holland, N. Y. 1983).

[51] M. V. Berry, N. L. Balazs, M. Tabor, A. Voros, Annals Phys. 122, 26 (1979); H. J. Korsch, M. V. Berry, Physica 3D, 627 (1981); J. S. Hutchinson, R. E. Wyatt, Phys. Rev. A. 23, 1567 (1981); Chem. Phys. Lett. 72, 378 (1980); G. P. Berman, A. R. Kolovskii, F. M. Izrailev, A. M. Iomin, Chaos, 1(2), 220 (1991).

[52] Results presented in Physics Computing '91 at San Jose. Refer to the supplemental Abstracts of the meeting.

[53] An initial Gaussian wave packet here will not be the ground state, but a linear combinations (completeness) of the eigen-functions if the initial state does not represent the ground state. See ref. 4.

[54] The corresponding classical motion is described by a single classical trajectory in this case, and by the Ehrenfest theorem the exact correspondence is established.

[55] N. D. Cartwright, Physica (Utrecht), **83A**, 210 (1976);
A. K. Rajagopal, Phys. Rev. A. **27**, 558 (1983).

[56] J. J. Henkel, M. Holthaus, Phys. Rev. A. **45**, 1978 (1992).

[57] J. H. Shirley, Phys. Rev. **138B**, 979 (1965).

[58] see for a comprehensive review, M. Tabor, *Chaos and Integrability in Nonlinear Dynamics* (John Wiley & Sons, N. Y. 1989), or
A. J. Lichtenberg, M. A. Lieberman, *Regular and Stochastic Motion* (Springer-Verlag, New York, 1985), p 462.

[59] J. Ford, G. Manteca, G. H. Ristow, Physica D, **50**, 493 (1991).

[60] J. C. Kimball, V. A. Singh, M. D'souza, Phys. Rev. A. **45**, 7065 (1992).

[61] L. Bonci, R. Roncaglia, B. J. West, P. Grigolini, Phys. Rev. A. **45**, 8490 (1992).

[62] See for more recent version of it, G. P. Berman, E. N. Bulgakov, G. M. Zaslavsky, Chaos, **2**, 257 (1992).

TABLE 3.I Data showing initial values for all the cases in this chapter. The initial Gaussian width is σ_G^2, and the Husimi trial function width is σ_H^2.

Figure	Case	q_o	p_o	ω	γ	μ	Δt	σ_G^2	σ_H^2
3.2-3	(a)	0.05	–0.02	2.0	0.2	N/A	0.005	N/A	N/A
	(b)					1.0		0.6	
	(c)					50.0		0.02	
	(d)					200.0		0.005	
3.4-5	(a)	0.05	–0.02	2.0	5.0	N/A	0.005	N/A	N/A
	(b)					1.0		0.6	
	(c)					50.0		0.02	
	(d)					200.0		0.005	
3.7-10	3.9	0.5	0.0	4/3	0.5	20.0	0.0038335	0.05	0.25
	3.10				1.25				
3.12		1.0	0.0	1.0	0.35	40.0	0.0038349	0.025	0.1
3.13		1.0	0.0	1.5	0.5	20.0	0.0051132	0.05	0.1

1

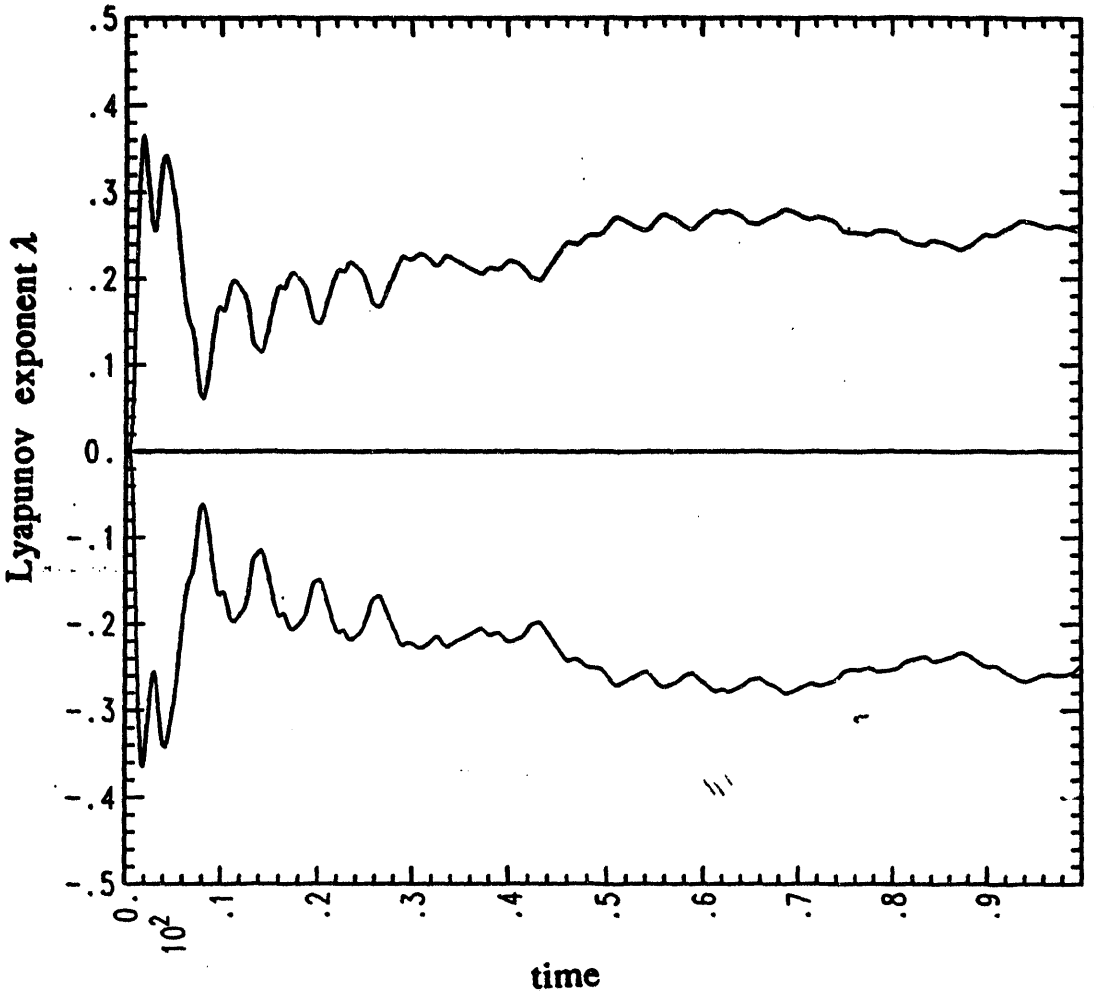

Figure 3.1 Time variations of Lyapunov exponents for the classically regular and the chaotic cases. Eventually, the exponents become stabilized to certain values

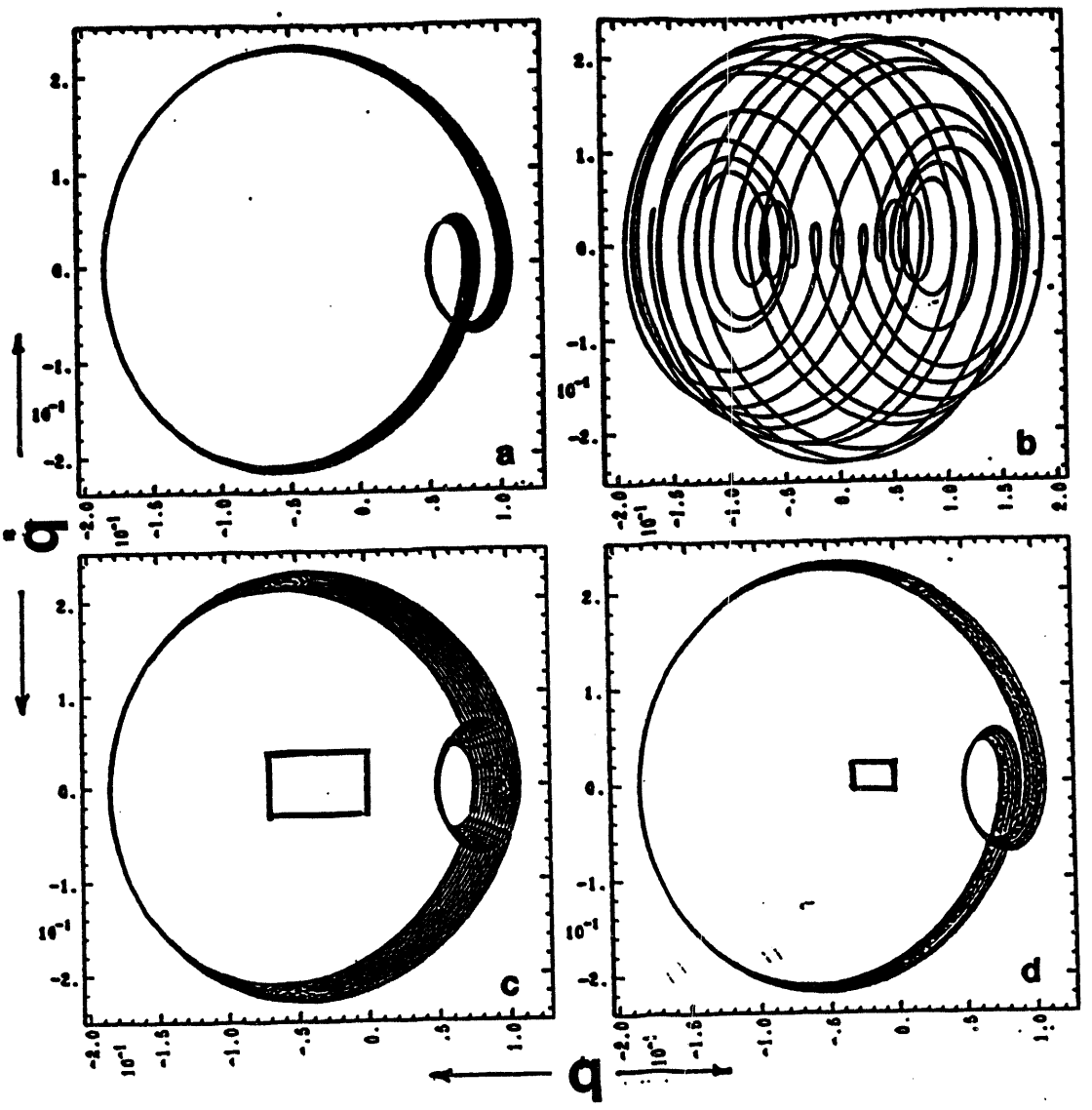

Figure 3.2 Phase-space trajectories in the classically regular regime. (a) classical trajectory (b)-(d) quantum expectation-value trajectories. Notice the better correspondence for larger values of μ. Two rectangles represent the typical uncertainty areas shadowing points on quantum trajectories.

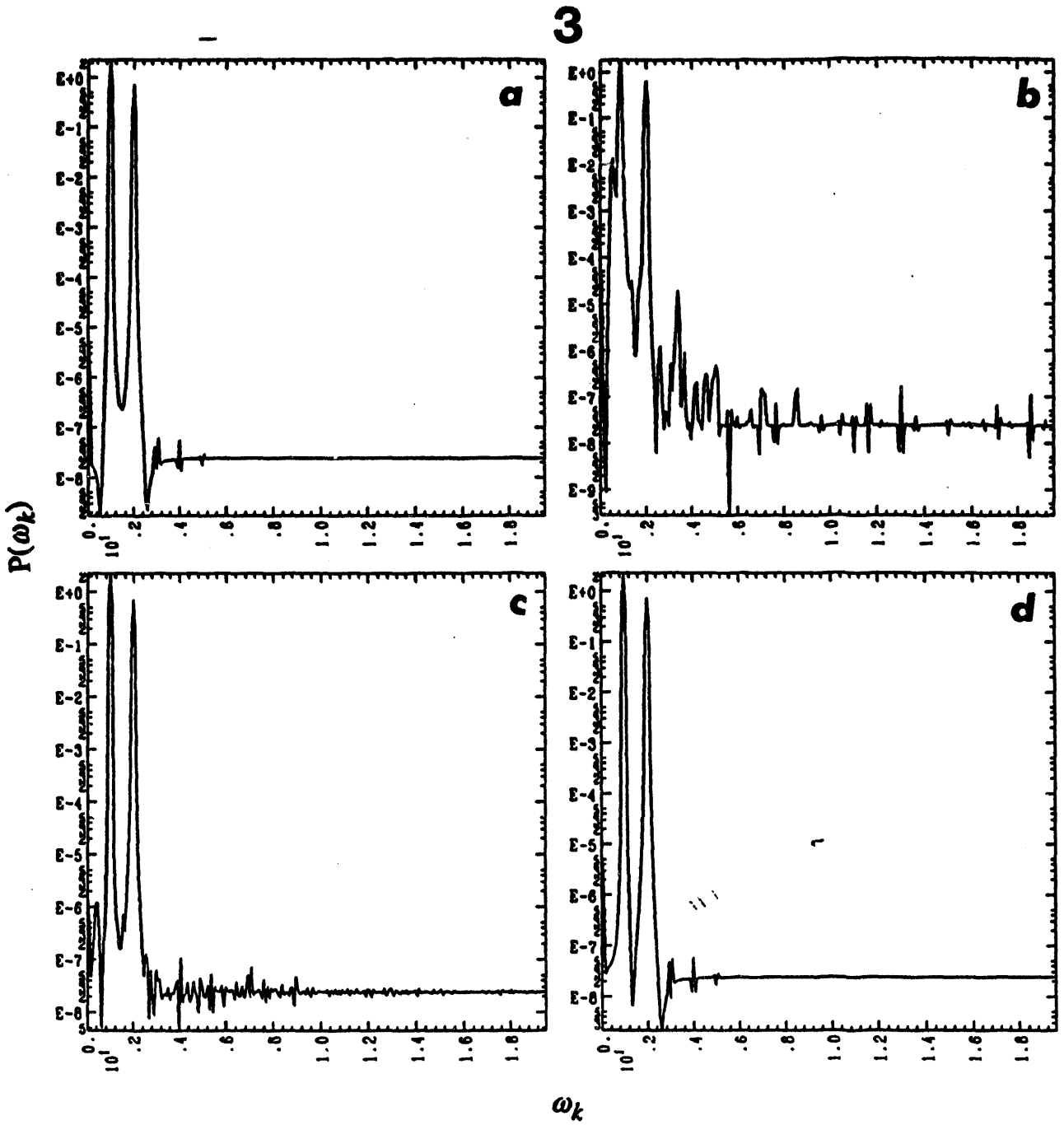

Figure 3.3 The power spectra corresponding to the previous figure. Notice the near-perfect correspondence between (a) and (d).

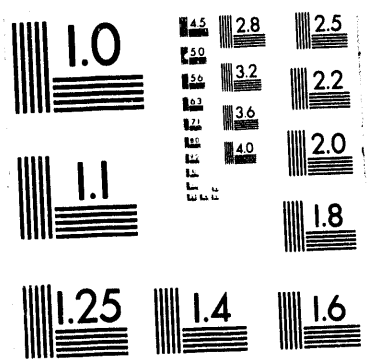
1.0
1.1
1.25
1.4
1.6
2.8
3.2
3.6
4.0
2.5
2.2
2.0
1.8

2 of 3

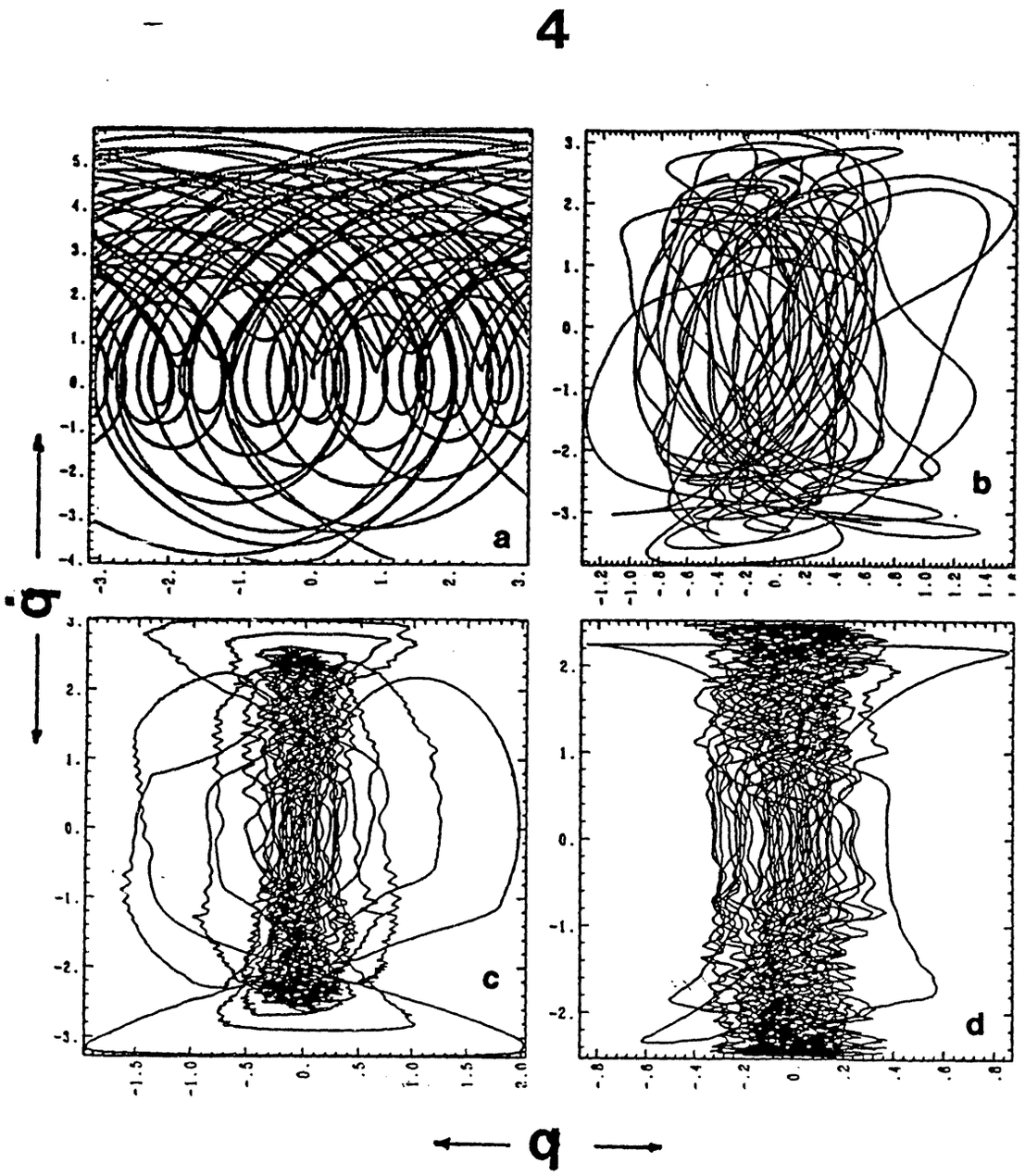

Figure 3.4 Phase-space trajectories in the classically chaotic regime. (a) classical trajectory (b)-(d) quantum expectation-value trajectories. Notice the failed correspondence even for larger values of μ. The more relaxation is clearly observed as μ increases.

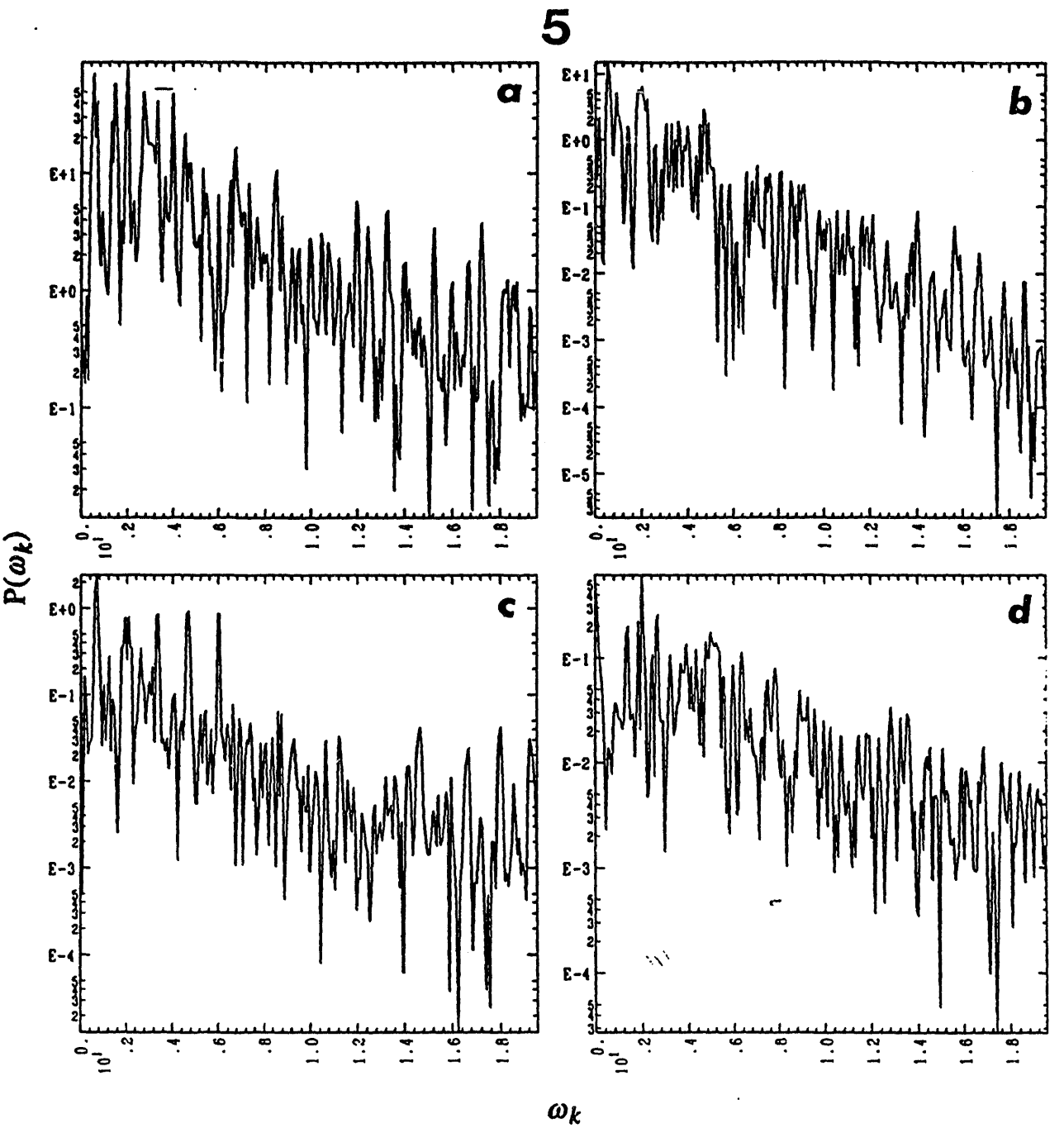

Figure 3.5 The corresponding power spectra to the previous figure. In this case no resemblance to each other can be found.

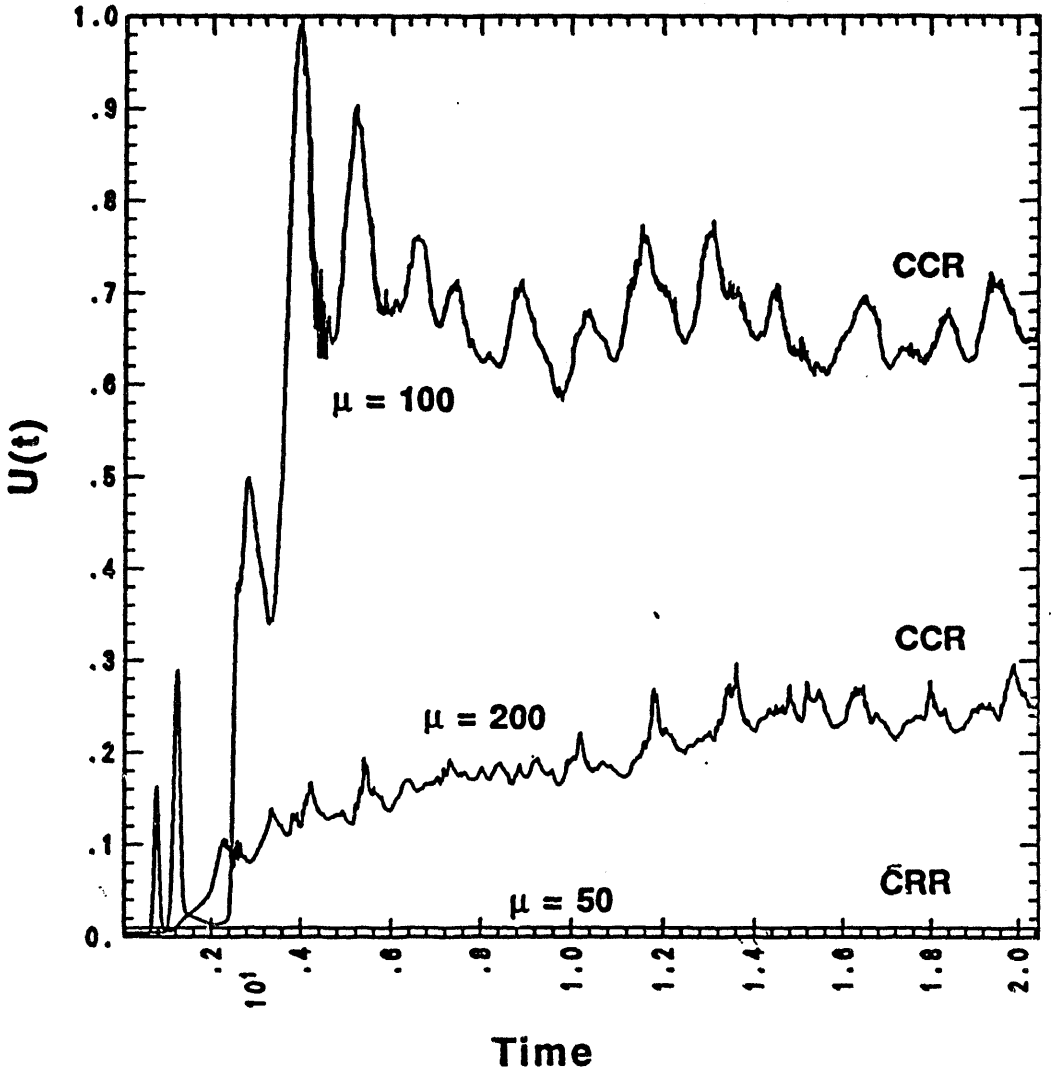

Figure 3.6 Time variations of the uncertainty products (areas). In classically regular regime (CRR), the steady variation is clear, whereas the exponential growth before the saturation can be assumed in classically chaotic regime (CCR). This large fluctuations are believed to be responsible for breaking the correspondence.

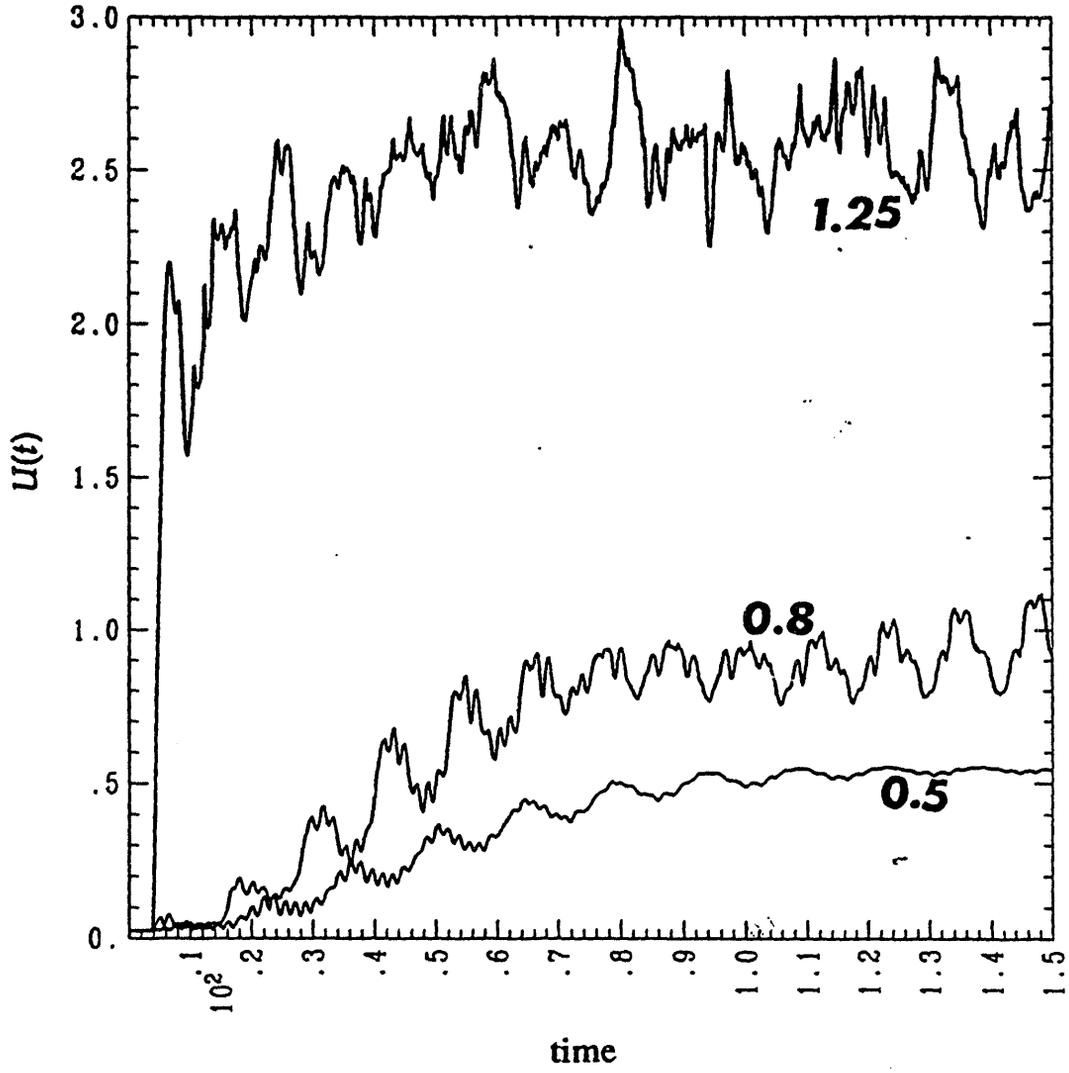

Figure 3.7 The uncertainty products showing cases that will be followed by figures 8-10. The numbers in the figure represent γ. For higher values of γ, the uncertainty grows as it should be.

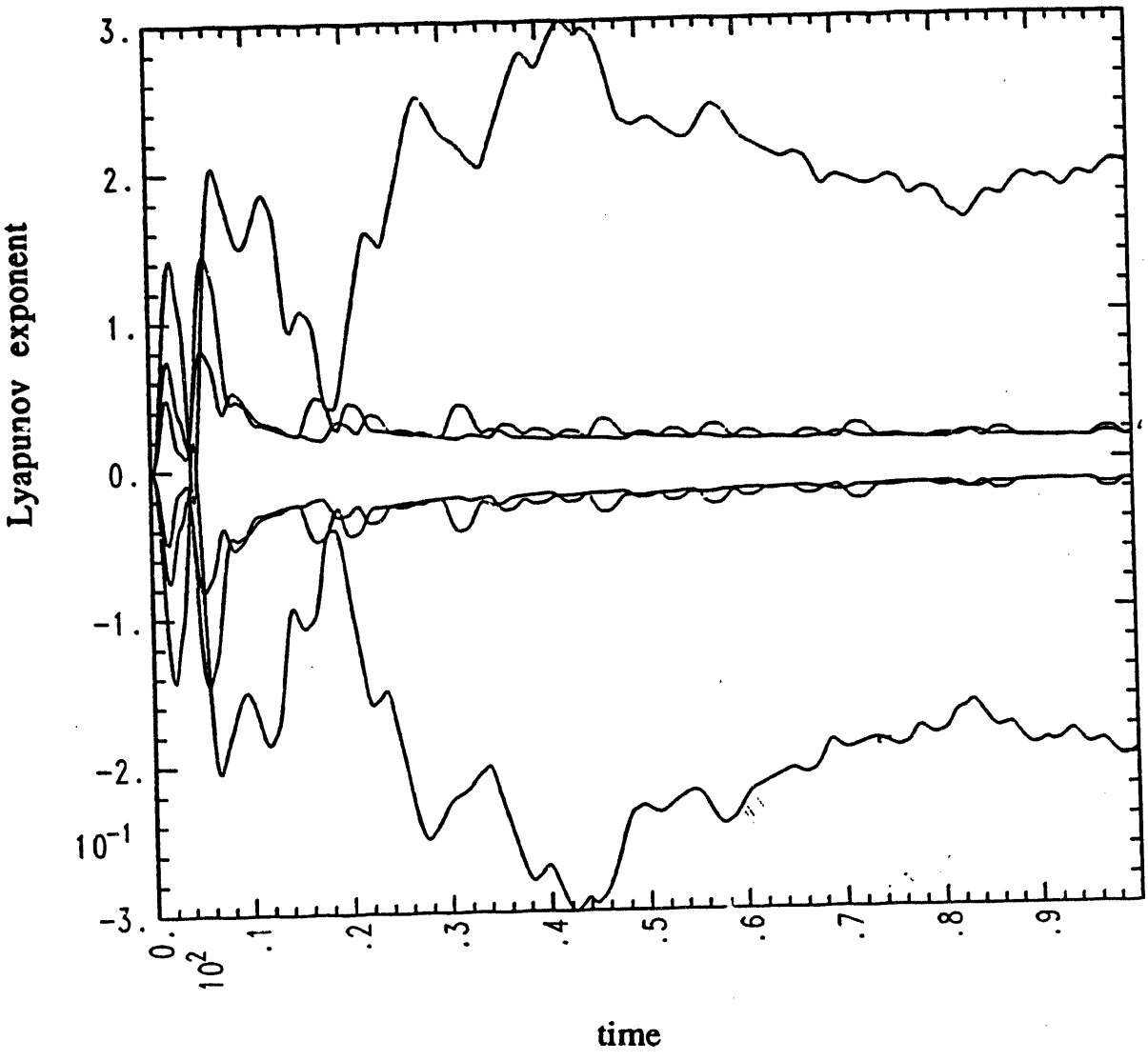

Figure 3.8 Lyapunov exponents showing a similar plot as Fig. 1. A larger positive exponent is found for higher γ.

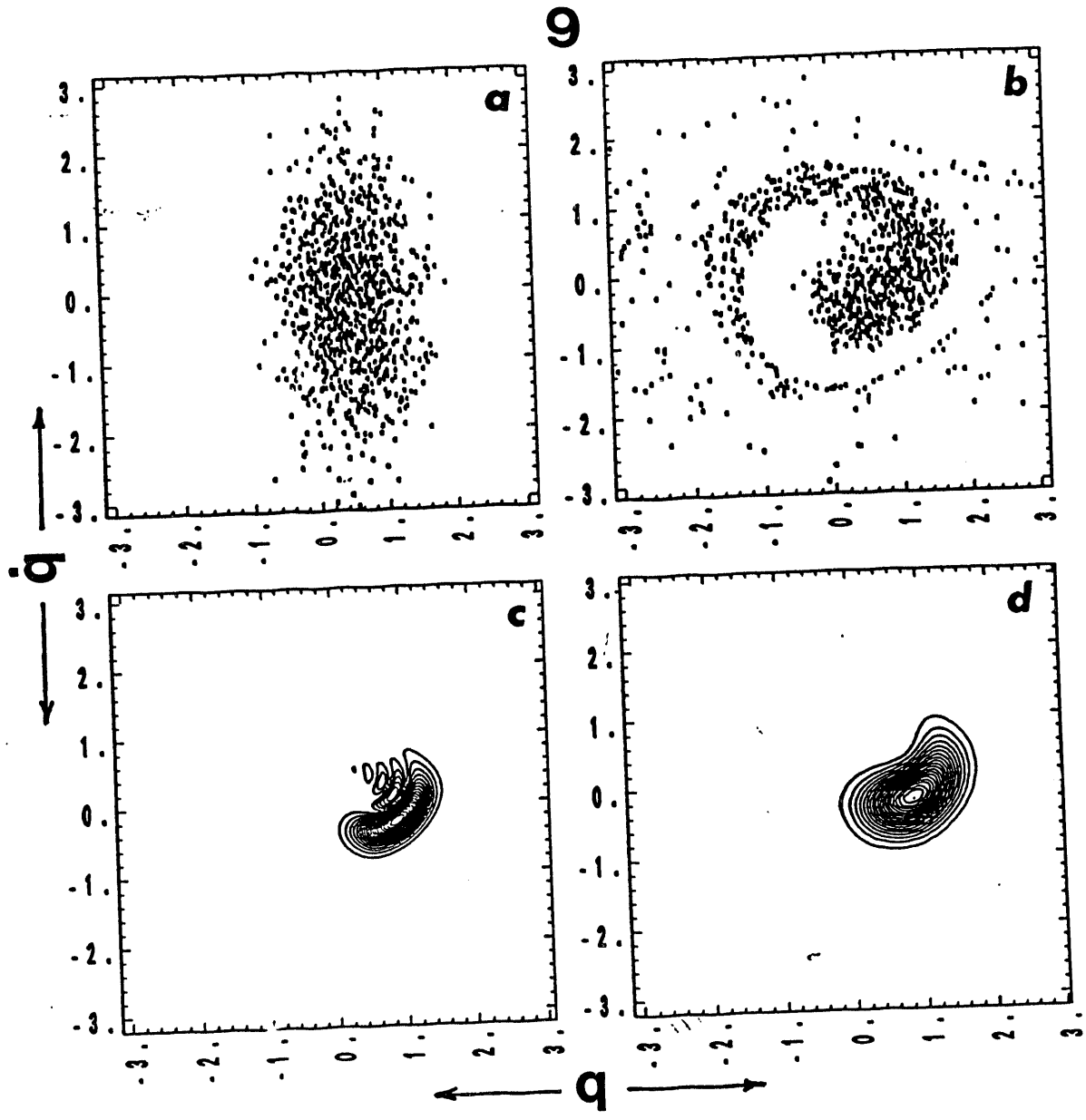

Figure 3.9 Plots of various distributions (a) the initial classical distribution (b) the later classical distribution (c) Wigner distribution (d) Husimi distribution. Notice that (d) is somewhat closer to (b) than (c).

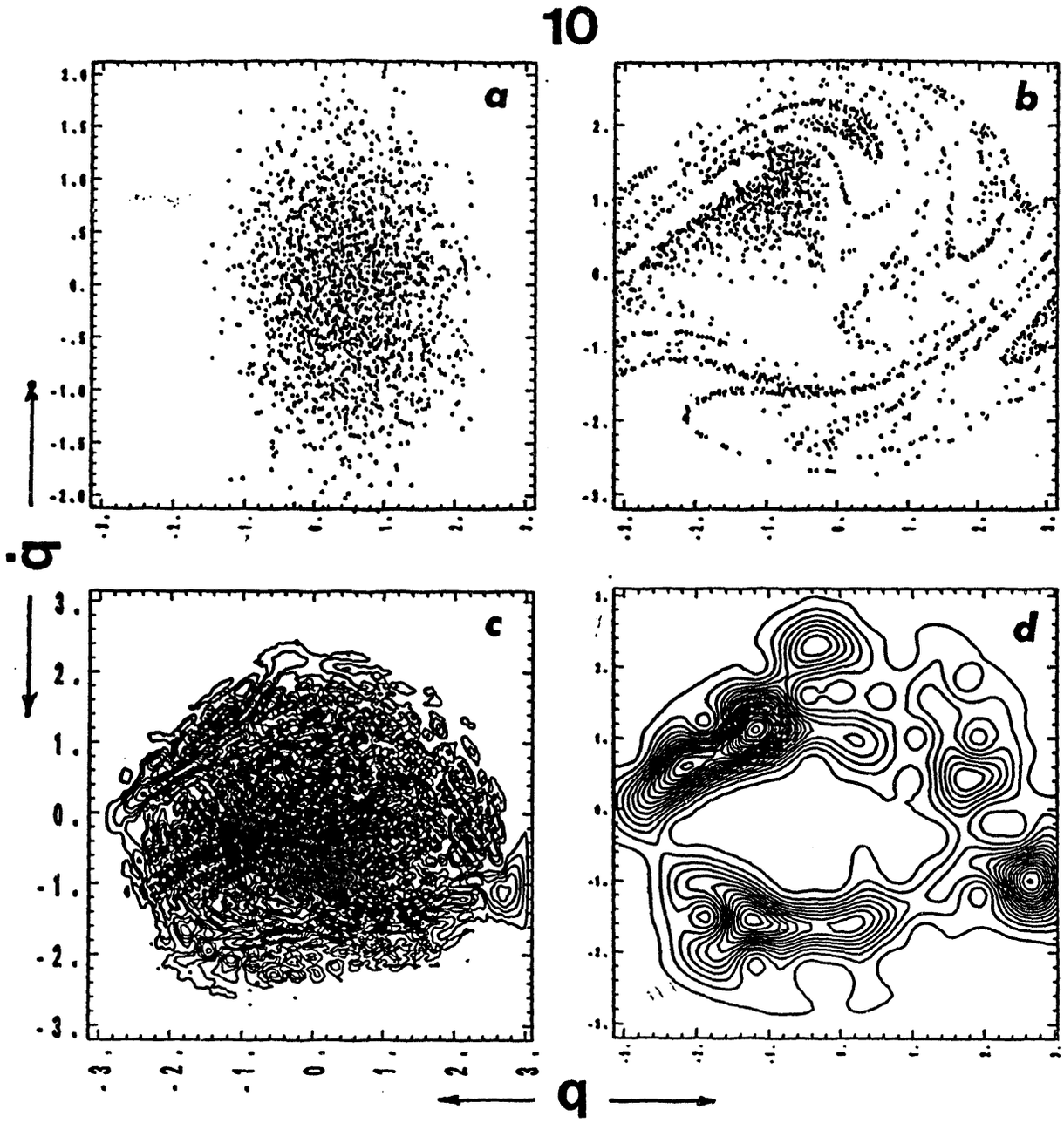

Figure 3.10 The same kind of plot as the previous figure. A larger value of γ is used this time. Clearly, the Husimi representation (d) is better than the Wigner one (c) in this case. The classical distribution (b) is chaotic since it has a large positive Lyapunov exponent as shown in Fig. 3.8.

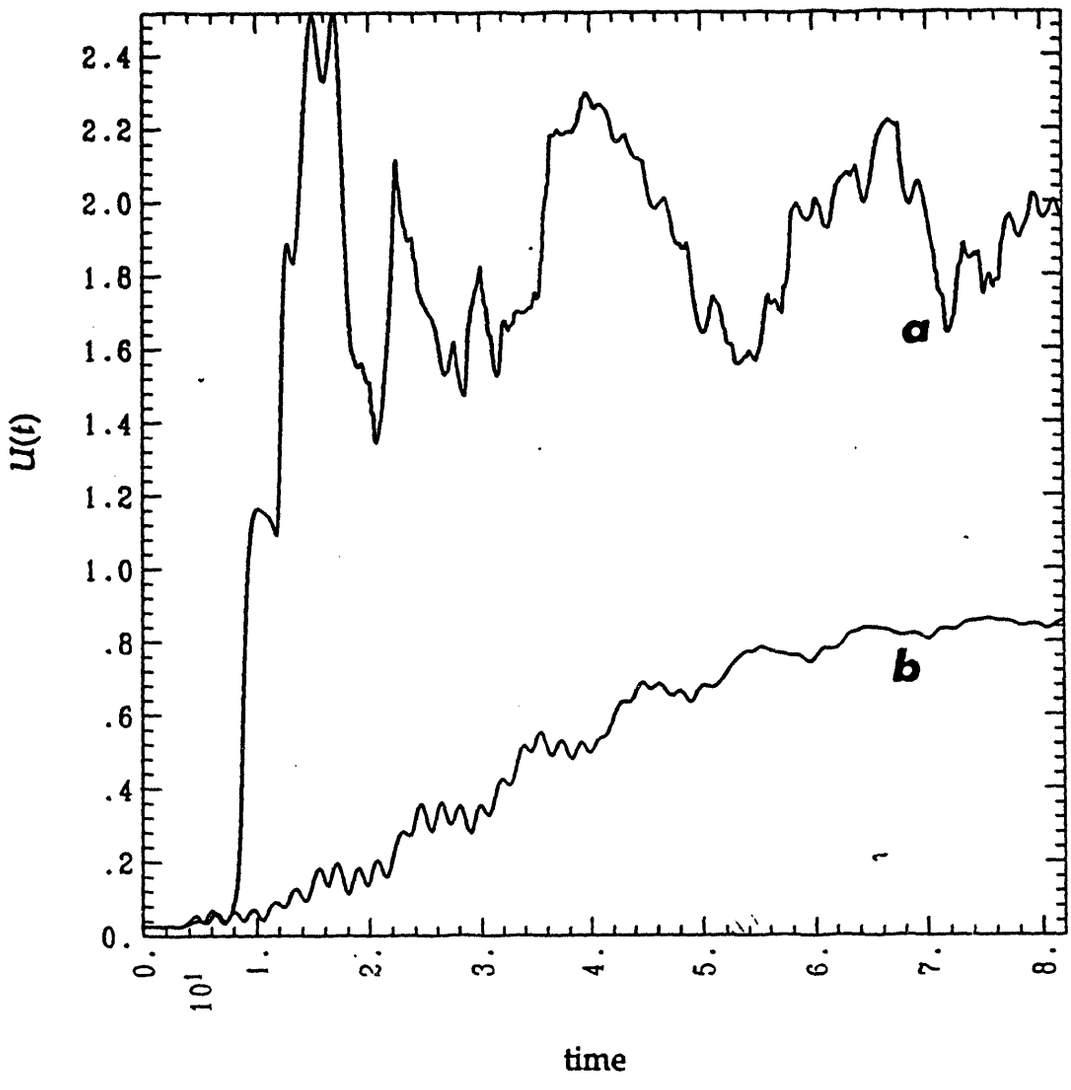

Figure 3.11 The uncertainty products of two more different cases. This suggests the correspondence to be failed due to the growth.

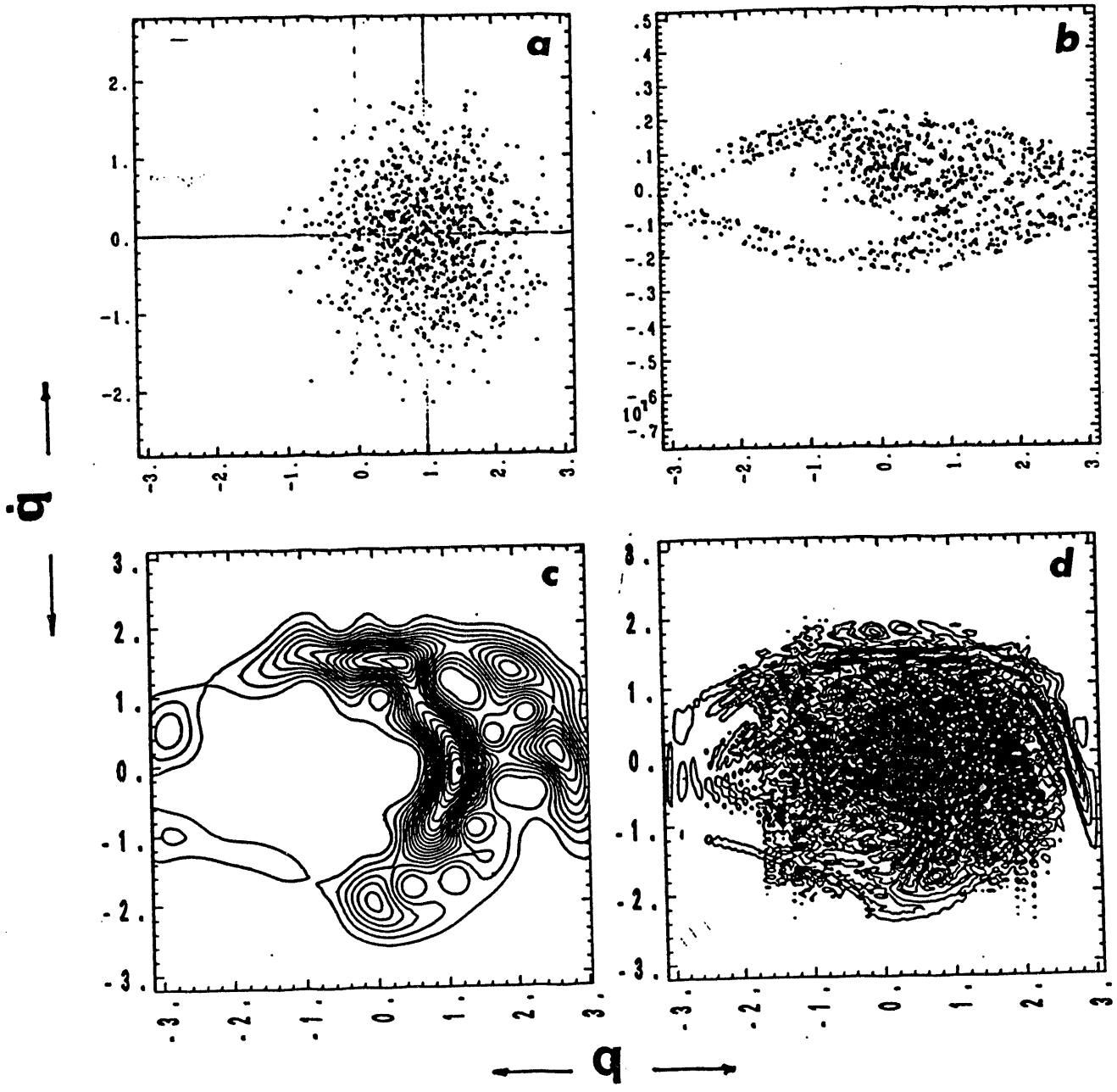

Figure 3.12 The classical distribution later (b) resembles Husimi distribution (c) more than Wigner one (d). This strongly supports the previous findings. However, the elapsed time was within the break time. Note that the Husimi is plotted in (c) and the Wigner in (d).

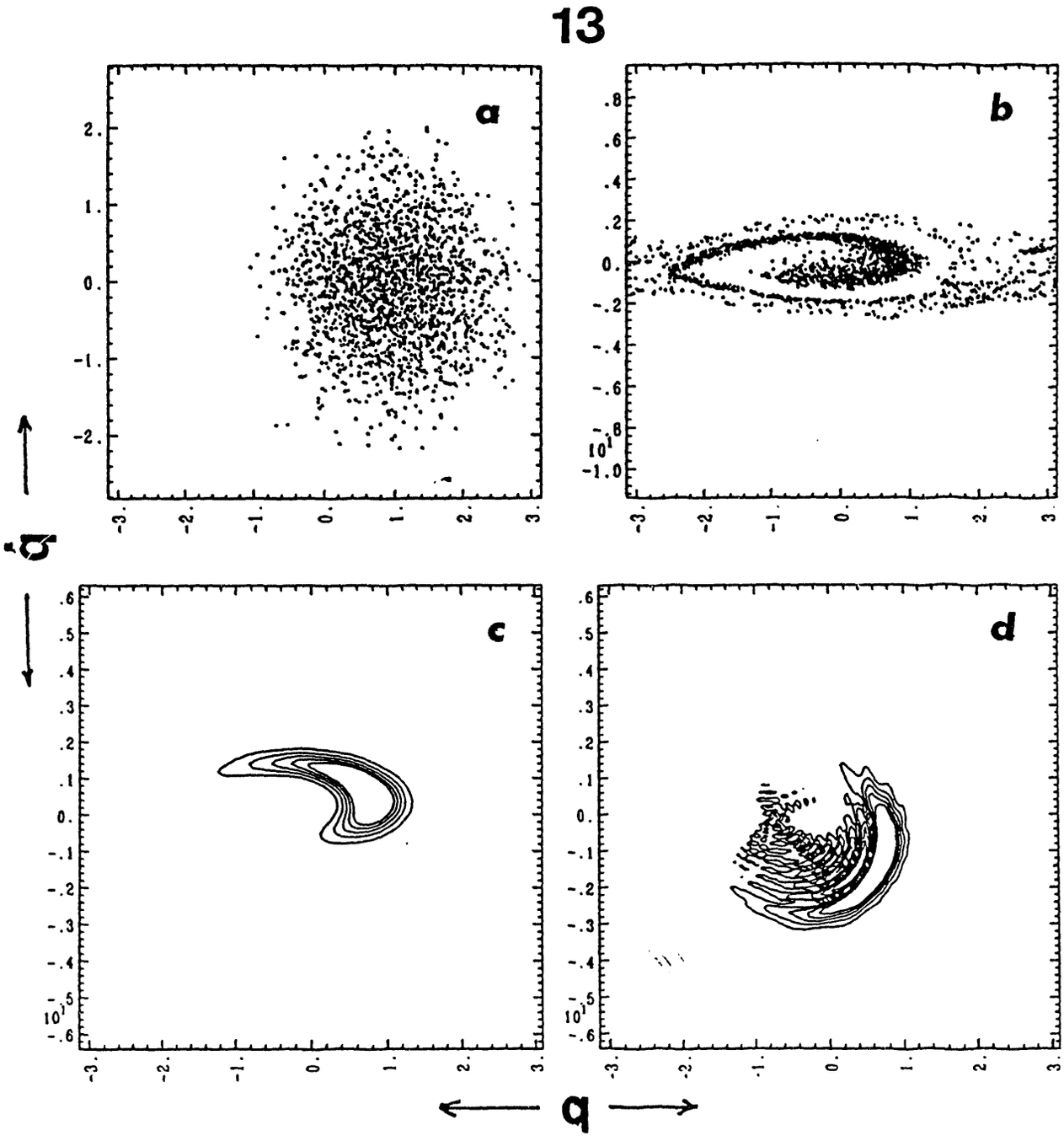

Figure 3.13 Another classically chaotic motions exhibited in (b). The spiral structure in (b) can be found in both (c) and (d), but its orientation is more closer to (c).

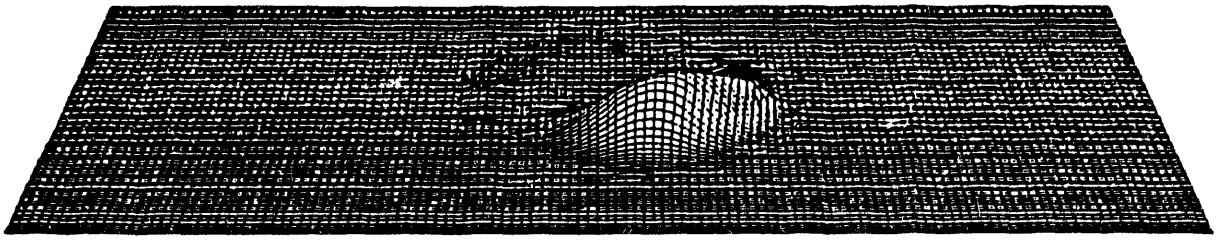

Husimi density function

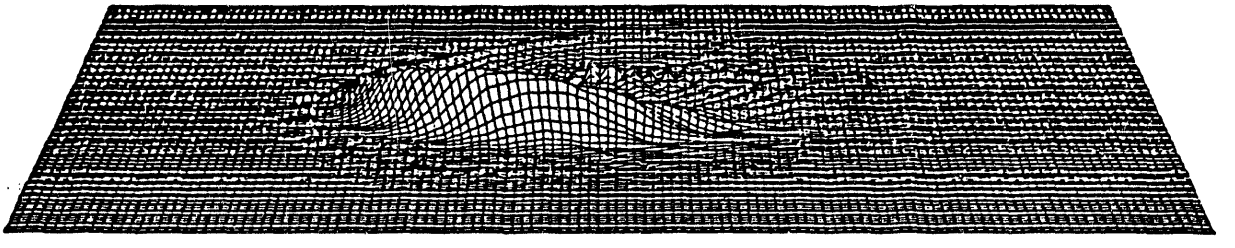

Wigner density function

Figure 3.14 Typical distributions in three dimensional view. Plots shows Husimi and Wigner distributions of the previous cases.

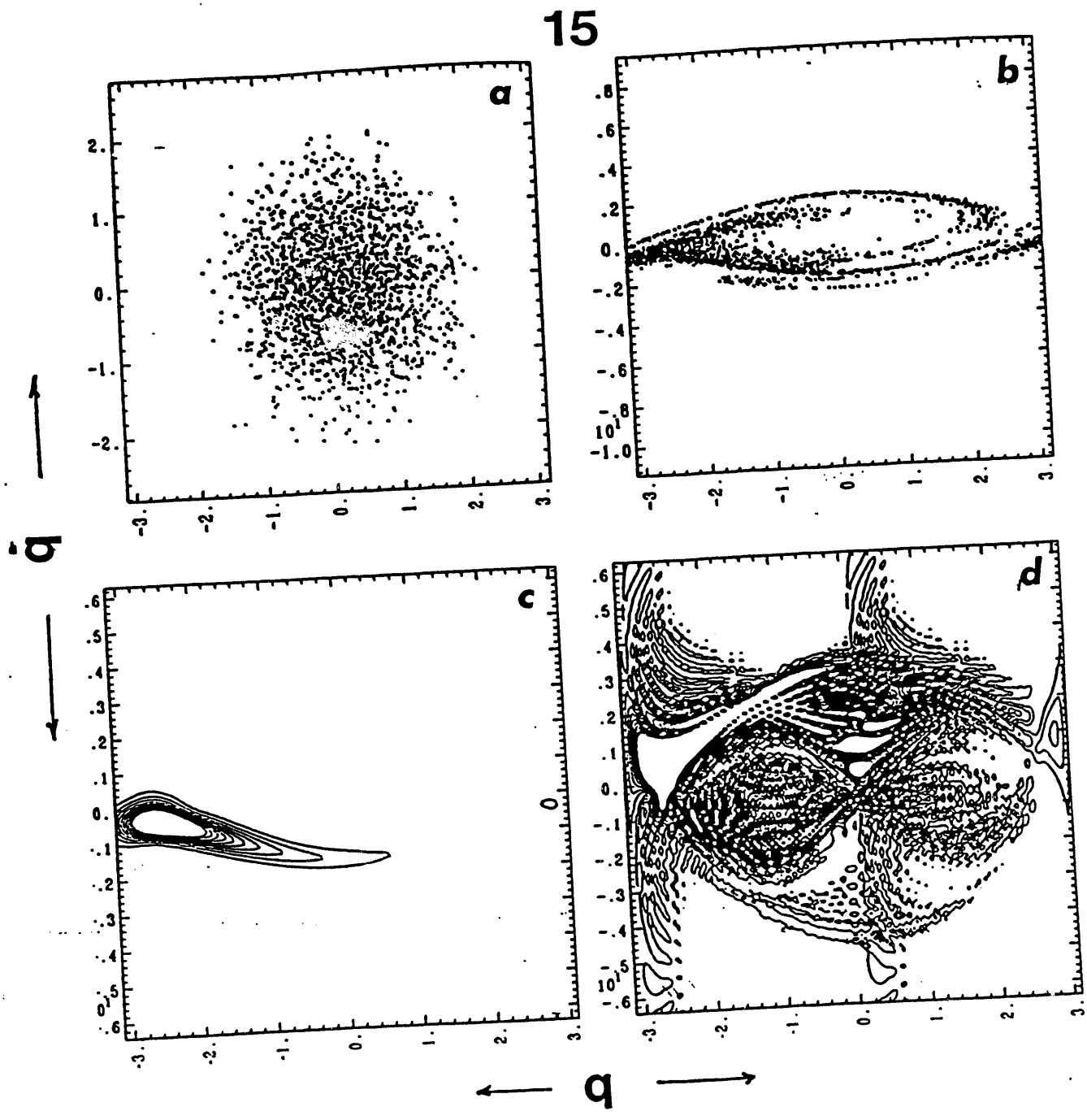

Figure 3.15 More examples in classically chaotic regimes. The overall structure in (b) initially started as in (a) resembles the one in (c). Wigner distribution in this case has somewhat resembled the classical one, but not as good as the Husimi one in (c).

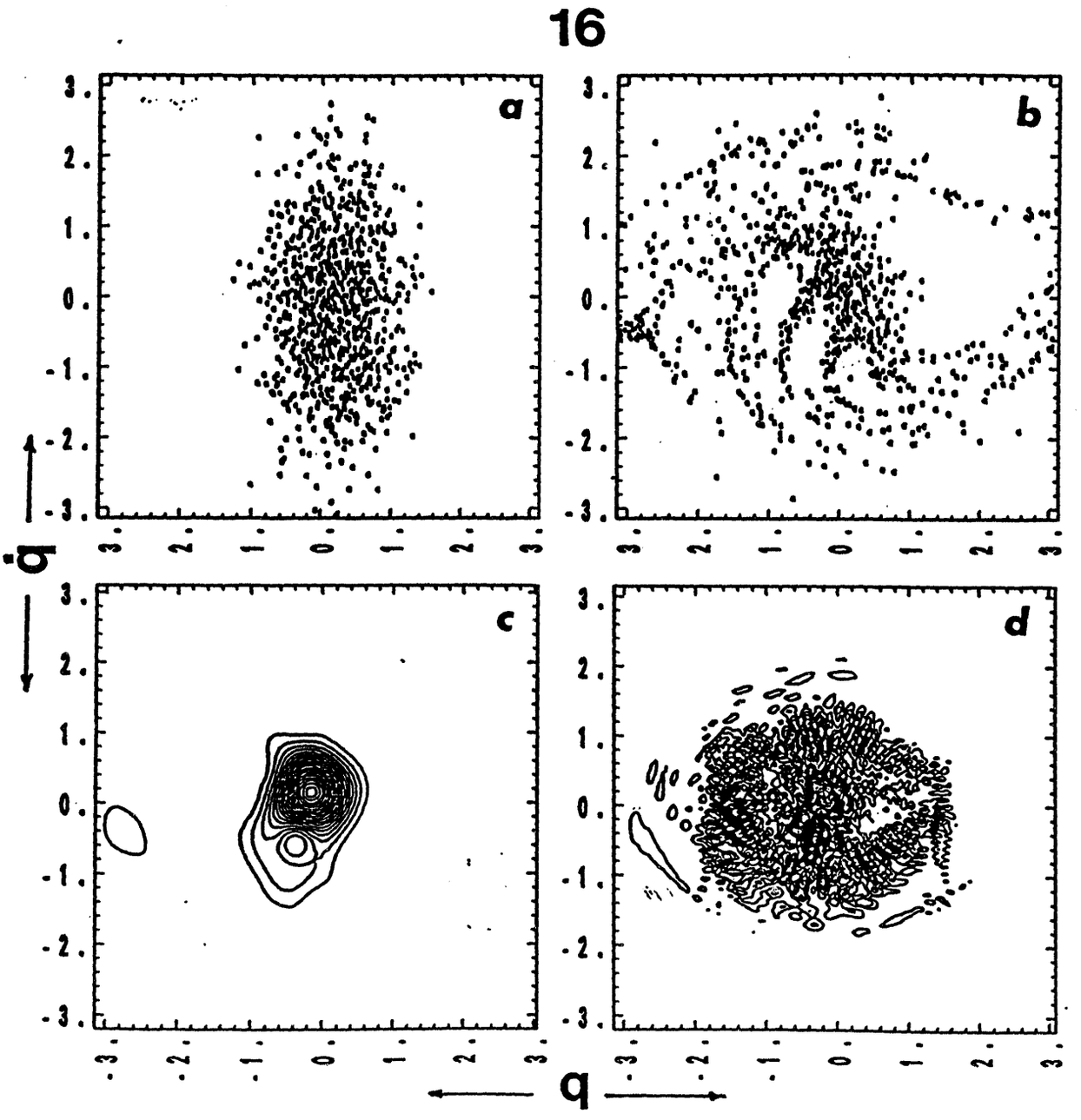

Figure 3.16 Another example showing the Husimi in (c) and the Wigner in (d). The judgment on the correspondence in this case is somewhat difficult.

CHAPTER 4

DISSIPATIVE SYSTEMS

But what could dictate that those laws of physics be 'the' laws of physics?

J. S. Bell's "Speakable and unspeakable in quantum mechanics"

The classical damping mechanism is added to Schrödinger equation regardless of its subtle point on Hermitian nature. The similar phase-space behaviors to the previous chapter are described. The results indicate the quantum damping mechanism resembles very closely classical one in classically regular regime, but fails in classically chaotic regime. This supports the conclusion in Chapter three.

4-1. Introduction

The correspondence principle has been known since the Bohr era. It provides that the dynamics of a system described by classical mechanics should agree with its quantum counterpart in the limit of large quantum numbers. This statement is well supported by Ehrenfest theorem [1] as well. In other words, the quantum mechanical expectation value gives a close representation of the classical variable if the potential energy changes by a negligible amount over the dimensions of a quantum wave packet [2].

However, in many cases classical dynamics contains a phenomenological viscous damping due to friction. It is known to depend on the velocity of a system. This kind of mechanism is not present in quantum mechanics since a micro-system does not experience classical-like friction. In addition, Schrödinger equation describes a thermally isolated system whereas classical equation with dissipation is generally for an open system interacting with its environment [3]. A closed system cannot exchange energy with the outside. Then a question may arise; is there any way to complete the correspondence for systems with the classical damping mechanism? If the statement that quantum mechanics is more fundamental is true, the answer must be positive and we should be able to describe an open system using Schrödinger equation. If so, what kinds of physical interpretations are possible?

In this chapter we are mainly concerned about the first question and trying to answer it. Over the last few decades, many attempts have been made with remarkable contributions to this subject. However, has no theory relating classical viscous dissipation to quantum so far been accepted as universal [4] in the context of correspondence. Recently, for example, the

dissipative tunneling problems have been studied in the Heisenberg picture (Heisenberg equation of motion) [5,6]. But these studies have no classical analogues. Our primary interest is in the direct application of classical damping mechanism to Schrödinger mechanics. To show the correspondence, we use the expectation-value trajectories in phase space by using the description of complex kinetic energy. Direct comparison with classical trajectories would indicate whether the introduction of our scheme to Schrödinger equation is valid or not.

We also review the Kubo-Fox approach that introduces thermally random stochastic potentials into the Hamiltonian description. In particular, we study the Kubo-Fox-Keizer mechanism which gives rise to dissipation by a purely random, Gaussian fluctuation in the Hamiltonian, and compare the advantages and disadvantages of the two approaches.

The Nosé-Hoover approach to quantum dissipation using the concept of nonequilibrium thermodynamics will be discussed and compared with the other two in the next chapter with some numerical examples. But the classical description of this method is reviewed in Sec. 4-2-2. Yet, we extensively use the complex kinetic energy method of quantum dissipation because of the reasons we offer in Sec. 4-3. Briefly, however, the complex kinetic energy approach can be outlined in a few sentences.

In wave optics, it is possible to consider an optical gain or loss by using the complex refractive index (complex potential) in wave equations with an idea of complex energy [7,8]. Then the probability amplitude (intensity) increases or decreases depending on the mechanism of gain or loss, respectively. The quantum mechanical analysis of this using the second quantization theory is also possible [9,10]. Then a similar idea to the complex potential can be adapted for the classical damping mechanism by assuming a

complex kinetic energy term which depends on velocity. We study more on this in Sec. 4-3, but first proceed by looking at the classical dissipation mechanisms.

4-2. Classical dissipation scheme

4-2-1. Lagrange-Rayleigh mechanics

The earlier chapter reveals signatures of quantum chaotic behavior in the semi-classical limit ($\mu \rightarrow \infty$) within the break time. The correspondence to the classical system in the Fourier power spectrum was also checked and verified in the non-dissipative driven pendulum.

In the case of dissipation, the classical motion with dissipation can be represented phenomenologically by a Rayleigh term [11]. Classical equations of motion with n degrees of freedom for a damped particle are described by the following Lagrange equations of motion for the Lagrangian $L = L(q_i, \dot{q}_i, t)$ and the Rayleigh term - we call it Rayleighian $R = R(\dot{q}_i)$.

$$\frac{d}{dt}\left(\frac{\partial L}{\partial \dot{q}_i}\right) - \frac{\partial L}{\partial q_i} + \frac{dR}{d\dot{q}_i} = 0, \qquad (4\text{-}1)$$

where the Rayleigh dissipation term $R(\dot{q}_i) = -\alpha_i [\dot{q}_i]^2$. A positive constant α_i represents the classical damping coefficient with an appropriate scaling.

The same equations of motion can be recovered by Hamilton's equations of motion where the Hamiltonian is expressed as

$$H(q_i, p_i, t) = T(p_i,t) + V(q_i, t) = \sum_{i=1}^{n} p_i \dot{q}_i - L(q_i, \dot{q}_i, t). \qquad (4\text{-}2)$$

Then the Hamilton's equations of motion become

$$\frac{\partial H}{\partial p_i} = \dot{q}_i \quad \text{and} \quad \frac{\partial H}{\partial q_i} - \frac{\partial R}{\partial \dot{q}_i} = -\dot{p}_i \,, \tag{4-3}$$

where in this case $R\,(p_i) = -\beta \dfrac{\mu\,(\dot{q}_i)^2}{2}$, where β is the damping coefficient seen from Sec. 1-2. Therefore, the resisting force due to friction $F_D = -\nabla_{\dot{q}_i} R$ such that $\dot{p}_i = -F_i + (F_D)_i$. We adopt the same concept of dissipation of kinetic energy to quantum mechanics. Note that $\mu\beta = b$, where $\mu = m\,l\sqrt{gl}$ in this classical case.

4-2-2. Nosé-Hoover mechanics

A more general dissipation mechanism than the Lagrange-Rayleigh phenomenological dissipation mechanism described in the previous section can be derived by using Nosé mechanics [12]. This description, discovered by Shúichi Nosé, is an extension of Hamiltonian mechanics.

In Nosé mechanics, the equations of motion in a reversible deterministic form of Hamiltonian mechanics make possible an exact analysis of thermodynamically-irreversible processes. Nosé's dynamical link between microscopic reversibility and macroscopic irreversibility is an important concept in non-equilibrium statistical mechanics. A recent modification of Nose's 1984 results was applied by Hoover to a variety of non-equilibrium problems [13]. Hoover also applied extensions of Nosé's classical idea to dissipative quantum dynamics and quantum statistical mechanics. We will tackle a very simple quantum system in the next chapter using this approach [13,14].

Because the friction coefficient, ς, in this approach corresponds to momentum, the equations of motion are time-reversible. They are given by

$$\begin{aligned} \dot{q} &= \frac{p}{m}, \\ \dot{p} &= -\frac{\partial V(q)}{\partial q} - \varsigma\, p, \\ \dot{\varsigma} &= \sum \left[\frac{p^2}{mkT} - 1 \right] / \tau^2, \end{aligned} \tag{4-4}$$

where the friction coefficient ς is itself determined by temperature-dependent time-reversible equation rather than being a constant number. τ is an arbitrary relaxation time. Here q and p are coordinate and momentum. The friction coefficient increases in those parts of phase space with above average temperature and decrease in those parts where the temperature is below average. This set of equations, can be shown to give the canonical distribution in an ergodic system [13]. In Nosé-Hoover mechanics, the coefficient ς can be either positive or negative depending upon the time history of the kinetic energy. By contrast, a negative friction coefficient cannot occur in Lagrange-Rayleigh mechanics. Many problems have been solved using this approach [13-15].

One of the amazing features in this Nosé-Hoover approach is to characterize strange-attractor fractal nature for nonequilibrium systems. Phase-space fractals are difficult to display in many-body case of nonequilibrium mechanics, but this dynamical approach shows that nonequilibrium phase-space distributions are typically (multi)fractal. This strange geometric objects are often appears in chaotic phenomena.

Moreover, with Nosé-Hoover dynamics, the phase-space deformation of nonlinear dynamics, the heat reservoirs of nonequilibrium molecular

dynamics, and the inexorable entropy increase of irreversible thermodynamics could all be linked together. For instance, the use of a particularly convenient form of heat reservoir, based on the Nosé-Hoover equations of motion (4-4), allows one to visualize the fact that phase-volume growth is impossible in the nonequilibrium steady state, which is equivalent to the macroscopic Second Law of Thermodynamics: *the entropy of the Universe can only increase.* Therefore, this Nosé-Hoover dynamical approach often produces multi-fractal objects obeying the Second Law of Thermodynamics and converting work into heat in multi-dimensional phase-space.

Nonequilibrium systems fundamentally differ from equilibrium systems in energy-transfer mechanisms of heat transfer and performing work. For instance, nonequilibrium systems maintained in stationary states require heat exchange with their surroundings, dissipating and depleting external energy sources. Since most of the state variables for nonequilibrium systems are the same as those used at equilibrium, it is natural to analyze nonequilibrium motions in a generalized phase space, extending or contracting the phase space, if need be, to include any strain rates, fields, or friction coefficients which vary with time and to satisfy any new constraints. But we expect that system variables for nonequilibrium states necessarily include external coordinates, capable of doing work, and external heat reservoirs, capable of exchange heat with selected system degrees of freedom. For more extensive discussions on the subject in this section, readers should consult the two books mentioned in Ref. 13 and references therein.

In the case of our model, with a positive constant friction coefficient, the equations of motion in Eq. (4-4) become those in Eq. (4-3). Therefore, our hydrodynamic drag force can be thought of as a special case resembling Nosé-

Hoover mechanics. Since we are only interested in energy-loss due to the drag force, we will use the Rayleighian in the quantum formulation of energy dissipation.

4-3. Quantum dissipation schemes

4-3-1. Kubo-Fox-Keizer method

Stochastic Liouville Equations first introduced by R. Kubo [16] deal essentially with a perturbation which is considered as a stochastic process. This stochastic process can be either additive or multiplicative. The prototype for the application of additive stochastic processes to physical phenomena is found in the theory of Brownian motion [17-19]. An additive stochastic external force is usually a purely random, stationary, Gaussian driving force. It corresponds with the true molecular force on the heavy particle which is produced by a great quantity of collisions in rapid succession, between the heavy particle and the molecules constituting the fluid. In Langevin equation, for instance, Brownian motion of a heavy particle with mass M and the velocity $v(t)$ in a fluid is described by

$$M\frac{dv(t)}{dt} = -\beta v(t) + \tilde{F}(t), \tag{4-5}$$

where β is the dissipative, friction coefficient, and $\tilde{F}(t)$ is a purely random, stationary, Gaussian driving force.

On the other hand, the multiplicative processes deal with a randomly modulated frequency [19,20] exhibiting dissipative thermal fluctuations. For

example, the length of a pendulum or the spring constant of a harmonic oscillator will fluctuate due to thermal fluctuations in surrounding environment. This gives rise to the fluctuations of the frequency of the oscillator. With the assumption that this frequency fluctuation may be characterized by the same type of a purely random, stationary, Gaussian process whose mean value is zero as in the additive process, it has proved [19] that the average values of the classical variables damp out in time. This dissipative mechanism must be distinguished from a damped oscillation which arises from the additive process in Brownian motion.

Suppose, for example, that the frequency fluctuation is described by the random, stationary Gaussian process, so that a harmonic oscillator can be expressed by the complex variable $a(t)$. Then the equation of motion for the multiplicative process becomes

$$\frac{d}{dt}a(t) = i\left[\omega_o - \tilde{\varphi}(t)\right]a(t), \tag{4-6}$$

where $\tilde{\varphi}(t)$ represents the Gaussian process, and ω_o is the frequency of oscillation. It has been shown rigorously that the average value becomes [19]

$$\frac{d}{dt} < a(t) >= [i\omega_o - \lambda] < a(t) >. \tag{4-7}$$

The constant λ is given in the following expression for the mean square correlation: $< \tilde{\varphi}(t)\tilde{\varphi}(s) >= 2\lambda\ \delta(t-s)$ with $< \tilde{\varphi}(t) >= 0$. The solution to this equation is clearly a damped oscillation. A general N-component real process then satisfies the equation where $\alpha = 1, 2, \ldots, N$,

$$\frac{d}{dt}a_\alpha(t)=\sum_{\alpha'}\left[A_{\alpha\alpha'}+\tilde{A}_{\alpha\alpha'}(t)\right]a_{\alpha'}(t), \qquad (4\text{-}8)$$

where the properties of a matrix $\tilde{A}$ can be written as $<\tilde{A}_{\alpha\alpha'}(t)>=0$ and $<\tilde{A}_{\alpha\beta}(t)\tilde{A}_{\mu\nu}(s)>=2Q_{\alpha\beta\mu\nu}\,\delta(t-s)$, $Q_{\alpha\beta\mu\nu}$ is a tensor with non-negative elements. The matrix representation of Schrödinger equation corresponds with this equation (4-8) by replacing $a(t)$ with the complex N-components $C_\alpha(t)$.

$$i\frac{d}{dt}C_\alpha(t)=\sum_{\alpha'}H_{\alpha\alpha'}C_{\alpha'}(t)+\sum_{\alpha'}\tilde{H}_{\alpha\alpha'}(t)C_{\alpha'}(t)\,. \qquad (4\text{-}9)$$

Both $H_{\alpha\alpha'}$ and $\tilde{H}_{\alpha\alpha'}$ are complex Hermitian matrices. The average value of (4-9) which is the quantum generalization of (4-7) becomes

$$\frac{d}{dt}<C_\alpha(t)>=-i\sum_{\alpha'}H_{\alpha\alpha'}<C_{\alpha'}(t)>+\sum_{\alpha'}\sum_{\beta}Q'_{\alpha\beta\beta\alpha'}<C_{\alpha'}(t)>. \qquad (4\text{-}10)$$

The sum $\sum_\beta Q'_{\alpha\beta\beta\alpha'}$ is Hermitian with nonnegative eigenvalues, and could be recognized as the classical-like friction coefficient. This (4-10) clearly indicates the dissipation of the average value.

In order to review the Hermiticity of this approach, we outline the work of Fox next. It is supposed that the individual states of a highly degenerated energy level in a many body system which is described by a many body Schrödinger equation are coupled by a phenomenological, stochastic coupling Hamiltonian. Therefore, the stochastic Schrödinger equation is

$$i\hbar\frac{\partial}{\partial t}\psi(t)=\tilde{\mathbf{H}}(t)\psi(t)+E\,\psi(t), \qquad (4\text{-}11)$$

where E is the energy of the degenerate level. The density matrix equation corresponding with this equation is

$$i\hbar\frac{\partial}{\partial t}\rho(t)=[\tilde{\mathbf{H}}(t),\rho(t)], \tag{4-12}$$

where is $\rho(t)$ defined by $\rho(t)\equiv|\psi(t)\rangle\langle\psi(t)|$, and the usual commutator relation is assumed. Notice that the Hamiltonian, $\tilde{\mathbf{H}}(t)$, is being taken to be Hermitian so that (4-12) has the form always found for ordinary Hamiltonians of the non-stochastic variety.

For an open system modeled by the stochastic Schrödinger equation to obtain the canonical density matrix in equilibrium, it is necessary to consider a subsystem coupled to a thermal reservoir. A strict phenomenological approach of Kubo-Fox's work describes the full system of reservoir and subsystem as their direct product in the Hilbert space. It is not difficult to justify the density matrix equation in this case in the full Hilbert space from Eq. (4-12). The equation is

$$i\hbar\frac{\partial}{\partial t}\rho(t)=[\tilde{\mathbf{H}}_{\mathbf{S}}\otimes\mathbf{1}_{\mathbf{R}},\rho(t)]+[\mathbf{1}_{\mathbf{S}}\otimes\tilde{\mathbf{H}}_{\mathbf{R}},\rho(t)]+[\tilde{\mathbf{H}}_{\mathbf{I}}(t),\rho(t)], \tag{4-13}$$

in which $\mathbf{1}_{\mathbf{R}}$ and $\mathbf{1}_{\mathbf{S}}$ are identity operators in the reservoir Hilbert space and the subsystem Hilbert space respectively. $\tilde{\mathbf{H}}_{\mathbf{I}}(t)$ is the stochastic interaction Hamiltonian and mixes the factor spaces of the full Hilbert space. The desired quantity is $<\rho(t)>$. Fox showed [19] rigorously using a reservoir of phonons for the thermal reservoir that the final result becomes

$$\frac{\partial}{\partial t}\langle\langle\rho_{\mathbf{S}}(t)\rangle\rangle=-\frac{i}{\hbar}[\tilde{\mathbf{H}}_{\mathbf{S}},\langle\langle\rho_{\mathbf{S}}(t)\rangle\rangle]-\mathbf{R}\langle\langle\rho_{\mathbf{S}}(t)\rangle\rangle, \tag{4-14}$$

where **R** is defined by

$$R_{\mu\nu\mu'\nu'} = \frac{1}{\hbar^2}\sum_k \{(Q^{kk}_{\theta\mu\theta\mu'}\eta_k + Q^{kk^*}_{\mu\theta\mu'\theta}(\eta_k+1))\delta_{\nu\nu'} + (Q^{kk}_{\theta\nu\theta\nu'}\eta_k + Q^{kk^*}_{\nu\theta\nu'\theta}(\eta_k+1))\delta_{\mu\mu'} - 2(Q^{kk}_{\mu\mu'\nu\nu'}(\eta_k+1) + Q^{kk^*}_{\mu\mu'\nu\nu'}\eta_k\} \quad . \tag{4-15}$$

Note that the double averaging $\langle\langle\ \rangle\rangle$ is used. For complete details of the derivations, readers should consult Ref. 4. It is clear the solution for (4-14) contains explicitly the dissipative part. In the special case of magnetic relaxation for a spin half magnetic moment, $\langle\langle\rho_S(t)\rangle\rangle$ is a 2×2 dimensional density operator. Fox has shown [21] for this case that Eq. (4-14) leads to a generalization of the H-theorem using the Helmholtz free energy.

The total probability is conserved on the average by (4-14) because

$$\frac{d}{dt}\mathrm{Trace}(\langle\langle\rho_S(t)\rangle\rangle) = -\frac{i}{\hbar}\mathrm{Trace}([\tilde{\mathbf{H}}_S,\langle\langle\rho_S(t)\rangle\rangle]) - \sum_\mu R_{\mu\nu\mu'\nu'}\langle\langle\rho_S\rangle\rangle_{\mu'\nu'} = -\sum_\mu R_{\mu\nu\mu'\nu'}\langle\langle\rho_S\rangle\rangle_{\mu'\nu'} = 0. \tag{4-16}$$

The second equality follows from the fact that the trace of the commutator of bounded operators is zero. The third equality can be proved by using Eq. (4-15). The equilibrium state corresponding with Eq. (4-14) is the canonical density operator

$$\langle\langle\rho_S(t)\rangle\rangle_{\text{canonical}} = \frac{1}{Z}\exp[-\beta\tilde{\mathbf{H}}_S], \tag{4-17}$$

in which Z is defined by $Z \equiv \mathrm{Trace}_S(\exp[-\beta \tilde{H}_S])$. Therefore, this method provides a useful opportunity in describing quantum systems in which interaction with a reservoir is significant since it preserves the Hermiticity and thus the total probability on the average. We will see that the complex energy approach described in the next section requires a constant artificial renormalization because of a loss of probability in time. However, the *generalized* density matrix defined by the *biorthonormal* Hilbert space [22] yields the conservation of the total probability on the average even as the system is dissipating.

To compare, we briefly present this theory: the generalization of the Feynman-Vernon-Hellwarth geometric representation [23,24] to the non-Hermitian Schrödinger equation. Consider the time-dependent Schrödinger equation,

$$i\hbar \frac{d}{dt}|\psi(t)\rangle = \hat{\mathrm{H}}(t)|\psi(t)\rangle, \tag{4-18}$$

where $\hat{\mathrm{H}}(t) = \hat{H}(t) - i\hat{D}(t)$, and $\hat{H}(t) = \hat{H}_o + H'(t)$. $\hat{H}_o$ is unperturbed Hamiltonian and $H'(t)$ is the perturbation term. $\hat{D}$ is the diagonal damping operator with eigenvalue d : $\hat{D}|\alpha\rangle = d|\alpha\rangle$ [25,26], where α is an eigenstate. So d can represent, for example, the spontaneous decay rate of level $|\alpha\rangle$. The conventional way to construct the density matrix yields the Liouville equation of the following form [27]:

$$\frac{\partial}{\partial t}\langle\langle\rho(t)\rangle\rangle = -\frac{i}{\hbar}[\hat{H}(t), \langle\langle\rho(t)\rangle\rangle]_- - \frac{1}{\hbar}\{\hat{D}, \langle\langle\rho(t)\rangle\rangle\}_+, \tag{4-19}$$

where $[A, B]_- = AB - BA$ and $\{A, B\}_+ = AB + BA$. Note the similarity between Eqs. (4-19) and (4-14). In other words, Eq. (4-19) also gives rise to dissipation.

However, due to the dissipative term, $\{\hat{D},\langle\langle\rho(t)\rangle\rangle\}_+$, the density matrix does not have a conserved norm and its trace. Trace($\langle\langle\rho(t)\rangle\rangle$) is decreasing in time. This causes difficulty in the description of the geometric phase as the density matrix is required to return to its initial value after a cyclic evolution of the system [28].

To avoid the difficulty, the following *generalized* density matrix has been considered:

$$\rho(t) = |\psi(t)\rangle\langle\chi(t)|, \tag{4-20}$$

defined by the *biorthonormal* Hilbert space. Here $\langle\chi(t)|$ is the solution of the Schrödinger equation with the adjoint Hamiltonian, $\hat{H}^+(t)$,

$$i\hbar\frac{\partial}{\partial t}|\chi(t)\rangle = \hat{H}^+(t)|\chi(t)\rangle. \tag{4-21}$$

The density matrix in (4-20) leads to the Liouville equation:

$$\frac{\partial}{\partial t}\langle\langle\rho(t)\rangle\rangle = -\frac{i}{\hbar}[\hat{H}^+(t),\langle\langle\rho(t)\rangle\rangle]_-, \tag{4-22}$$

the form of which is identical to the ordinary Liouville equation without dissipation. Further, in the biorthonormal Hilbert space, one has

$$\frac{\partial}{\partial t}\text{Trace}\langle\langle\rho(t)\rangle\rangle = \frac{\partial}{\partial t}\langle\chi(t)|\psi(t)\rangle = \frac{\partial}{\partial t}\langle\chi(0)|\psi(0)\rangle = 0\,. \tag{4-23}$$

So the total probability is conserved on the average, and this result is the same as (4-16). But this approach does not use the conventional density matrix and the normal Hilbert space. To overcome this subtlety, the Kubo-Fox

approach should be used. However, even though it does not satisfy the correct mathematical requirement in the formulation, not only the numerically equivalent, but much simpler treatment is also used in the next section in the Schrödinger's approach, in which the density matrix formulation is not necessary in our model since the model system deals with an one-dimensional pure state.

Therefore, Kubo-Fox method provides a completely valid description of quantum dissipative mechanism, whereas the later method uses an abnormal density matrix formulation more widely adapted in the field of quantum optics. Strictly speaking, the Kubo-Fox method is appropriate, but since our focus is not on the formulation of quantum dissipative mechanism, the later approach seems to be fitted. Moreover, since we are only concerned with the average values (expectation values) of classical observables to be damped out in time, we may take an *ad hoc*, bias version of the later approach. As mentioned, it is not even necessary for our model to be formulated in the density matrix representation, so we simply perform an artificial normalization. Still, we give extensive study of this empirical approach in which the possible physical background is provided. In summary, the choice is heavily weighed on the numerical preference rather than either on the physical significance or on the appropriate interpretation of the situation. It is safe to say that the two methods reviewed here would be more difficult to carry out numerically. At the same time, the author should warn the readers that there has not been enough theoretical background of the method chosen in the next section to be justified yet. The complex energy approach in the next section is somewhat closer to the generalized density matrix formulation theoretically, though it uses the Schrödinger momentum representation.

In contrast to the fact that the Schrödinger mechanics should always be time-reversible, Eqs. (4-14) and (4-22) are in general not time-reversible. In this context, our choice in the next section seems to be more appropriate. Nonetheless, this could well be an extensive topic for another kind of research.

It is edifying in my opinion to many readers to consider some of fluctuation properties [29] that are usually introduced through various parameters. These parameters are either dependent or independent of the system and the system state. We are not interested in studying the type of fluctuation term that is simply added to the deterministic equations in mathematical modeling. We are interested in *intrinsic* fluctuation. Both additive and multiplicative approaches provide the fluctuation-dissipation relation [30] which has a considerable effect on macroscopic variables. This macroscopic change of intrinsic fluctuations in a macrovariable systems has also exhibited surprising generality that just about any type of nonlinear transport process in a macroscopic system falls within the scope of a phenomenological theory of nonequilibrium thermodynamic fluctuations, as described by master equations [31]. This theory has widely been promulgated by J. Keizer [32], and has been applied successfully to many systems as diverse as chemical, hydrodynamic, electronic, and quantum. Additionally, the Kubo-Fox approach to fluctuations in macrovariable systems was unified with this Keizer's theory of fluctuations using the master equation [33].

Keizer's theory is phenomenological because it is based upon three postulates which Keizer formulated after he had made a detailed study of many transport processes such as chemical reactions, diffusion, electrode kinetics, heat transport and thermionic emission, etc [34]. The structure of the theory follows from three postulates which characterize the stochastic

properties of the transport processes. The macrovariables M_i are thought of in terms of a *deterministic* portion u_i and a fluctuating deviation v_i related to each other by

$$M_i = u_i + v_i \,, \tag{4-24}$$

where i=1, 2,..., N. The rate of change of u_i is given by the macroscopic transport law which is determined empirically. The theory describes that in many different cases these transport laws may always be expressed in terms of *elementary processes*. Associated with each elementary process is a forward rate V^+ and a backward rate V^-, where the system is characterized by a *largeness* parameter V which is often the volume in concrete situations. The rate of change in V is function of all the v's. During a certain elementary process, u_i changes by a microscopic amount ω_i in the forward direction, and by $-\omega_i$ in the backward direction. Keizer's ansatzes are

$$\text{(I)} \qquad \frac{d}{dt}u_i = \sum_{k=1}^{m} \omega_{ki}(V_k^+ - V_k^-); \tag{4-25}$$

where there are m elementary processes, and

$$\text{(II)} \qquad \frac{d}{dt}v_i = \sum_{k=1}^{N} H_{ik}(t)v_k + \tilde{g}_i(t); \tag{4-26}$$

where $H_{ik}(t) = \dfrac{\partial}{\partial v_k}\sum_{j=1}^{m} \omega_{ji}\left\{V_j^+(v) - V_j^-(v)\right\}$, and $\tilde{g}_i(t)$ is a stochastic Gaussian force with zero mean and correlation formula $<\tilde{g}_i(t)\tilde{g}_j(s)>= \gamma_{ij}(t)\delta(t-s)$. Also,

$$\text{(III)} \quad \gamma_{ij}(t) = \sum_{k=1}^{m} \omega_{ki}\left\{V_k^+(v) + V_k^-(v)\right\}\omega_{kj}. \tag{4-27}$$

These postulates provide a closed description because the deterministic portions of macrovariable are determined by Eq. (4-25) alone, and both H and γ are determined directly from the deterministic portions. The fluctuations satisfy a nonstationary but linear Langevin description.

Since this Keizer's formulation, numerous investigators have concluded that fluctuations in macroscopic variables - such as the mass, momentum, and internal energy densities used in hydrodynamics - satisfy Langevin-type equations obtained by linearization around the usual phenomenological macrovariable equations. The so-called Langevin equation approach is a useful method for dealing with a stochastic process, and it corresponds to a Markovian Gaussian process with Gaussian white noise which generally has to be nonstationary. Also, its noise power depends on the state of the system [34]. It is now widely appreciated that a complete macroscopic description of the stochastic dissipative process must include the deterministic macroscopic variables as well as the microscopic fluctuations, both of which reflect underlying microscopic dynamics [35-37]. However, while Langevin-type equation approach successfully describe a variety of physical and chemical phenomena for both stationary and nonstationary states, another important numerical work by Keizer suggests that this approach breaks down on chaotic attractors [38]. In the regard that the Kubo-Fox-Keizer [39] description of macroscopically chaotic and dissipative process is phenomenological and, in general, thermodynamically nonequilibrium, this approach is irreversible. The master equation is also irreversible. We

will come back to this soon. Nevertheless, we look at the relation between chaotic dynamics and the growth of intrinsic fluctuations first.

The macrovariables refer to the microscopic composition of real physical systems that are otherwise described by macrovariable equations. The macrovariables refer to macroscopic amounts of matter and, therefore, represent some sort of averaging over an underlying microscopic, or perhaps mesoscopic description. Consequently, associated with each macrovariable is an intrinsic fluctuation of microscopic origin. Frequently, these fluctuations are ignored and only the macrovariables are studied. However, light scattering [40] from a hydrodynamic system can be accounted for quantitatively only by working out the dynamics of the fluctuations as well as the macrovariables. Especially for chaotic macrovariable dynamics, it has been shown [39] that the intrinsic microfluctuations are amplified to macroscopic size so that the macrovariable description might be markedly modified. This large-scale intrinsic fluctuations amplified by chaotic trajectories in macrovariable physical systems may be linked together with the quantum uncertainty growth in the chaotic regime as we have seen in the previous chapter.

To be specific, a quantitative characterization of chaos is provided by the largest Lyapunov exponent, which when positive, implies chaos. The computation of the largest Lyapunov exponent directly utilizes the instantaneous values of the Jacobi matrix. Similarly, the growth of the intrinsic fluctuations is made quantitative by following the time evolution of the covariance matrix. In fact, it is well known [35,36] that the stochastic differential equations produce a nonstationary, Gaussian conditional probability distribution with vanishing mean and covariance $N \times N$ matrix $\mathbf{C}$, defined in general for a given N-component $\mathbf{X}$ by

$$\mathbf{C} = \begin{bmatrix} \langle \delta X_1 \, \delta X_1 \rangle & \langle \delta X_1 \, \delta X_2 \rangle & \cdots & \langle \delta X_1 \, \delta X_N \rangle \\ \langle \delta X_2 \, \delta X_1 \rangle & & & \\ \vdots & & \ddots & \\ \langle \delta X_N \, \delta X_1 \rangle & & & \langle \delta X_N \, \delta X_N \rangle \end{bmatrix}, \tag{4-28}$$

which solves the equation

$$\frac{d\,\mathbf{C}}{dt} = \mathbf{J}\mathbf{C} + \mathbf{C}\mathbf{J}^{+} + \Gamma \tag{4-29}$$

and in which Γ is the matrix of correlation coefficients for the fluctuating forces in the associated fluctuation equations for the given equations of a system. The Jacobian matrix of coefficients is J, which couples the given equations to the associated fluctuation equations. The solution of Eq. (4-29) is easily generated numerically using the conditional average solution obtained from the given equations. Then the largest Lyapunov exponent for this dynamics λ is given by

$$\lambda = \lim_{n\to\infty} \frac{1}{2n} \ln\left\{\mathrm{Tr}[\mathbf{J}^{+}(n)\mathbf{J}(n)]\right\}, \tag{4-30}$$

where n is the number of iterations. It should be noted that a recent study [38] of molecular fluctuations on the description of chaos by macrovariable equations using the Lorenz model shows that the exponential divergence of the covariance matrix, C for dissipative macrovariable fluctuations on a chaotic attractor is a general property of the usual fluctuation theories in the thermodynamic limit [35,36,38]. Indeed, chaotic dynamics can cause macroscopic growth of intrinsic fluctuations in a macrovariable system. If the

initial intrinsic noise level is n_0 and the largest Lyapunov exponent is λ, then the time, t, required for the noise level to reach n at t is of the order of

$$t = \frac{1}{\lambda} \ln\left[\frac{n}{n_0}\right]. \tag{4-31}$$

Generally, the significance of this amplification of intrinsic noise will be determined by a numerical simulation of model equations. This study also emphasize that this results refers only to macroscopic systems for which the dynamical processes are dissipative. However, in regard to the connection to the amplification of the quantum uncertainty, this could well be the solution. For more details, see Ref. 39.

As we have mentioned earlier, the KFK (Kubo-Fox-Keizer) method describes the irreversible behavior of a system. It is thus quite unlike the detailed microscopic equations of motion, e.g., the Schrödinger equation, which provide a description which is invariant under time-reversal. The methods we will tackle in the next section along with the Hoover's approach to quantum mechanical nonequilibrium case in Ch. 5 are time-reversible and based on the Schrödinger mechanics. It seems that one clear advantage using the KFK approach would be to make more physical sense in the context of understanding of the dissipative effects which lead to decrease of energy in many systems of interests because it is mathematically correct. Quantum mechanically, this dissipation effect is caused by the fluctuation that is capable of inducing transitions between the various unperturbed states. Another advantage of using KFK method would be its wide applicability to many physical systems. Unfortunately, the numerical method of the split operator scheme that is our prime tool in this thesis cannot be extended to this

approach. Moreover, initially our intention was to preserve the time-reversibility of Schrödinger equation. So it is a methodological question than the philosophical one as to which method we choose. It is also to try numerically empirical version of complex energy approach since its concept is widely used in wave optics and easier to apply whenever the type of Schrödinger equation is involved. This complex energy approach practically provides the same degree of difficult in solving the usual equilibrium Schrödinger equation.

4-3-2. Complex kinetic energy method

In the quantum counterpart of classical damping due to friction, it is not clear as to whether or not an equivalent Rayleigh dissipation term in the classical Lagrangian formulation is valid without introducing the kind of fluctuation discussed in the previous section. It could not be valid, but at the same time, it could be appropriate to assume that the damping mechanism in the context of correspondence may be in conjunction with the kinetic energy as the classical Rayleigh term represents. In general, a classical damped oscillator radiates heat so that the amplitude of its oscillation decreases in time. Moreover, as we have seen in the previous sections it is frequently assumed that this heat loss due to friction is a quadratic function of the velocity of a system (or perhaps of some higher time derivatives of the velocity). In this section, we presume that the quantum dissipation mechanism could be in association with the decrease of kinetic energy of the

corresponding classical one. Studies using the many-body treatment with a heat bath [3] will be considered in Ch. 5.

Contrary to the classical description, Schrödinger equation describes only thermally-isolated systems. Generally speaking, the possible, non-stochastic mechanism for dissipation of energy in this quantum mechanical isolated system is wave function tunneling mechanism. In other words, an isolated quantum system described by Schrödinger equation loses energy by decrease of the *relative* probability. The *relative* probability here means the probability compared to the previous one whereas the *absolute* probability means the real probability of finding the system. In fact, dissipative tunneling problem has been studied using a phenomenological damping term equivalent to the classical Rayleigh term in Heisenberg picture (Heisenberg equation of motion) [5,6]. The approaches studied in the previous section are not being considered here again. In Schrödinger picture, on the contrary, the damping term can be readily added to the solution of Schrödinger equation empirically. The generalized density matrix method in the previous section is somewhat mathematical background of our choice in which we take *ad hoc*.

In our model, we include the quantum dissipation as a decay of the kinetic energy equivalent to the classical Rayleigh term represents. Although the decreasing probability scheme may only be an approximate representation [41], the idea is to use the radiative loss of a wave function developed long ago by Heitler [42] and others [43,44] for the radioactive nucleus with the modification that includes the classical damping scheme to some extent. We compare the three approaches of dissipation mechanism by Nosé-Hoover, Kubo-Fox-Keizer, and using empirical version of complex energy in the last paragraph of this section.

Classically, the particle's anticipated dissipation neither changes its identity nor looses any part of itself. Therefore, the wave function must be normalized at all times artificially, whenever the absolute probability is concerned. The physics of the damping mechanism requires this process which agrees with the concept of the wave function moving in a frictional viscous potential in a dynamical point of view. In mathematical point of view, justification of this is still subtle.

On the other hand, one possible physical explanation could be that, within a given uncertainty, interactive vacuum fluctuations are the cause to reduce the system's kinetic energy. This idea is similar to the additive (or multiplicative) stochastic processes in the Langevin equation as we discussed in the previous section. But more work must be done on this problem at present. We will look at this problem a little more carefully once again in the Appendix.

In general, quantum analogs of the classical system can be found by changing classical variables to quantum operators. As a consequence, it is appropriate to introduce a dissipation operator (call it Rayleighian) comparable to the classical Rayleigh term that is proportional to kinetic energy p^2 in the classical Hamilton's formulation in the previous section. This $\widehat{R}$ operator which includes a minus sign is then applied to the time-dependent solution of Schrödinger equation (2-22).

$$i\hbar\frac{\partial\psi}{\partial t} = -\frac{\hbar^2}{2\mu}(1 - i\beta)\nabla^2\psi + V\psi, \qquad (4\text{-}32)$$

where the constant β corresponds to the classical damping coefficient divided by the natural frequency of the classical oscillator. This is dimensionally-

correct since the classical damping coefficient usually has an inverse time unit in the classical equations of motion. So we have the solution as

$$\psi(q, t+\Delta t) = \hat{\Theta} \exp\left[-i\int_t^{t+\Delta t} \hat{H}(t')\,dt'\right] \exp\left\{-\beta\int_t^{t+\Delta t} \hat{T}\,dt'\right\} \psi(q, t),$$

$$= \hat{U}(p, q, t; t')\,\hat{D}(p, t; t')\psi(q,t) + \vartheta\{(\Delta t)^3\}, \qquad (4\text{-}33)$$

$$= \hat{T}^{d}_{eff}\,\hat{Y}^{d}_{eff}\,\hat{T}^{d}_{eff},$$

where $\hat{D} = \exp\left\{-\beta\int_t^{t+\Delta t} \left[\frac{\Pi^2}{2\mu}\right] dt'\right\}$, and $\hat{U}$ is the same as (2-23). Here, we recall the mechanical (kinematical) momentum $\Pi = p + \frac{\mu\gamma}{\omega}\sin\omega t$, where p is canonical momentum. In this case, operators with dissipation $\hat{T}^{d}_{eff}$, $\hat{Y}^{d}_{eff}$ are

$$\hat{T}^{d}_{eff}(p) = \exp\left[-i(1-i\beta)\frac{p^2}{4\mu}\Delta t\right]$$
$$\times \exp\left[-i(1-i\beta)\frac{1}{2}\frac{p\gamma}{\omega}\left\{\sin(\omega t)\frac{\sin(\omega\Delta t)}{\omega} - \cos(\omega t)\left(\frac{\cos(\omega\Delta t)-1}{\omega}\right)\right\}\right], \qquad (4\text{-}34)$$

$$\hat{Y}^{d}_{eff}(q) = \exp\left[-i\mu(1-\cos q)\Delta t\right]$$
$$\times \exp\left[-i(1-i\beta)\frac{\mu\gamma^2}{2\omega^2}\left\{\frac{\Delta t}{2} - \sin(2\omega t)\frac{\cos(2\omega\Delta t)-1}{4\omega} - \cos(2\omega t)\frac{\sin(2\omega\Delta t)}{4\omega}\right\}\right], \qquad (4\text{-}35)$$

where we split the operator $\hat{D}$ by half and combine together with $\hat{T}^{d}_{eff}$, $\hat{Y}^{d}_{eff}$.

The split operator method takes advantage of the ease of treating operators (2-26) and (2-27) in their diagonal representations. However, the operator $\hat{D}$ is not diagonal in momentum space. Its operation is neither

unitary nor Hermitian in this case. Then the Rayleighian $\widehat{R}$ can be thought of giving complex eigen-values. An equivalent mathematical formulation to this analogy is to use a complex mass (see Appendix 4.I). Then the concept of complex energy becomes more apparent.

It is of importance that the wave function (4-33) should be normalized after numerical operations to avoid computational overflow due to the Rayleighian $\widehat{R}$ resulting in ever decreasing magnitude of (4-33). This makes more sense physically since the particle is not actually being absorbed, but losing its kinetic energy. The methods described in the previous section do not require this process, but they need considerably more computation time and effort. Only wanting the average values to be damped, we take this process. The normalization process at time t takes place by the following normalization constant N.

$$N = \left[\sum_{q_i} |\psi(q_i, t)|^2 (\Delta q)\right]^{-\frac{1}{2}}. \tag{4-36}$$

It is worth mentioning that we compare the results of the following two calculations to check numerically the accuracy of normalization processes for an undriven system. The first calculation is just the ratio between the normalization at initial time and at an arbitrary time t, which analytically should be

$$\frac{\int |\psi(q, t)|^2 \, dq}{\int |\psi(q, 0)|^2 \, dq} \sim \exp[\, -2\beta \langle T(t) \rangle \, t \,], \tag{4-37}$$

where <*T*> is the expectation-value of kinetic energy. This is just what we called the *relative* probability. Then the second calculation we compare is the numerical one which is just

$$\frac{\sum_q |\psi(q,t)|^2}{\sum_q |\psi(q,0)|^2}. \qquad (4\text{-}38)$$

The agreement is very good, and one might guess that for a smaller time step, the difference becomes even more negligible. Thus, the normalization process has no, or very small (but results in no changes) effect on the computation. It is worthwhile reminding the reader that the *absolute* probability must be equal to one after the normalization. This empirical version of (4-33) is relatively easy to find a solution since no complication with the usual Schrödinger equation exists.

Now, all the same kinds of numerical operations as in Chapter two can be applied, and the results are described in the next section. The distribution functions are also investigated using the formulas in Chapter three. In this case all we need is the wave function at a certain time since we only treat everything in Schrödinger picture. This empirical treatment for quantum description of classical dissipation is mainly used throughout the study.

4-4. Numerical results and discussions

All the initial values are summarized in Table 4.I. We first examine the simple harmonic oscillator case whose analytic solutions are not difficult to find classically. The quantum analysis of this case without an external force using raising and lowering operators can be found in Appendix II. The equation used in this case is Eq. (1-13). The upper two pictures in Figure 4.1 shows very close correspondence without an external field. The lower part also shows a good agreement qualitatively, but not as good as the case of upper part (notice a small discrepancy around the limit cycle). The real numerical values for different parameters in simple harmonic motions are specified in Table 4.II. From the figure and the table, therefore, it can be deduced that the proposition of the damping scheme is correct at least well within the break time. To support this, the driven damped pendulum in a classically regular regime follows a trajectory shown in Figure 4.2, where the corresponding classical one is depicted by the side. Limit cycles are evident in both cases. The lower part of power spectrum indicates the degree of their near perfect agreement. Figure 4.3 shows the overlap of two trajectories. The upper one is in the regular regime, and the lower one in the chaotic regime classically. The solid lines are quantum ones. Their actual numerical values are summarized in Table 4.III. It is very interesting to observe that this scheme also fails after the break time in the chaotic regime since their values are so different.

With the confidence that the correspondence will hold within the break time limit from the previous chapter, the three distributions are checked and compared. In Fig. 4.4, the time history of the classical distribution is plotted with the same parameter values as in Fig. 4.2. It is clearly observable

that the distribution contracts as time elapses until it reaches a steady state with a fixed area rotating in phase-space due to oscillation of the pendulum. Subsequent figures for the Wigner and the Husimi distributions in Fig. 4.5 and Fig. 4.6 indicate steady states well. This result is what we expect in the classically regular regime.

At this juncture, we increase γ with a rational value ω. Strange phenomenon is observed, as in Figure 4.7, although the classical motions are still in the regular regime. Even though both cases develop limit cycles eventually, their behaviors are quite different. Arrows in the figure indicate the correspondence limit where two trajectories do not match any longer in phase-space. It is interesting to see that they break off even before the system evolves one period of the external field. Power spectra at the bottom half are not similar either although both give distinct peaks. It is of interest to notice a rather sudden change in its expectation-value trajectory in quantum case.

As before, the time history of the classical distribution is depicted in Fig. 4.8, and shows the contraction of the volume due to dissipation. The corresponding Wigner and Husimi ones are plotted in Figs. 4.9, 4.10 respectively. Generally they appear to be similar to each other even though there exists a slight difference in the propagation time we picked in each scheme. Nonetheless, it is quite safe to judge that the Husimi is more representative in terms of the correspondence. However, we notice phenomena close to those in the previous chapter. That is, the structure of the Wigner tells us more about the dynamics through its details especially located around the middle of phase-space. With this information, the chaotic case should be examined.

Fig. 4.11 exhibits the trajectories and their power spectra in classically chaotic regime. The classical motion has a positive exponent and its phase-

space behavior displays chaotic motion. As in Fig. 4.7, locations of the arrows describe a rather short correspondence limit with a more drastic change in the trajectory in quantum expectation-value phase-space. Especially the arrow in quantum case indicates a sharp change. Their power spectra also show that the motion appears to be a quasi-periodic (or it becomes almost-periodic by ignoring transient) in quantum case. This quasi-periodic effect must be noted and will be mentioned later for more analysis. Now the classical, Wigner and Husimi distributions are plotted in Figs. 4.12 (4.13, too), 4.14 and 4.15 respectively. In this case, it becomes prominent that the Husimi resembles more than the Wigner as time elapses. As we have seen in Chapter three, the similar observation in the chaotic regime is recognized. The Husimi representation seems to be better, especially in the chaotic regime.

Several other results in the classically chaotic regime reveal that all the quantum mechanical motions with the dissipation mechanism become almost-periodic. For lesser values of β, it seems that it would take longer to be almost-periodic. It is worth pointing out that the uncertainty product manifests phase-space behaviors as shown in Figure 4.16. To our knowledge, there is no good explanation to this kind of phenomena at this time. However, we could certainly speculate that the kinds of periodic motions arising in quantum case are partly due to a large increase in U such that the average (expectation) values stabilize. This relaxation was also noted in the previous chapter.

Other classical strange attractors are compared with Wigner and Husimi representations in Figures 4.17, 4.18 and 4.19. It is now apparent that the Husimi exhibits a closer distribution to the classical one in its structure although its minute information is somewhat lost. Therefore it is safe to say from these figures that Husimi representation is a better representation than

the Wigner even in the presence of dissipation. The same conclusion was drawn in Chapter three in the absence of dissipation. The final two figures of Figs. 4.20, 4.21 depict the classical and the Husimi for further evidences. Hence, similar conclusions to the previous one in Chapter three can be summarized for this chapter. However, in the regular regime, the Husimi representation is not necessarily better than the Wigner representation for the quantum-classical correspondence. We were not interested in the regular regime where other representations are conceivable with relatively easier applications.

4-5. Summary

Several conclusions can be drawn from the results. It is evident that all the cases with an external force develop almost-periodic motions after the time when the damping ceases all the action if there is no external force. Our damping scheme forms periodic motion at times inversely proportional to the damping coefficient. In other words the fundamental frequency eventually disappears and only the external frequency and its subsequent harmonics remain as seen from the figures. A similar phenomenon is observed in the uncertainty calculations. Therefore with the exponential decay law (in the classical observables) adopted here, no quantum chaotic motion is observed for reasonable amount of damping coefficients.

For a case of small damping, it would take long time for the system to be in periodic motion. In this case, the exponential approximation scheme may be no longer valid. We believe the decay term in the solution of Schrödinger equation can in fact be treated separately. Therefore after the

damping dominates the primary motion of the system, the external field takes over the motion so that in this case, eventually, the periodic motion develops due to the periodic external field. No matter what kinds of external fields are applied, the resulting stationary state caused by decay of energy will resemble its external environment.

The problem however still remains: the existence of the time limitation that the approximation can be applied and its relation to the so-called break time that specifies the valid time limit that the correspondence principle can be applied. Within the short time of good correspondence, the exponential decay scheme certainly shows classical chaotic behavior. On the other hand, at large times the general exponential decay in quantum system is really a different damping scheme than the classical one as seen from the results. Much is in need of being investigated.

Chapters three and four have revealed that classical chaos does not manifest itself in the corresponding quantum systems as long as quantum mechanics expresses all the accessible classical states through its quantization. Inversely speaking, quantum mechanics does not manifest classical mechanics in the classically chaotic regime mainly because of the quantum uncertainty. We will see more examples of different kinds of systems in the next chapter to see if conclusions in Chapters three and four can be generalized.

Appendix 4. I Derivation of *dissipative* Schrödinger equation

Mathematically we can form a 'dissipative' Schrödinger equation with a non-Hermitian Hamiltonian without considering the loss of probability since our version is empirical. In Eq. (4-6) we included the dissipation term in the solution by substituting an imaginary kinetic energy with a specific coefficient β given by the corresponding classical damping term. This solution must then satisfy *dissipative* Schrödinger equation which will be derived here. We first start with an assumption that the kinetic energy term in Schrödinger equation is responsible for dissipation. The assumption is equivalent to consider the mass of a system to be complex; that is to say, m = Re{m} + iIm{m} = $m_r + im_i$. This is also equivalent to the complex energy of a system (E = Re{E} + iIm{E}), which we will show.

Substitute this complex mass into Schrödinger equation, and carry out the algebra, we finally find the following equation.

$$i\hbar\frac{\partial\psi}{\partial t} = -\frac{\hbar^2}{2\mu}(1-i\beta)\nabla^2\psi + V\psi = (1-i\beta)\,T\psi + V\psi, \qquad \text{(A4I-1)}$$

where $\beta = \frac{m_i}{m_r}$, and $\mu = m_r + \frac{m_i^2}{m_r}$; here, μ is not the effective mass. If one writes Re{E} = E_R, Im{E} = E_I, then this equation can be broken up into a set of coupled equations:

$$\hat{H}\psi = (\frac{p^2}{2\mu} + V)\psi = E_R\psi,$$
$$\hat{R}\psi = -\beta\frac{p^2}{2\mu}\psi = E_I\psi. \qquad \text{(A4I-2)}$$

It is obvious that if $\beta = 0$ (m_i=0), the usual Schrödinger equation is obtained.

Now, the spatial probability density $P(q, t)$ must be time-dependent such that the probability dissipates at a rate given by the classically damped kinetic energy. Then the quantum damping is assumed to be proportional to the kinetic energy of a wave packet. Whence, we propose that the integral of $P(q, t)$ over any fixed volume V

$$\int_V P(q,t)\, d\tau \sim exp\left(-\frac{\zeta T\, t}{\hbar}\right), \tag{A4I-3}$$

where $P(q, t) = |\psi(q, t)|^2$, and $P(q, 0) = 1$ with a positive constant ζ. The volume element of the integration is $d\tau$ which is just dq in one dimensional case. To find the appropriate value of ζ, consider the time variations of the normalization integral.

$$\frac{\partial}{\partial t}\int_V P(q,t)\, d\tau = \int_V \left[\psi^* \frac{\partial \psi}{\partial t} + \frac{\partial \psi^*}{\partial t}\psi\right] d\tau, \tag{A4I-4}$$

$$= \frac{i\hbar}{2\mu}\int_V \left[\psi^* \nabla^2\psi - (\nabla^2\psi^*)\,\psi\right] d\tau + \beta\frac{\hbar}{2\mu}\int_V \left[\psi^* \nabla^2\psi + (\nabla^2\psi^*)\,\psi\right] d\tau,$$

$$= -\frac{\hbar}{2i\mu}\int_V \nabla\left[\psi^* \nabla\psi - (\nabla\psi^*)\,\psi\right] d\tau + \beta\frac{\hbar}{2\mu}\int_V \nabla\left[\psi^* \nabla\psi + (\nabla\psi^*)\,\psi\right] d\tau - \beta\frac{\hbar}{2\mu}\int_V 2(\nabla\psi)\cdot(\nabla\psi^*)\, d\tau,$$

$$= -\int_V \nabla\cdot S \; d\tau - \int_V \nabla\cdot R \; d\tau - 2\beta\frac{\hbar}{2\mu}\int_V |\nabla\psi|^2 \, d\tau \,,$$

$$= -\int_V \nabla\cdot S \; d\tau - \int_V \nabla\cdot R \; d\tau - \frac{2\beta}{\hbar}\int_V \psi^*\left[\frac{\mu\hat{v}^2}{2}\right]\psi \, d\tau \,,$$

$$= -\int_A S_n \; dA - \int_A R_n \; dA - \frac{2\beta}{\hbar} < T > \,, \qquad \text{(A4I-5)}$$

where we identify $\frac{\hbar}{i\mu}\nabla$ as the velocity operator $\hat{v}$, and A describes a surface integral. Also, S is known as a probability current density given by

$$S(q,t) = \frac{\hbar}{2i\mu}\left[\psi^*\nabla\psi - (\nabla\psi^*)\psi\right] = Re\left[\psi^*\frac{\hbar}{i\mu}\nabla\psi\right],$$
$$R(q,t) = -\beta\frac{\hbar}{2\mu}\left[\psi^*\nabla\psi + (\nabla\psi^*)\psi\right] = \beta \, Im\left[\psi^*\frac{\hbar}{i\mu}\nabla\psi\right].$$

Note that the notations $R \neq \hat{R}$. In the case of a wave packet, for which ψ vanishes at great distances, the surface integrals are evidently zero when V is the entire space ($-\infty$ to ∞ in one dimension). For a wave function of a periodic structure at the boundaries, it can be also shown that the surface integrals vanish. So the normalization integral is negatively proportional to the expectation-value of kinetic energy. Then we can identify that ζ in (A4I-3) is equal to 2β. Therefore, the solution of (A4I-1) is expected to have the time dependence ~ exp[$(-iE-2\beta T)t$], where T is the kinetic energy of a system. We can show the same result by calculating P directly from Eq. (4-5). However, using Schrödinger equation (A4I-1), we have showed that Eq. (4-5) is indeed the required solution.

The equivalent differential form can be derived. It becomes

$$\frac{\partial P(q,t)}{\partial t} + \nabla\cdot\{S(q,t) + R(q,t)\} = -2\beta T \frac{P(q,t)}{\hbar} . \qquad \text{(A4I-6)}$$

This has a very similar relation to the conservation form of complex potential [7]. The similarity between the two is that the probability is not conserved, but the difference is the presence of the extra term, $\nabla\cdot R(q,t)$, in the differential form (A4I-6). If there is a region in which $\nabla\cdot\{S(q,t) + R(q,t)\}=0$, (A4I-6) obviously indicates the P decays exponentially in time according to (A4I-3). This is to be expected since a particle is experiencing a friction, and giving off its kinetic energy. One may include the zero point energy such that the solution cannot give energies smaller than the ground state energy.

The interpretation of a possible physical meaning in this quantum dissipation mechanism is the following: since we have to write the solution of the normalization integral as $\int P(q,t_2)dq = \int dq\, P(q,t_1)\, exp\left[-2\beta T\,(t_2-t_1)\right]$, where $t_2 > t_1$, the significant fact is only the ratio of $P(q,t_2)/P(q,t_1)$, the *relative* probability, so that the actual *absolute* probability can always be normalized. In other words, unlike to the case of complex potential where particles are being continuously absorbed, the probability to find a particle at position q is being reduced by the exponential factor which is proportional to the velocity of a particle in this case. So particles are staying somewhere in the system with reduced velocities. On the other hand, due to energy loss, the *relative* probability after Δt must be decreased compared to the previous one before normalization. In fact, this kind of esoteric process of normalization is not necessary if the generalized density matrix formulation in biorthonormal

Hilbert space is used as we have discussed in Ch. 4. The complete physical explanation of this quantum friction must be followed, and yet we do not have a good answer to this intriguing physics. A possible physical justification of mathematical process in the complex kinetic energy representation has been presented in this appendix to claim the validity of our choice of the method.

Appendix 4. II
Quantum analysis of a dissipative simple harmonic motion

In this appendix, we will derive the quantum solution of the harmonic oscillator with dissipation described earlier in this chapter. First, we set the lowering and raising operator as usual:

$$\begin{cases} \hat{a} = \sqrt{\frac{\mu\omega_o}{2\hbar}}(\hat{q} + \frac{i\hat{p}}{\mu\omega_o}) \\ \hat{a}^+ = \sqrt{\frac{\mu\omega_o}{2\hbar}}(\hat{q} - \frac{i\hat{p}}{\mu\omega_o}) \end{cases} . \qquad \text{(A4II-1)}$$

Note the following relationships:

$$[\hat{a}, \hat{a}^+] = 1, n = \hat{a}^+\hat{a}.$$

Then normally the Hamiltonian is just

$$\hat{H}_o = \hbar\omega_o(\hat{a}^+\hat{a} + \frac{1}{2}),$$

whereas the dissipative Hamiltonian becomes

$$\hat{H} = \frac{1}{4}\hbar\omega_o\left\{(\hat{a} + \hat{a}^+)^2 - (\hat{a} - \hat{a}^+)^2(1 - i\beta)\right\}.$$

This can be reduced to the following form with a simple arithmetic:

$$\hat{H} = \hbar\omega_o\left\{(\hat{a}^+\hat{a} + \frac{1}{2}) + \frac{i\beta}{4}(\hat{a} - \hat{a}^+)^2\right\}. \qquad \text{(A4II-2)}$$

Now to find the time-dependence on the operators, use the Heisenberg equations of motion.

$$\frac{d\hat{a}}{dt} = \frac{i}{\hbar}[\hat{H},\hat{a}],\ \frac{d\hat{a}^+}{dt} = \frac{i}{\hbar}[\hat{H},\hat{a}^+].$$

The final results is then just a coupled differential equation.

$$\begin{cases} i\hbar\dfrac{d\hat{a}}{dt} = \hbar\omega_o\left\{\hat{a}(1-\dfrac{i\beta}{2}) + \dfrac{i\beta}{2}\hat{a}^+\right\} \\ i\hbar\dfrac{d\hat{a}^+}{dt} = -\hbar\omega_o\left\{\hat{a}^+(1-\dfrac{i\beta}{2}) + \dfrac{i\beta}{2}\hat{a}\right\} \end{cases}, \qquad \text{(A4II-3)}$$

With the assignment

$$\bar{v} = \begin{pmatrix} \hat{a} \\ \hat{a}^+ \end{pmatrix}, \text{ and } \underline{A} = -i\omega_o \begin{pmatrix} 1-\dfrac{i\beta}{2} & \dfrac{i\beta}{2} \\ -\dfrac{i\beta}{2} & -1+\dfrac{i\beta}{2} \end{pmatrix}, \qquad \text{(A4II.4)}$$

we find a simple vector equation: $\dot{\bar{v}} = \underline{A}\bar{v}$. The general solution can be written

$$\bar{v}(t) = \exp(\underline{A}t)\bar{v}(0). \qquad \text{(A4II-5)}$$

Eigenvalues of the matrix $\underline{A}$ are easily found to be $\lambda = \pm\sqrt{1-i\beta}$. Next we diagonalize the matrix in the following manner:

$$\exp(\underline{A}t) = \bar{D}\exp(\underline{T}t)\bar{D}^{-1}, \qquad \text{(A4II-6)}$$

where $\bar{D}$= eigen-vector given by

$$\underline{\mathbf{D}} = \begin{pmatrix} 1 & 1 \\ 1+\dfrac{2i}{\beta}(1-\sqrt{1-i\beta}) & 1+\dfrac{2i}{\beta}(1+\sqrt{1-i\beta}) \end{pmatrix},$$

and its inverse becomes

$$\underline{\mathbf{D}}^{-1} = \frac{\beta}{4i\sqrt{1-i\beta}} \begin{pmatrix} 1+\dfrac{2i}{\beta}(1+\sqrt{1-i\beta}) & -1 \\ -1-\dfrac{2i}{\beta}(1-\sqrt{1-i\beta}) & 1 \end{pmatrix}.$$

Also, we have

$$\exp(\underline{T}t) = \begin{pmatrix} e^{-i\omega_o\sqrt{1-i\beta}t} & 0 \\ 0 & e^{i\omega_o\sqrt{1-i\beta}t} \end{pmatrix}.$$

Carry out the calculation (A4II-6), and one easily find

$$\begin{pmatrix} \hat{a} \\ \hat{a}^+ \end{pmatrix}(t) = \underline{R} \begin{pmatrix} \hat{a} \\ \hat{a}^+ \end{pmatrix}(0), \qquad \text{(A4II-7)}$$

where $\underline{R}$ is given by

$$\underline{R} = \frac{\beta}{4i\sqrt{1-i\beta}} \begin{pmatrix} R_{11} & R_{12} \\ R_{21} & R_{22} \end{pmatrix},$$

with

$$R_{11} = \left\{1+\frac{2i}{\beta}(1+\sqrt{1-i\beta})\right\} e^{-i\omega_o\sqrt{1-i\beta}t} - \left\{1+\frac{2i}{\beta}(1-\sqrt{1-i\beta})\right\} e^{i\omega_o\sqrt{1-i\beta}t},$$

$$R_{12} = e^{i\omega_o\sqrt{1-i\beta}t} - e^{-i\omega_o\sqrt{1-i\beta}t},$$

$$R_{21} = \left\{1+\frac{2i}{\beta}(1-\sqrt{1-i\beta})\right\}\left\{1+\frac{2i}{\beta}(1+\sqrt{1-i\beta})\right\}e^{-i\omega_o\sqrt{1-i\beta}t}$$
$$-\left\{1+\frac{2i}{\beta}(1-\sqrt{1-i\beta})\right\}\left\{1+\frac{2i}{\beta}(1+\sqrt{1-i\beta})\right\}e^{i\omega_o\sqrt{1-i\beta}t},$$
$$R_{22} = -\left\{1+\frac{2i}{\beta}(1-\sqrt{1-i\beta})\right\}e^{-i\omega_o\sqrt{1-i\beta}t} + \left\{1+\frac{2i}{\beta}(1+\sqrt{1-i\beta})\right\}e^{i\omega_o\sqrt{1-i\beta}t}.$$

Now we need to make an approximation to get a more simpler version. Further simplifications using $\sqrt{1-i\beta} \approx 1-\frac{i\beta}{2}$ yield the results:

$$R_{11} = \frac{4}{\beta}(\frac{\beta}{2}+i)\exp(-i\omega_o t)\exp(-\frac{\beta}{2}\omega t),$$
$$R_{12} = \exp(i\omega_o\sqrt{1-i\beta}t) - \exp(-i\omega_o\sqrt{1-i\beta}t),$$
$$R_{21} = 0,$$
$$R_{22} = \frac{4}{\beta}(\frac{\beta}{2}+i)\exp(i\omega_o t)\exp(\frac{\beta}{2}\omega t).$$

We can also approximate $\frac{\beta}{4i\sqrt{1-i\beta}} = \frac{\beta}{4(1+\frac{\beta^2}{2})}(\frac{\beta}{2}+i) \approx \frac{\beta}{4}(\frac{\beta}{2}+i)$, then $\underline{R}$ finally becomes the following matrix.

$$\underline{R} = \begin{pmatrix} (1+\frac{\beta^2}{4})e^{-i\omega_o t}e^{-\frac{\beta}{2}\omega t} & (\frac{\beta^2}{8}-i\frac{\beta}{4})(e^{i\omega_o t}e^{\frac{\beta}{2}\omega_o t}+e^{-i\omega_o t}e^{-\frac{\beta}{2}\omega_o t}) \\ 0 & (1+\frac{\beta^2}{4})e^{i\omega_o t}e^{\frac{\beta}{2}\omega_o t} \end{pmatrix}.$$

We get

$$\begin{pmatrix} \hat{a}(t) \\ \hat{a}^+(t) \end{pmatrix} = \begin{pmatrix} e^{-\frac{\beta}{2}\omega_o t}\cos(\omega_o t)\hat{a}_o - ie^{-\frac{\beta}{2}\omega_o t}\sin(\omega_o t)\hat{a}_o \\ \quad +2\cos(\omega_o t)\cosh(\frac{\beta}{2})\hat{a}_o^+ + i2\sin(\omega_o t)\sinh(\frac{\beta}{2})\hat{a}_o^+ \\ \\ e^{\frac{\beta}{2}\omega_o t}\cos(\omega_o t)\hat{a}_o^+ + ie^{\frac{\beta}{2}\omega_o t}\sin(\omega_o t)\hat{a}_o^+ \end{pmatrix}, \qquad \text{(A4II-8)}$$

where $\hat{a}_o = \hat{a}(0)$, and $\hat{a}_o^+ = \hat{a}^+(0)$. Now replace $\beta\omega_o$ with β_{qm} since we started with the dimensional damping coefficient whose unit is inverse-time. We need no dimension in quantum formulations, which means the replacement. This exactly corresponds to our claim since usually the classical damping coefficient has an inverse-unit. We have been accustomed without the subscript *'qm'*.

From the above expression, one can find

$$\begin{pmatrix} \hat{a}(t)+\hat{a}^+(t) \\ \hat{a}(t)-\hat{a}^+(t) \end{pmatrix} = \begin{pmatrix} (\hat{a}_o e^{-\frac{\beta}{2}t} + \hat{a}_o^+ e^{\frac{\beta}{2}t})\cos(\omega_o t) + i(\hat{a}_o^+ e^{\frac{\beta}{2}t} - \hat{a}_o e^{-\frac{\beta}{2}t})\sin(\omega_o t) \\ \quad +2\cos(\omega_o t)\cosh(\frac{\beta}{2})\hat{a}_o^+ + i2\sin(\omega_o t)\sinh(\frac{\beta}{2})\hat{a}_o^+ \\ \\ (\hat{a}_o^+ e^{\frac{\beta}{2}t} - \hat{a}_o e^{-\frac{\beta}{2}t})\cos(\omega_o t) + i(\hat{a}_o^+ e^{\frac{\beta}{2}t} + \hat{a}_o e^{-\frac{\beta}{2}t})\sin(\omega_o t) \\ \quad -2\cos(\omega_o t)\cosh(\frac{\beta}{2})\hat{a}_o^+ + i2\sin(\omega_o t)\sinh(\frac{\beta}{2})\hat{a}_o^+ \end{pmatrix}. \qquad \text{(A4II-9)}$$

It is obvious that the stationary undamped solution is obtained at t=0 since we have

$$\begin{pmatrix} \hat{q} \\ \hat{p} \end{pmatrix} = \sqrt{\frac{\hbar}{2\mu\omega_o}} \begin{pmatrix} 1 & 1 \\ i & -i \end{pmatrix} \begin{pmatrix} \hat{a}^+ \\ \hat{a} \end{pmatrix}.$$

It is not too clear analytically that the solution (A4II-9), yields the classical solution in the limit, but it exhibits the correspondence numerically. The analysis we have in this appendix is to determine analytic nature of the problem, and to come up with some ideas for comparison with classical solution. Unless we resolve the non-Hermitian nature contained in the solution, a further analysis does not seem necessary.

References

[1] P. Ehrenfest, Z. Physik, **45**, 455 (1927).

[2] See for example A. Yariv, *Quantum Electronics*, 3rd Edition, Ch. 1 (John Wiley & Sons, N. Y. 1989); J. L. Powell, B. Crasemann, *Quantum Mechanics* (Addison-Wesley, Reading, MA, 1961).

[3] V. B. Braginsky, V. P. Mitrofanov, V. I. Panov, *Systems with Small Dissipation* (The University of Chicago Press, Chicago, 1985); see also W. G. Hoover, B. Moran, C. G. Hoover, W. J. Evans, Phys. Lett. A. **133**, 114 (1988).

[4] B. A. Huberman, *Dynamical Systems and Chaos*, edited by L. Garrido (Springer-Verlag, New York, 1982).

[5] M. Razavy, Phys. Rev. A. **41**, 1211 (1990); **41**, 6668 (1990).

[6] M. Kamela, M. Razavy, Phys. Rev. A. **45**, 2695 (1992).

[7] L. I. Schiff, *Quantum Mechanics* (3rd edition) (McGraw-Hill, N. Y. 1968).

[8] E. M. Wright, J. C. Garrison, J. Opt. Soc. Am. **4**, 1751 (1987); M. D. Feit, J. A. Fleck, Jr. Appl. Opt. **20**, 848 (1981).

[9] See, for example, A. E. Siegman, *Lasers* (University Science Books, Mill Vally, CA, 1986).

[10] I. H. Deutsch, J. C. Garrison, E. M. Wright, J. Opt. Soc. Am. B. **8**, 1244 (1991).

[11] H. Goldstein, *Classical mechanics* (2nd Ed. Addison-Wesley, Reading, Ma, 1980)

[12] S. Nosé, Mol. Phys. **52**, 255 (1984); **57**, 187 (1986); J. Chem. Phys. **81**, 511 (1984); To see the recent development on Nosé-Hoover mechanics, consult, G. J. Martyna, M. L. Klein, J. Chem. Phys. **97**, 2635 (1992).

[13] W. G. Hoover, J. Stat. Phys. **42**, 587 (1986); Phys. Rev. A. **31**, 1695 (1985). For a detailed and comprehensive study, consult his books entitled, *Molecular Dynamics* (Springer-Verlag, Berlin, 1986), and *Computational Statistical Mechanics* (Elsevier, Amsterdam, 1992).

[14] W. G. Hoover, H. A. Posch, Phys. Lett. A. **113**, 82 (1985); Phys. Lett. A. **123**, 227 (1987).

[15] D. Kusnezov, A. Bulgac, W. Bauer, Ann. Phys. **204**, 155 (1990); **214** (1992); D. Kusnezov, Phys. Lett. A. **166**, 315 (1992).

[16] R. Kubo, J. Math. Phys. **4**, 174 (1963).

[17] P. Langevin, Compt. Rend. **146**, 530 (1908).
[18] R. F. Fox, G. E. Uhlenbeck, Phys. Fluids, **13**, 1893 (1970).
[19] R. F. Fox, J. Math. Phys. **13**, 1196 (1972); Phys. Rep. C. **48**, 179 (1978).
[20] R. Kubo, *Fluctuations, Relaxation and Resonance in Magnetic Systems* (Oliver and Boyd, Edinburgh, 1962).
[21] R. F. Fox, J. Math. Phys. **16**, 1214 (1976).
[22] S. I. Chu, Adv. Atom. Mol. Phys. 21, 97 (1985).
[23] R. P. Feynman, F. L. Vernon, R. W. Hellwarth, J. Appl. Phys. **28**, 49 (1957).
[24] S. I. Chu, Z. C. Wu, E. Layton, Chem. Phys. Lett. **157**, 151 (1989).
[25] W. E. Lamb Jr., R. R. Schlicher, M. O. Scully, Phys. Rev. A. **36**, 2763 (1987).
[26] T. S. Ho, S. I. Chu, Phys. Rev. A. **32**, 377 (1985).
[27] S. I. Chu, Adv. Chem. Phys. **73**, 739 (1989).
[28] Y. Aharonov, J. Anadan, Phys. Rev. Lett. **58**, 1593 (1987).
[29] D. K. C. MacDonald, *Noise and Fluctuations: An Introduction* (John Wiley & Sons, N.Y. 1962).
[30] See also, for example, H. B. Callen, *The Fluctuation-Dissipation Theorem and Irreversible Thermodynamics* in D. Ter Haar (ed.) *Fluctuations, Relaxations, and Resonance in Magnetic Systems* (Oliver & Boyd, London, 1962).
[31] For a comprehensive derivation, see for instance, F. Reif, *Fundamentals of Statistical and Thermal Physics*, Ch. 15 (McGraw-Hill, N.Y. 1965).
[32] J. E. Keizer, J. Chem. Phys. **63**, 398 (1975); **63**, 5037 (1975); **64**, 1679 (1976); **64**, 4466 (1976); **65**, 4431 (1976); **67**, 1473 (1977); J. Math. Phys, **18**, 1361 (1977): Phys. Fluids, **21**, 198 (1978).
[33] R. F. Fox, J. Chem. Phys. **70**, 4660 (1979).
[34] R. Kubo, K. Matsuo, K. Kitahara, J. Stat. Phys. **9**, 51 (1973).
[35] J. E. Keizer, *Statistical Thermodynamics of Nonequilibrium Processes* (Springer-Verlag, N.Y. 1987).
[36] N. C. van Kampen, *Stochastic Processes in Physics and Chemistry* (North-Holland, Amsterdam, 1981).
[37] R. F. Fox, J. E. Keizer, Phys. Rev. Lett, **64**, 249 (1990).
[38] J. E. Keizer, J. Tilden, J. Chem. Phys. **93**, 2811 (1989).
[39] R. F. Fox, J. E. Keizer, Phys. Rev. A, **43**, 1709 (1991).

[40] B. J. Berne, R. Percora, *Dynamic Light Scattering* (Wiley, N.Y. 1976).

[41] To see the explaination of non-exponetial decay, A. Peres, Anns. Phys. **129**, 33 (1980).

[42] W. Heitler, *The Quantum Theory of Radiation*, 3rd edition (Oxford, England, 1966), see Section 16.

[43] L. Fonder, G. C. Ghirardi, A. Rimini, Rep. Prog. Phys. **41**, 587 (1978); see also for a review, A. Sudbery, *Quantum Mechanics and The Particles of Nature* (Cambridge Univ. Press, Cambridge, N. Y. 1986); for a more recent version, see F. Haake, *Quantum Signatures of Chaos*, Vol 54 (Springer-Verlag, Berlin, 1991); R. Grobe, F. Haake, Phys. Rev. Lett. **62**, 2889 (1989); R. Grobe, F. Haake, H.-J. Sommers, Phys. Rev. Lett, **61**, 1899 (1988).

[44] E. C. G. Sudarshan, C. B. Chiu, V. Gorini, Phys. Rev. D. **18**, 2914 (1978); see also T. K. Bailey, W. C. Schieve, Nuovo Cimento, **47**, 231 (1978).

TABLE 4.I Data showing initial values for all the cases in this chapter. The initial Gaussian width is σ_G^2, and the constant Husimi trial function width is used.

Figure	Case	q_o	p_o	ω	γ	μ	β	Δt	σ_G^2
4.1	(a)	0.5	0.0	1.0	0.0	20	0.3	0.005	N/A
	(b)	0.5	0.0	2.0	0.5	20	0.3	0.005	N/A
4.2		0.2	0.0	2.0	1.0	20	0.1	0.005	N/A
4.3	(a)	0.5	–0.3	1.5	0.5	20	0.3	0.005	N/A
	(b)	–0.3	0.5	2/3	1.45	20	0.25	0.0025	N/A
4.4-4.6		0.2	0.0	2.0	1.0	20	0.1	0.005	0.1
4.7-4.10		0.5	0.0	4/3	1.5	20	0.25	0.0025	0.05
4.11-4.15		0.5	0.0	2/3	1.5	20	0.25	0.0025	0.05
4.16	(a)	0.5	0.0	2/3	1.5	20	0.25	0.0025	0.05
	(b)	0.5	0.0	4/3	1.5	20	0.25	0.0025	0.05
4.17-4.19		0.5	0.0	4/3	1.25	10	0.05	0.0023	0.1
4.20		0.0	0.5	2/3	0.5	10	0.25	0.0023	0.1

TABLE 4. II. Data showing classical values and quantum expectation-values of positions as well as velocities at various times specified by the number of integration steps n. Notice the good agreement in (a) and (b) since these are simple harmonic motions.

Case	n	$<\xi>$	$\xi_{classical}$	$<\dot{\xi}>$	$\dot{\xi}_{classical}$
(a)	3072	–0.3285601	–0.3090754	0.2111773	0.1832900
$\omega = 1.0$	5120	0.2591167	0.2260636	–0.0172164	–0.0107330
$\gamma = 0.0$	10240	0.1020580	0.0870070	–0.0236840	0.0011398
$\beta = 0.3$	20480	0.0142518	0.0128882	–0.0081721	–0.0009570
(b)	4096	–0.0835692	–0.0807721	–0.0356813	–0.0391514
$\omega = 2.3$	8192	–0.0973784	–0.0971143	–0.2715363	–0.2721665
$\gamma = 0.7$	16384	0.1390191	0.1330709	–0.2035585	–0.2030728
$\beta = 0.35$	32768	–0.1467359	–0.1370854	0.1934854	0.1915681

TABLE 4. III. Pendulum data showing classical values and quantum expectation-values of positions as well as velocities at various times specified by the number of integration steps n. Notice the good agreement in (a), but not in (b) where the classical motions are chaotic.

Case	n	$< q >$	$q_{classical}$	$< dq/dt >$	$dq/dt_{classical}$
(a)	256	0.4970575	0.4970063	–0.2986349	–0.2987335
$\omega = 1.5$	2560	0.3667574	0.3216246	–0.1905403	–0.2066624
$\gamma = 0.5$	4096	–0.0450927	–0.0395455	0.5584520	0.5441279
$\beta = 0.3$					
(b)	512	–0.2957375	–0.2959064	0.4185845	0.4187069
$\omega = 2/3$	4096	–1.2660619	–0.9159159	–0.7072607	–2.9014839
$\gamma = 1.45$	8192	–1.7320650	–2.0949545	–0.4502623	–0.2786042
$\beta = 0.25$	16384	–1.4317289	1.3972950	0.6264775	–2.2621542

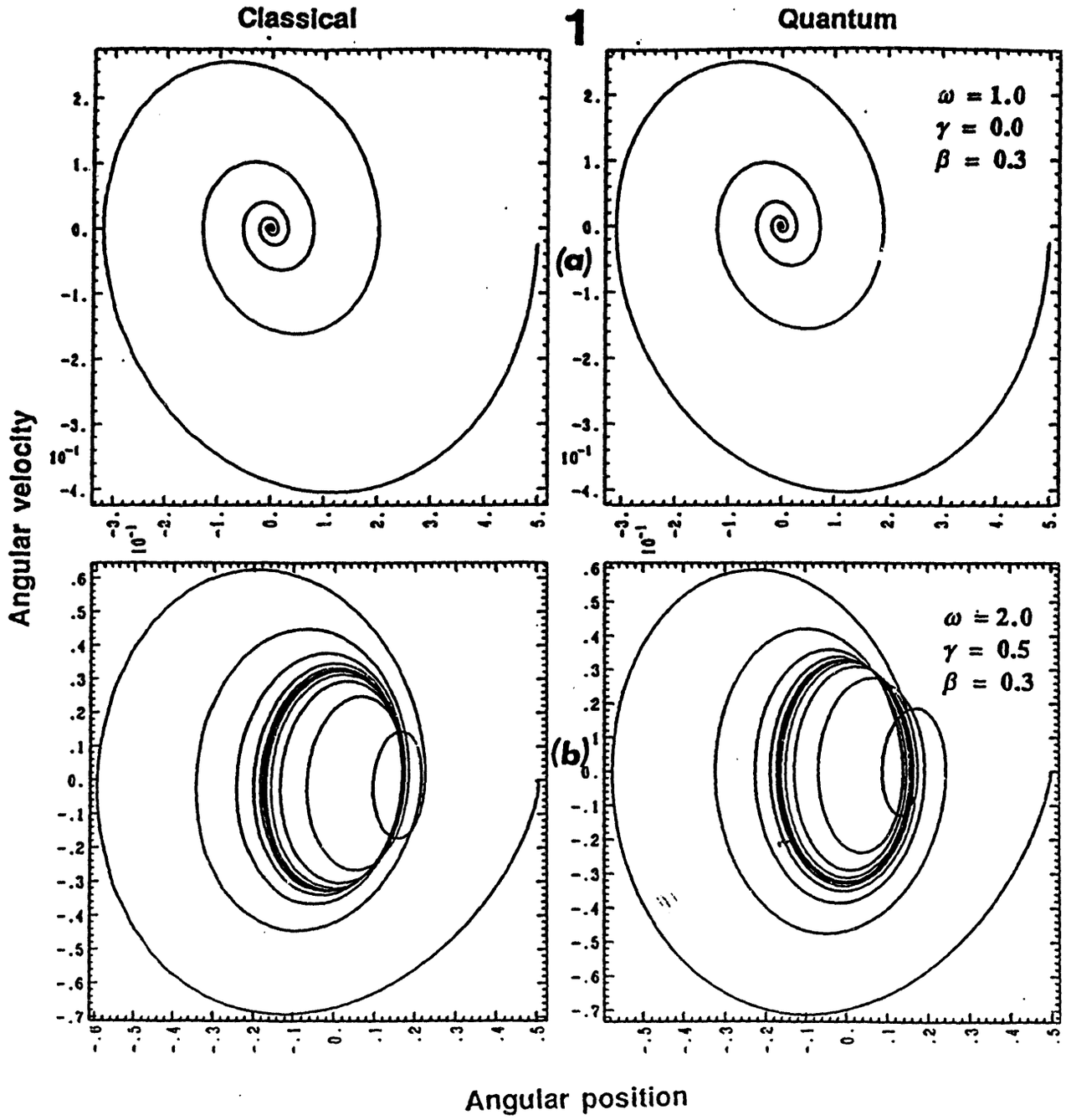

Figure 4.1 Phase-space trajectories of simple harmonic motions in (a) pure damping case (no external field) (b) damping with the driving force. The limit cycle is evident in (b).

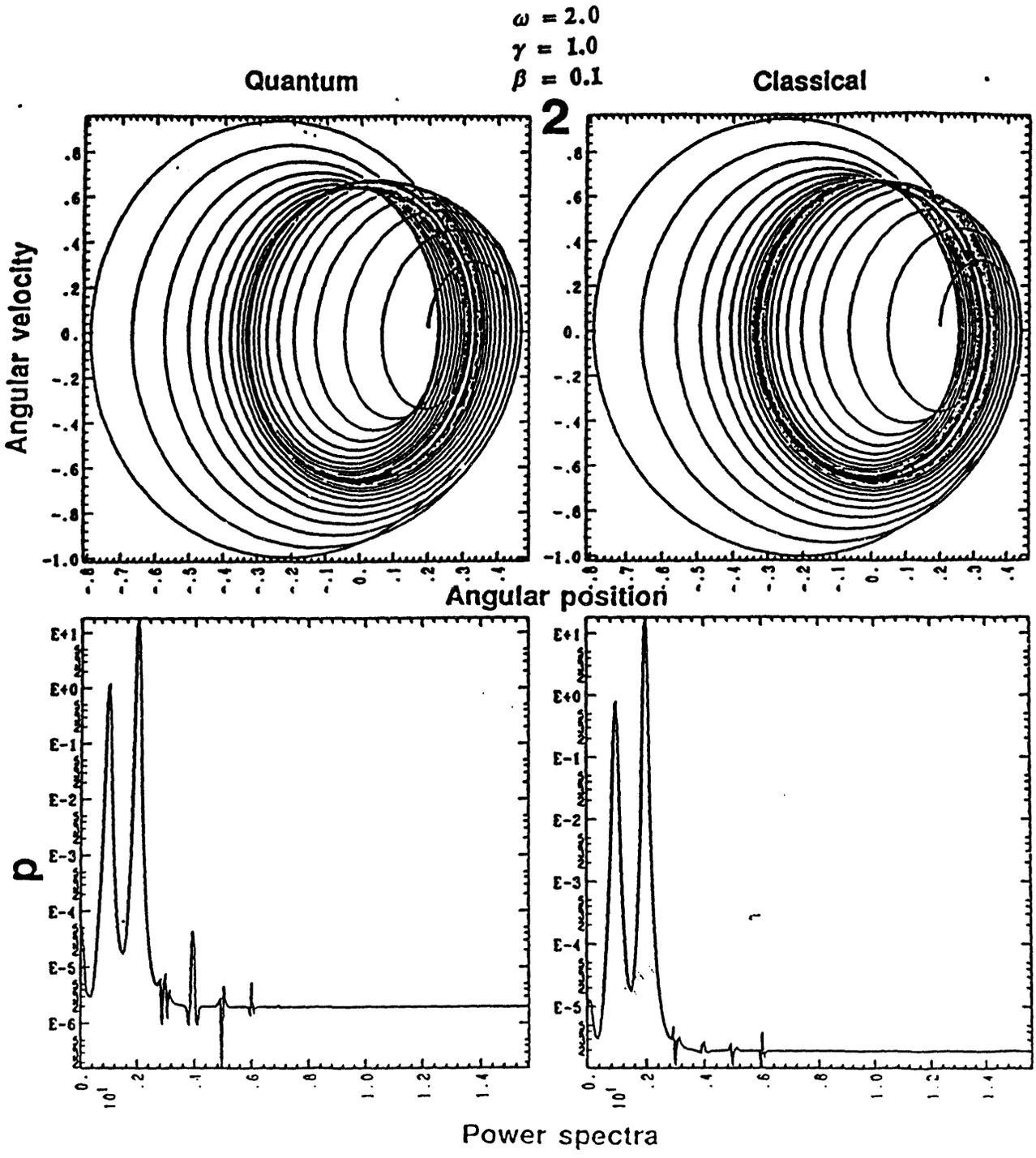

Figure 4.2 Phase-space trajectories of the forced pendulum. Power spectra at the bottom half indicate remarkably close resemblance to each other.

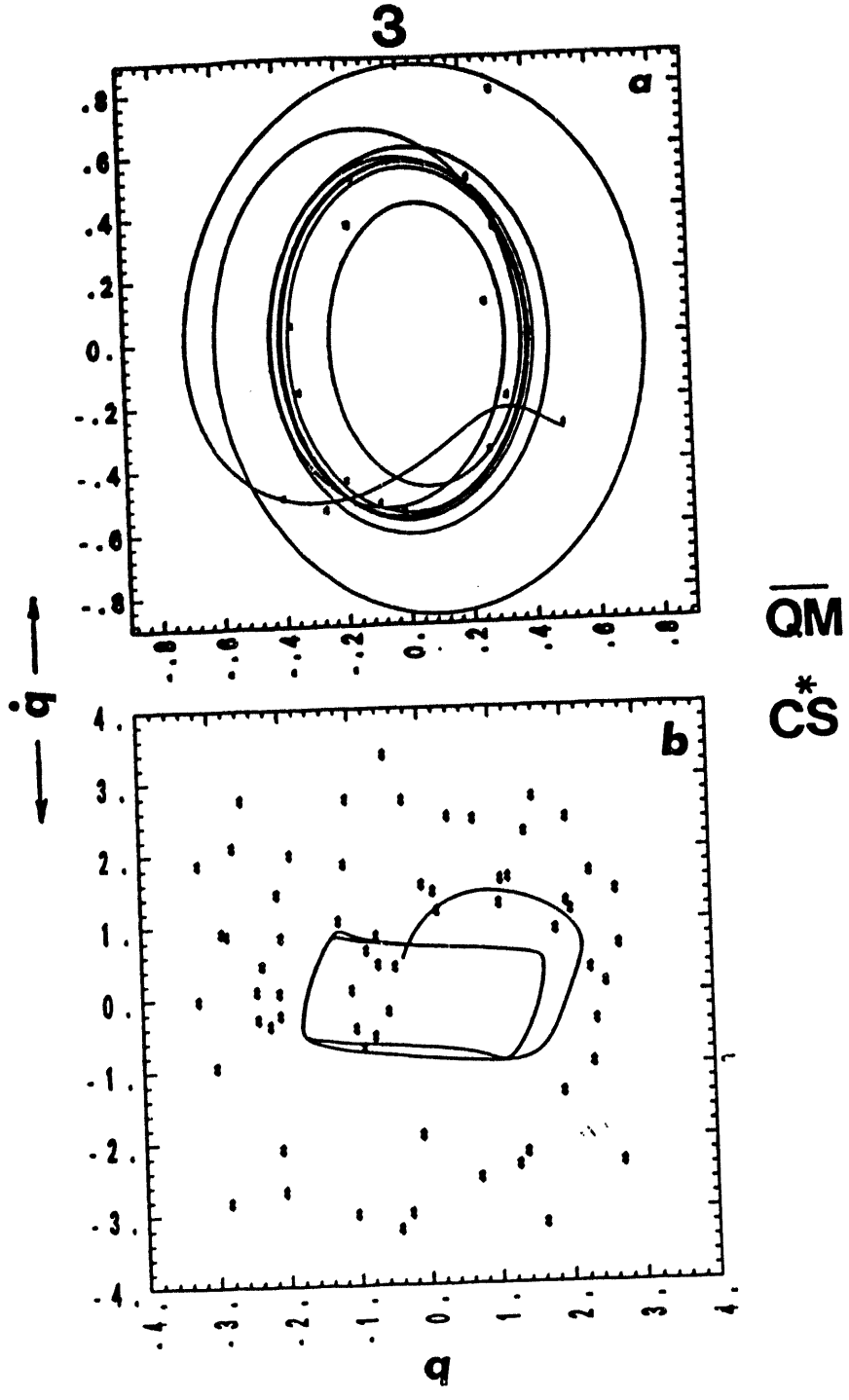

Figure 4.3 Overlaps of the trajectories in (a) regular regime, and (b) chaotic regime. Solid lines are for classical whereas the dotted stars for quantum. See Table 4.III for numerical comparison.

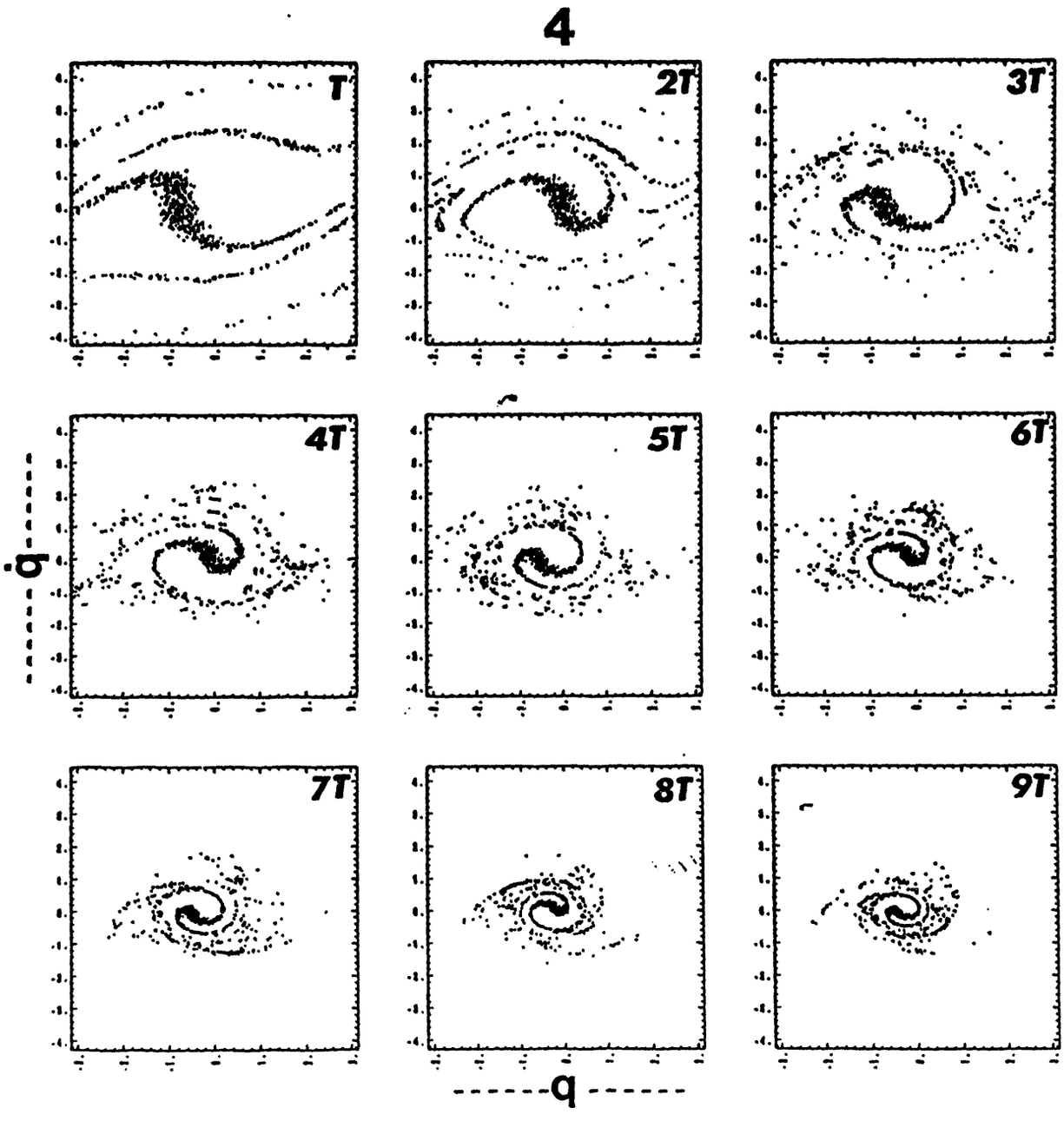

Figure 4.4 **The evolution of the classical distribution for the case depicted in Fig. 2. A rotating stationary distribution is evident as the time elapses.**

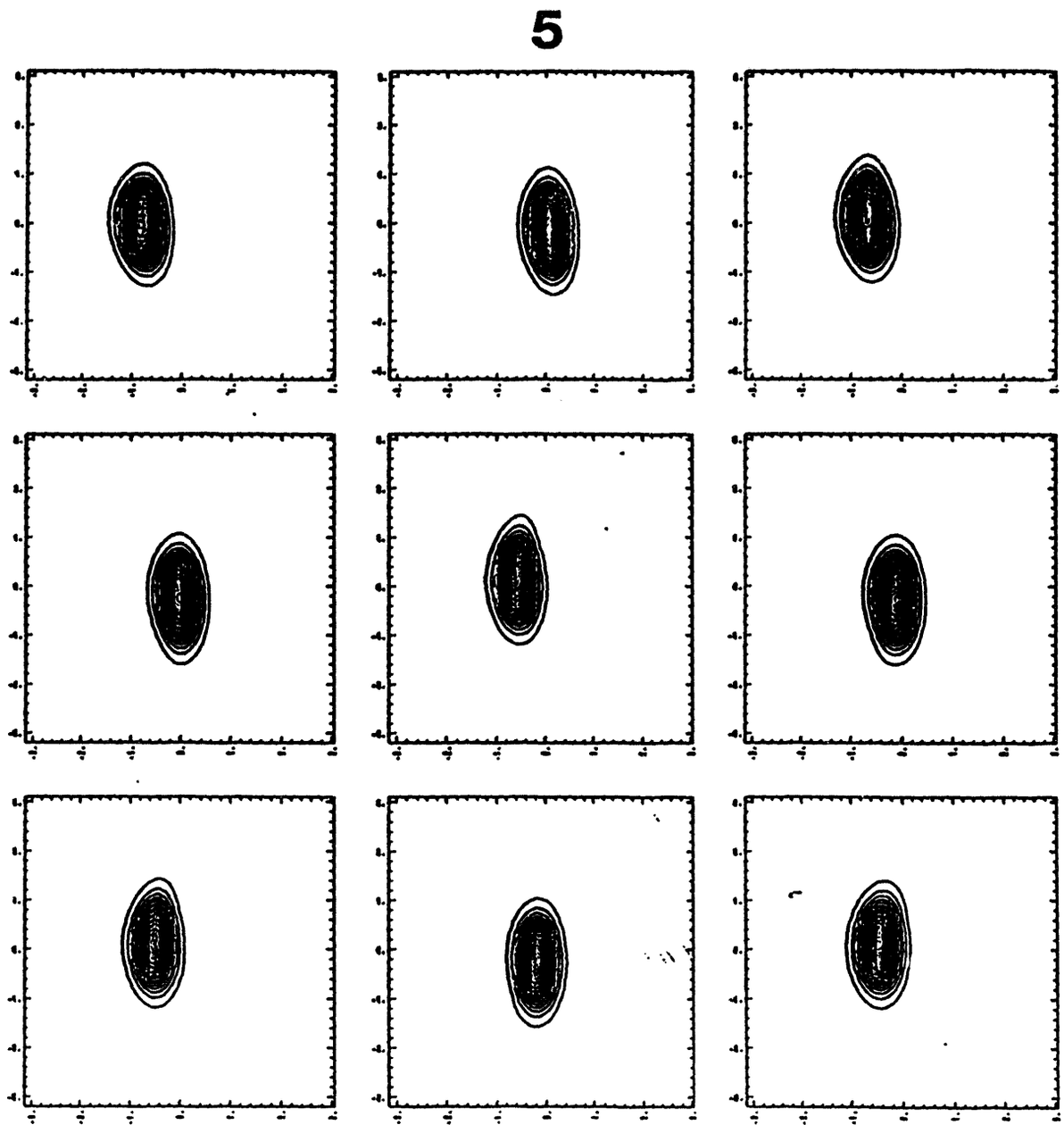

Figure 4.5 The evolution of the Wigner distribution for the same parameter values of the previous case depicted in Figs 2 and 4.

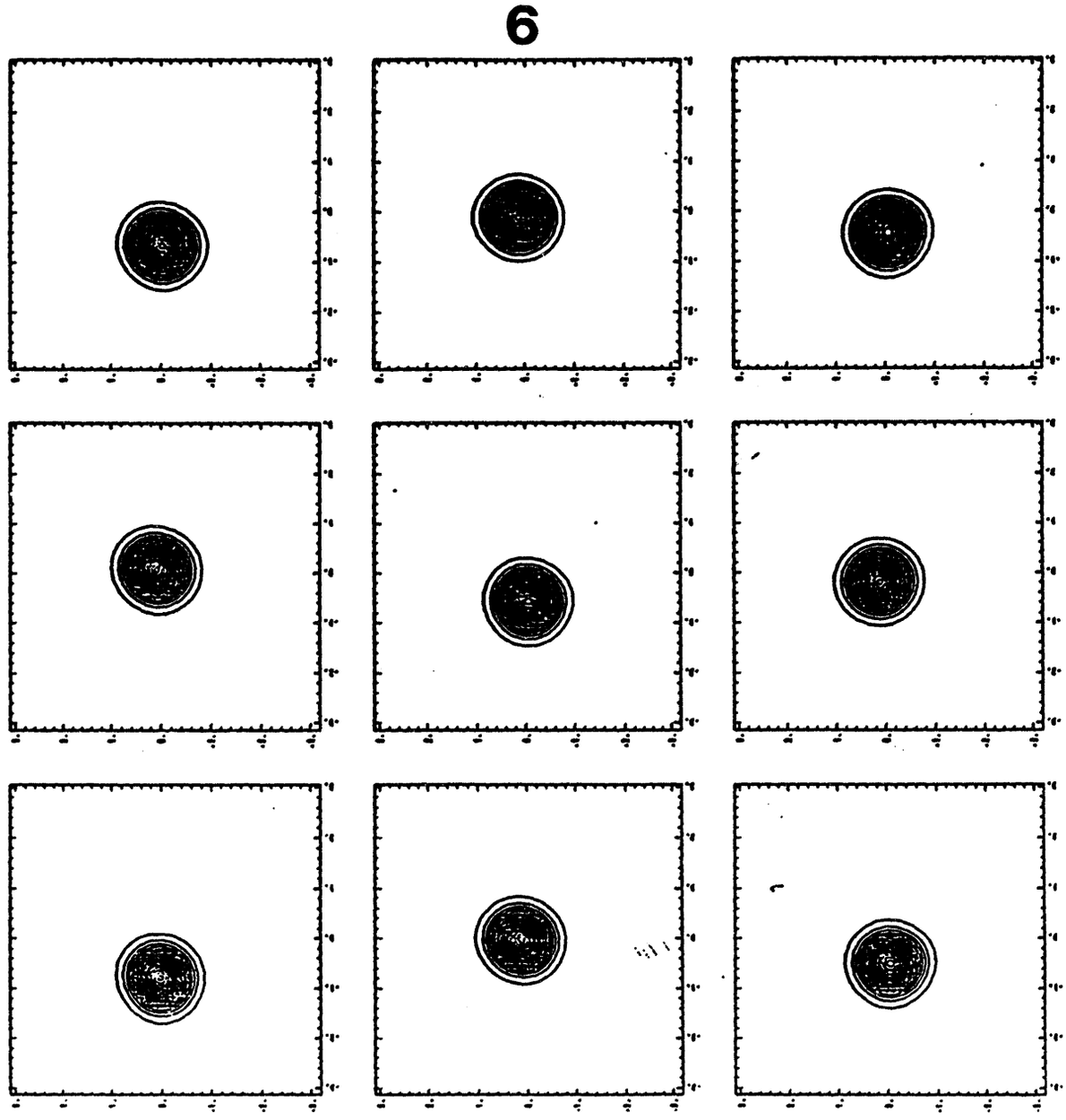

Figure 4.6 The evolution of the Husimi distribution with the same initial conditions as the previous figure.

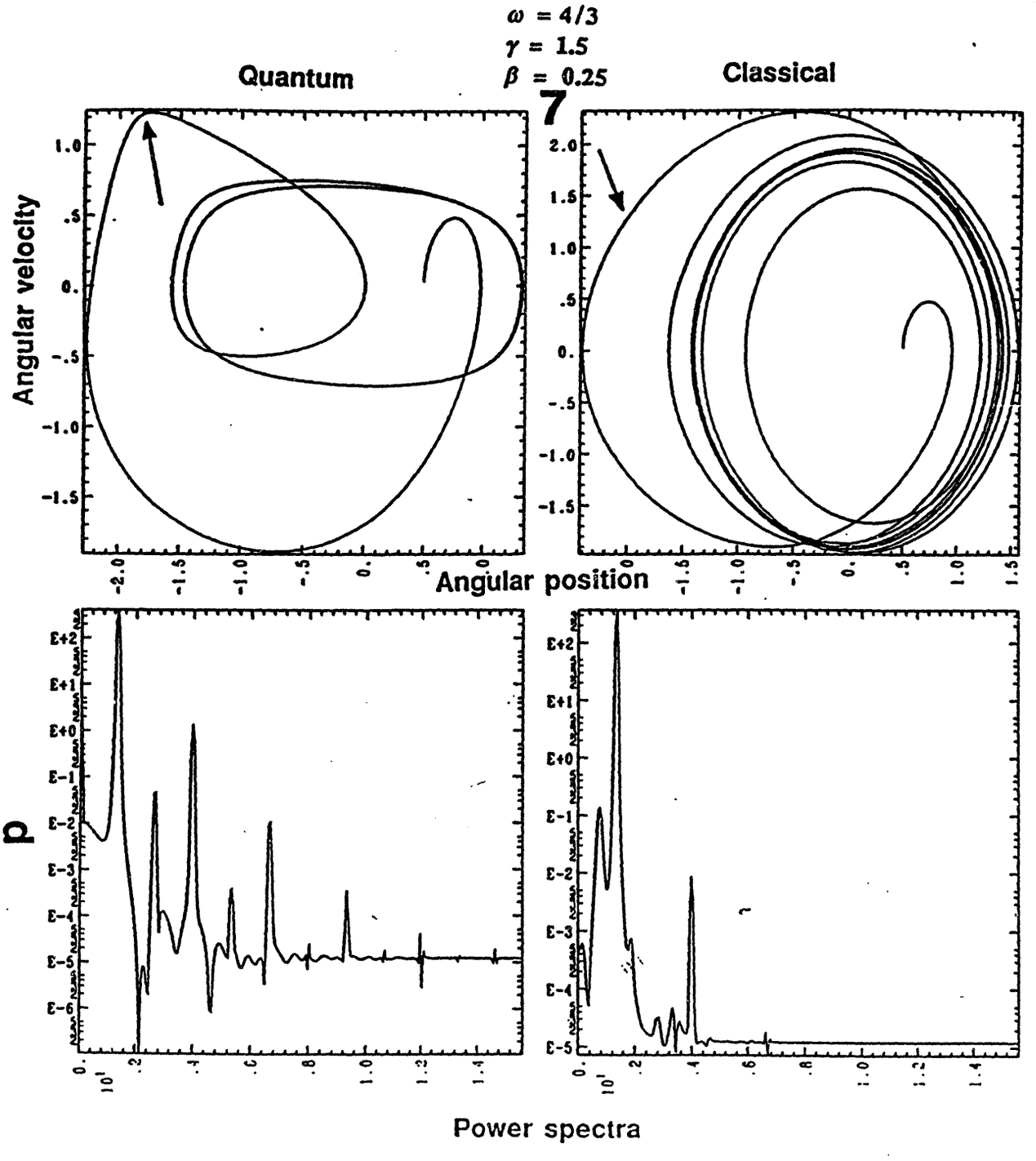

Figure 4.7 Phase-space trajectories of another forced case with moderate strength of damping. Two distinct limit cycles as one can observe from the power spectra at the bottom half are apparent.

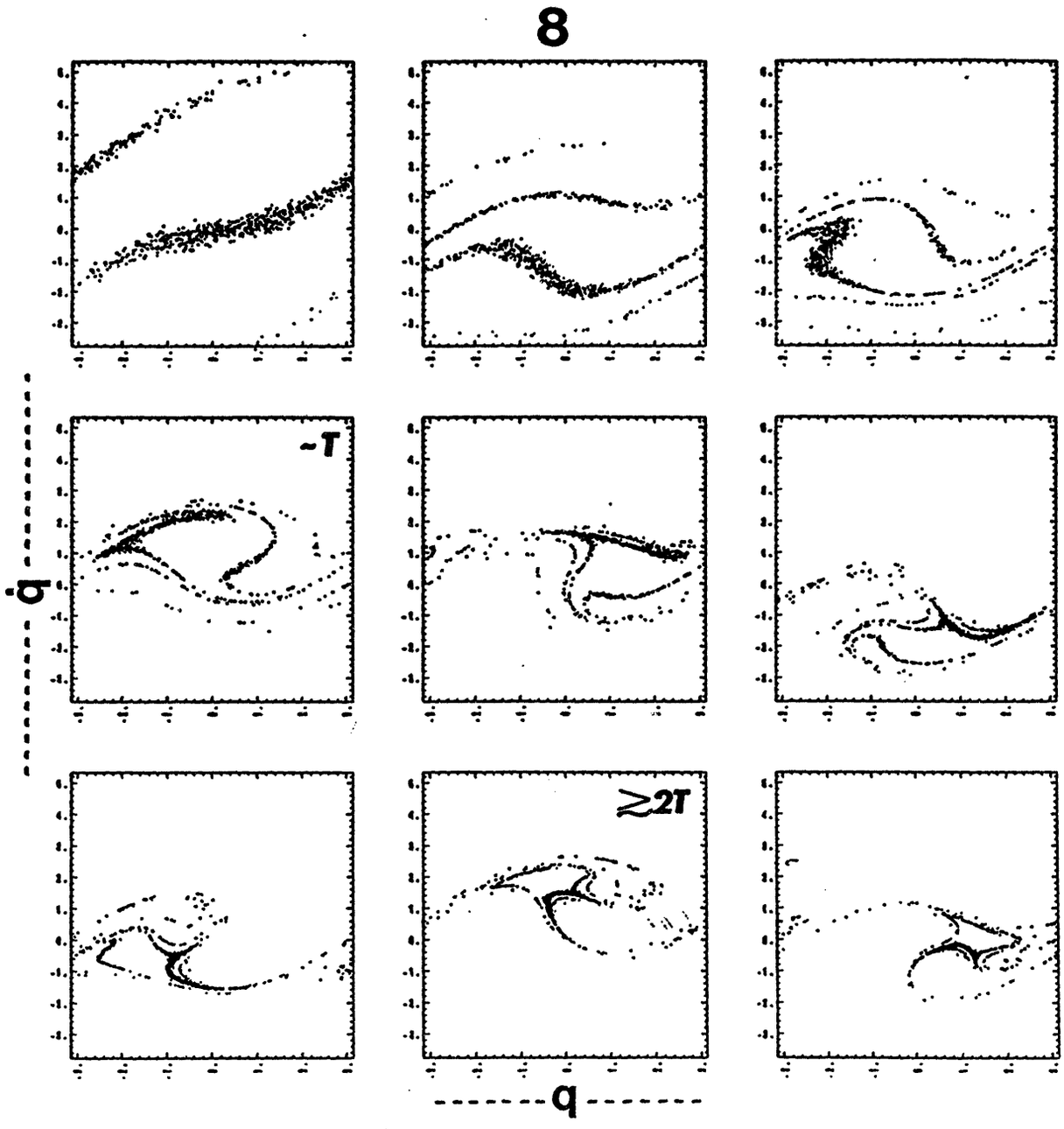

Figure 4.8 The time history of the classical distribution for the previous case in Fig. 4.7. An initially displaced Gaussian distribution revolves clockwise.

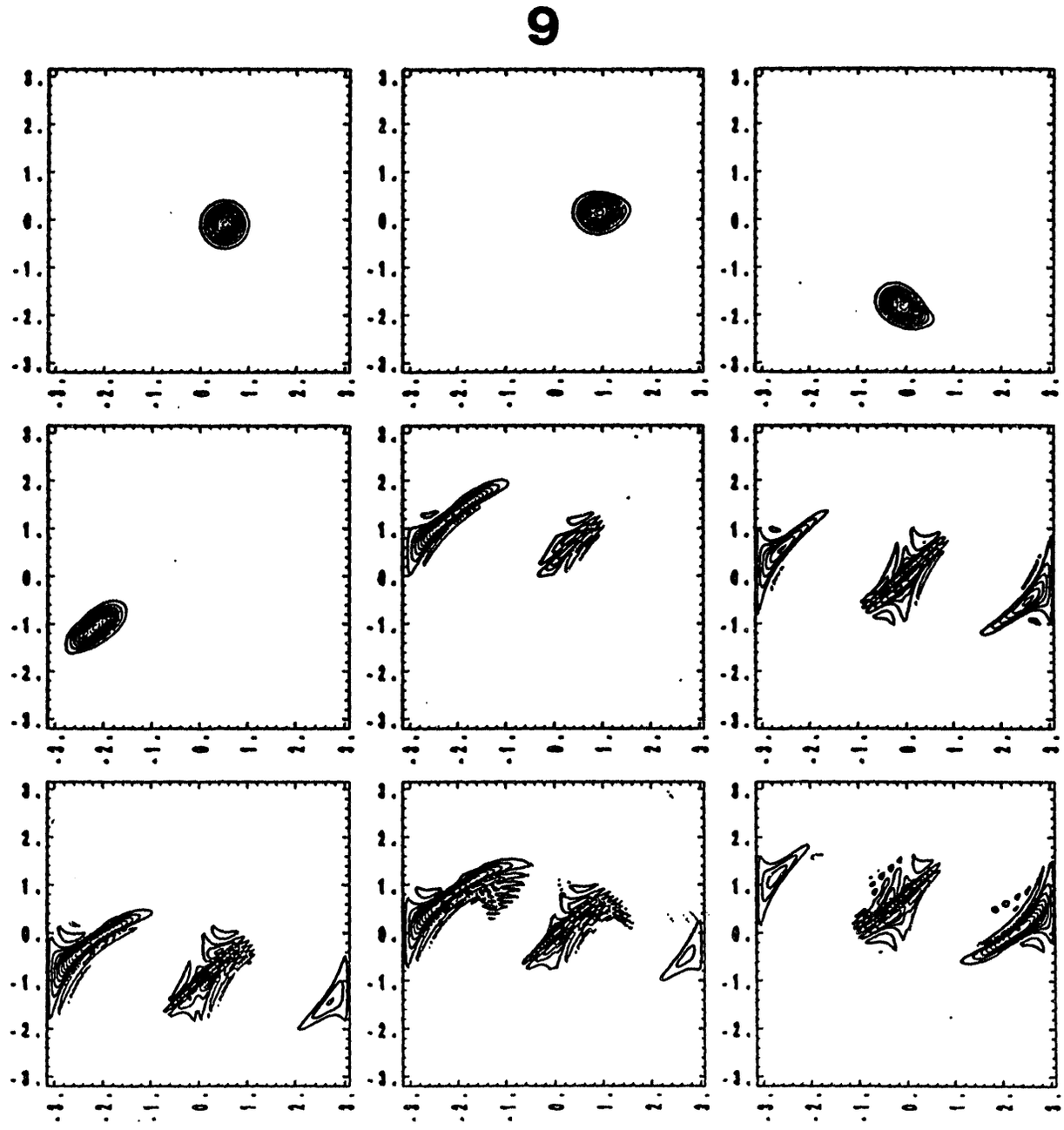

Figure 4.9 The corresponding Wigner distribution to the previous one in Fig. 4.8. The degree of the correspondence is noticeable low.

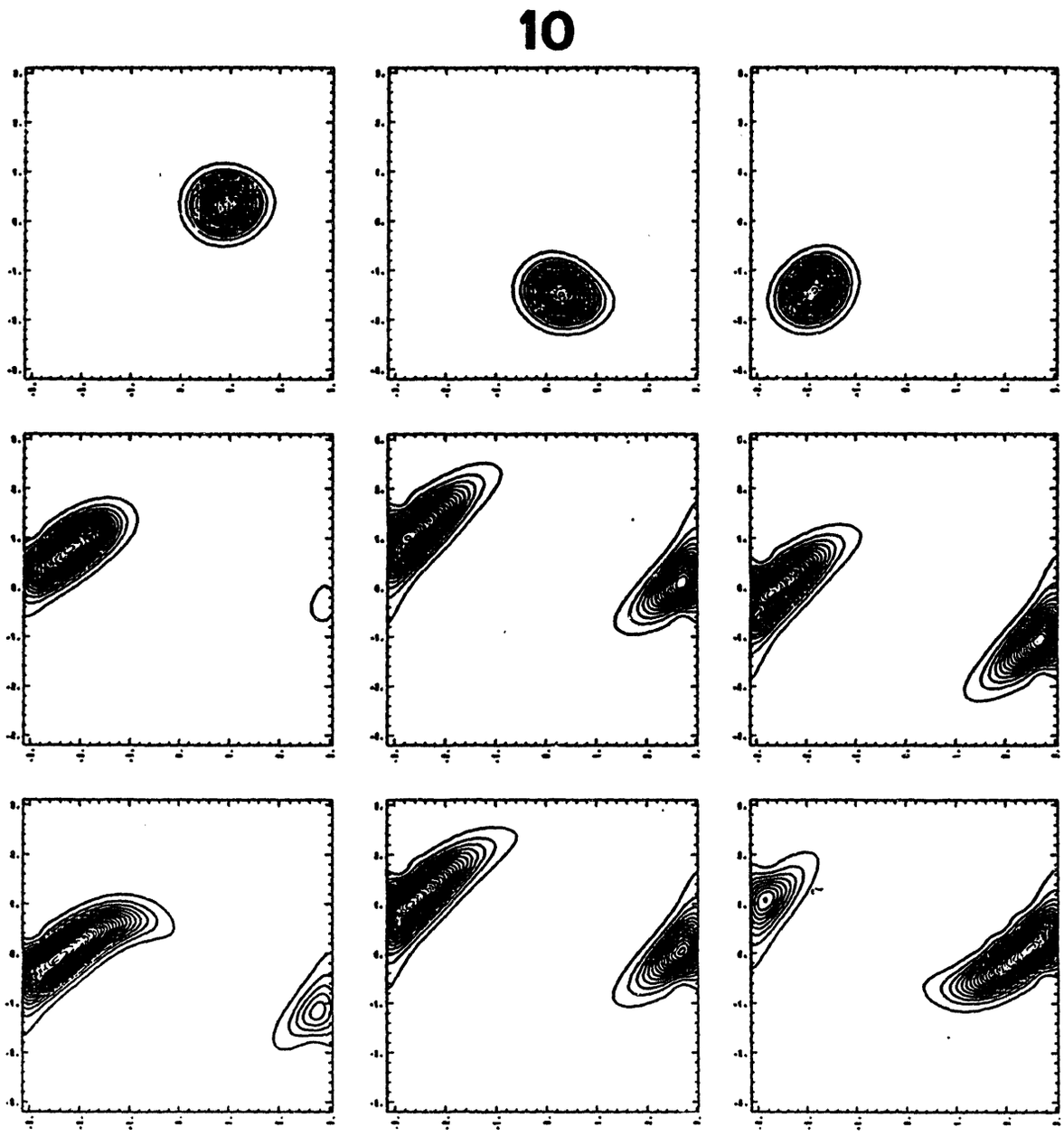

Figure 4.10 The corresponding Husimi distribution. The degree of the correspondence in this case is better than the Wigner one to some extent.

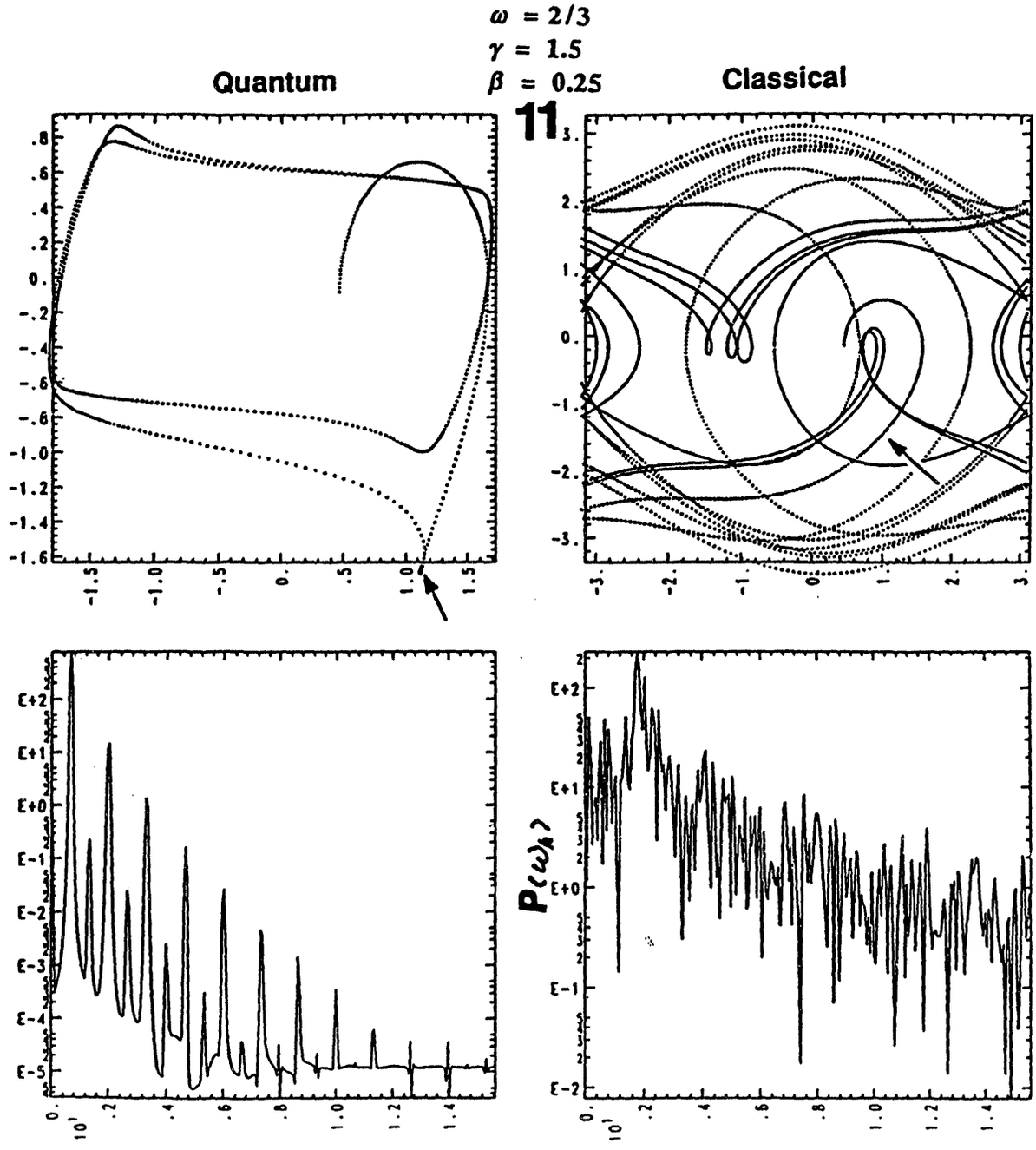

Classically chaotic regime

Figure 4.11 Phase-space trajectories and their power spectra in the classically chaotic regime with incommensurate rational driving frequency.

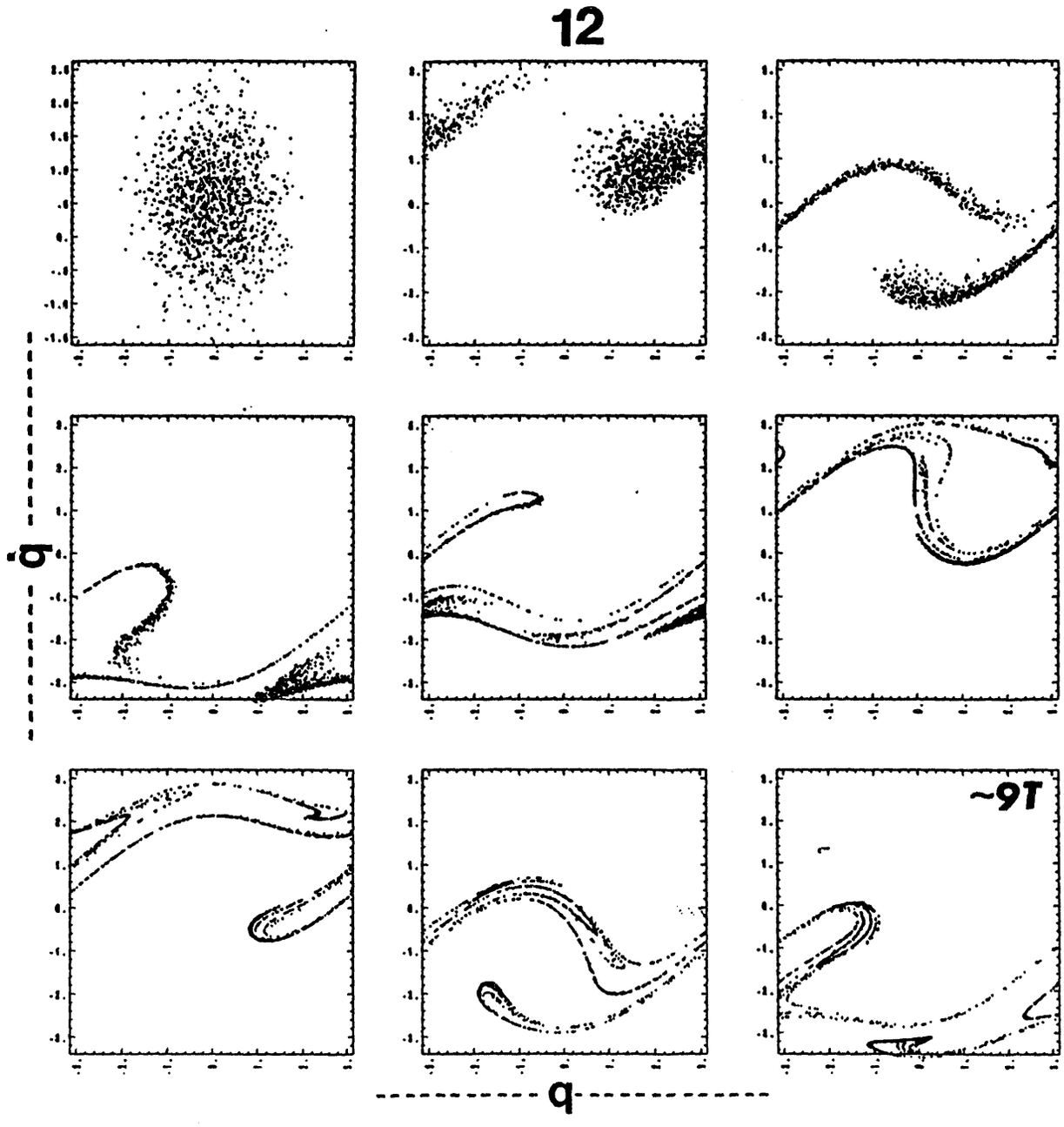

Figure 4.12 The classical distribution clearly evolves to strange attractors with self-similarity.

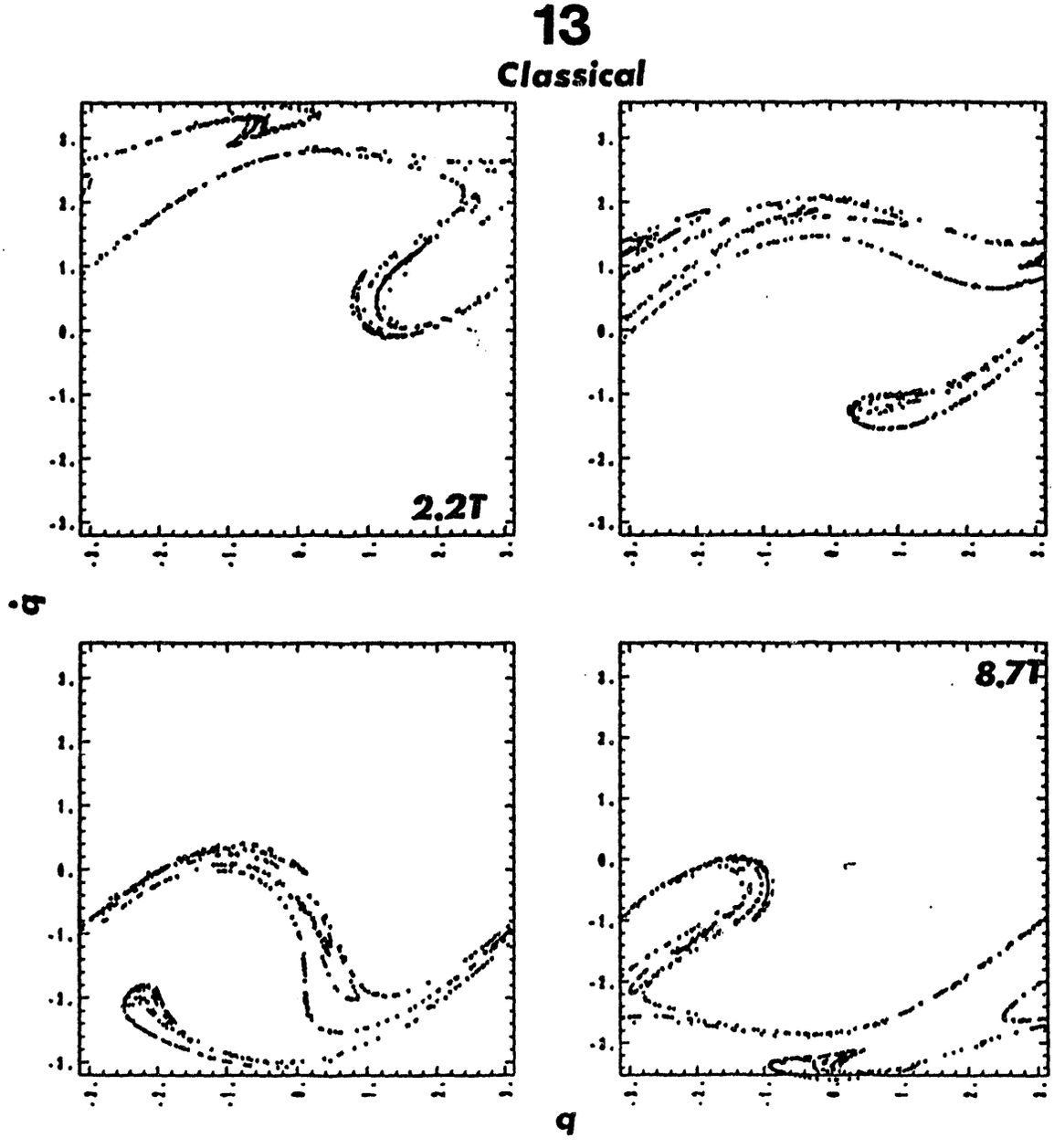

Figure 4.13 Blow-up of the previous figure. Note that the periodicity in configuration space (horizontal axis) at both ends of q.

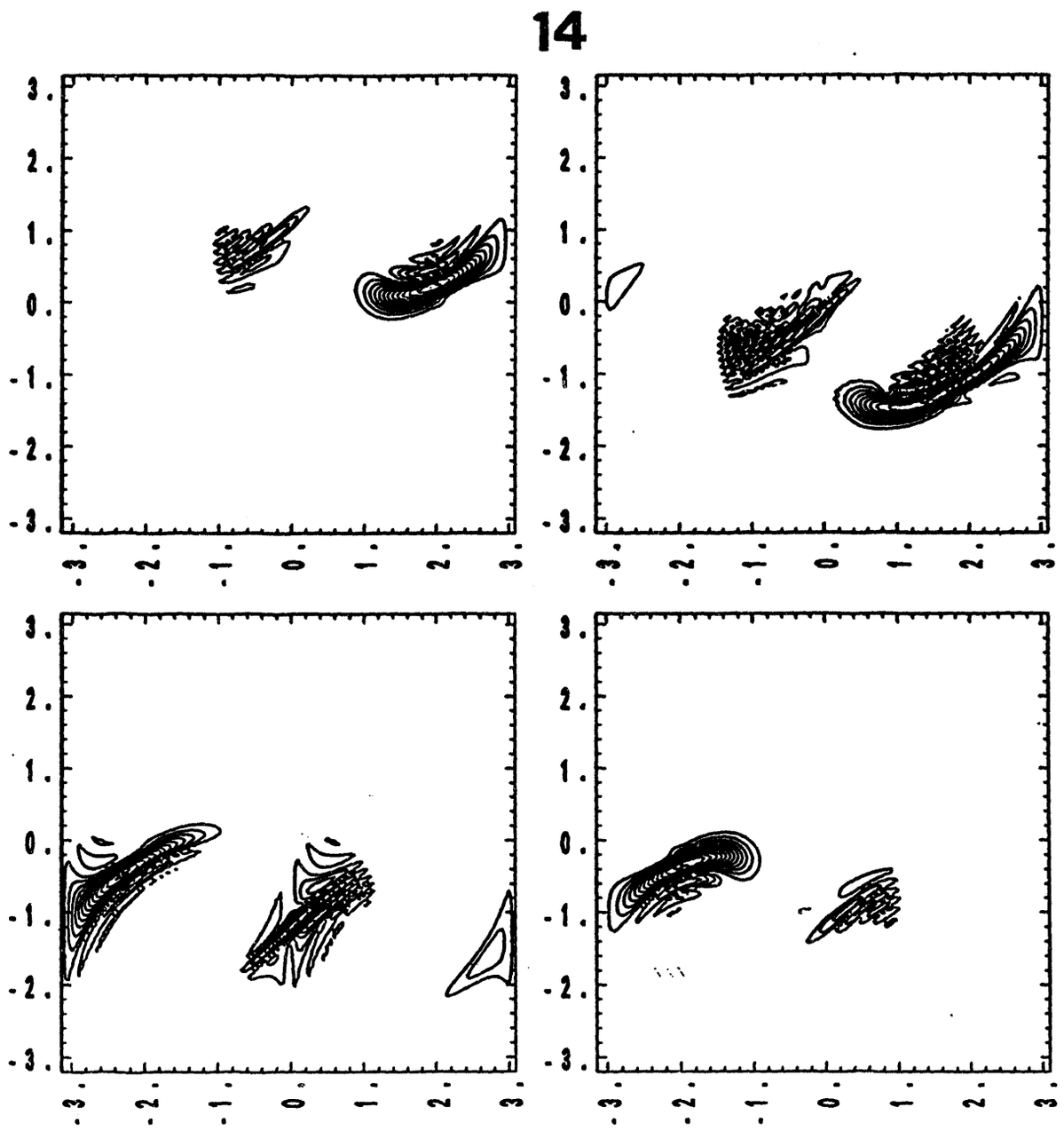

Figure 4.14 The evolution of the Wigner distribution. It resembles the previous figure somewhat.

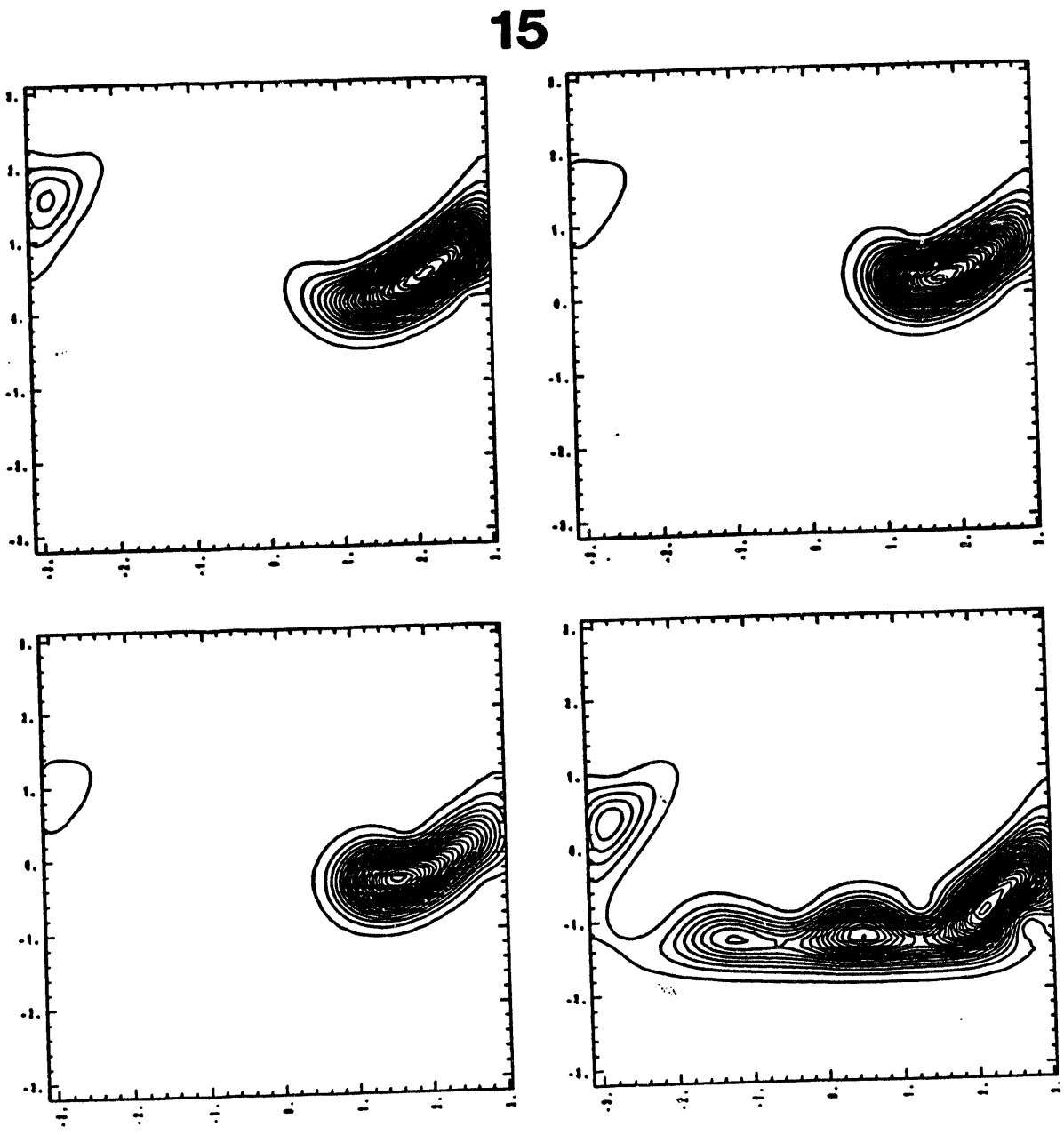

Figure 4.15 The evolution of the Husimi distribution. It resembles Fig. 4.13 more than the Wigner one in Fig. 4.14, especially when t ~ 8.7T, that is after the break time.

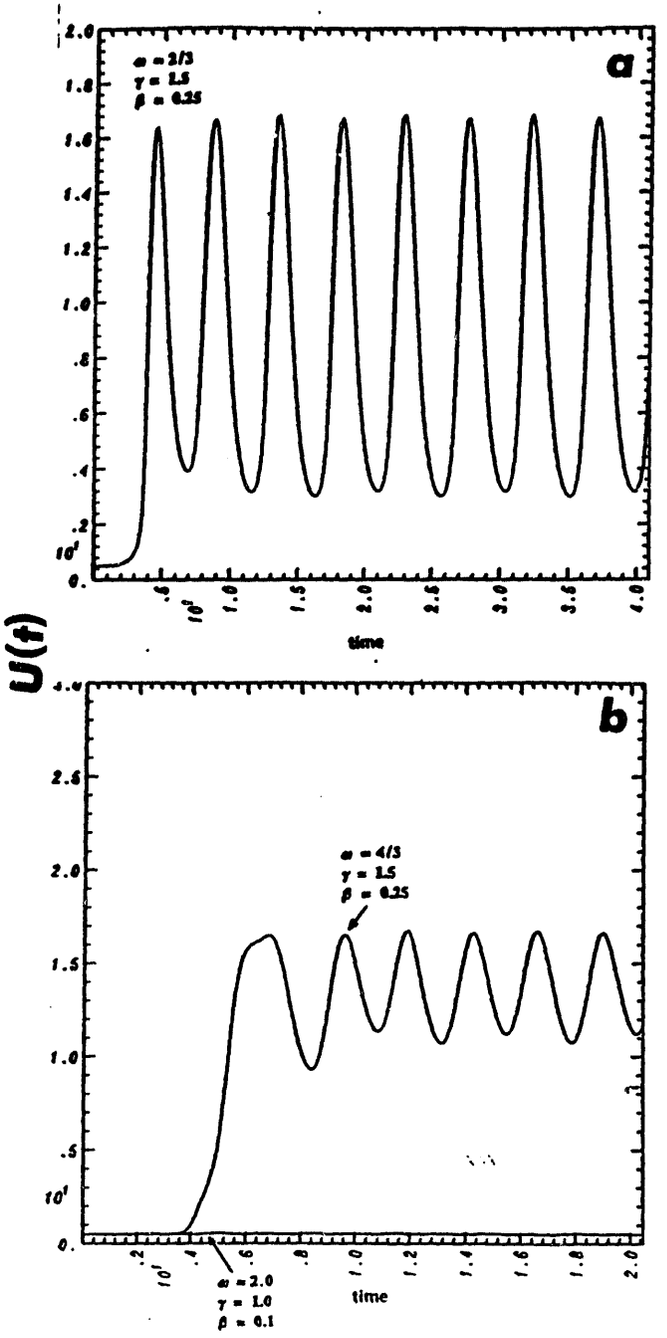

Figure 4.16 The evolution of the uncertainty products showing the previous two cases. Notice the large periodic fluctuations in both cases. It is believed that the correspondence still holds even after the break time because of this periodicity in U(t) although it has large fluctuations.

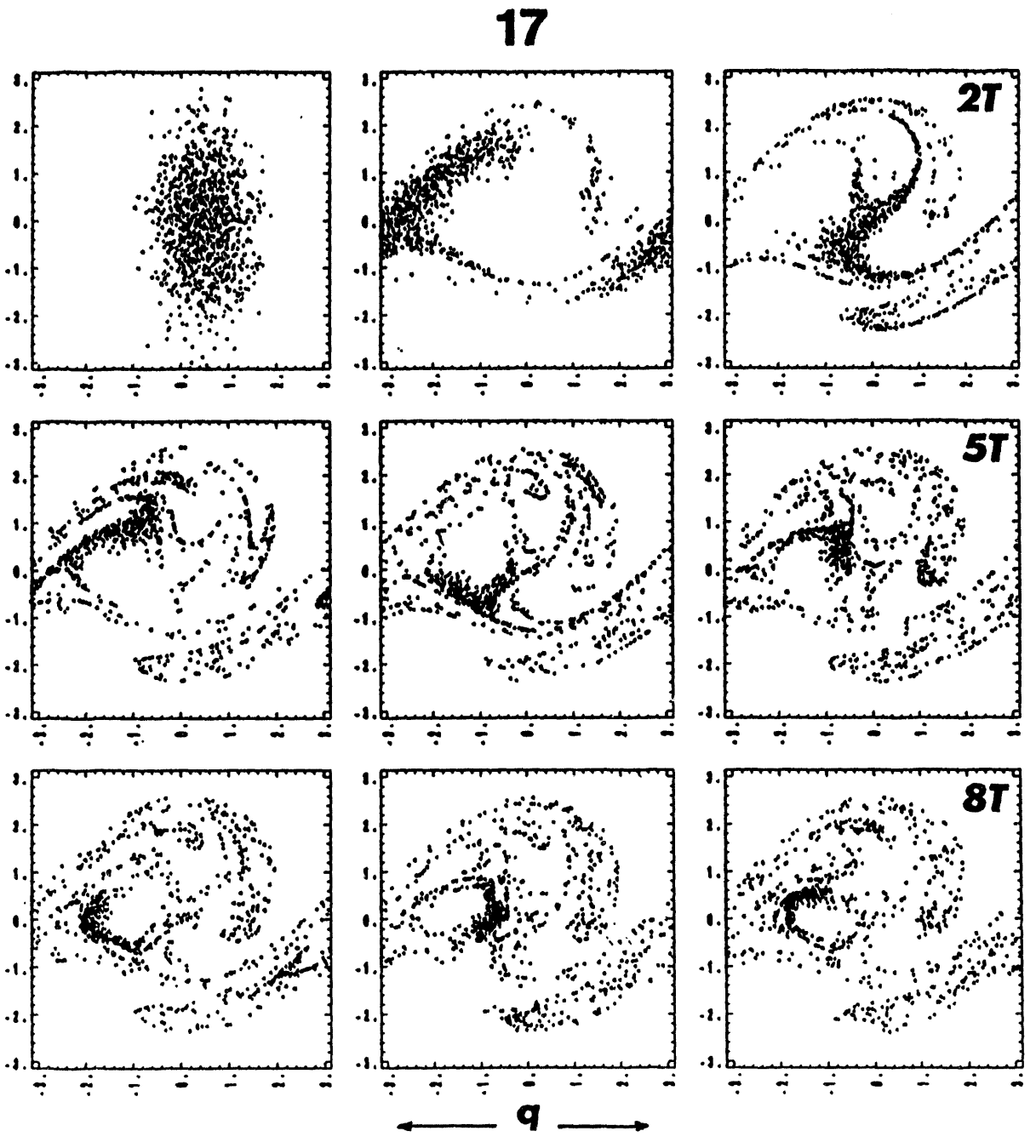

Figure 4.17 Another case of the classical distributions at various times. In this case, a rather small damping coefficient was used for the better correspondence.

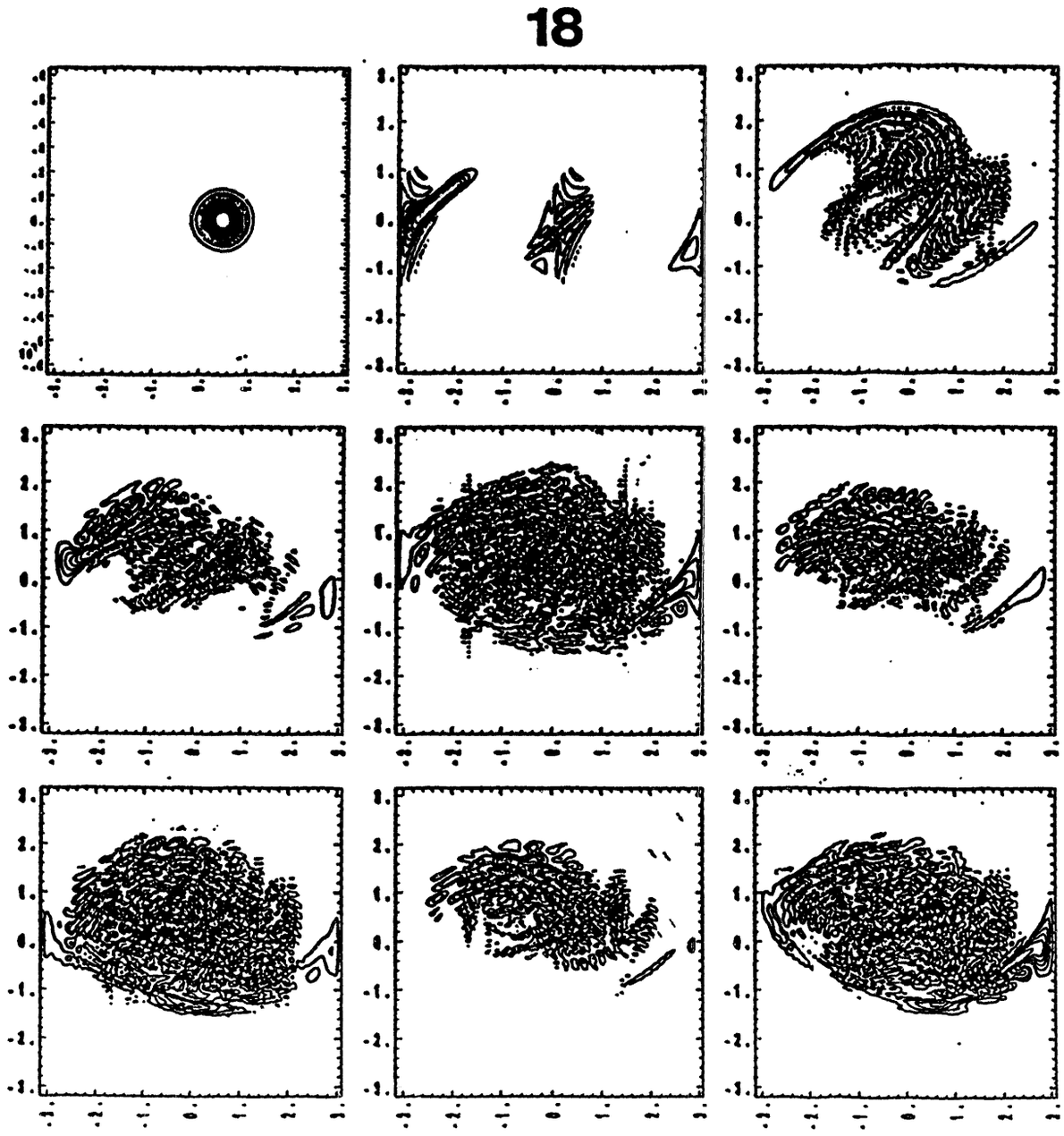

Figure 4.18 The Wigner distributions showing the detailed structures of the evolution of the quantum wave packet.

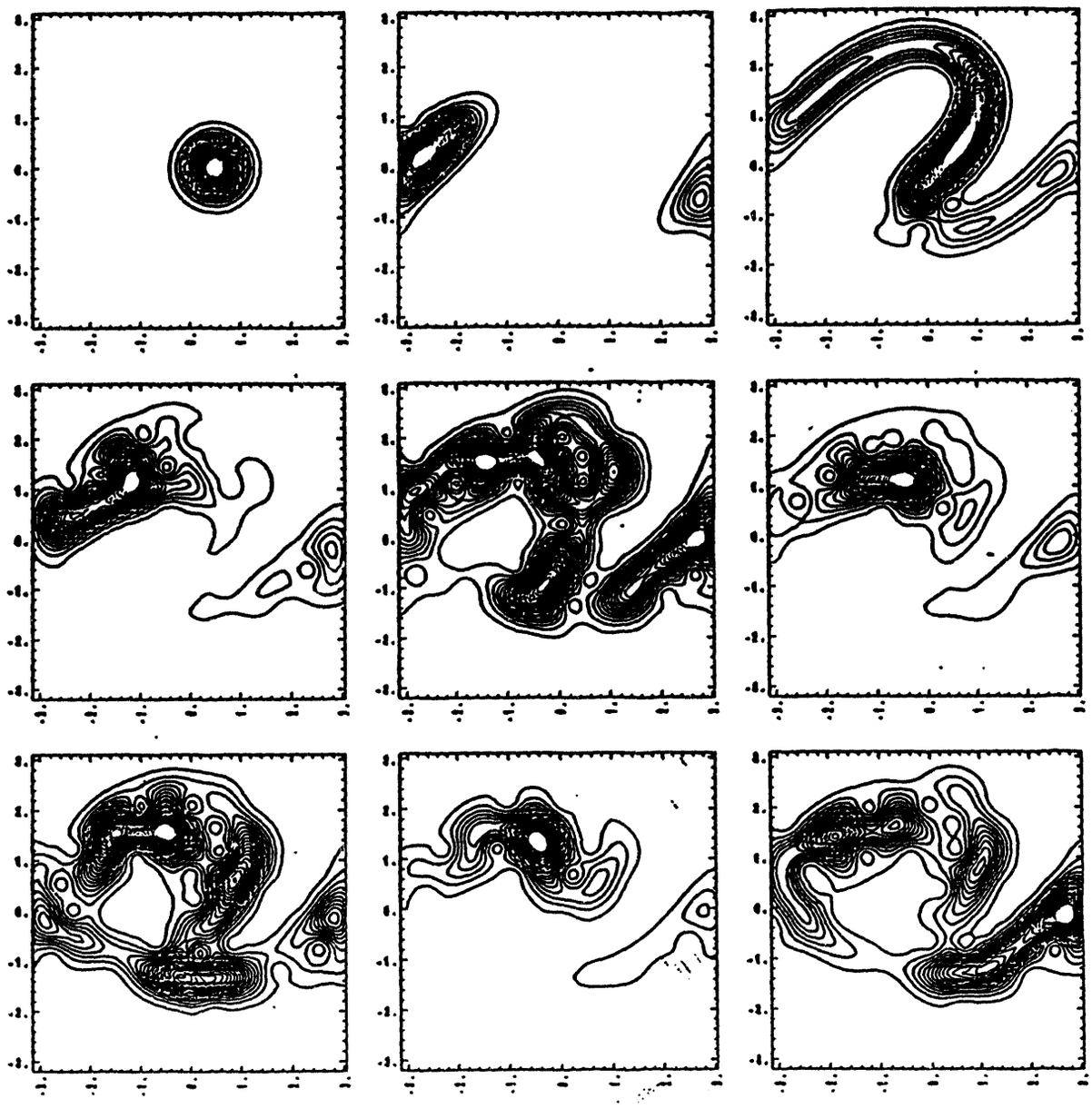

Figure 4.19 The Husimi distributions showing a close representation of the correspondence. It is remarkable that the quantum wave packet contains the information about the classical dynamics.

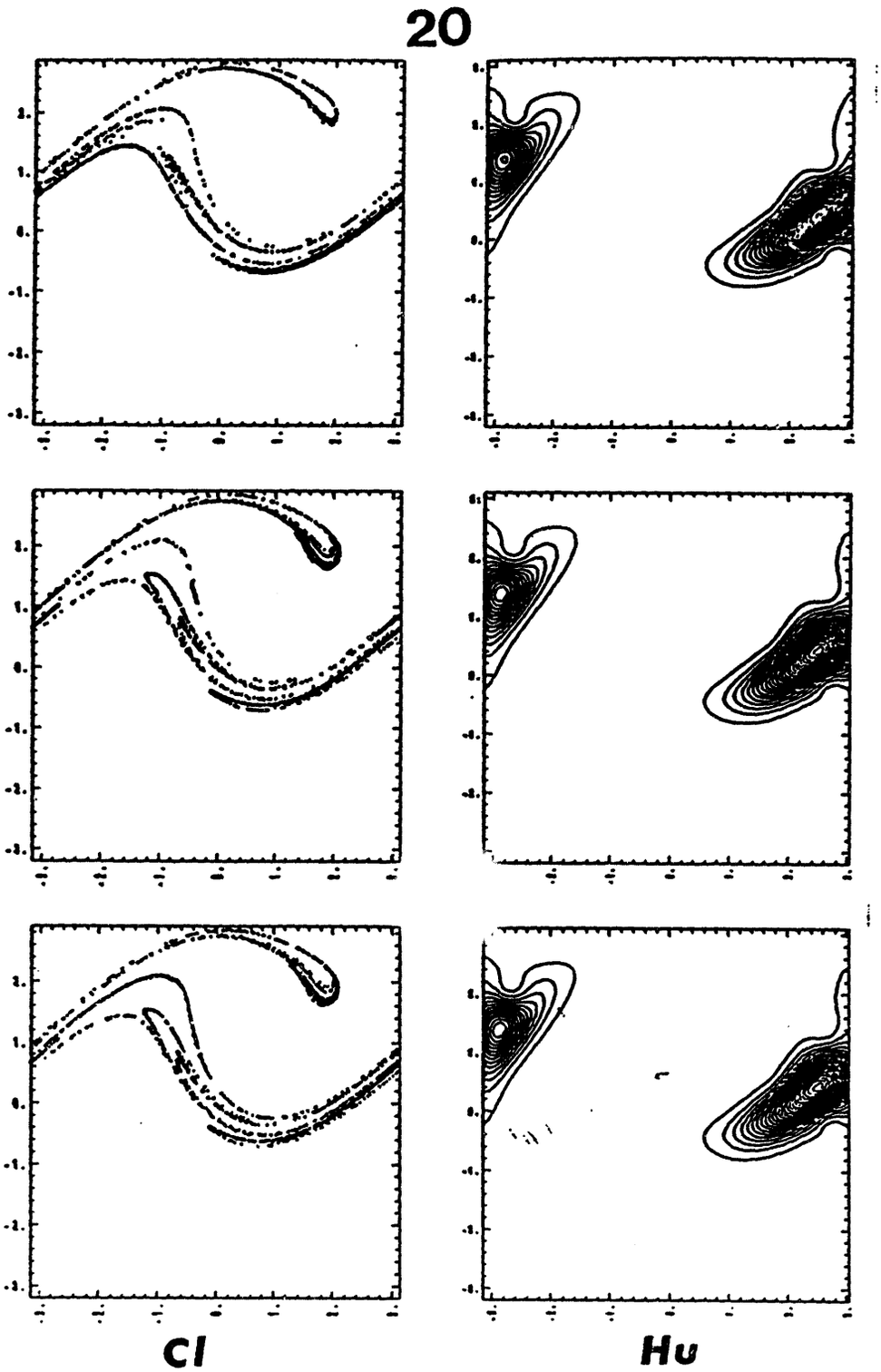

Figure 4.20 Classically strange attractors and their corresponding Husimi distributions. It becomes more apparent that our quantum dissipation scheme represents a good degree of the correspondence.

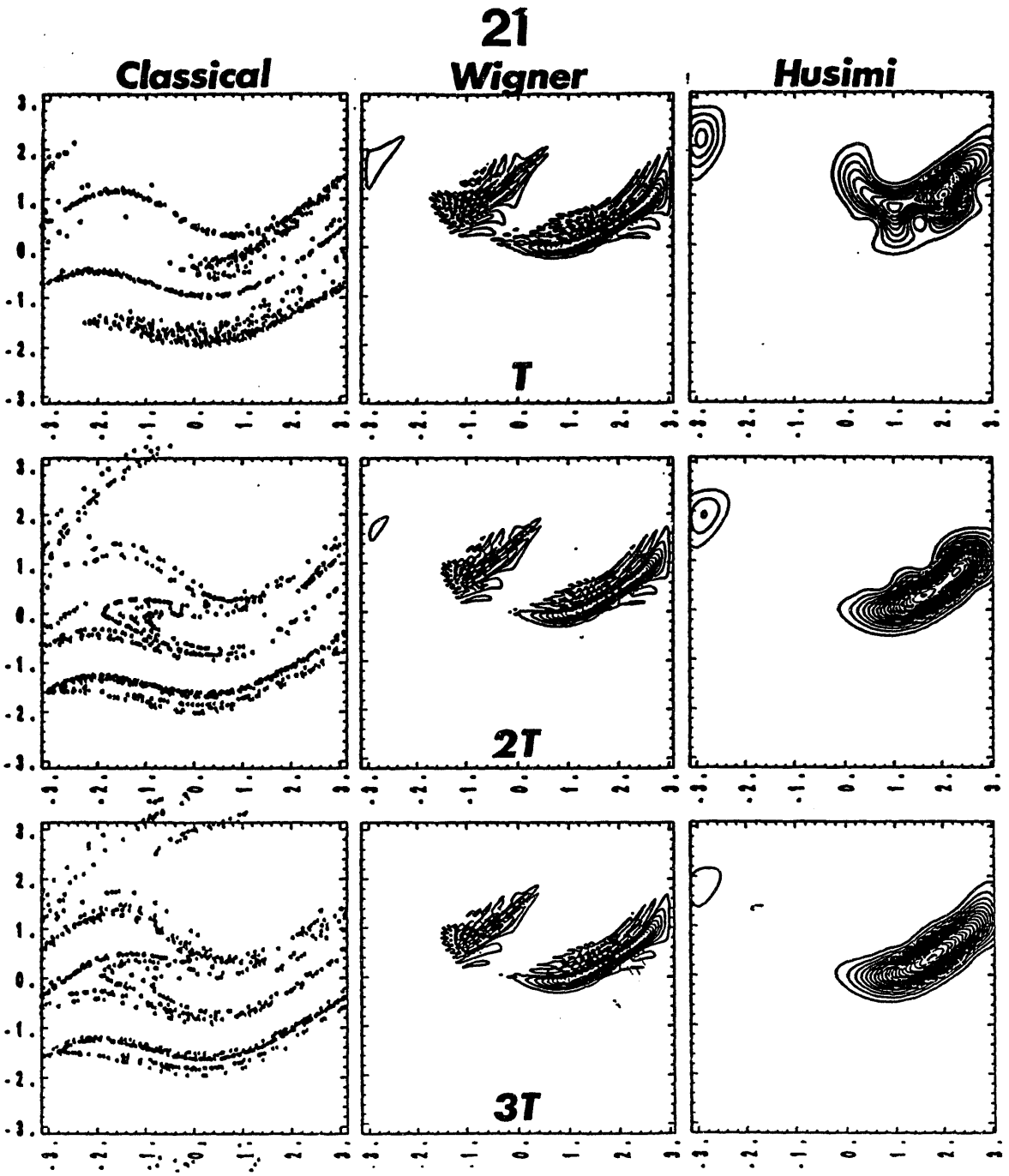

Figure 4.21 Another case with the quantum distributions that are similar to each other. The classical ones are not very close, yet the overall behavior resembles to the Husimi ones.

CHAPTER 5

APPLICATIONS

I had no technical knowledge. · · · It turned out that "allgemeine Übersicht"(general overview) over physical connections is often more valuable than specialist knowledge and routine.

A. Einstein confessing about his early years
(H. Woolf's "Some strangeness in the proportion")

Applications to some other models exhibiting classical chaos are considered. The kicked rotator and the Josephson junction reveal the similar phenomena as in the two previous chapters. In addition a two-dimensional problem is also tackled for Heller's scars. No signs of quantum chaos in terms of classical definitions are detected.

5-1. Kicked rotator

5-1-1. Characteristics of kicked rotators

To study more about quantum manifestations of classical chaos, a slightly different type of kicked rotator has been extensively adopted as an application of our method. The most commonly known model generates Standard mapping equation that exhibits classically chaotic behaviors at the so-called Chirikov threshold value [1]. Since our pendulum can be used as a kicked rotator as explained in Chapter two, exactly the same kinds of operations in the previous chapters can be applied. The two kinds of rotators will be discussed to compare the results from the previous studies [2-4].

First, the Hamiltonian (2-7) is

$$H = \frac{p^2}{2I} + \eta\ (1 - \cos q) \sum_{n=-\infty}^{\infty} \delta(t - nT). \tag{5-1}$$

The corresponding kinetic and potential energy operators are in this case much simpler. They are just

$$\hat{T}(p) = \exp[-i\ \frac{p^2}{4I} T],$$

$$\hat{Y}(q) = \exp[-i\ \eta\ (1-\cos q) T], \tag{5-2}$$

where T is the kick period in this case. It is important to point out that in this case the commutation error disappears, so the operations become exact. The solution of the type (2-22) is a full solution.

The conventional model giving standard equations has the Hamiltonian

$$H = \frac{p^2}{2I} + \eta \cos q \sum_{n=-\infty}^{\infty} \delta(t - nT). \tag{5-3}$$

The operators can be identified easily in this case. Then, we calculate expectation-values of energy and its power spectrum with phase-space behavior. The difference between Eqs. (5-1) and (5-3) is mentioned when we discussed Eq. (2-11) in Ch. 2.

5-1-2. Results and discussions

The first figure shows the map of classical Standard equations with increasing values of η from 0.5 to 1.13. The equation used is (2-11).

$$\begin{aligned} p_{n+1} &= p_n + K \sin q_n , \\ q_{n+1} &= q_n + p_{n+1}. \end{aligned} \tag{5-4}$$

With smaller values of K (or η) shown in Fig. 5.1 (a), two distinct islands are well separated for $\eta = 0.5$, but as η increases seen from (b) to (c), they start intermingling each other. The lower left picture (d) exhibits the appearance of a dark stochastic layer for $\eta = 0.972$ whose value characterizes the Chirikov criterion. All the pictures displayed in the figure use 5000 points, and the initial point is located at $q = 0.02$, $p = 0$ with $T = 1$.

Figure 5.2 also shows a similar phenomenon to Fig. 5.1 with the same initial conditions. This time we use the modified standard equations (2-11). We rewrite the equation here.

$$p_{n+1} = p_n - K \sin q_n ,$$
$$q_{n+1} = q_n + p_{n+1}. \qquad (5\text{-}5)$$

Two islands in the upper left (a) become connected as η increases from 1.35 in (a) to 2.0 in (d). Similar observation of dark stochastic layers and disappearance of islands to the case of conventional Standard mapping can be achieved for even higher vales of η.

It becomes clear that for values $\eta >> 1$, both figures give chaotic classical motions. One may calculate positive Lyapunov exponents for both cases. It is to note that the scales of momentum axis in both figures are not relevant.

Having solved for the classical results, we find differences in the quantum cases. Figures 5.3, 5.4 have the phase-space plots in upper parts (a) and the time variations in energy in lower parts (b) in the classically chaotic regime. The left side of the figures represents the conventional Standard map (5-5), and the right side the modified one (5-6). The bottom parts (c) of the figures show the power spectra of energies. Having said that, we find the same phenomena as Casati *et al* found in their energy variations [5,6]. Energy does not grow indefinitely and is interpreted as quasi-periodic variations of the states.

Figure 5.5 clearly exhibits that the uncertainty product neither grows nor fluctuates by a large amount as shown at the upper right (b). However, the correspondence still seems to be failing. The classical mapping equations (5-5) or (5-6) are discrete maps (difference equation), whereas solving Schrödinger equation using the split method is not a discrete map. Runge-Kutta as well as the quantum algorithms are to solve differential equation as we did in Chapters three and four. So starting with the differential equation

of (5-1) or (5-3), one could recover the correspondence even for a short time interval. Limpidly distinguishable peaks of power spectra at the lower half (c) and (d), support quasi-periodicity lying under the dynamics of the system. Therefore, in quantum cases, we find no evidence to quantum chaos, and the correspondence fails. Another example will be discussed in the next section where we focus on how the energy expectation-value varies in time.

5-2. Josephson junction and devil's staircase

The strange phenomenon known as the 'devil's staircase' in Josephson junction has been observed experimentally. Many numerical simulations of this phenomenon have showed the similar structures in their current vs. average voltage characteristic curves. However, the quantum mechanical treatment using solely Schrödinger equation has not been studied due to difficulties rising from many-body calculations with a dependence on temperature. In this section, we try to show a possible quantum treatment in the context of the classical-quantum correspondence. We shall not consider this topic rigorously here.

We first consider a Josephson junction whose classical equation is just (2-14). In a simplified form, it becomes

$$\ddot{q} + \sin q = \gamma_o + \gamma_1 \cos(\omega t) - \beta \dot{q}, \qquad (5\text{-}6)$$

where the phase difference between the two superconductors is denoted as q. It is obvious that the phase difference occurs because of quantum tunneling effect [5]. Yet the classical equation (5-6) describes the dynamics due to classical measurement of current and voltage. With the dissipation term, $-\beta\dot{q}$,

removed, the quantum version of the corresponding Hamiltonian takes the following form;

$$\hat{H} = -\frac{1}{2}\frac{\partial^2}{\partial q^2} + (1 - \cos q) - \gamma_1 q \cos(\omega t) - \gamma_0 q \,. \tag{5-7}$$

Representations of the external DC and AC currents are denoted as γ_0 and γ_1 in dimensionless forms. The relation $k\gamma = \Gamma$ specifies the proportional constant k whose magnitude or dimension is determined by the equations (2-14). Note there exists no equivalent mass term since we only deal with cooper pairs of electron [6]. The equivalent form of (5-7) is

$$\hat{H}_{\text{gauge}} = \frac{1}{2}\left[p + \gamma_1 \frac{\sin(\omega t)}{\omega} + \gamma_0 t \right]^2 + (1 - \cos q)\,, \tag{5-8}$$

whose gauges are simply in this case

$$\begin{aligned} \hat{\mathbf{A}} &= -\gamma_1 \frac{\sin(\omega t)}{\omega} - \gamma_0 t \,, \\ \hat{\chi} &= \gamma_1 q \frac{\sin(\omega t)}{\omega} + \gamma_0 q t \,, \end{aligned} \tag{5-9}$$

such that the gauge transformation with

$$\begin{aligned} \hat{\mathbf{A}}' &= \hat{\mathbf{A}} + \frac{\partial \hat{\chi}}{\partial q} = 0 \,, \\ \hat{\mathbf{V}}' &= \hat{\mathbf{V}} - \frac{\partial \hat{\chi}}{\partial t} = (1 - \cos q) - \gamma_1 q \cos(\omega t) - \gamma_0 q \,, \end{aligned} \tag{5-10}$$

yields the same Hamiltonian (5-7).

It is not difficult to show that the operators in this case become

$$\hat{T}_{eff}(p) = \exp[-i(1-i\beta)\frac{p^2}{4}\Delta t]$$
$$\times \exp\left[-i(1-i\beta)\frac{1}{2}\frac{p\gamma}{\omega}\left\{\sin(\omega t)\frac{\sin(\omega\Delta t)}{\omega} - \cos(\omega t)\left(\frac{\cos(\omega\Delta t)-1}{\omega}\right)\right\}\right],$$
$$\times \exp\left[-i(1-i\beta)\frac{p\gamma_0}{4}\{2t\,\Delta t + (\Delta t)^2\}\right] \qquad (5\text{-}11)$$

$$\hat{Y}_{eff}(q) = \exp[-i(1-\cos q)\Delta t]$$
$$\times \exp\left[-i(1-i\beta)\frac{\gamma^2}{2\omega^2}\left\{\frac{\Delta t}{2} - \sin(2\omega t)\frac{\cos(2\omega\Delta t)-1}{4\omega} - \cos(2\omega t)\frac{\sin(2\omega\Delta t)}{4\omega}\right\}\right],$$
$$\times \exp[-i(1-i\beta)(\{\frac{\gamma_0^2}{6}(3t^2\Delta t + 3t\,\Delta t^2 + \Delta t^3)\}$$
$$-\{\frac{\gamma_0\gamma_1}{\omega^2}((t+\Delta t)\cos(\omega(t+\Delta t)) - t\cos(\omega t))\}$$
$$+\{\frac{\gamma_0\gamma_1}{\omega^3}(\sin(\omega(t+\Delta t)) - \sin(\omega t))\})]. \qquad (5\text{-}12)$$

This rather long expression is not difficult to program. Now we are interested in current vs. voltage characteristic curve known as I-V curve. It is of importance to distinguish our version from the classical circle map. The circle map displays the rich forms of the devil's staircase with the concept of rational winding number. The physics is similar in each case, but the exact structure in Eq. (5-6) is quite different.

To find the devil's staircase in the I-V curve, we must first take the time average of the voltage. Figure 5.6 shows a typical classical I-V curve with

rather large staircase. The blow-up of this flat plateau with finer scales would display more plateaus forming Cantor-set like structure [7].

However, the quantum case does not show any similar devil's staircase structure as seen in Figure 5.7. There seems to exist one at around 0.13, but the numerical study with a more resolution suggests that it is due to either numerical fluctuations or the uncertainty variations in that region. By taking the long time limit in the order of hundreds of the driven field period, which is more close to a experimental situation, a small steady increase replaces the fluctuating part running from 0 to about 0.18.

Thus, we also find no direct evidences of correspondence between classical and quantum mechanical treatment of the junction. So far none of our examples are in contradiction with our earlier conclusions from the pendulum. In fact, the examples here uphold the core idea that it is arduous to track down quantum manifestations of classical mechanics in chaotic regime although we scent some in the distribution functions.

5-3. Search for 'scars' in 2-dimensional Duffing's potentials

It is interesting to study more about quantum chaos using different, but simple techniques. One of the available techniques is known as the Heller's scar [8-10] for actual visualization of dynamical properties of the quantum wave packet. It is regarded as the remnant of the dynamical wave functions in the potential field (configuration space). Since we have been solving Schrödinger equation, the scar of bound states can be determined for appropriate potentials. It is better for us to use a two-dimensional potential (it is difficult to visualize the scar in one dimensional potential). Duffing's potential which gives rise to a classical Duffing's oscillator [11] seems to be a

good choice. It should be noted that the stadium problem [12] requires the cylindrical geometry. Because of the difficulty emerging from the Fourier-Bessel transformation in our scheme, the same problem is not being chosen, and a simpler version of Duffing's potential is established. The model Hamiltonian for this Duffing's oscillator is

$$H(x,y,p_x,p_y)=\frac{p_x^2}{2}+\frac{p_y^2}{2}+V(x,y), \tag{5-13}$$

where the potential is

$$V(x,y)=-\frac{1}{2}a(x^2+y^2)+\frac{1}{4}b(x^4+y^4). \tag{5-14}$$

This potential is depicted in the three-dimensional diagram in the next page (upper one). The potential we use numerically, V_{true}, has a scalar difference from (5-14) since we are interested in the potential whose minimum is at least 0 for numerical reasons (the minimum value of (5-14) is negative, $-\frac{a^2}{4b}$). So we have

$$V_{true}(x,y)=-\frac{1}{2}a(x^2+y^2)+\frac{1}{4}b(x^4+y^4)+\frac{a^2}{4b}. \tag{5-15}$$

It would be interesting to study a similar, but cylindrially symmetric potential of the following form which is also depicted in the next page (lower one):

$$V_{true}(x,y)=-\frac{1}{2}a(x^2+y^2)+\frac{1}{4}b(x^2+y^2)^2+\frac{a^2}{4b}, \text{ or}$$
$$V_{true}(r)=-\frac{1}{2}ar^2+\frac{1}{4}br^4+\frac{a^2}{4b}. \tag{5-16}$$

Diagram describing the two-dimensional potentials.

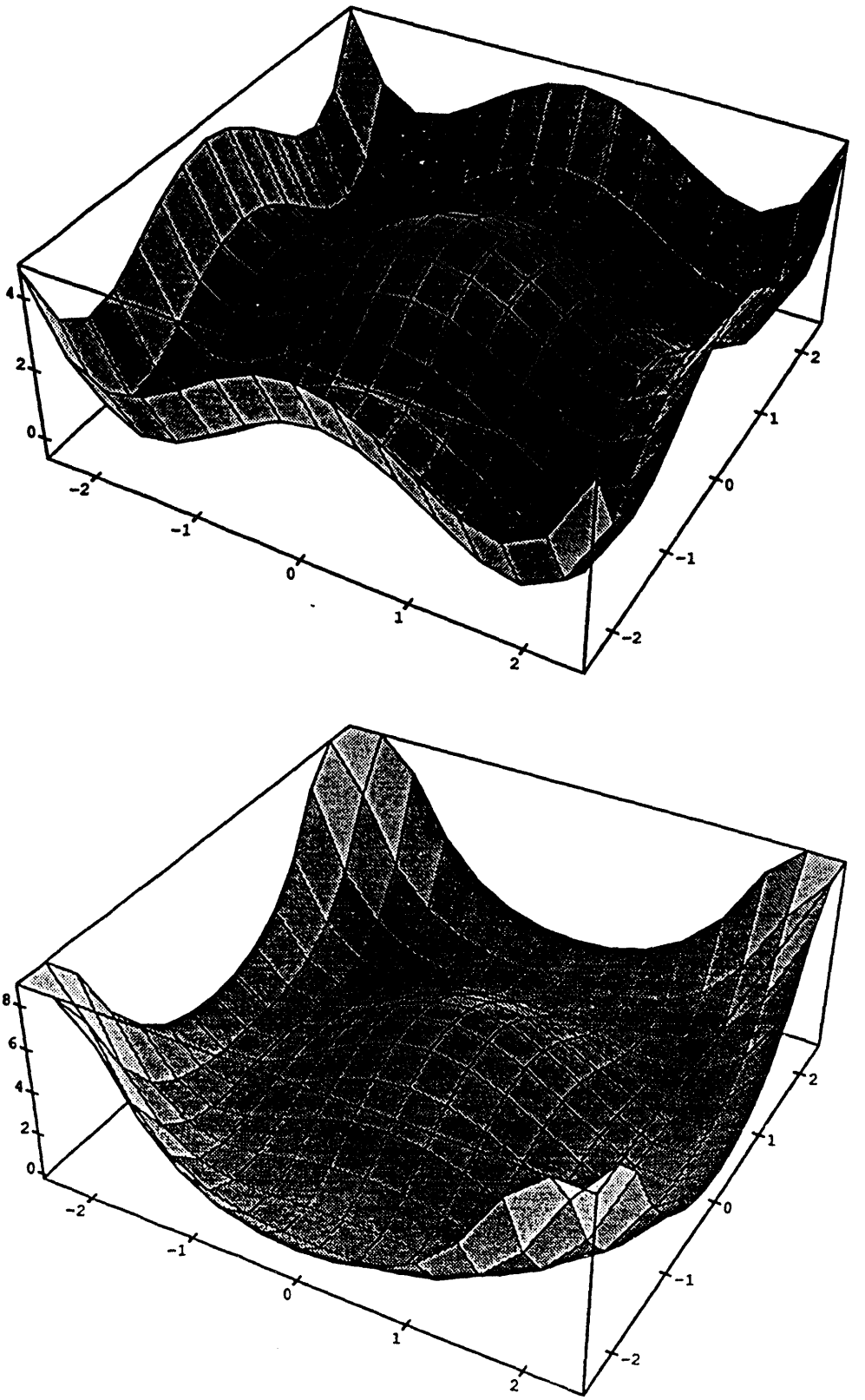

The Hamiltonian (5-13) is then utilized by the method described in Ch. 2. We are interested in the wave packet at different times in two-dimensional potential configuration space. It is expected that the contours of the quantum wave packet amplitudes would reveal the scar of bound states resembling classical trajectory in the same space. Classically chaotic cases most likely associated with unbound states, therefore, will not be considered here.

The corresponding classical equations of motion becomes using (2-2)

$$\begin{cases} \ddot{x} - ax + bx^3 = 0 \\ \ddot{y} - ay + by^3 = 0. \end{cases} \tag{5-17}$$

We use an initial wave function of the form:

$$\psi_o(x,y,p_x,p_y) = \frac{1}{\sqrt{\pi\delta}} \exp\left[-\frac{(x-x_o)^2}{2\delta}\right] \exp\left[-\frac{(y-y_o)^2}{2\delta}\right]$$

$$\times\left\{(x-x_o)^2 + (y-y_o)^2\right\}^n, \tag{5-18}$$

where n specifies the power of the polynomial function. It is not difficult to conjecture that the doughnut shape of ψ_o is close to that of the ground state because of the bump in the middle of the potential as shown in the diagram.

The results of calculations display an interesting aspect: overlaps of many classical trajectories. Fig. 5-8 is a typical classical trajectory for bound motions in x-y space with four different, but arranged initial conditions (all initial momenta are set to zero). Since all the motions are regular, symmetry given by the potential must exist. The next figure in Fig. 5-9 lists the time history of the wave packet in x-y plane with an initial condition of classically bound motions. An initial wave function is displaced asymmetrically. The

wave function quickly develops into the near four-fold symmetric forms, and their orientations marked by dark area of condensed contours are similar to the classical trajectories. Figs. 5-10 and 5-11 are exhibiting similar phenomena. The wave forms started from the initial wave function that was located at the center in Fig. 5-11 clearly indicate a four-fold symmetry – the finding of this symmetry is not objective but subjective, so one may have a different observation. One could notice, however, the similarity between Fig. 5-8 and Figs. 5-9 ~ 5-11. Therefore, the scars can be checked using the method described so far. The possible extension to the cylindrical coordinate or even to the spherical one could provide many applications. Ours are limited to the Cartesian coordinate. Note the parameter values $a = -0.7$, $b = 1.0$, and $n = 6$.

5-4. Three coupled nonequilibrium oscillators

In this section, we discuss the nonequilibrium quantum mechanical analog of Nosé-Hoover mechanics, briefly discussed in Section 4-2-2. We study a quantum mechanical nonequilibrium constrained system. By analogy with Gauss' principle of least constraint [13], we constrain some kinetic energies to be constants in time. The total mass is fixed.

Gauss' principle of least constraint states that any dynamical constraint should be imposed by using the least possible constraint force. This statement is

$$\sum_{k=1}^{N} \frac{F_c^2}{2m} \text{ minimum,} \tag{5-19}$$

where the constrained system has N degrees of freedom. By adding small variations to the constraint forces, (5-19) is equivalent to

$$\sum_{k=1}^{N} \frac{F_c \cdot \delta F_c}{m} = 0. \tag{5-20}$$

Gauss' principle, when used to impose isothermal conditions, by constraining the kinetic energy, produces exactly the same equations of motion as Nosé-Hoover's equations of motion in Eq. (4-4).

We shall apply Gauss' least-constraint idea to quantum mechanics by restricting Schrödinger equation in order to explore quantum chaos. Heat and work can be included in Schrödinger equation by imposing three constraints [14]:

$$C_{mass} = \sum_i (\psi_i^R \psi_i^R + \psi_i^I \psi_i^I) - 1 = 0, \tag{5-21a}$$

$$C_{momentum} = \sum_i (\psi_i^R \nabla \psi_i^I + \psi_i^I \nabla \psi_i^R) - SJ(t) = 0, \tag{5-21b}$$

$$C_{kinetic\ energy} = \sum_i -\frac{1}{2}(\psi_i^R \nabla^2 \psi_i^R + \psi_i^I \nabla^2 \psi_i^I) - SE(t) = 0. \tag{5-21c}$$

S is the number of available sites, J is the current, and E is the energy per site. Superscripts R and I represent the real and imaginary parts of ψ respectively. Hoover's analog of Gauss' principle [14] for quantum mechanics (HMS equation for Hoover's Modified Schrödinger equation) is

$$\left[\frac{\partial \psi}{\partial t}\right]_{Gauss} = \left[\frac{\partial \psi}{\partial t}\right]_{Schr} - \sum_j [\lambda_j(\psi) \nabla_\psi C_j]. \tag{5-22}$$

The subscript *Schr* stands for the usual Schrödinger equation. The Lagrange multipliers are λ_j and vary with time. The sum includes the constraints (5-21). Each gradient in Eq. (5-22) is computed with respect to the corresponding wave-function amplitude appearing on the left-hand side. The usual Schrödinger equation, $\dot{\psi}_{Schr} = -i\hat{H}\psi_{Schr}$, can be written as $\dot{\psi}^R_{Schr} = \hat{H}\psi^I_{Schr}$ and $\dot{\psi}^I_{Schr} = -\hat{H}\psi^R_{Schr}$. We consider the simple case of three-coupled oscillators with constraints (5-21a) and (5-21c), but not (5-21b).

Before solving the problem, we describe the evaluation of the Lagrange multipliers. Because the multipliers depend upon ψ, Eq. (5-22) is nonlinear. In the case of n constraints,

$$\begin{bmatrix} C_1 = \sum_{i,j} M^1_{ij}\,\psi_i\psi_j - c_1(t) = 0 \\ C_2 = \sum_{i,j} M^2_{ij}\,\psi_i\psi_j - c_2(t) = 0 \\ \vdots \\ C_k = \sum_{i,j} M^k_{ij}\,\psi_i\psi_j - c_k(t) = 0 \\ \vdots \\ C_n = \sum_{i,j} M^n_{ij}\,\psi_i\psi_j - c_n(t) = 0 \end{bmatrix}. \qquad (5\text{-}23)$$

M^k_{ij} represents the symmetric matrix element of the kth constraint for spatial indices i and j running for both the real and imaginary parts of ψ. For simplicity, we consider the one-dimensional case. Each constraint is subject to $c_k(t)$. For example, the matrix $\underline{M}$ would be diagonal if the constraint is to conserve mass. Two non-zero blocks of tri-diagonal matrices would form the symmetric matrix $\underline{M}$ (in a finite-difference scheme) if the constraint is to conserve kinetic energy. In the case of the conservation of momentum, we also have two blocks of bi-diagonal matrices with non-zero elements being

nearest neighbors to the right or left depending on the use of the forward or backward scheme.

$\underline{\underline{M}} = \begin{bmatrix} \underline{\underline{M}}_{aa} & \underline{\underline{M}}_{ab} \\ \underline{\underline{M}}_{ba} & \underline{\underline{M}}_{bb} \end{bmatrix}$, $\underline{\underline{M}}_{aa}$ and $\underline{\underline{M}}_{bb}$ = tri- or bi-diagonal. $\underline{\underline{M}}_{ab} = \underline{\underline{M}}_{ba} = \underline{\underline{0}}$.

One can always break up this matrix into two smaller diagonal pieces, $\underline{\underline{M}}_{aa}$ and $\underline{\underline{M}}_{bb}$, to treat the real and imaginary parts of ψ separately. Matrix elements for our model are written explicitly in (5-34).

The quantum ansatz equation (5-22) can be rewritten as

$$\dot{\psi}_i = [\dot{\psi}_i]_{Schr} - \sum_{k=1}^{n} \lambda_k \sum_j M_{ij}^k \psi_j \,. \tag{5-24}$$

From the time derivatives of the constraints (5-23), we get

$$\begin{bmatrix} \sum_{ij} M_{ij}^1 (\psi_i \dot{\psi}_j + \psi_j \dot{\psi}_i) = \dot{c}_1(t) \\ \sum_{ij} M_{ij}^2 (\psi_i \dot{\psi}_j + \psi_j \dot{\psi}_i) = \dot{c}_2(t) \\ \vdots \\ \sum_{ij} M_{ij}^k (\psi_i \dot{\psi}_j + \psi_j \dot{\psi}_i) = \dot{c}_k(t) \\ \vdots \\ \sum_{ij} M_{ij}^n (\psi_i \dot{\psi}_j + \psi_j \dot{\psi}_i) = \dot{c}_n(t) \end{bmatrix} . \tag{5-25}$$

Substitution of the equations, (5-24), into the required conditions, (5-25), yields the linear system of equations:

$$\begin{cases} A_{11}\lambda_1 + A_{12}\lambda_2 + \cdots + A_{1n}\lambda_n = \alpha_1 \\ A_{21}\lambda_1 + A_{22}\lambda_2 + \cdots + A_{2n}\lambda_n = \alpha_2 \\ \quad \vdots \\ A_{k1}\lambda_1 + \cdots + A_{kl}\lambda_l + \cdots + A_{kn}\lambda_n = \alpha_k \\ \quad \vdots \\ A_{n1}\lambda_1 + A_{n2}\lambda_2 + \cdots + A_{nn}\lambda_n = \alpha_n \end{cases}, \tag{5-26}$$

where we have

$$\alpha_k = \sum_{ij} M_{ij}^k \left([\dot{\psi}_i]_{Schr} \psi_j + [\dot{\psi}_j]_{Schr} \psi_i \right) - \dot{c}_k(t), \tag{5-27}$$

$$A_{kl} = \sum_{ij} M_{ij}^k \left(\psi_j \sum_m M_{mi}^l \psi_m + \psi_i \sum_m M_{mj}^l \psi_m \right). \tag{5-28}$$

A further simplification is possible since $\underline{M}$ is symmetric.

The solution of a linear system such as Eq. (5-26) is well-known. We write the determinant of the matrix $\underline{A}$ as $\|A\|$. Then the multiplier λ_k becomes

$$\lambda_k = \frac{1}{\|A\|} \begin{vmatrix} A_{11} & A_{12} & \cdots & A_{1,k-1} & \alpha_1 & \cdots & A_{1n} \\ A_{21} & A_{22} & \cdots & A_{2,k-1} & \alpha_2 & \cdots & A_{2n} \\ \vdots & \vdots & & & \vdots & & \vdots \\ A_{n1} & A_{n2} & \cdots & A_{n,k-1} & \alpha_n & \cdots & A_{nn} \end{vmatrix}. \tag{5-29}$$

These Gauss-Lagrange multipliers perform thermodynamic work and extract heat. These procedures are repeated during every time integration step to get $\dot{\psi}_{Gauss}$ in Eq. (5-22) (or Eq. (5-24)).

Here, we consider explicitly the special case in which three coupled harmonic oscillators are constrained in their motion by external heat reservoirs with one end hot and the other end cold. We employ the finite-

difference form of the constraints (5-21) and the classic fourth-order Runge-Kutta method for the time integration of Eq. (5-24). The schematic diagram below describes the one-dimensional situation:

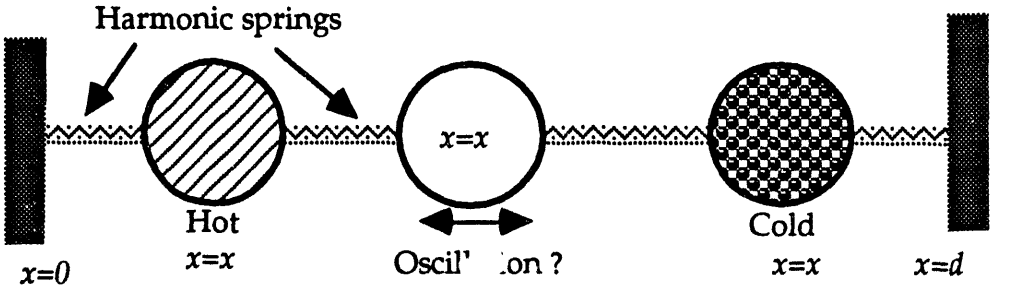

Numerically, we examine three distinguishable particles that interact with each other through harmonic springs with fixed temperatures at both ends in a discrete space. The Hamiltonian of this system (see Appendix 5.I) is

$$H = \frac{p_{Hot}^2}{2} + \frac{p_?^2}{2} + \frac{p_{Cold}^2}{2} + \frac{1}{2}[(q_{Hot})^2 + (q_{Hot} - q_?)^2 + (q_{Cold} - q_?)^2 + (q_{Cold})^2], \quad (5\text{-}30)$$

where the position coordinate q is measured from the position of equilibrium and thus the momentum $p = \dot{q}$. For convenience, we set the masses, the spring constants and the equilibrium spring lengths equal to unity. Computations of the discrete momenta p (derivatives with respect to x) are carried out according to the finite difference method through ψ with the Hamiltonian in the laboratory frame that is,

$$H = \frac{p_1^2}{2} + \frac{p_2^2}{2} + \frac{p_3^2}{2} + \frac{1}{2}[(x_1 - 1)^2 + (x_2 - x_1 - 1)^2 + (x_3 - x_2 - 1)^2 + (3 - x_3)^2]. \quad (5\text{-}31)$$

The classical-mechanical analysis of this Hamiltonian is listed in Appendix 5.I with its complete analytic description of motion and the normal modes of vibration without constraints. In this appendix, analysis with general constraint forces is also considered as an overview of application. Here we are interested in the dynamics of this model under quantum mechanical constraints.

The specific constraints in this case are

$$\begin{cases} C_{mass} = C_1 = \sum_i (\psi_i^R \psi_i^R + \psi_i^I \psi_i^I) - 1 = 0 \\ C_{KE(Hot)} = C_2 = \sum_i -\frac{1}{2}(\psi_i^R \nabla_H^2 \psi_i^R + \psi_i^I \nabla_H^2 \psi_i^I) - f(t) = 0 \\ C_{KE(Cold)} = C_3 = \sum_i -\frac{1}{2}(\psi_i^R \nabla_C^2 \psi_i^R + \psi_i^I \nabla_C^2 \psi_i^I) - g(t) = 0. \end{cases} \tag{5-32}$$

The computation uses 3 spatial grid points equally spaced with the distance one so that 27 distinguishable particle sites are available. These constraints, given by (5-32), can simply be written as

$$\begin{cases} \sum |\psi|^2 = 1 \\ \dfrac{\langle \nabla_{Hot}^2 \rangle}{2} = \langle T_H \rangle = f(t) \\ \dfrac{\langle \nabla_{Cold}^2 \rangle}{2} = \langle T_C \rangle = g(t). \end{cases} \tag{5-33}$$

The time-dependent HMS equation is then solved for the 54 nonvanishing values of the real and imaginary wave function. In other words, we solve the set of the 54 coupled, nonlinear, first-order ordinary differential equations for ψ^R and ψ^I, with the number of grid points fixed at 3 for an equilibrium case (a)

with no constraint, and the same case of which, with the constraints, (b) $f(t) = 1, g(t) = 1$. We consider the nonequilibrium cases of which (c) $f(t) = 1, g(t) = 0.5$, and (d) $f(t) = 1 - 0.5 \sin^2 t, g(t) = 1$.

Therefore, the matrix elements, M_{ij}^k, for $i = 1, 2, .., 54$ and $j = 1, 2, ., 54$ in these cases are

$$M_{ij}^1 = \frac{1}{54}\delta_{ij}, \text{ and the } 18\times18 \text{ matrix,}$$

$$\underline{\underline{M}}^2 = \begin{bmatrix} \underline{m} & & 0 \\ & \ddots & \\ 0 & & \underline{m} \end{bmatrix}, \text{ where the } 3\times3 \text{ matrix, } \underline{m} = \begin{bmatrix} -2 & 1 & 0 \\ 1 & -2 & 1 \\ 0 & 1 & -2 \end{bmatrix}.$$

$$\underline{\underline{M}}^3 = \begin{bmatrix} \underline{n} & 0 \\ 0 & \underline{n} \end{bmatrix}, \text{ where the } 27\times27 \text{ matrix, } \underline{n}_{ij} = \begin{cases} -2\delta_{ij}, & \\ 1, & i = j \pm 9 \\ 0, & \text{otherwise} \end{cases}. \tag{5-34}$$

For complete details of the program, see the supplemental program attached at the end of the text.

It is also worthwhile to note that a fast, modern computing facility currently available runs typically up to 10^{12} binary operations per second. With this power, it is possible to increase the number of grid points so that the "real" many-body problem could be tackled. In our case, during each time-integration step, the operations of Eqs. (5-27), (5-28) and (5-29) are carried out for the set of the 54 coupled nonlinear ordinary differential equations. In actual computations with three 54×54 matrices using Cray Y-MP, the preliminary investigation of the equilibrium case with the routines that calculate the multipliers indicates the approximate CPU-time consumed for 800 time-integration steps is about one minute with 14 decimal digit-accuracy. However, one can reduce this computation time drastically using only non-

zero elements of the three matrices. Eliminating zero components increases the computation efficiency by almost 18 folds so that 14,000 time steps can be integrated during one minute with the same accuracy. With 40 CRAY hours, for instance, we would be able to integrate more than 1000 time steps for 21 grid points.

Before we describe the results of the nonequilibrium calculations, it is readily noticeable that all the multipliers should be zero in the case of the equilibrium. Since Hoover's ansatz must satisfy the usual Schrödinger equation in that case, the nonlinearity has to disappear. All the cases (a), (b), (c), and (d) are checked to be time-reversible.

Next, several different sizes of time step have been examined for 1,000 time steps to estimate the appropriate time-integration step. The time step Δt = 0.01 seems to be the optimum value for the overall accuracy during the total integration time within 0.5%. More specifically, in overall we have

$$\begin{cases} \sum|\psi|^2 = 1 \pm 0.002 \\ \langle T_H \rangle = f(t) \pm 0.005. \\ \langle T_C \rangle = g(t) \pm 0.005 \end{cases}$$

We arrive at this accuracy by first reducing Δt from 0.16 to 0.08 for 32 time-steps and 64 time-steps, respectively, during which several oscillations are possible (the total integration time is 5.12). The table in the next page lists the actual numbers generated after this integration time interval for the cases (c) and (d). The numbers shown are rounded off at the seventh decimal places.

Δt	$\sum\|\psi\|^2$		$< T_H >$		$< T_C >$	
	(c)	(d)	(c)	(d)	(c)	(d)
0.16	0.6596001	0.6699084	0.4975876	0.3853349	0.4726473	0.4932859
0.08	0.8783244	0.8883579	0.8159243	0.5028487	0.7847145	0.4965302
0.04	0.9736894	0.9818584	0.9640282	0.5696386	0.5109516	0.5075137
0.02	0.9959078	0.9971853	0.9963953	0.5793542	0.5062504	0.5043565
0.01	0.9994252	0.9994024	1.0008584	0.5796416	0.5028223	0.5019154
0.005	0.9999200	0.9997906	1.0009196	0.5791773	0.5012421	0.5008270
exact	1.0	1.0	1.0	0.5785733	0.5	0.5

We observe no real significant changes in the accuracy with an even smaller time step. In the equilibrium case (a) with no constraint, $\sum|\psi|^2 = 0.9747478$, 0.9991336, 0.9999724 for $\Delta t = 0.1$ (32 time steps), 0.05 (64 time steps), 0.0025 (128 time steps), respectively.

We are also interested in number densities, ρ for hot, cold and middle atoms using the expectation value of number operator $\hat{O}$. Its value at a certain time is

$$\rho_i = \langle O_i \rangle / 3, \qquad (5\text{-}35)$$

where $\langle O_i \rangle = \sum_{j,k} \left[|\phi_{ijk}|^2 + |\phi_{jki}|^2 + |\phi_{kij}|^2 \right]$, $i, j, k = 1, 2, 3$ for the hot, middle, cold atom respectively. Also the following notation is used; $\phi_{ijk} = \psi_{[i+3(j-1)+9(k-1)]}$ For the hot atom, for example, we have

$$\langle O_1 \rangle = \langle O_H \rangle = \sum_{j,k=1}^{3} \left[|\phi_{1jk}|^2 + |\phi_{jk1}|^2 + |\phi_{k1j}|^2 \right]$$
$$= 3|\psi_1|^2 + 2|\psi_2|^2 + 2|\psi_3|^2 + 2|\psi_4|^2 + |\psi_5|^2 + |\psi_6|^2$$
$$+ 2|\psi_7|^2 + |\psi_8|^2 + 2|\psi_9|^2 + 2|\psi_{10}|^2 + |\psi_{11}|^2 + |\psi_{12}|^2$$
$$+ |\psi_{13}|^2 + |\psi_{16}|^2 + 2|\psi_{19}|^2 + |\psi_{20}|^2 + |\psi_{21}|^2 + |\psi_{25}|^2 .$$

Thus, $\rho_H + \rho_M + \rho_C = 1$ since we put the denominator 3 in (5-35) for three atoms. The actual computer program is attached at the end of the text for those who want to reproduce the results.

We also summarize the initial data used in the calculations for Figs. 5.12 to 5.15 in the following table:

Case	ψ_1	ψ_{10}	$f(0)$	$g(0)$	n
(a) Fig. 5.12	1.0	0.0	N/A	N/A	3000
(b) Fig. 5.13	1.0	0.0	1.0	1.0	4000
(c) Fig. 5.14	$1/\sqrt{2}$	$1/\sqrt{2}$	1.0	0.5	2000
(d) Fig. 5.15	$1/\sqrt{2}$	$1/\sqrt{2}$	1.0	0.5	4000

The time step is 0.01 for these calculations. For Figs. 5.16, and 5.17, we use Δt = 0.05 and 0.03 for the cases (c) and (d), respectively. For Fig. 5.18, we use two different initial conditions other than the cases (a), (b), (c), and (d) above. The plots in the left column shows the case with initial conditions: the real parts of wave functions, $\psi_1 = \psi_4 = \psi_{14} = \psi_{23} = 0.5$ and $\langle T_H \rangle = 1 - 0.5 \sin^2 t$, $\langle T_C \rangle = 0.75$. The right column is for $\psi_1 = \psi_4 = \psi_5 = \psi_9 = \psi_{10} = \psi_{14} = \psi_{18} = \psi_{23} = \psi_{27} = 1/\sqrt{9}$ and $\langle T_H \rangle = 8/9$, $\langle T_C \rangle = 8/18$. The time steps for these two cases are 0.02.

All the abscissas in Figs. 5.12 to 5.18 represent time in an arbitrary unit. In Fig. 5.12, we first test the equilibrium case (a). As we expected, both the total

energy of the system and the probability conserve even with the greater accuracy of about 10^{-6}. In this case, we choose arbitrarily that all three atoms are initially at x_1 so that the average kinetic energy of the far right one is the largest. This expected result is shown in the figure. In Fig. 5.13, we constrain the atoms at both ends to be at the same temperature with the same initial conditions as those in (a). We tried a few other choices of initial values of ψ other than ψ_1 and ψ_{10}; there are 54 possible initial values of ψ. Those results indicate very similar behavior as shown in the figure. In Fig. 5.14 for the nonequilibrium case (c), we did not observe any chaotic behavior for small perturbations on the constraints. This is rather clear because the model system with the same kind of constraints is classically not chaotic, either. For another nonequilibrium case (d) depicted in Fig. 5.15, we see the expected variations of $<T_H>$ with the period of oscillation, π. Note the overall similarity between the multipliers for the conservation of mass and for $<T_H>$. In Fig. 5.16, the readers can readily notice the periodic motions of the average kinetic energies of the middle atoms for the cases (c) and (d). In this figure, we also plot the time average of both the difference in the multipliers for $<T>$, and the expected values of total energies. The results indicate steady states as we expected. Thus chaotic phenomena seem to be suppressed in the expectation values of various variables. The right column in Fig. 5.16 indicates that the nonequilibrium cases (c) and (d) eventually reach the steady state with constant heat flows. Since the multipliers act as thermostats, the steady time average of their difference can be interpreted as a steady heat flow from the hot to cold atom. In Fig. 5.17, we plot the time history of number densities for cases (c) and (d). It is clearly shown here that the number densities calculated from (5-35) become periodic. It is also clear from the Fig. 5.18 that the plots in the right side display the periodic variations of the

number densities. We observe that even the number densities plotted in the left become periodic in a longer time interval. These last two plots do not support the existence of chaotic behavior in this system.

In addition, we observe no significant change in the time-history patterns of various values listed in Figures 5.14, 5.15, and 5.18 after we make the small changes in ψ_{10} by 5% of ψ_1. This indicates no sensitivity to a small initial perturbation. Apparently, the results from this three-body model indicate no chaos in nonequilibrium cases (c) and (d) and cases in Fig. 5.18. But this type of approach certainly be extendible to more than three body systems that might exhibit chaotic nature. It is also important to note that the time average of expected values of energies can be used to measure the degree of chaotic dynamics by checking its fluctuations. The computations were checked to be time-reversible.

All runs but (a) are computed with the constraints. The cases (b), and (d) were carried out more than 10,000 time steps, and the results indicate the same patterns as shown in Figures 5.13 and 5.15. We plot the first 4,000 time steps in order to display more details in these cases.

We can apply this method with an additional momentum constraint. It is expected that time averages of the current (in momentum) can be expected to resemble its classical, elastic, and hydrodynamical counterpart [14]. Some interesting systems have been thoroughly investigated in this context including the analysis of Lyapunov stability [15,16].

In this thesis, we only looked at the simplest possible problem to show the nonequilibrium treatment of many-body molecular dynamics using HMS mechanism. More complex problem like the Galton board system on a hexagonal finite-difference grid has been studied. It is worthwhile noting that the results from the quantum Galton Board also reveal the absence of the

quantum analog of Lyapunov instability which underlies the Second Law of Thermodynamics and the classical irreversibility although the distributions of mass, momentum, and energy approach the fractal distributions found classically. From the standpoint of the quantum-classical correspondence, this agrees with our previous points from the pendulum model, which indicates the breaking of the correspondence for the classically chaotic system in the chaotic regime.

5-5. Summary

From the examples in this chapter, a more clear picture of the quantum chaos with classical counterparts has emerged: The uncertainty breaks their correspondence near the break time to form quasi-periodicity. Evidently very thin stochastic layers intermingled with tori, and the islands within islands in Figs. 5-1 and 5-2 are wiped away in quantum mechanics. Therefore a detailed structure in the coarse-grained quantum phase-space due to a small but finite $\hbar$ can almost all be neglected [17]. Then quantum behavior appears regular even if the corresponding classical system appears chaotic. This effect becomes more apparent when the uncertainty rapidly grows. The observations made by Casati *et al.* on the quantum kicked rotator [18] and by Marcus [19] for the quantum Hénon-Heiles problem confirm this core idea. However, using HMS dynamical description, chaotic behavior in quantum system might be possible, but requires more than three bodies. In the next chapter, we will look at the possible reasons and solutions of quantum regularity in the normal Schrödinger mechanics.

Appendix 5. I Classical-mechanical analysis of the coupled oscillators

For the complete classical description of motion for this system, we ignore any constraints. We will use the normal modes of the system to solve this problem. To do that, we set x_i as the position coordinate for ith atom, where i = 1(Hot), 2(?), and 3(Cold). The distance between the two walls is denoted by d (the position of the left wall is zero) and the equilibrium distances of atoms b (equilibrium spring length). Then the potential energy of the system with spring force constant k in the laboratory coordinates is

$$V = \frac{k}{2}[(x_1 - b)^2 + (x_2 - x_1 - b)^2 + (x_3 - x_2 - b)^2 + (d - x_3 - b)^2]. \qquad \text{(A5I-1)}$$

We now introduce coordinates relative to the equilibrium positions [20]:

$$q_i = x_i - x_{oi},$$

where

$$x_{o1} = x_{o2} - x_{o1} = x_{o3} - x_{o2} = d - x_{o3} = b.$$

In discrete space, the distance d can be replaced with an integer N specifying the total number of spatial grid points with equal distance apart being one (b=1). The potential energy in the equilibrium displacement coordinates q_i then reduces to

$$V = \frac{k}{2}[q_1^2 + (q_2 - q_1)^2 + (q_3 - q_2)^2 + q_3^2], \qquad \text{(A5I-2)}$$

since $x_{o3} = d - b$ (or $=N+1-b=N$) and $q_3 = x_3 - x_{o3}$. The kinetic energy takes the following simple form in this coordinates:

$$T = \frac{m}{2}[\dot{q}_1^2 + \dot{q}_2^2 + \dot{q}_3^2]. \qquad \text{(A5I-3)}$$

Eqs. (A5I-2) and (A5I-3) give the Hamiltonian (5-30). Similarly, since $\dot{q}_i = \dot{x}_i$, one can establish another form of Hamiltonian (5-31) using (A5I-1) in the laboratory frame with $b = 1$, $d = 4$. The Lagrangian, $L(q_i, \dot{q}_i)$, is $T - V$, which we can write as

$$L = \frac{1}{2}\sum_{i=1}^{3}\sum_{j=1}^{3}(T_{ij}\dot{q}_i\dot{q}_j - V_{ij}q_iq_j), \qquad \text{(A5I-4)}$$

where

$$\mathbf{T} = \begin{pmatrix} m & 0 & 0 \\ 0 & m & 0 \\ 0 & 0 & m \end{pmatrix} \text{ and } \mathbf{V} = \begin{pmatrix} -2k & -k & 0 \\ -k & -2k & -k \\ 0 & -k & -2k \end{pmatrix}. \qquad \text{(A5I-6)}$$

It is useful to write **T** and **V** as matrices so that we could generalize to different cases. This approach also makes an even simpler introduction of the constraint forces to the system.

Using Lagrange's equation, we find the equations of motion:

$$\mathbf{T}\ddot{\underline{q}} + \mathbf{V}\underline{q} = \mathbf{0}, \qquad \text{(A5I-7)}$$

where we have defined the vector $q = (q_1, q_2, q_3)^T$. The normal modes are collective motions where all three blocks move with the same frequency. Since there are three degrees of freedom there will be three normal modes, For each one, the solution is of the form

$$\underline{q(t)} = \mathbf{a}_j(t)\exp(i\omega_j t). \qquad \text{(A5I-8)}$$

We substitute this (A5I-8) into the equations of motion (A5I-7), we get a matrix equation for the matrix $\mathbf{a}_j(t)$,

$$(\mathbf{V}-\omega_j^2\mathbf{T})\mathbf{a}_j=0. \qquad \text{(A5I-9)}$$

In order for a nontrivial solution to exist, the following secular equation must be vanished:

$$\left|\mathbf{V}-\omega^2\mathbf{T}\right|=\begin{vmatrix} 2k-\omega^2 m & -k & 0 \\ -k & 2k-\omega^2 m & -k \\ 0 & -k & 2k-\omega^2 m \end{vmatrix}=0. \qquad \text{(A5I-10)}$$

This leads to a cubic equation in ω^2, with roots $\omega_1^2 = 2k/m$, $\omega_2^2=(2+\sqrt{2})k/m$, and $\omega_3^2=(2-\sqrt{2}))k/m$. If we insert these frequencies into Eq. (A5I-9), we are to solve for the three normal modes, for which we choose the normalization prescription $\mathbf{a}^T\mathbf{T}\mathbf{a}=1$. Subject to this condition, our normal modes are

$$\mathbf{a}_1=\frac{1}{\sqrt{2m}}\begin{pmatrix}1\\0\\-1\end{pmatrix},\ \mathbf{a}_2=\frac{1}{2m}\begin{pmatrix}1\\\sqrt{2}\\1\end{pmatrix},\ \text{and}\ \mathbf{a}_3=\frac{1}{2m}\begin{pmatrix}1\\-\sqrt{2}\\1\end{pmatrix}. \qquad \text{(A5I-11)}$$

The frequencies of vibration can be obtained from $f_i = \omega_i/2\pi$. These normal modes of vibration are depicted for the corresponding frequencies.

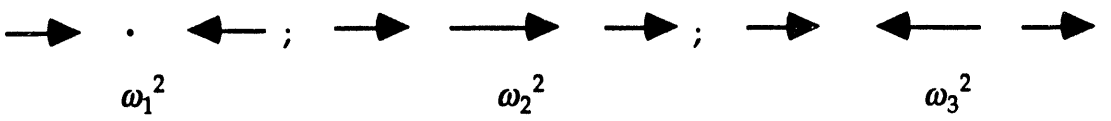

From Eq. (A5I-8), we could also find the position of each atom at any later time if the initial conditions are given.

Now, suppose we apply a force $\mathbf{F}(t)$ to keep the average kinetic energies of some atoms in the system constants of motion. However, because the constraints in this case (Eq. 5-31) are quantum mechanical, not applicable to classical case, the exact form of $\mathbf{F}(t)$ is not obtainable. The expectation-values in quantum mechanics are interpreted as average values over many measurements at a given time in classical language. So, this meaning of average makes us unable to formulate a specific description of constraint nonlinearly. Moreover, the fact that the constraints we deal with are nonholonomic adds additional difficulty to the problem. But we can still discuss the general overview of the problem by assuming the force $\mathbf{F}(t)$.

Since we now can use the vectors in (A5I-11) as a basis set to write an arbitrary displacement as

$$\underline{q(t)} = \xi_1 \mathbf{a}_1 + \xi_2 \mathbf{a}_2 + \xi_3 \mathbf{a}_3, \tag{A5I-12}$$

where ξ_i are called normal coordinates, our equations of motion are

$$\mathbf{T}\left(\sum_{i=1}^{3} \ddot{\xi}_i \mathbf{a}_i\right) + \mathbf{V}\left(\sum_{i=1}^{3} \xi_i \mathbf{a}_i\right) = \mathbf{F}(t). \tag{A5I-13}$$

We use the matrix equation for a normal mode vector, (A5I-9), to rewrite $\mathbf{V}\mathbf{a}_i$ as $\omega_i^2 \mathbf{T}\mathbf{a}_i$. If we now multiply on the left by $\mathbf{a}_j^T$ and use the orthogonality condition, $\mathbf{a}_i^T \mathbf{T} \mathbf{a}_j = \delta_{ij}$, the normal modes decouple and we obtain the equations of motion for the normal coordinates:

$$\ddot{\xi}_i + \omega_i^2 \xi_i = f_i(t), \tag{A5I-14}$$

where we have defined $f_i(t) = \mathbf{a}_i^T \mathbf{F}(t)$. At this juncture, if the particular force **F** is given, one could compute $f_i(t)$. Then, with the certain initial conditions on ξ_i, the solution of (A5I-14) allows us to find the motion of a specific atom in terms of the equilibrium displacement coordinates q_i. Although it is quantum mechanical, our model could be investigated in the same context, especially for q_2 .

References

[1] B. V. Chirikov, Phys. Rep. **52**, 263 (1979).

[2] T. Hogg, B. A. Huberman, Phys. Rev. Lett. **48**, 711 (1982); Phys. Rev. **28A**, 22 (1983).

[3] H. G. Schuster, Phys. Rev. **28B**, 381 (1983).

[4] F. M. Izraelev, D. L. Shepelyanskii, Theor. Math. Phys. **43**, 417 (1980).

[5] J. Clarke, A. N. Cleland, M. H. Devoret, D. Esteve, J. M. Martinis, Science, **239**, 992 (1988).

[6] According to BCS theory, two electrons in superconducting material form a pair by a weak attraction between them. The attractive force is caused by the repulsion between electrons nearby. For more information on the theory, see any modern superconducting theory textbook available, for instance, D. R. Tilley, J. Tilley, *Superfluidity and Superconductivity*, 3rd ed (AIP, N. Y. 1992) or H. Y. Fan, *Elements of Solid State Physics* (John Wiley & Sons, 1987).

[7] See for example, H. G. Schuster, *Deterministic Chaos: An Introduction* (2nd Edition, VCH, N. Y. 1988).

[8] S. Tomsovic, E. J. Heller, Phys. Rev. Lett. **67**, 664 (1991).

[9] E. J. Heller, *Chaos and Quantum Physics*, edited by M. J. Giannoni, et al. (Elsevier Science, Amsterdam, 1990).

[10] E. J. Heller, *Quantum Chaos and Statistical Nuclear Physics*, edited by T. H. Seligman, *et al.* (Springer-Verlag, 1986).

[11] J. M. T. Thompson, H. B. Stewart, *Nonlinear Dynamics and Chaos* (John Wiley and Sons, N. Y. 1986).

[12] S. W. McDonald, A. N. Kaufman, Phys. Rev. Lett, **42**, 1189 (1979).

[13] L. A. Pars, *A Treatise on Analytical Dynamics* (Oxbrow Press, Woodbridge, Ct., 1979).

[14] W. G. Hoover, B. Moran, C. G. Hoover, D. J. Evans, Phys. Lett. A. **133**, 114 (1988).

[15] See [14] and also W. G. Hoover, H. A. Posch, Phys. Lett. A. **113**, 82 (1985); **123**, 227 (1987).

[16] W. G. Hoover, B. Moran, Phys. Rev. A. **40**, 5319 (1989).

[17] I. C. Percival, Adv. Chem. Phys. **36**, 1 (1977).

[18] G. Casati, B. V. Chirikov, J. Ford, Phys. Lett. **77A**, 91 (1980); E. Ott, Rev. Mod. Phys. **53**, 655 (1981).

[19] R. A. Marcus, in R. H. G. Helleman (ed.), op cit, p. 169 (1980).
[20] H. Goldstein, *Classical Mechanics*, 2nd Edition, see Ch. 6-4 (Addison-Wesley, Reading, MA, 1980).

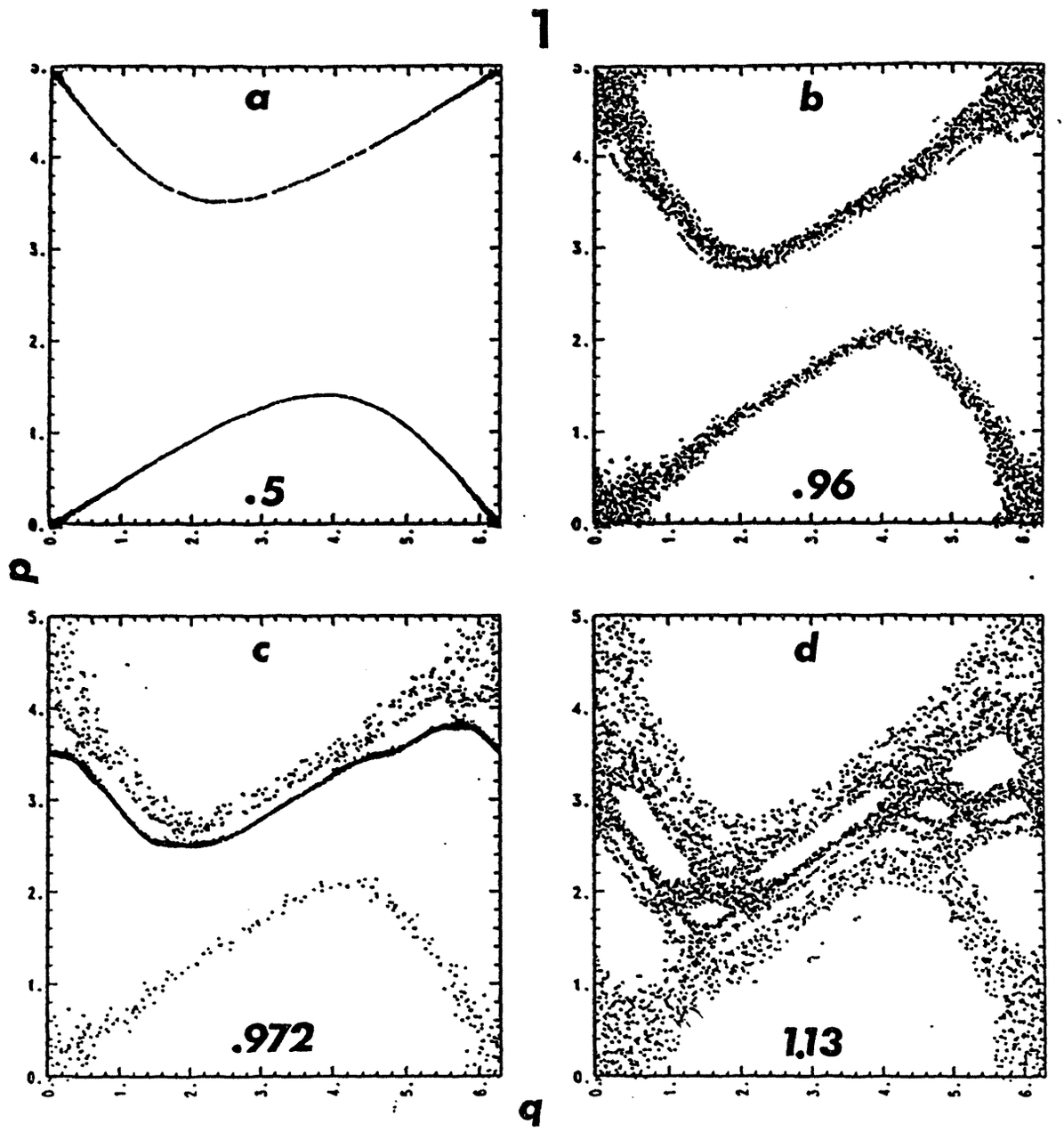

Figure 5.1 Phase-space diagrams at various kick strengths for the standard map. Regular motion is in (a). A dark chaotic layer is emerged in (c). Two islands intermingle in (d). Numbers inside the plots represent the kick strength.

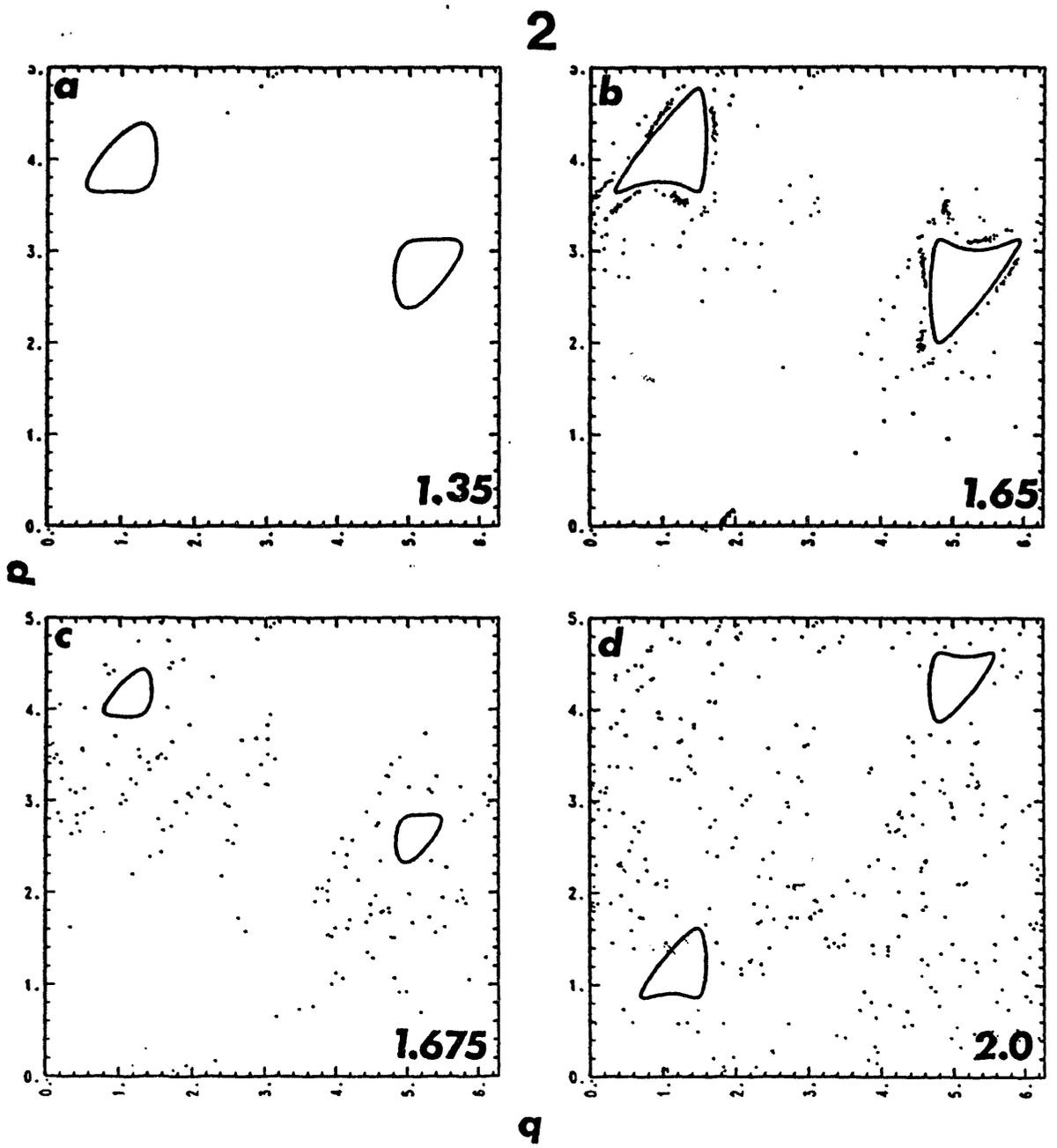

Figure 5.2 Phase-space diagrams at various kick strengths for a modified standard mapping (5-3). The similar observation can be made as the previous figure even though the dark strip of chaotic layer is not evident in this case.

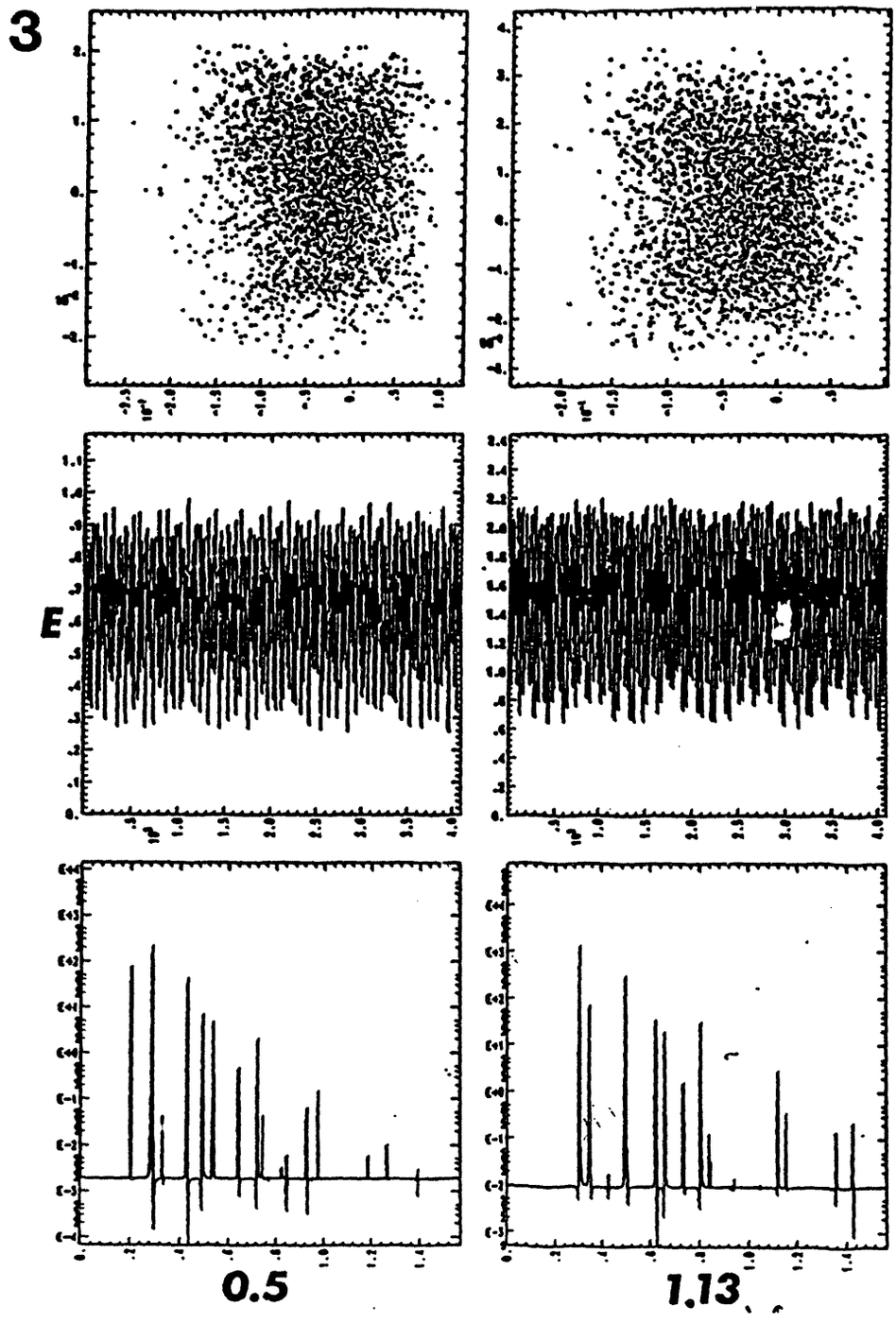

Figure 5.3 Phase-space plots are located at the top and energy variations over time at the middle. Power spectra of energy variations at the bottom display distinct peaks. Left column shows data from Eq. (5-5), whereas right one shows data from Eq. (5-6).

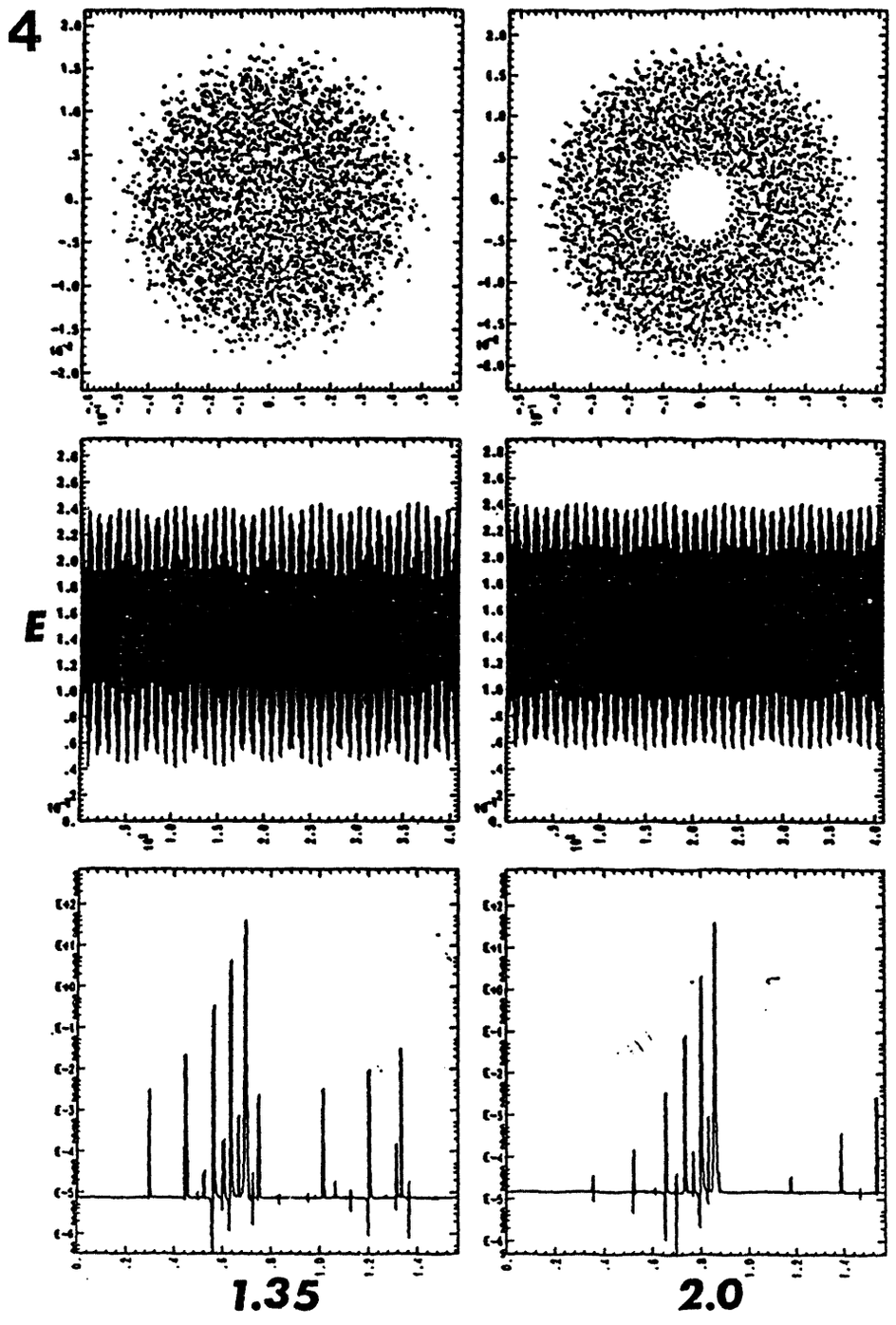

Figure 5.4 The same kind of plots as Fig. 5.3 with larger values of kick strength. Spectral peaks are well distinguishable in both cases.

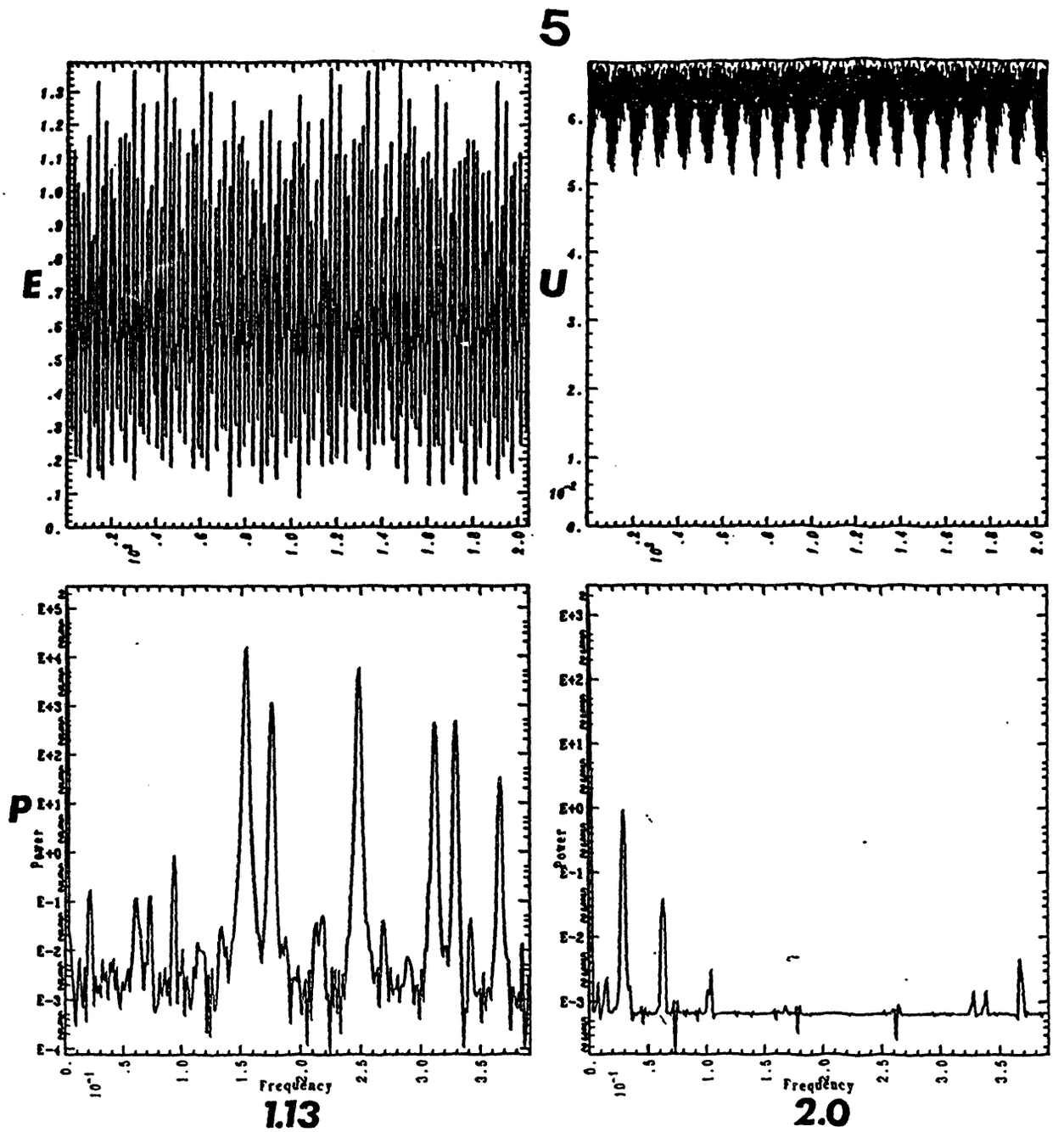

Figure 5.5 This shows the energy and the uncertainty variations in the upper panels. Their corresponding power spectra are shown in the lower panels with higher resolution than previous cases. No chaotic spectra are observed.

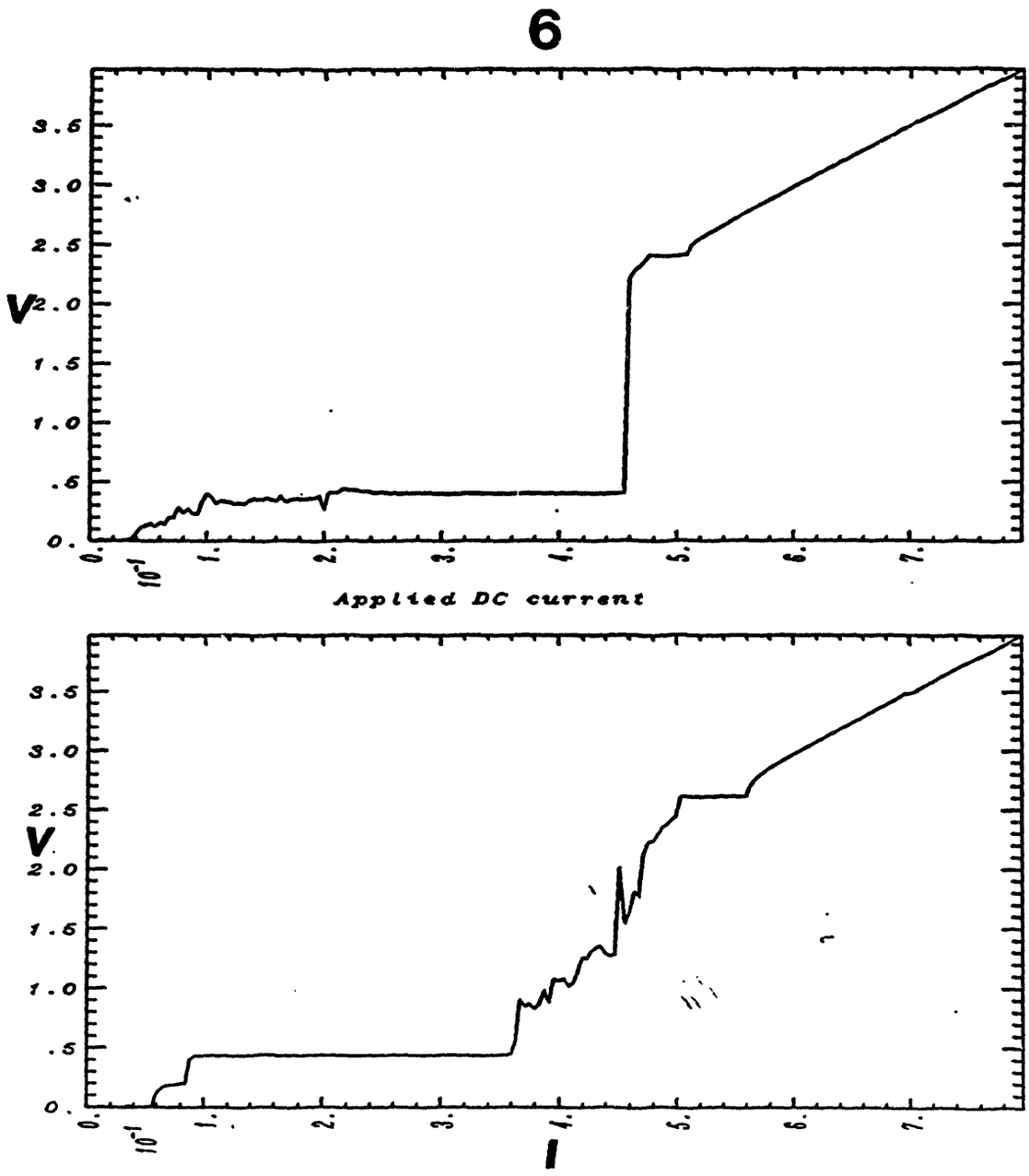

Figure 5.6 Typical classical devil's staircases. Large plateaus are clearly shown.

7

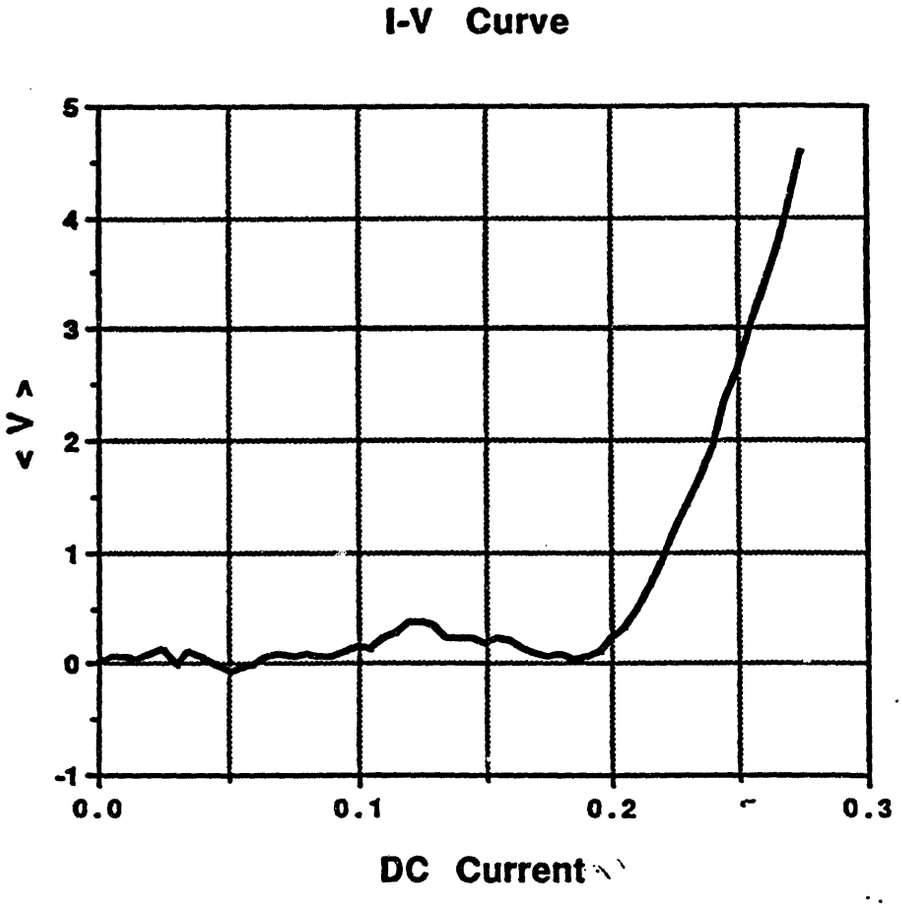

Figure 5.7 The result from the quantum calculation. No apparent plateaus are observable.

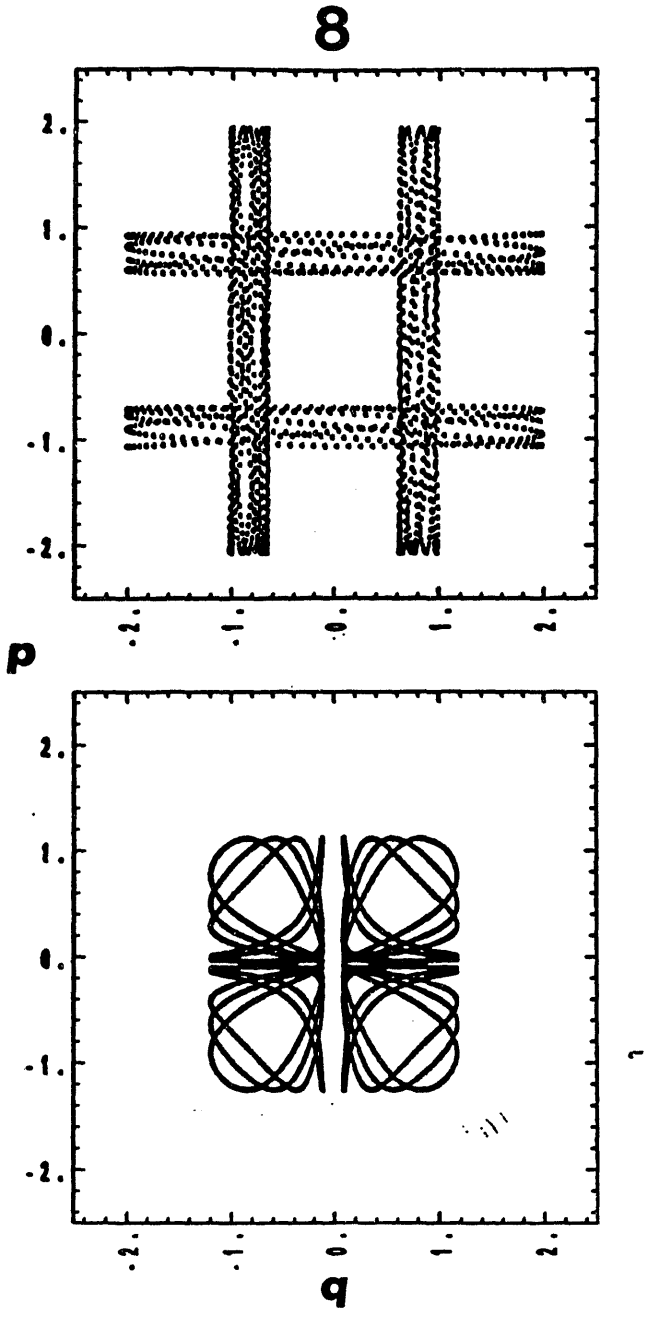

Figure 5.8 Classical trajectories of the Duffing's oscillator at various initial points in space.

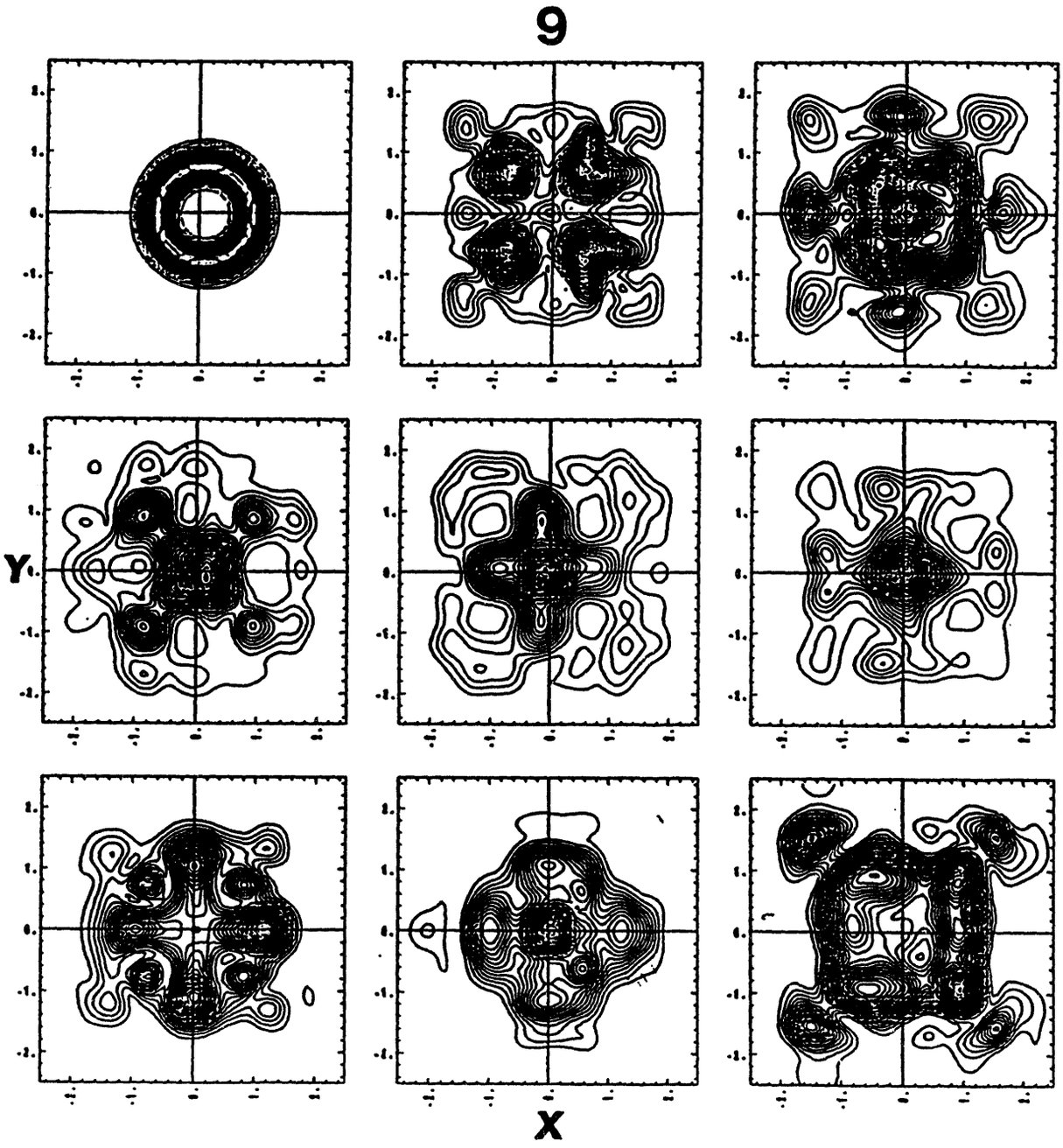

Figure 5.9 A time history of a wave packet in space. There is neither external force nor damping. Note the rectangular shape and the circular shape formed by condensed contours similar to the classical trajectories.

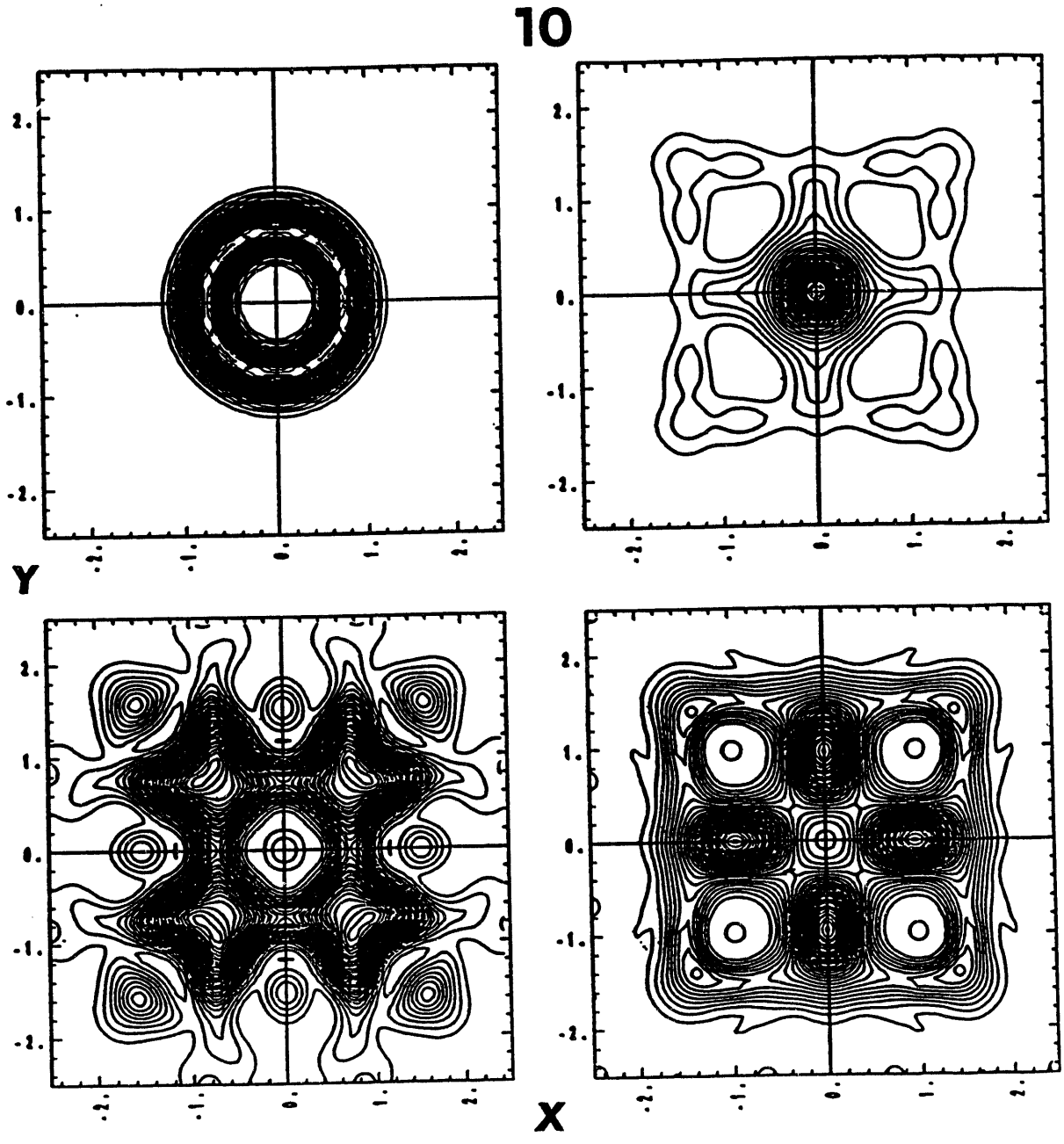

Figure 5.10 Another example of quantum calculations showing the spatial variations of the wave packet.

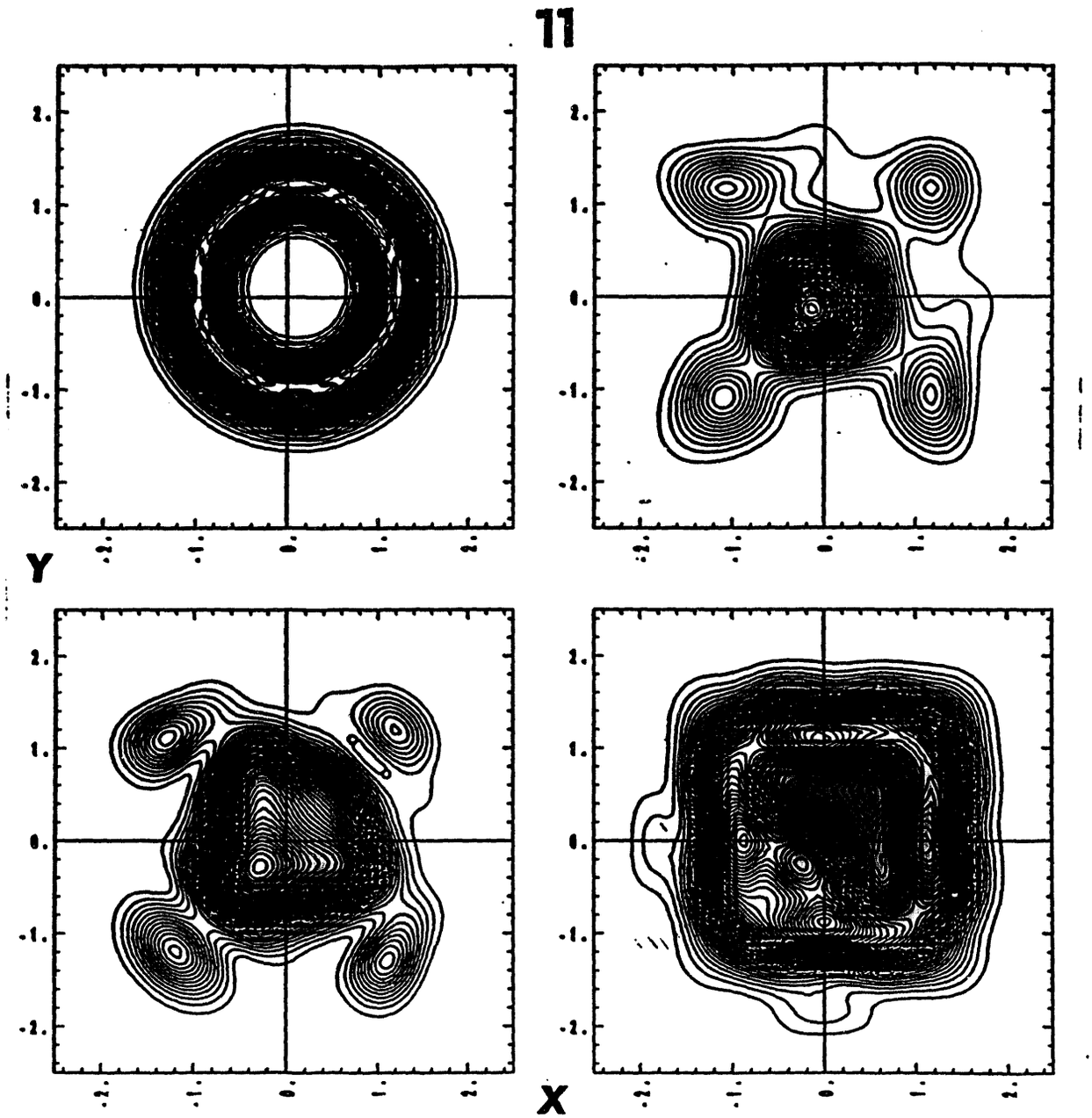

Figure 5.11 More example with a centrally located initial wave packet. Note the symmetry in this case.

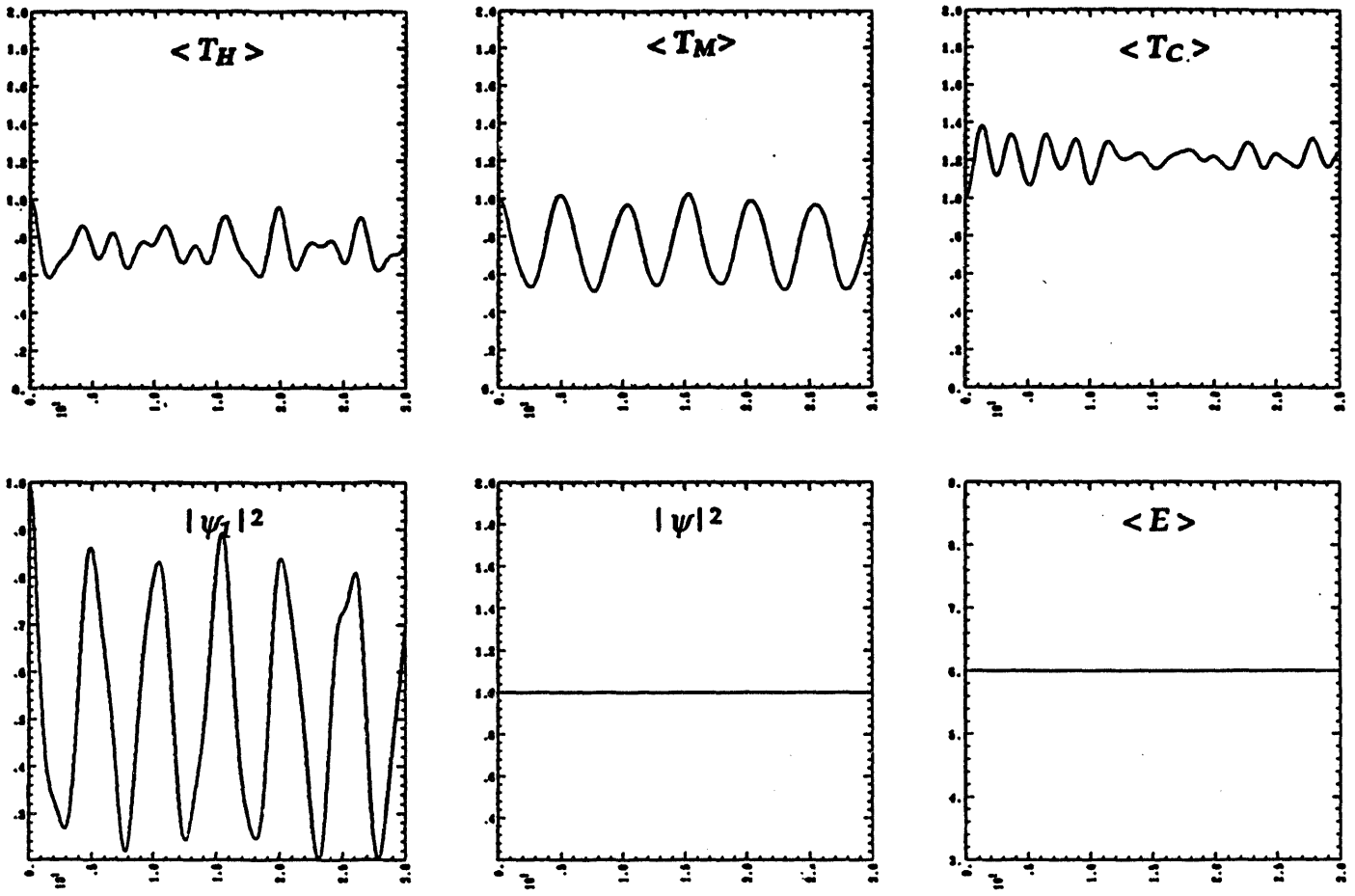

Figure 5.12 Time variations of the kinetic energies <*T*>, the probability amplitudes, the total energy <*E*> for equilibrium case (a) without any constraint. The usual Schrödinger equation is solved in this case. All the horizontal axes represent time in arbitrary unit.

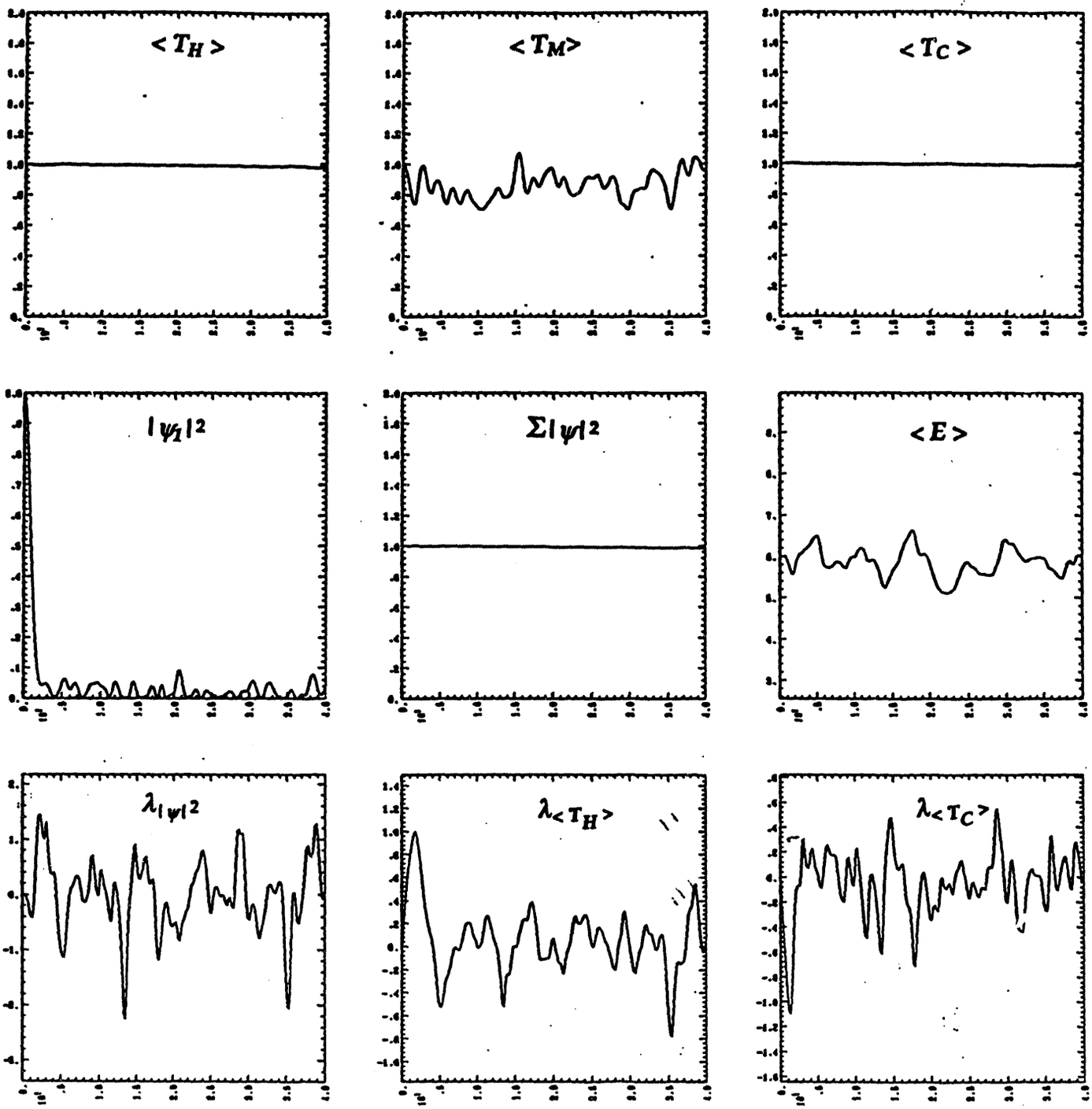

Figure 5.13 The previous case with the constraints, $< T_H >=1$, $< T_C >=1$, and $\Sigma|\psi|^2=1$. The HMS equation is solved in this case for (b). All the abscissas represent time.

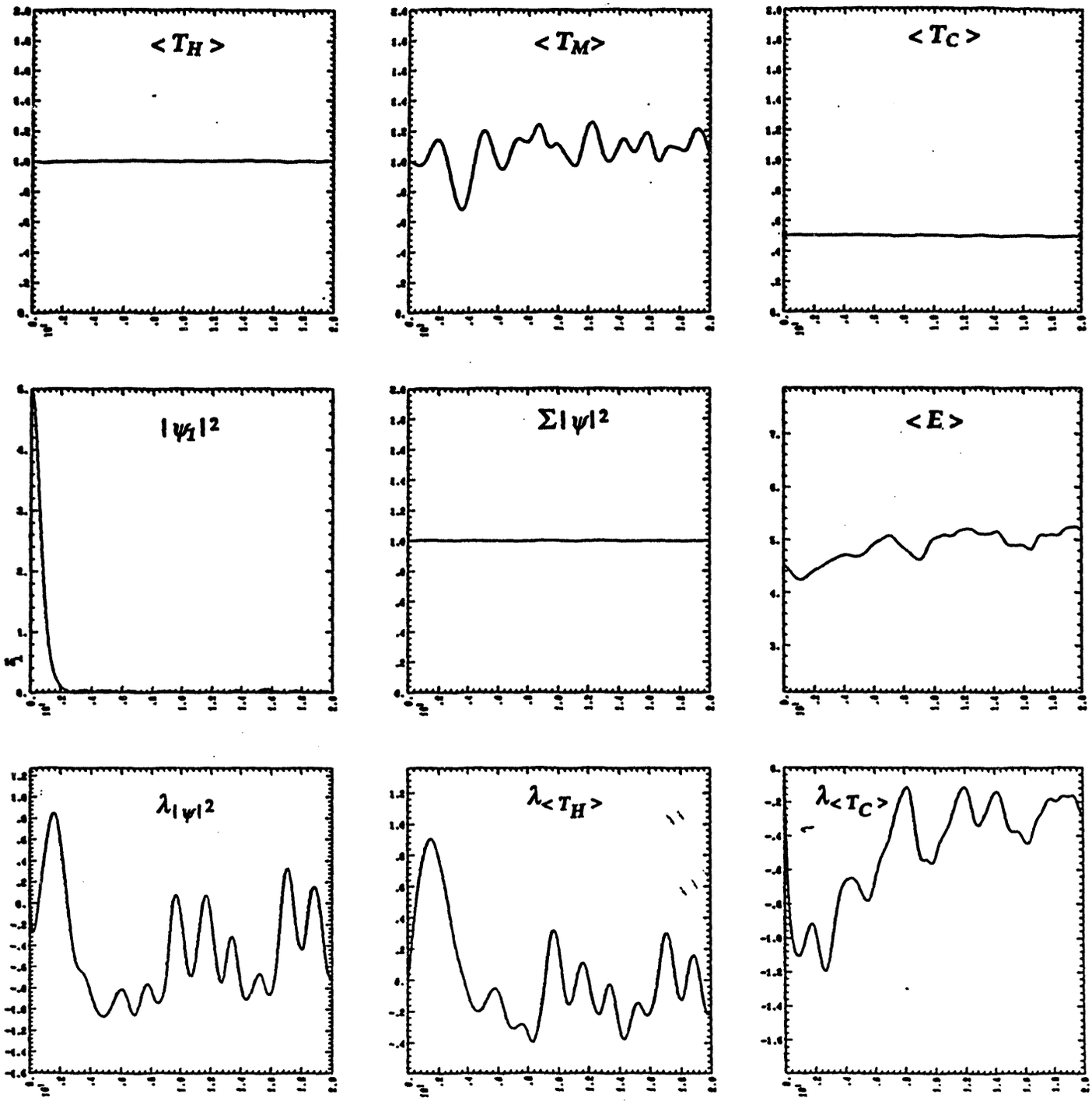

Figure 5.14 Nonequilibrium case (c) with the constraints, $< T_H > = 1$, $< T_C > = 0.5$, and $\Sigma|\psi|^2 = 1$. All the abscissas represent time.

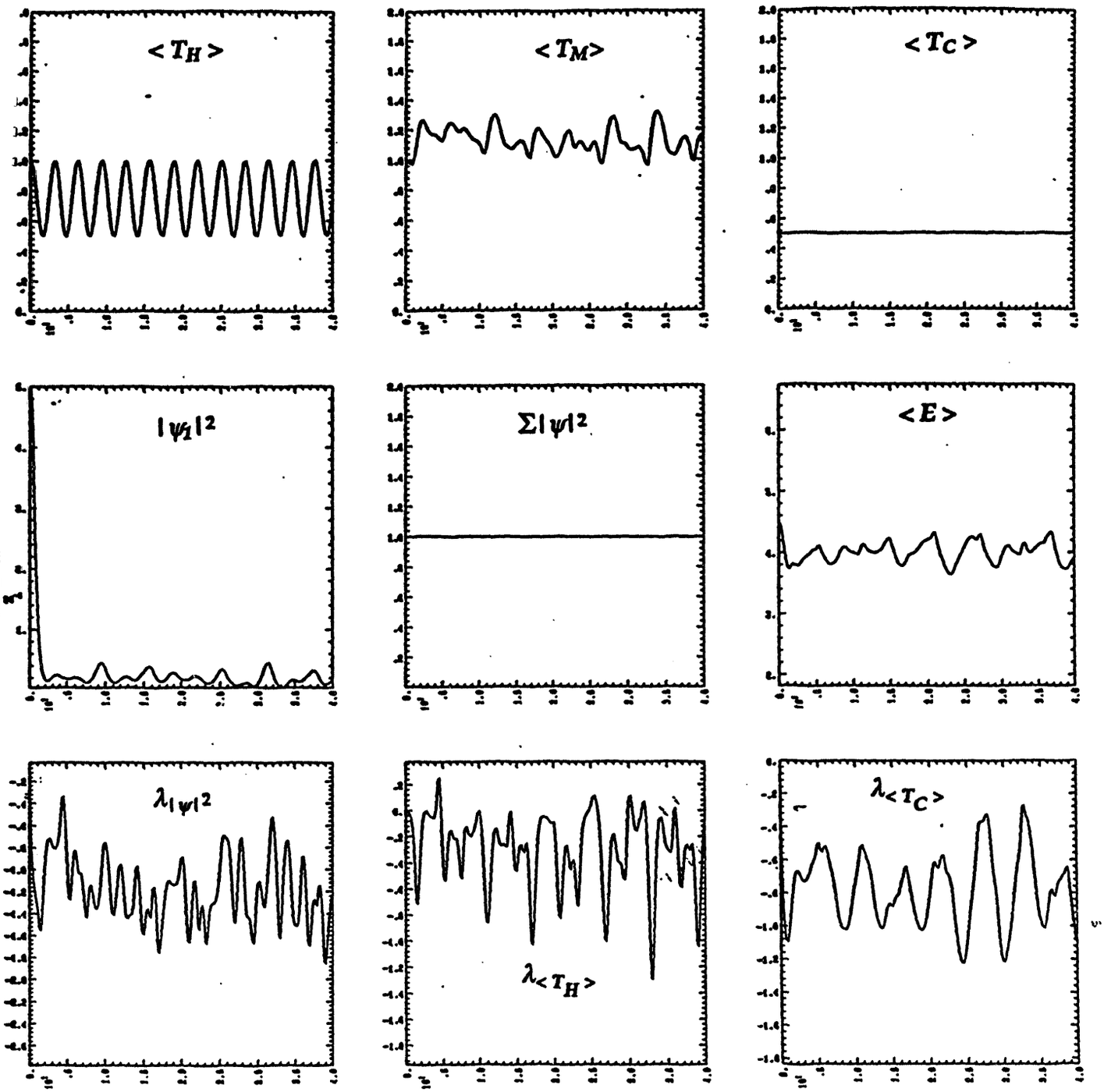

Figure 5.15 Nonequilibrium case (d) with the constraints, $< T_H > = 1 - 0.5 \sin^2 t$, $< T_C > = 0.5$, and $\Sigma|\psi|^2 = 1$. All the abscissas represent time.

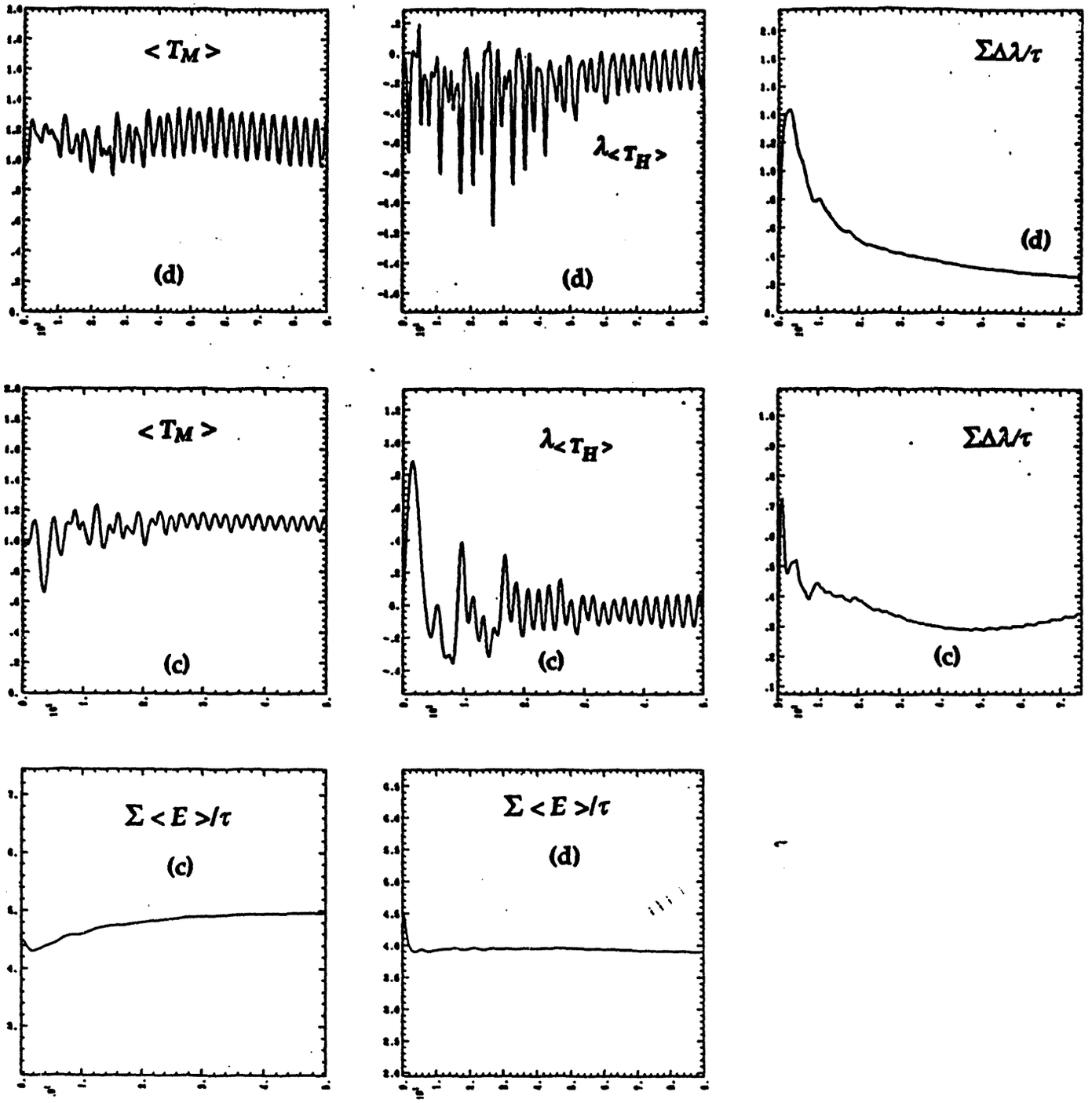

Figure 5.16 Periodic motions of the middle atom are apparent from the above two rows for the cases (d) and (c), respectively. The time-averages of both the difference in the multipliers and the expected value energies reach steady states. The time steps for these calculations are 0.03, and 0.05 respectively. τ is the total integration time.

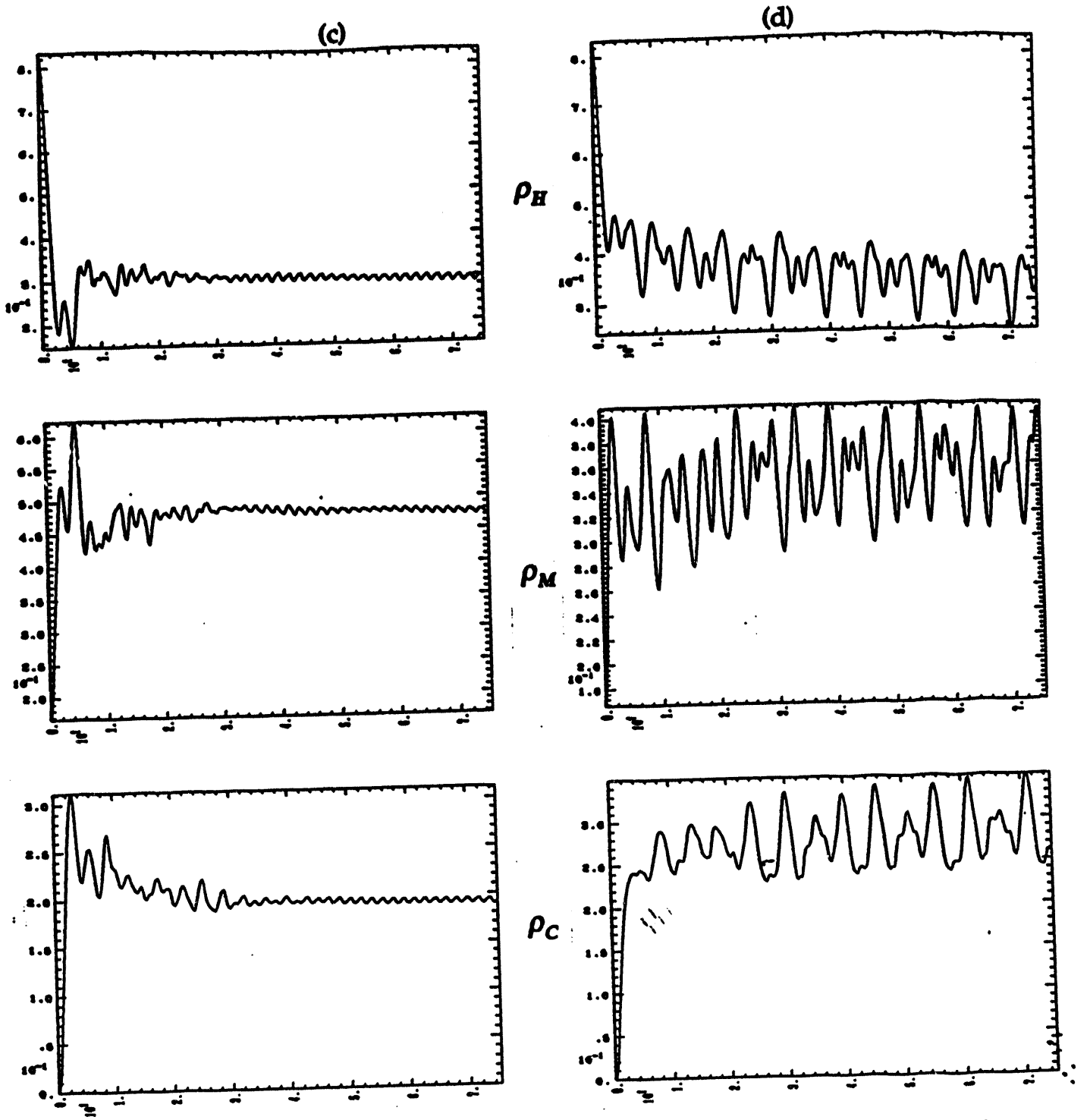

Figure 5.17 Time variations of the number densities. All the abscissas represent time. The left column is for the case (c), and the right for the case (d). It is apparent that the number densities are periodic in time.

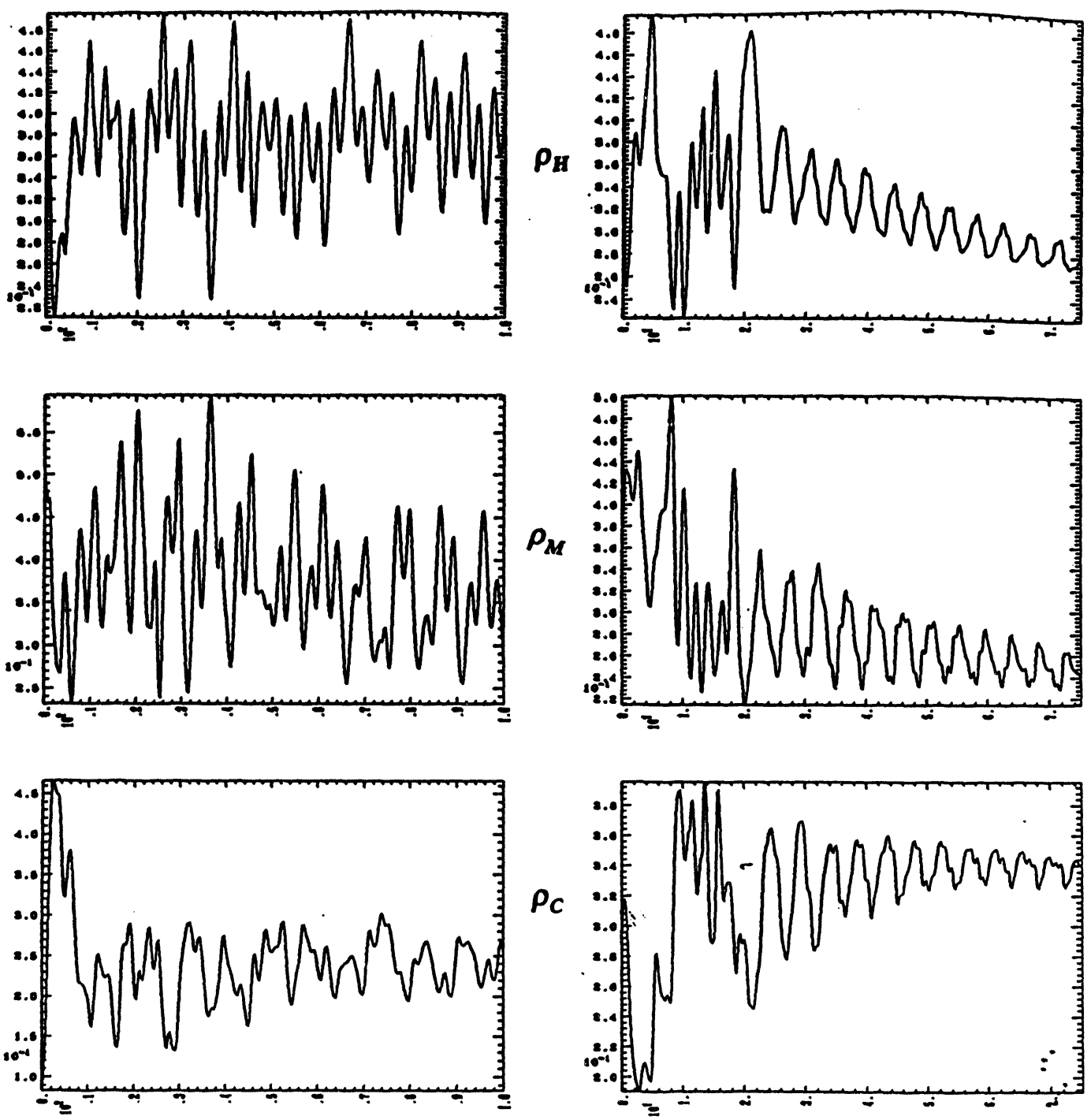

Figure 5.18 Time variations of the number densities. Nonequilibrium cases with the constraints, $< T_H > = 1 - 0.5 \sin^2 t$, $< T_C > = 0.75$ for the plots in the left column, and $< T_H > = 8/9$, $< T_C > = 8/18$ for the plots in the right. The densities become periodic for the plots in the left in a longer time interval. Initial conditions for these cases are listed in the text.

CHAPTER 6

CONCLUSIONS AND FUTURE

A quantum physicist and student of quantal paradoxes: Macroscopic objects ... can't be in two mutually exclusive states at the same time; quantal objects can be, and often are .... Quantum physics seems to contain classical physics as a limiting case ....

Alice (a graduate student): Why do you say "seems to"? Surely physicists know by now whether it does or doesn't?

Alice in quantum land

(D. Layzer's "Cosmogenesis")

We summarize our results in this chapter. The quantum measurement problem is also considered in the context of quantum chaos qualitatively.

6-1. Conclusions

Extensive, though not complete, search for quantum chaos has been carried out throughout the previous chapters. Since the principal conclusions are described in the summary sections of each chapter, we will list a few important properties worth mentioning again here.

First, we found the claim that quantum mechanics generally embraces classical physics is valid even though exactly the same measurement is not possible. No trace of violation of the claim was found. The expectation-values we calculated were the statistical averages of many possible measurements ignoring actual perturbations due to the measurement (or observation) processes of a quantal system. Because of this perturbation, its physical state must change discontinuously. This will in fact changes the Hamiltonian of a system whenever there is a measurement. Also, the measurement would reduce the uncertainty to the minimum value allowed by its process. With this perturbing part excluded, the statistical averages relax to smaller values as the time elapses. This relaxation effect was seen from the results in the classically chaotic regime in Ch. 3. Those results indicate the change in the uncertainty is not small. This however does not mean that the claim fails. In other words, the large uncertainty variation prevents us from knowing the exact state. Therefore, someone like Einstein asserted that the physical state of a quantal system is unknowable. He thought that quantum physics is just computational device for calculating the probability of observable events. Nonetheless, this probability can represent classical mechanics in the regular regime, but not in the chaotic regime. Instead, quantum distribution functions permit us a good level of correspondence in the chaotic regime. It is worthwhile printing again that the Husimi representation is not necessarily

better for the quantum-classical correspondence than the Wigner one in the classically regular regime. Therefore, bearing the uncertainty in mind, the quantum violation of classical dynamics was not found, and the claim stands.

As we have noticed from the previous three chapters, quantum mechanics does not manifest classical mechanics, especially in classically chaotic regime mostly because observation is impossible in quantum mechanics. This was described in the previous paragraph. On the contrary, a close correspondence was observed in the regular regime. We also found a higher degree of correspondence in more classical limits ($\hbar \to 0$ or $\mu \to \infty$). The uncertainty growth or fluctuation is believed to be partly responsible for the breaking of the correspondence. The uncertainty principle does not restrict the shape of a micro-cell (P-cell) whose volume in phase-space is equal to or greater than Planck's constant. Thus, the effect of relaxation effect discussed before can be a rough measure of which variable is responsible for the breaking of the correspondence. In other words, we may be able to distinguish the specific variable that has the relatively high level of uncertainty at the specific time.

The interaction with the environment, especially through frictional dissipation, was approximately treated, and found to be a good representation. Using this technique, quantum treatment of classical strange attractor was studied to check signatures in phase-space. Quantum signatures of chaos were discovered using the Wigner and the Husimi distribution functions even in the chaotic regime. To represent the correspondence, the Husimi seemed to be better, although the Wigner contained more detailed information on classical dynamics through its contours. It is of importance to remind the reader that no evidence of quantum chaos was found in phase-space trajectories. Therefore, these distributions deserve more attention in the

context of a quantum chaos search. At any rate, it is realized that some finite, bounded, undriven quantum systems are not chaotic [1]. Also the study considering a quantum version of the Arnol'd cat map claims a failure of the correspondence even in an appropriate limit of the chaotic regime [2]. Chaotic quantum phenomena, however, can be observed using numerical simulations of a nonlinear Hartree equation [3] or of a mean-field approximation [4] without a classical counterpart.

In addition, a quantum wave packet carries dynamical information of classical trajectory as we have seen through some Heller's scars, though we did not study the chaotic regime. This was expected because the quantum distribution functions containing wave packets resembled classical one closely. But perhaps most importantly, it appears that classically chaotic phenomena would eventually be suppressed by the quantum uncertainty even in the semi-classical limits.

Finally, the split operator method was very effective in solving the time-dependent Schrödinger equation. This could have many possible applications in quantum dynamical problems even though our study was limited to the Cartesian coordinates. One immediate application of the method is to study the overlap of energy levels of the Floquet states [see Ref. 22 in Ch. 4] in which the transition from regular to chaotic states might be characterized. The level broadening of the Floquet states in the chaotic regime would result in the complicated, mixed state. For instance, the multiphoton process in the Rydberg state of atom undergoing the transition could be extensively analyzed by using the split operator method with the spectral method mentioned in Eqs. (2-40) ~ (2-42).

6-2. Future

As E. Wigner once called it, the 'pre-quantum-mechanical' laws of physics told us how to predict the future state of a physical system. This concept fails to be valid in the state of the pre-quantum-mechanical chaos (classical chaos). This unpredictable feature originating in classical chaos contradicts the linear nature of the predictability in quantum mechanics.

We, human beings, experience the classical chaotic phenomena in the world around us everyday. However, quantum phenomena are also applicable over vastly different and larger scales than just atomic physics, even though we seldom experience it directly. For example, experientially neutrons show both particle and wave nature over the energy (mass) range from 10^{-7} eV to over 10^{8} eV. Today there is no experimental evidence that points to the break down of the quantum theory. Then why have no quantum manifestations of classical chaos been observed? Why can't we control the uncertainty? Where does the uncertainty come from? I think the problem is this: quantum mechanics is fundamentally about 'observations'. It necessarily divides the world into two parts, a part which is observed and a part which does the observing.

In my opinion, the only thing that the existing quantum mechanical equations allow us to postulate about chaotic behavior is a quantum state of object plus a classical apparatus for the outcome of the measurement that has a definite value. Observer's worlds of quantum mechanics [5-7] have produced a paradox such as the Schrödinger's cat almost seven decades ago. Such a long time interval has inevitably made many propositions on quantum measurement theories [8-11]. It is now believed by some that

quantum theory of chaos has to come in conjunction with the measurement theory.

This concept of a global Schrödinger equation for a quantum system plus environment has obviously an implication of fundamental change in our description of the basic rules of nature. In fact, there are some elaborated postulates taking care of specific problems. A classical approach to non-equilibrium Schrödinger equation using the concept of Lagrange's multipliers and Gauss' least constraint principle could generates chaos [12-14] as we have discussed in Section 5-4. The so-called stochastic dynamical reduction equation that includes an unusual operator in the normal Schrödinger equation has also been suggested [15,16]. The importance of the Kubo-Fox method [17] cannot also be emphasized enough. In many aspects, its approach has a clear advantage as we discussed in Ch. 4. Moreover, addition of a nonlinear term to Schrödinger equation has been studied [18,19]. However, they do not seem to have universal validity. Each of these postulates has its own advantage for different problems. Especially, Hoover's postulate has a distinguishable advantage in treating non-equilibrium quantum many-body situation. His approach provides the necessary mechanism in treating an open system as we have discussed in both Sections. 4-2-2 and 5-4.

In my opinion, Schrödinger equation may need an additional nonlinear term that couples the classical world with a coupling coefficient specifying the strength of the coupling. Without a measurement, the coefficient is zero and the normal quantum mechanics resumes. Yet no specific postulate exists. At this juncture, further extensive investigations are necessary.

I think that either a change in Schrödinger equation or the need to interpret quantum mechanics differently using classical mechanics is not a

lunatic idea. I also believe that the *measurement* approach to quantum chaos [20] would provide considerable progress towards a better, though not complete understanding. This problem is also related to the paradox of classical locality and quantum nonlocality. Both problems can be regarded in the same context. I must say as well that it is perhaps conceivable to search for quantum chaos in a totally different context than the one we have been considering in this study. Currently, on the other hand, many researchers are turning into the possible future application of this still low-profile, enigmatic subject as the semi-classical (or one may prefer both classical and quantum) regime in many areas of physics are becoming more important.

6-3. Epilogue

Almost three years have passed since the collection of the first numerical data in its initial interpretation. The core structure of the computer program using the celebrated split operator method had been set up even before that time with a great help from Mike Feit. The skeleton of the computer program for the material in Sec. 5-4 was provided by Bill Hoover.

Frankly, the investigation was started with an expectation that a quantum system exhibits chaos for a sufficient time to be observed, although the present evidence weighs heavily against this [21]. Regardless, if this thesis suggests that ubiquitous chaotic nature in a macroscopic level is not observable in underlying microscopic level, so be it. My hope is that this study would be considered as a certain contribution to the field. At any rate, even after the careful processes of many revisions, many parts of my work may still contain some defects. In his words, Warren S. McCulloch seems to describe my emotion at this moment:*"Don't bite my finger - look where it's pointing."*

References

[1] J. Ford, M. Ilg, Phys. Rev. A. **45**, 6165 (1992).

[2] J. Ford, G. Manteca, G. H. Ristow, Physica D, **50**, 493 (1991).

[3] G. Jona-Lasinio, C. Presilla, Phys. Rev. Lett. **68**, 2269 (1992).

[4] C. Presilla, G. Jona-Lasinio, F. Capasso, Phys. Rev. B. **43**, 5200 (1991).

[5] N. Herbert, *Quantum Reality: Beyond the New Physics* (Anchor Press, N. Y. 1985).

[6] D. Layzer, *Cosmogenesis: The Growth of Order in the Universe* (Oxford, N. Y. 1990).

[7] A. Pais, *Einstein on particles, fields and quantum theory,* in *Some strangeness in the proportion* (H. Woolf, Editor).

[8] M. Cici, J-M. Lévi-Leblond (edititors), *Quantum Theory without Reduction* (Adam-Hilger, N. Y. 1990).

[9] D. M. Greenberger (editior), *New Techniques and Ideas in Quantum Measurement Theory* (N.Y. Academy of Science, N.Y. 1986).

[10] B. J. HIley, F. D. Peat (editors), *Quantum Implications: Essays in honour of David Bohm* (Routhledge & Kegan Paul, N. Y. 1987).

[11] J. S. Bell, *Speakable and Unspeakable in Quantum Mechanics* (Cambridge, England, 1987).

[12] W. G. Hoover, B. Moran, C. G. Hoover, D. J. Evans, Phys. Lett. A. **133**, 114 (1988).

[13] W. G. Hoover, Physica A, **118**, 111 (1983).

[14] D. J. Evans, W. G. Hoover, B. H. Failor, B. Moran, A. J. C. Ladd, Phys. Rev. A. **28**, 1016 (1983).

[15] P. Pearle, Am. J. Phys. **35**, 742 (1967); Int. J. Theor. Phys. **48**, 489 (1986).

[16] L. E. Ballentine, Rev. Mod. Phys. **42**, 358 (1970); *Measurements and Time Reversal in Objective Quantum Theory* (Pergamon, Oxford, 1975).

[17] See references listed in Ch. 4 for the Kubo-Fox method.

[18] G. Jona-Lasinio, C. Presilla, Phys. Rev. Lett. **68**, 2269 (1992).

[19] G. Benettin, M. Casartelli, L. Galgani, A. Giorgilli, J.-M. Strelcyn, Nuovo Cimento, **44B**, 183 (1978).

[20] See, for example, P. Cvitanovic, I. Percival, A. Wirzba (Editors), *Quantum Chaos-Quantum Measurement,* NATO ASI Series (Kluwer Academic Pub, Dordrecht, Belgium, 1992).

[21] J. Ford, in *Directions in Chaos*, Vol. II, edited by H. Bai-Lin (World Scientific, Singapore, 1988); see also by the same author, *The New Physics*, edited by P. Davis (Cambridge Univ. Press, Cambridge, 1989).

Bibliography

Aharonov, Y., Anadan, J., Phys. Rev. Lett. **58**, 1593 (1987).

Aitchison, I. J. R., Hey, A. J. G., *Gauge Theories in Particle Physics* (2nd Ed., Adam Hilger, Bristol, England, 1989).

Arnold, V. I., Sov. Math. Dokl. **3**, 136 (1963); **4**, 1153 (1963).

Bailey, T. K., Schieve, W. C., Nuovo Cimento, **47**, 231 (1978).

Bak, P., Physics Today, **39** (Dec. 1986).

Baker, G. L., Gollub, J. P., *Chaotic dynamics*, (Cambridge Univ. Press. N. Y., 1990).

Ballentine, L. E., Rev. Mod. Phys. **42**, 358 (1970); *Measurements and Time Reversal in Objective Quantum Theory* (Pergamon, Oxford, 1975).

Bardsley, J. N., Szöke, A., Comella, J. M., J. Phys. B. **21**, 3899 (1988).

Berne, B. J., Percora, R., *Dynamic Light Scattering* (Wiley, N.Y. 1976).

Batt, J., Faltenbacher, W., Horst, E., Arch. Rat. Mech. Anal. **93**, 159 (1986).

Belykh, V. N., Pedersen, N. F., Soerensen, O. H., Phys. Rev. B. **16**, 4853 (1977).

Benettin, G., Casartelli, M., Galgani, L., Giorgilli, A., Strelcyn, J.-M., Nuovo Cimento, **44B**, 183 (1978).

Berman, G. P., Kolovskii, A. R., Izrailev, F. M., Iomin, A. M., Chaos, **1**(2), 220 (1991).

Berry, M. V., Balazs, N. L., Tabor, M., Voros, A., Annals Phys. **122**, 26 (1979).

Berry, M. V., *Dynamical Chaos* (Princeton Univ. Press, Princeton, N. J. 1987).

Berry, M. V., Phil. Trans. Roy. Soc. **A287**, 237-71 (1977); J. Phys. A. **10**, 2083 (1977).

Berry, M. V., Robnik, M. , J. Phys. A. **19**, 1365 (1986).

Bishop, A. R., Nature, **344**, 290 (1990).

Bohm, D., Phys. Rev. **85**, 166 (1952); **85**, 180 (1952); Nature, **315**, 294 (1985).

Bonci, L., *et al*, Phys. Rev. A. **45**, 8490 (1992).

Braginsky, V. B., Mitrofanov, V. P., Panov, V. I., *Systems with Small Dissipation* (The University of Chicago Press, Chicago, 1985).

Brown, R. C., Heller, E. J., J. Chem. Phys. **75**(1),186 (1981).

Callen, H. B., *The Fluctuation-Dissipation Theorem and Irreversible Thermodynamics* in D. Ter Haar (ed.) *Fluctuations, Relaxations, and Resonance in Magnetic Systems* (Oliver & Boyd, London, 1962).

Carruthers, P., Zachariasen, F.,Rev. Mod. Phys. **55**, 245 (1983).

Cartwright, N. D., Physica (Utrecht), 83A, 210 (1976).
Casati, G., Chirikov, B. V., Ford, J., Phys. Lett. 77A, 91 (1980); Ott, E., Rev. Mod. Phys. 53, 655 (1981).
Casati, G., Ford, J., Guarneri, I., Vivaldi, F., Phys. Rev. A. 34, 1413 (1986).
Casiti, G.(Ed), *Chaotic Behavior in Quantum Systems* (NATO ASI Series,Plenum Press, New York, 1983).
Cerdeira, H. A., Ramasmeny, R., Gutzwiller, M. C., Casati G. (editors), *Quantum Chaos* (World Scientific, Singapore, 1991).
Chelkowski, S., Bandrauk, A. D., Phys. Rev. A. 44, 788 (1991).
Chirikov, B. V., Izrailev, F. M., Shepelyansky, D. L., Soviet Sci. Rev. C. 2, 209 (1981).
Chirikov, B. V., Phys. Rep. 52, 263 (1979).
Chu, S. I., Adv. Atom. Mol. Phys. 21, 97 (1985); Adv. Chem. Phys. 73, 739 (1989).
Chu, S. I., Wu, Z. C., Layton, E., Chem. Phys. Lett. 157, 151 (1989).
Cici, M., Lévi-Leblond, J-M., (edititors), *Quantum Theory without Reduction* (Adam Hilger, N. Y. 1990).
Clarke, J., Cleland, A. N., Devoret, M. H., Esteve, D., Martinis, J. M., Science, 239, 992 (1988).
Cohen, L., J. Math. Phys. 7, 781 (1966).
Cvitanovic, P., et. al. (Editors), *Quantum Chaos-Quantum Measurement,* NATO ASI Series (Kluwer Academic Pub, Dordrecht, Belgium, 1992).
D'Humieres, D., Beasley, M. R., Hubermann, B. A., Libchaber, A., Phys. Rev. A. 26, 3483 (1982).
Degond, P., Guyot-Delaurens, F., J. Comput. Phys. 90, (1990).
Deutsch, I. H., Garrison, J. C., Wright, E. M., J. Opt. Soc. Am. B. 8, 1244 (1991).
Eckhardt, B., Phys. Rep. 163, 205 (1988).
Ehrenfest, P., Z. Physik, 45, 455 (1927).
Evans, D. J., Hoover, W. G., Failor, B. H., Moran, B., Ladd, A. J. C., Phys. Rev. A. 28, 1016 (1983).
Feingold, M., Fishman, S., Physica D, 25, 181 (1987).
Feit, M. D., Fleck, Jr, J. A., Appl. Opt. 19, 1154 (1980); 20, 848 (1981); 20, 2843 (1981).
Feit, M. D., Fleck, Jr, J. A., J. Chem. Phys. 78(1), 301 (1983).
Feit, M. D., Fleck, Jr, J. A., J. Chem. Phys. 80, 2578 (1984).
Feit, M. D., Fleck, Jr, J. A., Steiger, A., J. Comput. Phys. 47, 412 (1982).

Feit, M. D., Fleck, Jr., J. A., Appl. Opt. **20**, 848 (1981).

Feyman, R. P.,*The Feynman Lectures on Physics*, Vol III (Addison-Wesley, Reading, Ma. 1964).

Feyman, R. P., Vernon, F. L., Hellwarth, R. W., J. Appl. Phys. **28**, 49 (1957).

Firth, W., *et al*, *Quantum Measurement and Chaos*, edited by E.R. Pike, S. Sarkar (Nato ASI Series, Plenum Press,1986), p 251.

Fishman, S., Grempel, D. R., Prange, R. E., Phys. Rev. Lett. **49**, 509 (1982).

Fonder, L., Ghirardi, G. C., Rimini, A., Rep. Prog. Phys. **41**, 587 (1978).

Ford, J., Ilg, M., Phys. Rev. A. **45**, 6165 (1992).

Ford, J., in *Directions in Chaos*, Vol. II, edited by H. Bai-Lin (World Scientific, Singapore, 1988).

Ford, J., *The New Physics*, edited by P. Davis (Cambridge Univ. Press, Cambridge, 1989).

Ford, J., Manteca, G., Ristow, G. H., Physica D, **50**, 493 (1991).

Fox, R. F., Uhlenbeck, G. E., Phys. Fluids, **13**, 1893 (1970).

Fox, R. F., J. Math. Phys. **13**, 1196 (1972); J. Math. Phys. **16**, 1214 (1976); Phys. Rep. C. **48**, 179 (1978); J. Chem. Phys. **70**, 4660 (1979); Phys. Rev. A. **41**, 2969 (1990).

Fox, R. F., Keizer, J. E., Phys. Rev. Lett, **64**, 249 (1990); Phys. Rev. A, **43**, 1709 (1991).

Freedman, D. H., Science, **253**, 626 (1991)

Frensley, W. R., Phys. Rev. B. **36**, 1570 (1987).

Ghosh, S. K., Dhara, A. K., Phys. Rev. A. **44**, 65 (1991).

Goldstein, H., *Classical mechanics* (2nd Ed. Addison-Wesley, Reading, Ma, 1980).

Gradshteyn, I. S., Ryzhik, I. M., *Table of Integrals, Series, and Products* (Academic Press, Orlando, Fl. 1980).

Greenberger, D. M., (editior), *New Techniques and Ideas in Quantum Measurement Theory* (N. Y. Academy of Science, N. Y. 1986).

Grempel, D. R., Phys. Rev. A. **29**, 1639-47 (1984).

Grobe, R., Haake, F., Phys. Rev. Lett. **62**, 2889 (1989).

Grobe, R., Haake, F., Sommers, H.-J., Phys. Rev. Lett, **61**, 1899 (1988).

Gutzwiller, M. C., *Chaos in Classical and Quantum Mechanics* (Springer-Verlag, 1990).

Gwinn, E. G., Westervelt, R. M., Phys. Rev. Lett. **54**, 1613 (1985); Phys. Rev. A. **33**, 4143 (1986).

Haake, F., *Quantum Signatures of Chaos* (Springer-verlag, Berlin, 1991).
Harris, F. J., Proceedings of IEEE, **66**, 51 (1978).
Heitler, W.,*The Quantum Theory of Radiation*, 3rd edition (Oxford, England, 1966).
Heller, E. J., *Chaos and Quantum Physics*, edited by Giannoni, M. J., *et al.* (Elsevier Science, Amsterdam, 1990).
Heller, E. J., Phys. Rev. Lett. **16**, 1515 (1984).
Heller, E. J., Physica 7D, 356 (1983).
Heller, E. J., *Quantum Chaos and Statistical Nuclear Physics*, edited by Seligman, T. H., *et al.* (Springer-Verlag, 1986).
Henkel, J. J., Holthaus, M., Phys. Rev. A. **45**, 1978 (1992).
Herbert, N. *Quantum Reality: Beyond the New Physics* (Anchor Press, N. Y. 1985).
Hillery, M., *et al*, Phys. Rep. **106**, 121 (1984).
Hirakawa, K., Sakaki, H., Phys. Rev. B. **33**, 8291 (1986).
Ho, T. S., Chu, S. I., Phys. Rev. A. **32**, 377 (1985).
Hogg, T., Huberman, B. A., Phys. Rev. A. **28**, 22 (1983); Phys. Rev. Lett. **48**, 711 (1982).
Hoover, W. G., Physica A, **118**, 111 (1983); J. Stat. Phys. **42**, 587 (1986); Phys. Rev. A. **31**, 1695 (1985); Phys. Rev. A. 40, 5319 (1989); *Molecular Dynamics* (Springer-Verlag, Berlin, 1986), *Computational Statistical Mechanics* (Elsevier, Amsterdam, 1992).
Hoover, W. G., Moran, B., Hoover, C. G., Evans, W. J., Phys. Lett. A. **133**, 114 (1988).
Hoover, W. G., Posch, H. A., Phys. Lett. A. **113**, 82 (1985); Phys. Lett. A. **123**, 227 (1987).
Hornbeck, R. W., *Numerical Method* (Prentice-Hall, N. J. 1975).
Huberman, B. A., *Dynamical Systems and Chaos*, edited by Garrido, L. (Springer-Verlag, New York, 1982).
Husimi, K., Pro. Phys. Math. Soc. Jpn. **22**, 264 (1940).
Hutchinson, J. S., Wyatt, R. E., Phys. Rev. A. **23**, 1567 (1981); Chem. Phys. Lett. 72, 378 (1980).
Izraelev, F. M., Shepelyanskii, D. L., Theor. Math. Phys. **43**, 417 (1980).
Izrailev, F. M., Phys. Rep. **196**, 299 (1990).
Jensen, J. H., Phys. Rev. A. **45**, 2686 (1992).

Joachain, C. J., *Quantum Collision Theory*, 3rd edition (part III) (North-Holland, N. Y. 1983).

Jona-Lasinio, G.,Presilla,C., Phys. Rev. Lett. **68**, 2269 (1992).

Kamela, M., Razavy, M., Phys. Rev. A. **45**, 2695 (1992).

Keizer, J. E., J. Chem. Phys. **63**, 398 (1975); **63**, 5037 (1975); **64**, 1679 (1976); **64**, 4466 (1976); **65**, 4431 (1976); **67**, 1473 (1977); J. Math. Phys, **18**, 1361 (1977): Phys. Fluids, **21**, 198 (1978).

Keizer, J. E., *Statistical Thermodynamics of Nonequilibrium Processes* (Springer -Verlag, N.Y. 1987).

Keizer, J. E., Tilden, J., J. Chem. Phys. **93**, 2811 (1989).

Kim, Y. S., Wigner, E. P., Am. J. Phys. **58**(5), 439 (1990).

Kimball, J. C., Singh, V. A., D'souza, M., Phys. Rev. A. **45**, 7065 (1992).

Kincaid, D., Cheney, W., *Numerical Analysis* (Brooks/Cole Pub. Co., Pacific Grove, CA. 1991).

Klüksdahl, N. C., *et al*, Phys. Rev. B. **39**, 7720 (1989).

Kolmogorov, A. N., Dokl. Akad. Nauk. SSSR, **98**, 527 (1954).

Korsch, H. J., Berry, M. V., Physica 3D, 627 (1981).

Kubo, R., J. Math. Phys. **4**, 174 (1963).

Kubo, R., *Fluctuations, Relaxation and Resonance in Magnetic Systems* (Oliver and Boyd, Edinburgh, 1962).

Kubo, R., Matsuo, K.,Kitahara, K., J. Stat. Phys. **9**, 51 (1973).

Kuo, S. S., *Computer Applications of Numerical Method* (Addison-Wesley, N. Y. 1972).

Kusnezov, D., Bulgac, A., Bauer, W., Ann. Phys. **204**, 155 (1990); **214** (1992).

Kusnezov, D., Phys. Lett. A. **166**, 315 (1992).

Lalovic, D., Dacidovic, D. M., Bijedic, N., Phys. Rev. A. **46**, 1206 (1992).

Lamb Jr., W. E., Schlicher, R. R., Scully, M. O., Phys. Rev. A. **36**, 2763 (1987).

Lan, B. L., Fox, R. F., Phys. Rev. A. **43**, 646 (1991).

Landau, L. D., Lifshitz, E. M., *Quantum Mechanics* (Non relativistic Theory, 3rd Edition, Pergamon Press, 1977).

Langevin, P., Compt. Rend. **146**, 530 (1908).

Layzer, D., *Cosmogenesis: The Growth of Order in the Universe* (Oxford, N. Y. 1990).

Lee, H. W., Scully, M. O., J. Chem. Phys. **73**, 2238 (1980).

Leforestier, C., *et al*, J. Comp. Phys. **94**, 59 (1991).

Lichtenberg, A. J., Lieberman, M. A., *Regular and stochastic Motion* (Springer-Verlag, New York, 1985).

Lorenz, E. N., *Deterministic Nonperiodic Flow*, J. Atmos. Sci. **20**, 130 (1963).

Marcus, R. A., in Helleman, R. H. G. (ed.), op cit, p. 169 (1980).

Marion, J. B., *Classical Dynamics of Particles and Systems* (2nd Ed., Academic Press, Orlando, Fl, 1970).

Martyna, G. J., Klein, M. L., J. Chem. Phys. **97**, 2635 (1992).

MacDonald, D. K. C., *Noise and Fluctuations: An Introduction* (John Wiley & Sons, N.Y. 1962).

McCumber, E. E., J. Appl. Phys. **39**, 3113 (1968).

McDonald, S. W., Kaufman, A. N., Phys. Rev. Lett, **42**, 1189 (1979).

McLaughlin, J. B., J. Stat. Phys. **24**, 375 (1981).

Mikeska, J. J., Frahm, J., *Chaos, Noise and Fractals* edited by E. R. Pike, L. A. Lugiato (Adam Hilger, Bristol, England, 1987).

Moser, J., Nachr. Akad. Wiss. Göttingen. Math. Phys. **K1**, 1 (1962).

Moyal, J. E., Proc. Cambridge Philos. Soc. **45**, 99 (1949).

Nier, F., Ph.D. Thesis (Ecole Polytechnique, Palaiseau Cedex, France, 1991).

Noid, D. W., Koszykowski, M. L., Marcus, R. A., Annu. Rev. Phys. Chem. **32**, 267 (1981).

Nordholm, K. S. J., Rice, S. A., J. Chem. Phys. **61**, 203 (1974); **61**, 768 (1974); **62**, 157 (1975).

O'Connel, R. F., Wang, L., Willians, H. A., Phys. Rev. A. **30**, 2187 (1984).

Pais, A. ,*Einstein on particles, fields and quantum theory*, in *Some strangeness in the proportion* (H. Woolf, Editor).

Pars, L. A., *A Treatise on Analytical Dynamics* (Oxbrow Press, Woodbridge, Ct., 1979).

Pearle, P., Am. J. Phys. **35**, 742 (1967); Int. J. Theor. Phys. **48**, 489 (1986).

Percival, I. C., Adv. Chem. Phys. **36**, 1 (1977).

Percival, I. C., Phys. B. **6**, L229 (1973).

Peres, A., Anns. Phys. **129**, 33 (1980).

Povlsen, J. H.,Davidsen, P., Jacobsen, G., J. Opt. Soc. Am. **72**, 1506 (1982).

Powell, J. L., Crasemann, B., *Quantum Mechanics* (Addison-Wesley, Reading, MA, 1961).

Presilla, C., Jona-Lasinio, G., Capasso, F., Phys. Rev. B. **43**, 5200 (1991).

Prugovecki, E., Ann. Phys. **110**, 102 (1978).

Radons, G., Prange, R. E., Phys. Rev. Lett. **61**, 1691 (1988).

Rajagopal, A. K., Phys. Rev. A. **27**, 558 (1983).

Ravaioli, U., *et al*, Physica, **134B**, 36 (1985).

Razavy, M., Phys. Rev. A. **41**, 1211 (1990); **41**, 6668 (1990).

Reif, F., *Fundamentals of Statistical and Thermal Physics*, Ch. 15 (McGraw-Hill, N.Y. 1965).

Reinhardt, W. P., *Chaotic Behaviors in Quantum Systems: Theory and Applications*, edited by G. Casati (Plenum, N. Y. 1985).

Sakurai, J. J., *Modern Quantum Mechanics* (Benjamin Cummings, Menlo Park, CA, 1985).

Schiff, L. I., *Quantum Mechanics* (3rd edition) (McGraw-Hill, N. Y. 1968).

Schuster, H. G., *Deterministic Chaos* (Physik-Verlag, Berlin, 1984).

Schuster, H. G., *Deterministic Chaos: An Introduction* (2nd Edition, VCH, N. Y. 1988).

Schuster, H. G., Phys. Rev. **28B**, 381 (1983).

Seligman, T. H. (Ed.) *et al., Quantum Chaos and Statistical Nuclear Physics* (Springer-Verlag, 1986).

Shaw, R., Z. Naturforsch, **36A**, 80 (1981).

Shirley, J. H., Phys. Rev. **138B**, 979 (1965).

Siegman, A. E., *Lasers* (University Science Books, Mill Vally, CA, 1986).

Stewart, W. C., Appl. Phys, Lett. **12**, 277 (1968).

Stoer, J., Bulirsch, R., *Introduction to Numerical Analysis* (Springer-Verlag, N. Y. 1980).

Sudarshan, E. C. G., Chiu, C. B., Gorini, V., Phys. Rev. D. **18**, 2914 (1978).

Sudbery, A., *Quantum Mechanics and The Particles of Nature* (Cambridge Univ. Press, Cambridge, N. Y. 1986).

Tabor, M., *Chaos and Integrability in Nonlinear Dynamics* (John Wiley & Sons, N. Y. 1989).

Takahasi, K., J. Phys. Soc. Jpn. **55**, 762 (1986).

Takahasi, K., Saito, N., Phys. Rev. Lett. **55**, 645 (1985).

Tatarskii, V. I., Sov. Phys. Usp. **26**, 311 (1983).

Teich, M. C., Saleh, B. E. A., Physics Today, **43**, 26 (June 1990).

Thachuk, M., Schatz, G. C., J. Chem. Phys. **97**, 7297 (1992).

Thompson, J. M. T., Stewart, H. B., *Nonlinear Dynamics and Chaos* (John Wiley & Sons, N. Y. 1986).

Tilley, D. R., Tilley, J., *Superfluidity and Superconductivity*, 3rd ed (AIP, N. Y. 1992).

Tomsovic, S., Heller, E. J., Phys. Rev. Lett. **67**, 664 (1991).
van Kampen, N. C., *Stochastic Processes in Physics and Chemistry* (North-Holland, Amsterdam, 1981).
Weissman, Y., Jortner, J., J. Chem. Phys. **77**, 1486 (1982).
Wigner, E. P., Phys. Rev. 40, 749 (1932).
Wolf, A., Swift, J. B., Swinney, H. L., Vastano, J. A., Physica 16D, 285 (1985).
Wright, E. M., Garrison, J. C., J. Opt. Soc. Am. **4**, 1751 (1987).
Yariv, A., *Quantum Electronics*, 3rd Edition (John Wiley & Sons, N. Y. 1989).
Zaslavsky, G. M., Phys. Rep. **80**, 157 (1981) *Chaos in Dynamic systems* (Harwood, N. Y. 1985).

The following books are also used: J. Stat. Phys, **68**, July issue (1992) and*The Random House Dictionary of the English Language*, 2nd Edition, Unabridged, Random House (N. Y., 1987).

Supplement

The core structure of the split operator algorithm is listed conceptually in this supplemental section. The computer program for Section 5-4 is also provided.

```
      BEGIN

c Set up n number of initial grids and kinetic, potential
energy operators.

      DO i=1, n
         q(i), p(i)
         T(i), V(i)
      DONE

c Set up initial wave function y0.

      DO i=1, n
         y0(i)
         y(i)=y0(i)
      DONE

c Propagate initial wave function for m time steps.
c Split the kinetic energy operator once.

      DO 1 j=1, m

         Fourier transform of y(i)

         DO i=1, n
            y(i)=y(i)*T(i)
            Expectation values of p
         DONE

         Inverse Fourier transform of y(i)

         DO i=1, n
            y(i)=y(i)*V(i)
            Expectation values of q
         DONE


c Calculate normalization and correlation function.

         DO i=1, n
         C(j)=C(j)+y0(i)*y(i)
         DONE

c Call subroutine to compute eigen-energies and eigen-
functions
```

```
c using spectral method

        CALL  SUBROUTINES

1     DONE

c Calculate the power spectra from here

-------------------------------------------------------------
c For the Wigner and Husimi distribution functions, set up
c momentum grids (index jj) for phase-space contour plots

      FOR  WIGNER
      DO  i=1,  n
         DO  j=1,  n
          ii  for  shifted  spatial  coordinates
           W(ii,jj)=W(ii,jj)
                +complex  conjugate(y(x-y/2))*(y(x+y/2))
         DONE
      Fourier  transform  in  terms  of  the  momentum  index  jj
      DONE

      FOR  HUSIME
      DO  i=1,  n
         DO  j=1,  n
            DO  k=1,  n
            H(ii,jj)=H(ii,jj)+Gaussian  test  function*y(k)
            DONE
         DONE
      DONE

-------------------------------------------------------------
-------------------------------------------------------------
c Subroutines for Eigen-functions yk(j,k) and eigen-values
E(k)
-------------------------------------------------------------
            Fourier transform of the correlation function C(i)

            Apply Line-fitted method to get E(k)
-------------------------------------------------------------
            kth eigen-value
            DO  i=1,  n
          yk(i,k)=yk(i,k)+y(i)*exp[complex(i)*E(k)*time]
            DONE

-------------------------------------------------------------
```

The above listing describes very simply the core structure of the program. One can add more possible operations for different purposes.

```
      program HMSeqn

c Calculation of the time-dependent Schroedinger equation for a chain
c of three harmonic oscillators bounded by the fixed walls at both ends.

      real t,dt,tm,const,aa,cc,gsum
      dimension yr(3,3,3),yi(3,3,3),yy(54),yyp(54),yyps(54)
      dimension sum1(54),sum2(54),sum3(54),psi(3,10000)
      common/deg/ c1(54,54),c3(54,54),pr(54,54),em(3,3)

c Initial conditions
      write(6,*)
     *  'Enter initial values for y1,y2,....,y27'
      read(5,*) yr(1,1,1),yr(2,1,1).....yr(3,3,2),

c Input parameters
c ncase=1: turn on all the constraints
c iwnt=1: turn on the sinusoidal kinetic energy constraint
c n is the total number of integration steps
      write(6,*) 'Case,dt,n,iwnt'
      read(5,*) ncase,dt,n,iwnt

c Integration
      do 10 i=1,3
      do 10 j=1,3
      do 10 k=1,3
      ijkr=i+3*(j-1)+9*(k-1)
      ijki=ijkr+27
      yy(ijkr)=yr(i,j,k)
      yy(ijki)=yi(i,j,k)
      prosum=prosum+yy(ijkr)**2+yy(ijki)**2
  10  continue

c Set up the matrix elements
      do 14 i=1,54
       pr(i,i)=1.
       c1(i,i)=-2.
       c3(i,i)=-2.
  14  continue
      do 15 i=1,18
       jn=i-1
       c1(1+jn*3,2+jn*3)=1.
       c1(2+jn*3,1+jn*3)=1.
       c1(2+jn*3,3+jn*3)=1.
       c1(3+jn*3,2+jn*3)=1.
  15  continue
      do 16 k=10,45
       c3(k,k-9)=1.
       c3(k,k+9)=1.
  16  continue
      do 17 jj=1,9
       c3(jj,jj+9)=1.
  17  continue
      do 18 kk=46,54
       c3(kk,kk-9)=1.
  18  continue
      do 181 i=19,27
       c3(i,i+9)=0.
 181  continue
      do 182 j=28,36
       c3(j,j-9)=0.
 182  continue

c Normalize the initial wave function
      cnorm=1./sqrt(prosum)
      do 19 i=1,27
       yy(i)=cnorm*yy(i)
       yy(i+27)=cnorm*yy(i+27)
  19  continue
```

```
c ********** MAIN PROGRAM ****************************
      do 100 ii=1,n
      t=t+dt

      do 21 i=1,3
      do 20 j=1,3
      do 20 k=1,3
      ijkr=i+3*(j-1)+9*(k-1)
      ijki=ijkr+27
      yr(i,j,k)=yy(ijkr)
      yi(i,j,k)=yy(ijki)
      sum1(ijkr)=0.0
      sum1(ijki)=0.0
      sum2(ijkr)=0.0
      sum2(ijki)=0.0
      sum3(ijkr)=0.0
      sum3(ijki)=0.0
   20 continue
      psi(i,ii)=0.0
   21 continue

      prosum=0.0
      enesum=0.0
      enesum2=0.0
      ene1=0.0
      ene2=0.0
      ene3=0.0
      do 22 i=1,3
      do 22 j=1,3
      do 22 k=1,3
      ijkr=i+3*(j-1)+9*(k-1)
      ijki=ijkr+27
      pot=0.5*((i-1)**2+(j-i-1)**2+(k-j-1)**2+(k-3)**2)
      dsqr1=-2.*yr(i,j,k)
      dsqr2=-2.*yr(i,j,k)
      dsqr3=-2.*yr(i,j,k)
      dsqi1=-2.*yi(i,j,k)
      dsqi2=-2.*yi(i,j,k)
      dsqi3=-2.*yi(i,j,k)
      if (i.gt.1) dsqr1=dsqr1+yr(i-1,j,k)
      if (j.gt.1) dsqr2=dsqr2+yr(i,j-1,k)
      if (k.gt.1) dsqr3=dsqr3+yr(i,j,k-1)
      if (i.gt.1) dsqi1=dsqi1+yi(i-1,j,k)
      if (j.gt.1) dsqi2=dsqi2+yi(i,j-1,k)
      if (k.gt.1) dsqi3=dsqi3+yi(i,j,k-1)
      if (i.lt.3) dsqr1=dsqr1+yr(i+1,j,k)
      if (j.lt.3) dsqr2=dsqr2+yr(i,j+1,k)
      if (k.lt.3) dsqr3=dsqr3+yr(i,j,k+1)
      if (i.lt.3) dsqi1=dsqi1+yi(i+1,j,k)
      if (j.lt.3) dsqi2=dsqi2+yi(i,j+1,k)
      if (k.lt.3) dsqi3=dsqi3+yi(i,j,k+1)

c Calculate kinetic energies
      ene1=ene1-0.5*(yr(i,j,k)*dsqr1+yi(i,j,k)*dsqi1)
      ene2=ene2-0.5*(yr(i,j,k)*dsqr2+yi(i,j,k)*dsqi2)
      ene3=ene3-0.5*(yr(i,j,k)*dsqr3+yi(i,j,k)*dsqi3)

c Calculate the total probability and total energy
      prosum=prosum+yr(i,j,k)**2+yi(i,j,k)**2
      enesum=enesum+pot*(yr(i,j,k)**2+yi(i,j,k)**2)-0.5*
     1       yr(i,j,k)*(dsqr1+dsqr2+dsqr3)-0.5*yi(i,j,k)*
     2       (dsqi1+dsqi2+dsqi3)
   22 continue

      if (ncase.ne.1) go to 1000

      do 211 mm=1,54
      do 211 nn=1,54
       if ((c1(mm,nn).eq.0.).and.(c3(mm,nn).eq.0.)) go to 211
        sum1(nn)=0.0
        sum2(nn)=0.0
        sum3(nn)=0.0
```

```
      alp=alp+pr(mm,nn)*(yyps(mm)*yy(nn)+yyps(nn)*yy(mm))
      bth=bth+c1(mm,nn)*(yyps(mm)*yy(nn)+yyps(nn)*yy(mm))
      gam=gam+c3(mm,nn)*(yyps(mm)*yy(nn)+yyps(nn)*yy(mm))
       do 212 ll=1,54
        sum1(nn)=sum1(nn)+pr(nn,ll)*yy(ll)
        sum2(nn)=sum2(nn)+c1(nn,ll)*yy(ll)
        sum3(nn)=sum3(nn)+c3(nn,ll)*yy(ll)
 212    continue
      em(1,1)=em(1,1)+pr(mm,nn)*(yy(mm)*sum1(nn)+yy(nn)*sum1(mm))
      em(1,2)=em(1,2)+pr(mm,nn)*(yy(mm)*sum2(nn)+yy(nn)*sum2(mm))
      em(1,3)=em(1,3)+pr(mm,nn)*(yy(mm)*sum3(nn)+yy(nn)*sum3(mm))
      em(2,1)=em(2,1)+c1(mm,nn)*(yy(mm)*sum1(nn)+yy(nn)*sum1(mm))
      em(2,2)=em(2,2)+c1(mm,nn)*(yy(mm)*sum2(nn)+yy(nn)*sum2(mm))
      em(2,3)=em(2,3)+c1(mm,nn)*(yy(mm)*sum3(nn)+yy(nn)*sum3(mm))
      em(3,1)=em(3,1)+c3(mm,nn)*(yy(mm)*sum1(nn)+yy(nn)*sum1(mm))
      em(3,2)=em(3,2)+c3(mm,nn)*(yy(mm)*sum2(nn)+yy(nn)*sum2(mm))
      em(3,3)=em(3,3)+c3(mm,nn)*(yy(mm)*sum3(nn)+yy(nn)*sum3(mm))
 211  continue
      if (iwnt.eq.1) then
      bth=bth-2.*sin(t)*cos(t)
      endif

c Calculate the multipliers
      call rlamda(alp,bth,gam,em,aa,bb,cc)

      alp=0.
      bth=0.
      gam=0.
 1000 continue

c Calculate the number densities
      do 57 m=1,3
      do 56 jj=1,3
      do 56 kk=1,3
      psi(m,ll)=psi(m,ll)+(yr(m,jj,kk)**2+yi(m,jj,kk)**2)+
     *          (yr(jj,kk,m)**2+yi(jj,kk,m)**2)+
     *          (yr(kk,m,jj)**2+yi(kk,m,jj)**2)
 56   continue
      psi(m,ll)=psi(m,ll)/3.0
 57   continue

      write(6,799) t,prosum,enesum,ene1,ene2,ene3,aa,bb,cc

c Perform the time integration
      call runkut(dt,yy,yyp,yyps,aa,bb,cc)

  100 continue
  799 format(f6.3,1x,2(f8.4,1x),3(f6.3,1x),3(f8.3,1x))

      call exit
      end
```

```
      subroutine runkut(dt,yy,yyp,yyps,aa,bb,cc)
      parameter(neq=54)

      dimension yy(neq),yyp(neq),yyps(neq)
      dimension yak1(neq),yak2(neq),yak3(neq),yak4(neq),ynew(neq)
      common/sam/ prbsum(54),c1s(54),c3s(54)
      common/deg/ c1(54,54),c3(54,54),pr(54,54),em(3,3)

      do 32 ijkr=1,27
      ijki=ijkr+27
      prbsum(ijkr)=0.
      prbsum(ijki)=0.
      c1s(ijkr)=0.
      c1s(ijki)=0.
      c3s(ijkr)=0.
      c3s(ijki)=0.
      do 32 jjj=1,27
       prbsum(ijkr)=prbsum(ijkr)+pr(ijkr,jjj)*yy(jjj)
       prbsum(ijki)=prbsum(ijki)+pr(ijki,jjj+27)*yy(jjj+27)
       c1s(ijkr)=c1s(ijkr)+c1(ijkr,jjj)*yy(jjj)
       c1s(ijki)=c1s(ijki)+c1(ijki,jjj+27)*yy(jjj+27)
       c3s(ijkr)=c3s(ijkr)+c3(ijkr,jjj)*yy(jjj)
       c3s(ijki)=c3s(ijki)+c3(ijki,jjj+27)*yy(jjj+27)
32    continue

      call fcn(dt,yy,yyp,yyps,aa,bb,cc)
      do 1 i=1,neq
1     yak1(i)=yyp(i)
      do 2 i=1,neq
2     ynew(i)=yy(i)+(0.5*dt)*yak1(i)
      call fcn(dt,ynew,yyp,yyps,aa,bb,cc)

      do 3 i=1,neq
3     yak2(i)=yyp(i)

      do 4 i=1,neq
4     ynew(i)=yy(i)+(0.5*dt)*yak2(i)
      call fcn(dt,ynew,yyp,yyps,aa,bb,cc)

      do 5 i=1,neq
5     yak3(i)=yyp(i)

      do 6 i=1,neq
6     ynew(i)=yy(i)+dt*yak3(i)
      call fcn(dt,ynew,yyp,yyps,aa,bb,cc)
      do 7 i=1,neq
7     yak4(i)=yyp(i)

      do 8 i=1,neq
8     yy(i)=yy(i)+dt*(yak1(i)+2.*yak2(i)+2.*yak3(i)+yak4(i))/6.0

      return
      end
```

```
      subroutine fcn(dt,y,yp,yps,aa,bb,cc)
      parameter(neq=54)
      dimension y(neq),yp(neq),yr(3,3,3),yi(3,3,3),yps(neq)
      common/sam/ prbsum(54),c1s(54),c3s(54)
      common/deg/ c1(54,54),c3(54,54),pr(54,54),em(3,3)

      do 30 i=1,3
      do 30 j=1,3
      do 30 k=1,3
      ijkr=i+3*(j-1)+9*(k-1)
      ijki=ijkr+27
      yr(i,j,k)=y(ijkr)
      yi(i,j,k)=y(ijki)
30    continue

      do 35 i=1,3
      do 35 j=1,3
      do 35 k=1,3
      pot=0.5*((i-1)**2+(j-i-1)**2+(k-j-1)**2+(k-3)**2)
      dsqr1=-2.*yr(i,j,k)
      dsqr2=-2.*yr(i,j,k)
      dsqr3=-2.*yr(i,j,k)
      dsqi1=-2.*yi(i,j,k)
      dsqi2=-2.*yi(i,j,k)
      dsqi3=-2.*yi(i,j,k)
      if (i.gt.1) dsqr1=dsqr1+yr(i-1,j,k)
      if (j.gt.1) dsqr2=dsqr2+yr(i,j-1,k)
      if (k.gt.1) dsqr3=dsqr3+yr(i,j,k-1)
      if (i.gt.1) dsqi1=dsqi1+yi(i-1,j,k)
      if (j.gt.1) dsqi2=dsqi2+yi(i,j-1,k)
      if (k.gt.1) dsqi3=dsqi3+yi(i,j,k-1)
      if (i.lt.3) dsqr1=dsqr1+yr(i+1,j,k)
      if (j.lt.3) dsqr2=dsqr2+yr(i,j+1,k)
      if (k.lt.3) dsqr3=dsqr3+yr(i,j,k+1)
      if (i.lt.3) dsqi1=dsqi1+yi(i+1,j,k)
      if (j.lt.3) dsqi2=dsqi2+yi(i,j+1,k)
      if (k.lt.3) dsqi3=dsqi3+yi(i,j,k+1)

      ijkr=i+3*(j-1)+9*(k-1)
      ijki=ijkr+27

      yps(ijkr)=-0.5*(dsqi1+dsqi2+dsqi3)+pot*yi(i,j,k)
      yp(ijkr)=yps(ijkr)-aa*prbsum(ijkr)-bb*c1s(ijkr)-cc*c3s(ijkr)
      yps(ijki)=0.5*(dsqr1+dsqr2+dsqr3)-pot*yr(i,j,k)
      yp(ijki)=yps(ijki)-aa*prbsum(ijki)-bb*c1s(ijki)-cc*c3s(ijki)
35    continue

      return
      end

      subroutine rlamda(alp,bth,gam,em,aa,bb,cc)
      dimension em(3,3),d(3,3),rl(3)

      denom=em(1,1)*em(2,2)*em(3,3)-em(1,1)*em(2,3)*em(3,2)+
     *      em(1,2)*em(2,3)*em(3,1)-em(1,2)*em(2,1)*em(3,3)+
     *      em(1,3)*em(2,1)*em(3,2)-em(1,3)*em(2,2)*em(3,1)

      rnum1=alp*em(2,2)*em(3,3)-alp*em(2,3)*em(3,2)+
     *      em(1,2)*em(2,3)*gam-em(1,2)*bth*em(3,3)+
     *      em(1,3)*bth*em(3,2)-em(1,3)*em(2,2)*gam
      rnum2=em(1,1)*bth*em(3,3)-em(1,1)*em(2,3)*gam+
     *      alp*em(2,3)*em(3,1)-alp*em(2,1)*em(3,3)+
     *      em(1,3)*em(2,1)*gam-em(1,3)*bth*em(3,1)
      rnum3=em(1,1)*em(2,2)*gam-em(1,1)*bth*em(3,2)+
     *      em(1,2)*bth*em(3,1)-em(1,2)*em(2,1)*gam+
     *      alp*em(2,1)*em(3,2)-alp*em(2,2)*em(3,1)

      do 3 i=1,3
      do 3 j=1,3
      em(i,j)=0.0
3     continue

      aa=rnum1/denom
      bb=rnum2/denom
      cc=rnum3/denom
      return
      end
```

DATE
FILMED
5/4/94
END